Ubiquitin E3 Ligases in Lung Disease

by

Travis Bradley Lear

BA, Saint Mary's College of Maryland, 2012

Submitted to the Graduate Faculty of the

Department of Environmental and Occupational Health

Graduate School of Public Health in partial fulfillment

of the requirements for the degree of

Doctor of Philosophy

University of Pittsburgh

2020

UNIVERSITY OF PITTSBURGH

GRADUATE SCHOOL OF PUBLIC HEALTH

This dissertation was presented

by

Travis Bradley Lear

It was defended on

March 6, 2020

and approved by

Aaron Barchowsky, PhD, Professor, Environmental and Occupational Health, Graduate School
of Public Health, University of Pittsburgh

Bruce R. Pitt, PhD, Professor, Environmental and Occupational Health, Graduate School of
Public Health, University of Pittsburgh

Toren Finkel, MD, PhD, Professor of Medicine, Department of Medicine, School of Medicine,
University of Pittsburgh

Dissertation Advisor: Bill B. Chen, PhD, Associate Professor of Medicine, Department
of Medicine, School of Medicine, University of Pittsburgh

Bill B. Chen, PhD

Ubiquitin E3 Ligases in Lung Disease

Travis Bradley Lear, PhD

University of Pittsburgh, 2020

Abstract

Diseases of the lung form the one of the largest causes of death globally. Inflammatory diseases such as Acute Respiratory Distress Syndrome, and fibrosis such as interstitial lung disease, in particular have high mortality rates with limited therapy. Thus, there is an unmet public health need for new avenues of intervention. Inflammatory, fibrotic, and nutrient lung diseases are driven by cellular signaling pathways, leading to pathological cell responses. Effector lung cells naturally dampen these deleterious signaling pathways; dysfunction of these dampening mechanisms play causal roles in lung disease, notably through excessive destruction of critical signal transduction proteins. Modulation of signal transduction protein degradation may have therapeutic effect by controlling deleterious signaling. The ubiquitin-proteasome system is the major cellular mechanism controlling protein degradation. Ubiquitin E3 ligase proteins are a critical part of ubiquitination, specifically targeting substrates for degradation. Research shows the importance of protein degradation in lung disease, however the potential to identify and inhibit specific E3-ligase-substrate interactions remains unexplored. Through both candidate-based and unbiased high-throughput screening techniques, we probed the importance of E3 ligases in lung disease through their targeted degradation of signal transduction proteins, and the therapeutic potential of E3 ligase inhibition. We investigated three aspects of lung disease – 1) inflammation and innate immunity, 2) fibrosis and interstitial lung disease, and 3) regulation of nutrient sensing mechanisms. Here we report multiple E3 ligase-substrate axes, including those associated with

fibrosis: FIEL1-PIAS4; KLHL42-PPP2R5e, with innate immunity: PPP1R11-TLR2, RNF113A-CXCR4, KIAA0317-SOCS2, RNFT2-IL3Ra, and with nutrient sensing: RNF186-SESN2. We observed that E3 ligases potently control inflammatory signaling through control of cytokine receptors and signal modulators during acute inflammation and bacterial infection. We uncovered that E3 ligases are significantly associated with fibrotic signaling in interstitial lung fibrosis, and can be targeted by small molecules. Finally, we detected new mechanisms of nutrient sensor control leading to manipulation of anabolism. These results show the criticality of ubiquitin e3 ligases in the biology of lung inflammation, fibrosis, and nutrient sensing. Further, these studies validate ubiquitin E3 ligases as potential targets for therapeutic intervention to provide new tools to combat lung diseases.

Table of Contents

List of Tables

List of Figures

Preface

This research was only possible through the unending generosity and support of my mentor and PI Dr. Bill Chen. Working with Dr. Chen has been a wonderful and productive journey as a lab technician and graduate student that has given me the scientific foundation

My committee members, Dr. Barchowsky, Dr. Pitt, and Dr. Finkel, have been supporters and teachers throughout my graduate career. The EOH Department has been immensely supportive and a beautiful place of learning and research. I owe thanks to several collaborators in both the Pulmonary Division and the Aging Institute, specifically Dr. Yuan Liu, who has been a wonderful teacher and collaborator for many years.

These studies have been a team effort from the Chen Lab, encompassing many great scientists and friends over the years. In completing my doctoral work, I leave a great group involving Dr. John Evankovich, Dr. Yanwen Chen, Karina Lockwood, Dan Camarco, V. White, John Villandre, and Dr. Tuncer. Friends and colleagues from earlier iterations of the Chen lab deserve mention as well, such as Yurong, Dr. Yao Tong, Alison McKelvey, Sarah Dunn, Shristi Rajbhandari, William Connelly, and my first supervisor and hirer, Tiffany Coon.

Finally, I'd like to thank my wonderful parents for their unending patience and support. Their guidance and wisdom molded me into someone strong enough to undertake this venture. I couldn't have finished this endeavor without the support of my partner Janine. Janine, thank you for all your patience with me and my work. Many other friends have been key support, notably Dr. Phu T Van, the one who encouraged me to move to Pittsburgh in the first place. PhD is a long road and their infinite supply of patience, guidance, and enthusiasm have been invaluable.

1.0 Introduction

The human lung system is the critical organ system for respiratory function. Separated into two multi-lobed segments, the lungs are part of the lower respiratory system tasked with gas exchange to the circulatory system. Connecting to the upper-respiratory system at the trachea, the architecture of the lung becomes increasing complex deeper into the airway. The lungs are connected to the trachea and the upper respiratory system through large airways known as bronchi. Bronchi branch into smaller and more numerous sub-airways, decreasing in diameter and increasing in total surface area. The lung terminates in collections of hollow cavities termed alveoli. Pulmonary alveoli are coated with capillary vasculature, and their proximity to the alveolar epithelial cells allow for gas exchange of oxygen and carbon dioxide, which is used to maintain homeostasis in the systemic vascular system.

1.1 Diseases of Lung

Lung respiratory efficacy is reliant on the integrity and health of the alveolar spaces and surrounding and supporting interstitial tissue. As outside air is processed for gas exchange, the lung is exposed to environmental and occupational exposures, several of which may cause damage or disease.

1.1.1 Global Public Health Significance of Lung Disease

Diseases of the lung collectively account for the majority of global human hospitalization and mortality (1, 2). The World Health Organization has identified five major disease types that account for the largest proportion of lung diseases, chronic obstructive pulmonary disease (COPD), tuberculosis, lung cancer, asthma, and lower respiratory infections (2). Lower respiratory infections are particularly of public health concern due to little change in mortality despite decades of research and therapy (3). Lower respiratory infections can arise from bacterial, viral, or sometimes fungal causes, leading to acute immune responses, pneumonia, sepsis, and in many cases, respiratory failure (4, 5). Inflammation in the lung, and particularly the alveolar spaces is an important determinant of disease course during respiratory infection, as a balance needs to be struck between enough immune response to clear infection, while restraining the response from causing damage to the lung and host (5). In addition to the predominant lung diseases, numerous other pathologies arise in the lung, including interstitial lung disease (fibrosis), pulmonary arterial hypertension, and cystic fibrosis. Further, many of these diseases show an increase prevalence and mortality among aged patients, an area for concern as the global human population grows older in the coming decades.

In these dissertation projects, we sought to investigate new protein-protein relationships in cellular signaling that are biologically relevant in lung disease, and the potential to chemically intervene to improve the underlying disease. As a proof of principle, we focused on three types of lung disease: 1) pulmonary fibrosis, 2) lung inflammation related to infection and acute lung injury, and 3) mechanisms of aging through pilot studies into nutrient sensing. We believe these research efforts have highlighted new mechanisms of disease-related signaling and new avenues for therapeutic intervention and targeting.

1.1.2 Fibrosis in the Lung

Interstitial lung disease is a collection of pathologies characterized by the hardening of the interstitial space in the lung and between the alveolar cavities (6). During normal injury repair processes, fibrosis response is a healthy mechanism to repair damaged tissue, and restore normal function (7). However, aberrant and pathological fibrosis results in runaway fibrotic deposition of collagenous material with an increase in inflammatory signaling. Interstitial lung disease can arise from environmental or occupational exposures such as silica or asbestos or an underlying medical condition such as sarcoidosis or systemic auto-immune diseases such as Scleroderma/Systemic sclerosis (8, 9). However, one type, idiopathic pulmonary fibrosis, has no understood cause (10).

1.1.2.1 Idiopathic Pulmonary Fibrosis

Adapted from: Lear and Chen, Therapeutic targets in fibrotic pathways, Cytokine. 2016 Dec;88:193-195. doi: 10.1016/j.cyto.2016.09.008. Epub 2016 Sep 19. (11)

Idiopathic pulmonary fibrosis (IPF) is the most common interstitial lung disease with no cure and a grim median survival time of 3 years. This disease afflicts over 50 people per 100,000; and disproportionately affects the elderly: up to 0.2% of those over 75 years of age (12). Excessive fibrous deposition in the alveolar space results in pulmonary failure. Interestingly, there is profound heterogeneity in disease course and severity among patients, necessitating research into the molecular mechanisms of pathogenicity. Despite years of research, the sub-cellular molecular etiology of pulmonary fibrosis remains unclear. Several groups have sought to clarify the pathogenesis of pulmonary fibrosis.

1.1.2.2 Determinants of IPF Pathology

Both genetic and environmental insults show association with the development of IPF. Research from the Armanios lab has implicated telomere distress as a causal agent in a subset of cases, as part of generational genetic anticipation (13). Additionally, research has shown several genetic hotspots, such as the MUC5B promoter, associate with a worsened phenotype (14). Extra-cellular matrix proteins such as integrins and matricellular proteins have been associated with fibrosis (15, 16). Most saliently important is the cytokine Transforming Growth Factor β (TGF-β), which is well accepted as a driver of cellular fibrosis (16, 17). TGF-β is sequestered in the extracellular matrix of cells in a latent form prior to cleavage and activation. Reed and colleagues demonstrated the importance of integrin-mediated latent-TGF-β activation in the context of liver and pulmonary fibrosis, as well as the potential for therapeutic targeting (18). Active TGF-β is a ligand for the TGF-β receptor, which initiates the SMAD signaling cascade (19). TGF-β signaling transduces through SMAD proteins, which dimerize prior to nuclear translocation and regulation of gene expression (20). Gao and colleagues demonstrated Ubiquitin E3 ligases directly regulate SMAD signal transduction, and Imoto and colleagues observed direct SUMOylation of SMADs leading to signaling suppression (21-23).

1.1.2.3 Therapeutic Options for IPF

Until recently, IPF had few therapeutic options and was an orphan drug disease. Researchers halted triple treatment of immuno-suppressants and N-acetylcysteine due to concerns of increased mortality among study patients (24). However, in 2014, the FDA approved two therapeutics for IPF treatment. Several groups developed Nintedanib as a small-molecule treatment for idiopathic pulmonary fibrosis, culminating in the INPULSIS trials and FDA approval (25). Nintedanib inhibits multiple tyrosine kinases, such as vascular endothelial growth factor

(VEGF), fibroblast growth factor (FGF), and platelet-derived growth factor (PDGF). This therapy shows efficacy in critical metrics of pulmonary function. Concurrently, several research groups developed Pirfenidone, culminating in the ASCEND Study trial (26). The discreet targets of Pirfenidone still remain unclear, yet it shows efficacy in delaying disease progression (27). Due to the heterogeneity of this disease, multiple targets in the fibrotic pathway lay open for potential intervention (28) (Figure 1).
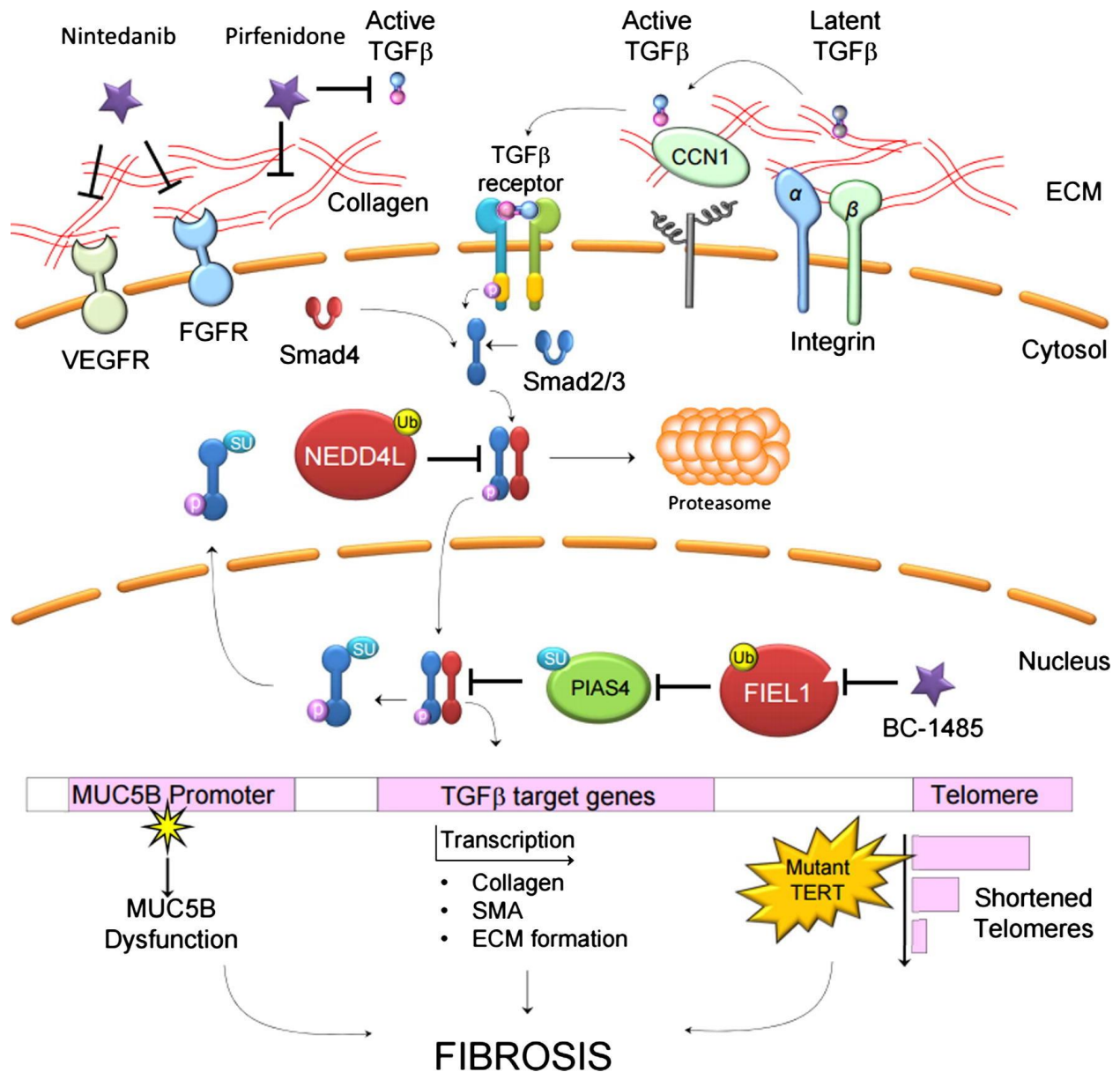
Figure 1 Therapeutic Targets in Fibrotic Pathways

Membrane proteins such as integrins and secreted proteins in the extracellular matrix (ECM) such as CCN1 interact and facilitate the conversion of latent, ECM-sequestered TGFβ to its active form. Active TGFβ is ligand to the TGFβ receptor on epithelia, fibroblasts, and immune cells. Receptor stimulation causes a signaling cascade via SMAD proteins, leading to the nuclear translocation of a SMAD complex and the transcriptional activation of pro-fibrotic genes. Ubiquitin-E3 ligases, such as NEDD4L, regulate SMAD signaling through proteasome-mediated degradation. Additionally, SUMO-E3 ligases, such as PIAS4, regulate SMAD signaling by forcing its nuclear export. Direct regulators of SMAD signaling are themselves regulated, as FIEL1 catalyzes the degradation of PIAS4. In addition to transcriptional regulation of pro-fibrotic genes and gene products such as collagens, smooth muscle action and fibronectin, genetic abnormalities associate with fibrosis. Mutation within the MUC5B promoter and shortened telomeres caused by telomerase mutations both associate with worsened fibrosis. The current therapeutics Nintedanib and Pirfenidone target growth receptors, ECM formation, and TGFβ. Novel compound BC-1485 targets downstream profibrotic protein FIEL1, which may serve as a new therapeutic approach for the future IPF therapy.

1.1.3 Inflammation in the Lung

The inflammatory response in the lung is a critical deterrent to infection such as acute lower respiratory infections, and in maintaining pulmonary homeostasis. Inflammation induces cytokine signaling leading to immune responses to respiratory infections. Sentinel cells, including pulmonary epithelia, detect pathogens, and initiate innate inflammatory responses via cytokine signaling cascades (29). Cytokine signaling pathways rely on receptor protein complexes that detect extracellular signals or patterns to initiate signaling. Two common classes of cellular signaling species are Pathogen Associated Molecular Patterns (PAMPs) and Damage Associated Molecular Patterns (DAMPs). PAMPs are molecular patterns distinct to invading pathogens, often part of their structural make-up. Lipopolysaccharide is a classic PAMP from Gram-negative bacteria such as E. coli or P. aeruginosa (30). Peptidoglycan species are Gram-positive PAMPs from S. aureus (31). DAMPs are often released as a product of ongoing stress and damage to the host and include proteins like HMGB1 and free nuclei acids (32). PAMPs are key to innate immunity, as they are recognized by pattern-recognition receptors, such as Toll-Like Receptors, on sentinel pulmonary cells which then initiate cytokine signaling cascades. Pro-inflammatory cytokine signaling leads to gene expression programs and the generation of immune recruitment markers such as cytokines to activate the systemic immune response. Research has shown pulmonary epithelial cell models that closely mimic effector cells in the alveolar compartment are able release pro-inflammatory cytokines upon stimulation with PAMPs, suggesting that alveolar epithelial cells are important initiators of pulmonary inflammation (33, 34). The increase in cytokine secretion also has paracrine and autocrine effect on the alveolar epithelial cells, as cytokines such as chemokines and interleukins modulate signaling. Indeed several studies have suggested lung sensitization or a "double-hit" where a combination of cytokine and PAMP

exacerbates the inflammatory response (35-37). This cytokine release facilitates the activation of resident alveolar macrophages and the recruitment of leukocytes from the vasculature to the afflicted area (38).

This innate immunological response is critical to containing and clearing a respiratory infection. However, the inflammatory response induces changes to the pulmonary landscape (39). Dysregulated or pulmonary inflammation leads to capillary damage, disruption of pulmonary barrier function, and alveolar damage caused by leukocytes (40). These cells cause lung injury through the release of toxic species such as proteases and reactive oxygen species that affect the integrity of epithelial cells and their intercellular junctions, leading to edema formation and reduced gas exchange across the alveolus (41). This disruption of the alveolar architecture and functional is termed Diffuse Alveolar Damage: a classic hallmark of pulmonary distress resulting from excessive inflammatory response (5, 42, 43). This uncontrolled pulmonary inflammation is the characteristic and causal of several acute pathologies, such as acute respiratory distress syndrome (ARDS), pneumonia, and exacerbations of chronic diseases (44). For example, ARDS affects almost 0.25 million patients annually, whom suffer over 40% mortality (45, 46).

One pathway, nuclear factor-kappa B (NF-κB), potently stimulates the release of inflammatory cytokines such as IL-1, IL-6, and TNF (47). These and other chemotactic cytokines promote endothelial activation, in which the pulmonary vasculature loosens and allows the migration of immune cells into the alveolar space (48). Subsequent research has shown that NF-κB signaling promotes the transcription of cytokines involved in ARDS pathogenesis (49-52). Indeed, isolated alveolar macrophages from ARDS patients show more activated NF-κB than control (49). NF-κB signaling has been implicated with pulmonary inflammation leading to cardiovascular distress (53, 54). Cytokine signaling pathways utilize signal modulating proteins to

accelerate or dampen the signaling process depending on the cellular context (55, 56). Signal-suppressing proteins, such as SOCS, work to repress cytokine signaling (57). Previous studies by the Mallampalli and Chen Labs have shown that key proteins that modulate inflammatory responses in the lung are dysregulated during inflammatory disease and injury (58-62). We sought to investigate novel E3 ligase-substrates relationships in lung inflammation, and if the E3 ligases were druggable.

1.1.4 Nutrient Sensing in the Lung

Nutrient sensing is a critical molecular process driving cellular responses during homeostasis, anabolism, and catabolism (63-65). The major mechanism of sensing amino acids and nutrients is the mechanistic target of rapamycin (mTOR) network (66, 67). Activated mTORC1 promotes cellular processes such as protein translation, glucose metabolism, and fatty acid synthesis, while suppressing autophagy (68-70). Dysfunctional nutrient sensing is characteristic of cancer, metabolic disorders, immune dysregulation, and is considered a major hallmark of aging itself (68, 71). Inhibition of mTORC1 has shown clinical promise, specifically for use in immunosuppression and in treating mTOR-sensitive tumors, however mTORC1 inhibitors suffer from adverse side effects (72-75), illustrating the need for new therapies. Further, mTORC1 inhibition is one of the sole mechanisms for extended longevity in multiple experimental systems(76), raising the question as to alternative approaches of intervention. Researchers have uncovered an intricate network of over 30 proteins that directly control mTORC1 (70, 77, 78). *mTORC1 regulators* are critically important in activating or inhibiting mTORC1, as loss-of-function and mutational studies of individual regulator result in impaired mTORC1 function. For example, depletion of the mTORC1-inhbitor nutrient sensor Sestrin-2, led to constitutive

activation of mTORC1, even during nutrient deprivation when mTORC1 is inactive (77, 79). mTORC1 regulator mutation and dysfunction occurs in numerous pathologies including metabolic diseases, neurological disorders, and neoplasia, leading to disruption of mTORC1 homeostasis (80-84). However, the role of mTORC1 regulator protein stability and their mechanisms of degradation remain poorly characterized. The mechanisms underlying mTORC1 regulator control could represent a new area for selective therapeutic inhibition to modulate mTORC1 activity. Previous research has suggested some mTORC1 regulators are controlled by ubiquitination (81); however, a systematic analysis of the protein stability of the mTORC1 regulator landscape has not been conducted.

1.2 Protein Degradation

1.2.1 Protein Lifespan

Cellular proteins are dynamically regulated in time and space through numerous post-translational modifications. Key to these modifications is the observation that cellular proteins tend to exhibit differential permanence over time, likely due to differences in individual protein stabilities. These seemingly intrinsic proteins of specific proteins have been termed protein lifespan or "half-life", signifying an estimation before degradation of the protein. Differential protein half-life occurs due to functional differences in the underlying proteins ranging from sensitive transcription factors to long-lived structure proteins. Overall, the scope of cellular proteins have been estimated to have half-lives ranging from minutes to many hours (85-87). Protein half-life is also modulated due to context specific cellular needs, such as changes in cell

production due to cell proliferation, growth, metabolism, or immune response (88). For example, researchers observed cell-cycle specific changes in protein degradation rates, as proteins become more stable around the moment of cytokinesis (89). Protein stability has consequences in disease, as infection can manipulate endogenous cellular protein stability processes to favor the pre-mature degradation of otherwise anti-viral proteins, such as the hijacking of ubiquitination activity by HIV to preserve infectivity (90-92). These observations utilized the hijacking of a cell's E3 ligase, which is part of the ubiquitin proteasome system, an integral regulator of protein stability. Moreover, inhibition of the process of protein degradation has been an effective avenue of disease therapy, as inhibition of the proteasome has shown efficacy in combating cancers such as multiple myeloma (93).

1.2.2 The Ubiquitin Proteasome System

The Ubiquitin Proteasome System is the major cellular mechanism for protein degradation and recycling (94). This system utilizes the 76 amino-acid protein Ubiquitin as a molecular tag for substrate proteins through post-translational modification. The C-terminus of ubiquitin is covalently bound to target residues of the substrate protein, usually the ε-amino group of a substrate lysine (Lys) residue. Ubiquitin has the interesting ability to be itself ubiquitinated, with a second ubiquitin forming peptide bonds to Lys residues within the initial ubiquitin. From this, substrates can become poly-ubiquitinated, with long chains of linked ubiquitin moieties (95). Poly-ubiquitination offers an additional level of coding, as ubiquitin has seven Lys sites that can be substrate sites for ubiquitination (Lys-6, 11, 27, 29, 33, 48, 63). In addition, ubiquitin can form linear assemblages through methionine-1 (Met-1) serving as the substrate site for subsequent ubiquitination (96). Research has shown that specific poly-ubiquitin chain linkage types can signal

11

for specific fates of the ubiquitinated substrate (97, 98). For example, Lys-63 linked poly-ubiquitin chains are implicated directed substrates for degradation in the lysosome rather than the proteasome (99). Met-1 linear ubiquitination plays a key role in controlling NF-κB signaling (100). Lys-48 specific poly-ubiquitination is the canonical signal for degradation in the proteasome, a massive protein structure that recycles proteins to their amino acids (101). The fate of ubiquitin itself during proteasomal substrate degradation is an developing topic of research, recent studies have suggested that the proximal ubiquitin attached the substrate is degraded along with the substrate protein, while the distal poly-ubiquitin chains are cleaved of their isopeptide bonds by de-ubiquitinases, and recycled to the intracellular space (102).

The conjugation of ubiquitin to target substrates is accomplished in an enzymatic cascade. First, using ATP, the catalytically active cysteine (Cys) residue of the E1-activating enzyme forms a high energy thioester bond to the C-terminal glycine of ubiquitin (Ub). Then, using another ATP, the E1 enzyme transfers ubiquitin to the active center Cys of the E2 Ub conjugating enzyme (Ubc)(103). Finally, ubiquitin is covalently attached to target substrates through the aid of ubiquitin E3 ligases. Within this enzymatic cascade, E3 ligases play the critical role in identifying and binding the substrate protein fated for ubiquitination.

1.2.3 Ubiquitin E3 Ligases

The third enzyme class in the ubiquitination pathway cascade is the Ubiquitin E3 Ligase. E3 ligases play the critical role in targeting and binding substrates fated for ubiquitination. Substrates are then ubiquitinated either through E3 ligase steric orientation that allows the E2 conjugating enzyme to be in close proximity to the substrate, or through intrinsic E3 ligase enzymatic activity. Research has identified over 800 unique E3 ligase proteins, which quite

numerous compared to the 20 E2 enzymes and single E1 activating enzyme complex (19, 20).

Ubiquitin E3 ligases can be classified into several distinct families, including Cullin-RING-Ligase (CRL) complexes, Really Interesting New Gene (RING) Domain, U-box, and E6-AP Carboxyl Terminus (HECT) domain (Figure 2) (103-106). Distinct E3 ligase families demonstrate different mechanistic and functional attributes, for example, HECT E3 ligases possess a unique feature in which they accept ubiquitin from an E2 ubiquitin-conjugating enzyme in the form of a thioester bond and directly transfer the ubiquitin to the substrate. An active site within the C-terminal of the HECT domain containing a cysteine residue is required for ubiquitin-thioester formation (107). In contrast, F-box E3 ligases, which serve as the substrate receptor subunit of the Cullin-RING-Ligase 1 (CRL1) E3 ligase complex, function to bind substrate proteins, which are then ubiquitinated by the accompanying E2 enzyme (108-112). RING finger E3 ligases contain a unique RING (Really Interesting New Gene) finger domain that consists of two zinc finger type domains (113-115). RING domains facilitate the coordination of ubiquitin E2 domains, but some RING E3 ligases exhibit ligase activity independent of a scaffolding framework of a CRL complex (116, 117). Of these E3 ligase families, HECT-domain and RING-domain E3 ligases remain poorly characterized (118). There are about 30 HECT E3 ligases in mammalian cells, and functional data is only available for a select few including E6AP, Smurf, HECTD2 and NEDD4 (118, 119). Functional data are available for only about a dozen of the over 300 predicted RING E3 ligases , such as MDM2 and several RNF and TRIM proteins (120-123).
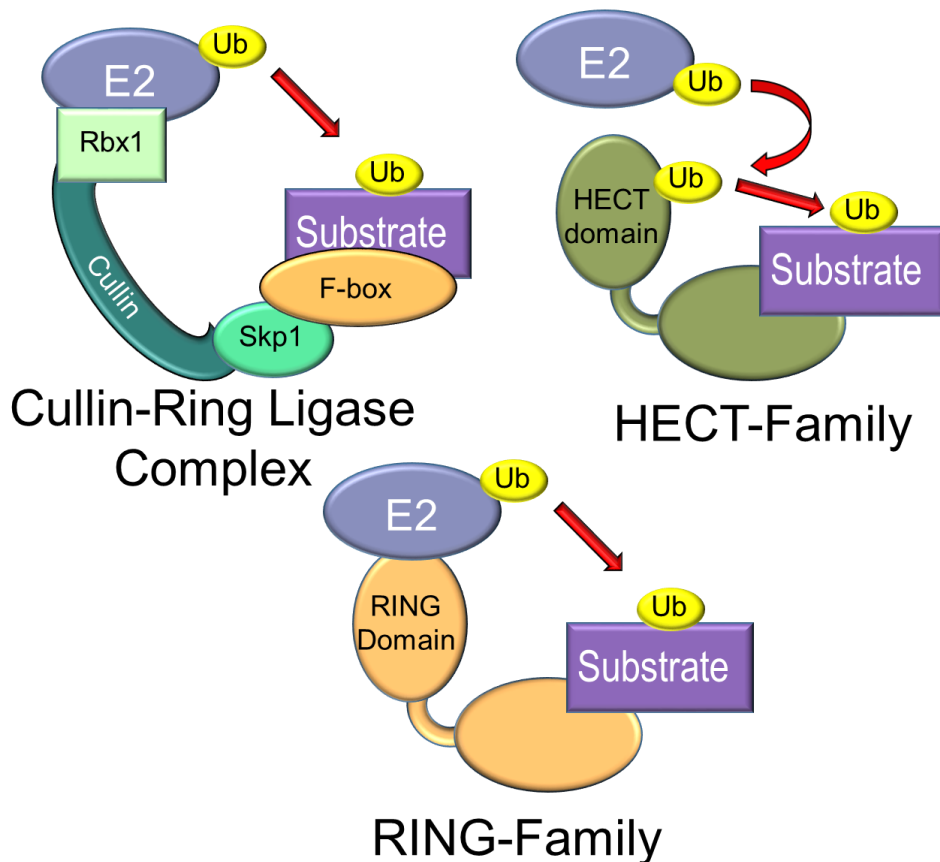
Figure 2 Ubiquitin E3 ligase Sub-Families

Schematic of different Ubiquitin E3 ligase sub-families and diagrams of their mechanisms of action for ubiquitination and substrate engagement. RING and Cullin-RING E3 ligase complexes rely on E2 ubiquitin conjugating enzymes to faciliate substrate ubiquitiantion, while HECT E3 ligases have instrinsic ligase activity to directly ubiqutinate substrate proteins.

1.2.3.1 Ubiquitin E3 Ligases in disease

Dysfunction of E3 ligases lay at the heart of many diseases, as aberrant E3 ligase activity disrupts substrate homeostasis. The RING E3 ligase Mdm2 is a classic example of E3 ligase dysfunction in disease. Mdm2 is a RING-family E3 ligase and has been described to negatively regulate the ubiquitination and stability of the tumor suppressor p53 (124). Genetic mutations or amplification of Mdm2 has been described in numerous oncological cases, as Mdm2 hyperactivity leads to reduced p53, and increased tumorigenesis (124-126). Indeed, Mdm2 has been the target for therapeutic development to combat cancer, with inhibitors and antagonists such as Nutlin-series

compounds undergoing clinical trials (124, 127, 128). The genes BReast-CAncer susceptibility gene (BRCA) 1 and 2, encode proteins with RING-domains and ubiquitin E3 ligase activity. Research suggests BRCA1/2 function in DNA damage repair; disease-associated mutations impair their activity, thus leading to increased risk of cancer. (129) (130). Clinical studies have shown that mutations in BRCA1/2 confer around 70% cumulative risk for breast cancer and reduced but significant risk for ovarian cancer (131). BRCA1/2 mutations are of such clinical risk that prophylactic risk-reducing mastectomy has become an increasingly used therapy; evaluations of its efficacy are ongoing (132). The ligase Parkin, belonging to the smaller RING-between-RING E3 ligase family, is named for its associations with Parkinson's' Disease. Mutations with Parkin have been associated with hereditary early onset Parkinson's Disease (133). Subsequent mechanistic research has uncovered that Parkin plays a critical role in the selective autophagy of mitochondria, termed mitophagy (134). During mitophagy, Parkin is recruited to the outer-mitochondrial membrane of damaged mitochondria and catalyzes the ubiquitination of numerous surface proteins. These ubiquitinated proteins signal the autophagy machinery to initiate mitophagy of the damaged mitochondria (135). The Von Hippel–Lindau tumor suppressor gene (VHL) encodes the VHL ubiquitin ligase that functions as part of the cullin-2-ring ligase complex (CRL2) (136). The VHL-CRL2 complex mediates the ubiquitination and degradation of Hypoxia-Inducible Factor (HIF) proteins, with numerous downstream consequences in oxygen sensing, tumorigenesis, and innate immune activation, including in the lung (137-139) . VHL was originally uncovered as a genetic determinant for the rare neurological disease, Von Hippel-Laud disorder; nicely reviewed by Gossage et al. (140). These observations demonstrate the ubiquitin e3 ligases are both causal and potentially targetable in human diseases. From this, we hypothesize that additional substrate-E3 ligase interactions are yet to be uncovered in lung diseases.

1.3 Specific Aims

Increasingly, research has shown that Ubiquitin E3 ligases are biologically relevant in lung diseases. Concomitantly, there is un-tapped therapeutic potential in the selective targeting and inhibition of specific disease related E3 ligases to ameliorate lung diseases. These dissertation studies have focused on novel ubiquitin E3 ligase-substrate interactions and their effects on downstream signaling pathways with the goal of understanding if 1.) ubiquitin E3 ligases-substrate interactions biologically important for lung diseases, and 2.) Can we target E3 ligase for inhibition and therapeutically intervene in lung disease?

To test these concepts, we approached in three specific aims, which have resulted in peer-reviewed publications:

Aim 1: To determine the role of Ubiquitin E3 ligases in regulating lung fibrosis mechanisms

Sub-aim 1.1: Ubiquitin E3 Ligase FIEL1 Regulates Fibrotic Lung Injury through SUMO-E3 Ligase PIAS4

Sub-aim 1.2: Kelch-like Protein 42 is a Pro-Fibrotic Ubiquitin E3 Ligase in Systemic Sclerosis

Aim 2: Innate immunity and inflammatory signaling can be manipulated by E3 ligase targeting

Sub-aim 2.1: RING Finger E3 Ligase PPP1R11 Regulates TLR2 Signaling and Innate Immunity

Sub-aim 2.2: 3.2 KIAA0317 Regulates Pulmonary Inflammation Through SOCS2 Degradation

Sub-aim 2.3: The RNFT2/IL-3Rα axis regulates IL-3 signaling and innate immunity

Sub-aim 2.4: RNF113A Regulates CXCR4 stability and signaling

Aim 3: Nutrient sensing mechanisms are controlled by E3 ligase-mediated ubiquitination

Sub-aim 3.1: The RING-type E3 ligase RNF186 ubiquitinates Sestrin-2 and thereby controls nutrient sensing

These studies utilized both candidate-based and unbiased methods to determine biologically relevant substrates. E3 ligases for specific substrates were determined through narrow, targeted screens, or larger high-throughput RNAi-based screens. Finally, the biologic effects of the E3 ligase-substrate axis were investigated in biochemical, molecular, cellular, animal and translational manners.

2.0 Ubiquitination in Fibrosis

In our first aim, we investigated the role of ubiquitin e3 ligases in fibrosis through their targeted degradation of anti-fibrotic proteins. This research focused on mediators of the TGFβ signaling pathway in idiopathic pulmonary fibrosis, and in the lung manifestation of systemic sclerosis. These studies also investigated the therapeutic potential in designing inhibitors of Ubiquitin E3 ligase activity to prevent degradation of anti-fibrotic substrates, and to intervene in fibrotic signaling and disease.

2.1 Ubiquitin E3 Ligase FIEL1 Regulates Fibrotic Lung Injury through SUMO-E3 Ligase PIAS4

2.1.1 Study Overview

The E3 SUMO-protein ligase PIAS4 is a pivotal protein in regulating the TGFβ pathway. Here we discovered a new protein isoform encoded by *KIAA0317*, termed FIEL1 (Fibrosis Inducing E3 Ligase 1), which potently stimulates the TGFβ signaling pathway through the site-specific ubiquitination of PIAS4. FIEL1 targets PIAS4 using a "double locking" mechanism which

is facilitated by the kinases PKCζ and GSK3β. Specifically, PKCζ phosphorylation of PIAS4 and GSK3β phosphorylation of FIEL1 are both essential for the degradation of PIAS4. FIEL1 protein is highly expressed in lung tissues from patients with Idiopathic Pulmonary Fibrosis (IPF), whereas PIAS4 protein levels are significantly reduced. FIEL1 overexpression significantly increases fibrosis in bleomycin murine model, while FIEL1 knockdown attenuates fibrotic conditions. Further, we developed a first-in-class small molecule inhibitor towards FIEL1 that is highly effective in ameliorating fibrosis in mice. This study provides a basis for IPF therapeutic intervention by modulating PIAS4 protein abundance.

2.1.2 Introduction

Idiopathic Pulmonary Fibrosis (IPF) is a fibrotic disease of unknown etiology, but it is characterized by deposition of extracellular matrix into the interstitium and destruction of alveolar architecture resulting in progressive impairment in gas exchange and ultimately death (142-145). IPF is the most common form of interstitial lung disease with a prevalence of 50 per 100,000 cases, and it almost exclusively affects patients older than 50 (146). Despite its unknown etiology, the downstream effectors of IPF are well-characterized. Samples from IPF patients show increased levels of transforming growth factor beta (TGFβ) across all three isoforms (147). TGFβ promotes several IPF-relevant phenotypes: the differentiation of fibroblasts to myofibroblasts, the activation of epithelial to mesenchymal transition, and the promotion of lung epithelial cell apoptosis (148-151). TGFβ transduces downstream signaling in part through the mothers against decapentaplegic homolog (SMAD) protein family. SMAD proteins regulate a variety of cellular processes, such as differentiation, proliferation, tumorigenesis, and immune responses (152-154). The SMAD family is comprised of receptor-SMADs (R-SMAD), inhibitor SMADs (I-SMAD), and the common

mediator SMAD (co-SMAD) (155). TGFβ signal transduction commences with the phosphorylation of R-SMADs, often SMAD2 or SMAD3, which form a trimeric structure with the co-SMAD, SMAD4, and translocate to the nucleus. In the nucleus, the trimer binds to the SMAD binding element (SBE) in the JunB promoter to activate the transcription of pro-fibrotic genes (156). Therefore, TGFβ is a major pro-fibrotic growth factor through the downstream SMAD signaling pathway (157, 158).

2.1.2.1 PIAS proteins and SMAD signaling

PIAS (protein inhibitor of activated STAT) proteins are a family of proteins that are known to negatively control and regulate gene transcription and inflammatory pathways in cells (159). There are four characterized PIAS family members, PIAS1, PIASx (PIAS2), PIAS3, and PIASy (PIAS4), each with specificity toward different pathways (160). Specifically, PIAS4 has been shown to suppress TGFβ signaling by several mechanisms (23, 161). First, TGFβ promotes the interaction of PIAS4 with SMAD3 and SMAD4 to form a ternary complex (161). PIAS4 is known to possess small ubiquitin-like modifier (SUMO) E3 ligase activity within its RING-type domain (162). It promotes the sumoylation of SMAD3, in turn stimulating its nuclear export and inhibiting SMAD3/4-driven pro-fibrotic transcription (22, 163). Furthermore, PIAS4 directly recruits and interacts with histone deacetylase 1 (HDAC1) to repress SMAD3-driven transcriptional activation (161). In all, PIAS4 is an important negative regulator of TGFβ signaling.

In this study, we discovered a new protein isoform encoded by *KIAA0317*, termed FIEL1 (Fibrosis Inducing E3 Ligase 1). We also revealed a new molecular pathway in which FIEL1 regulates TGFβ signaling through the ubiquitin-mediated degradation of PIAS4. Under TGFβ stimulation, two kinases, PKCζ and GSK3β, phosphorylate PIAS4 and FIEL1 respectively. Phosphorylated FIEL1 targets phosphorylated PIAS4 and mediates its ubiquitination and

degradation, thereby exaggerating TGFβ signaling. These studies provide a new molecular model of fibrotic lung injury and lead to the development of a small molecule antagonist that exerts potent anti-fibrotic activity by regulating the abundance of PIAS4.

2.1.3 FIEL1-PIAS4 pathway in pulmonary fibrosis

PIAS4 degradation occurs in a ubiquitin-dependent manner through the proteasome (Figure 3A-B). We next screened our E3 ligase library and determined that the HECT domain E3 ligase KIAA0317 regulates PIAS4 protein stability (data not shown). *KIAA0317* encodes two major isoforms, of lengths 823 and 789 residues. The longer isoform has been previously characterized as AREL1 and contains an additional 34 residues in the C-terminal HECT-domain (164). However, we found that the shorter isoform (789 residues, termed FIEL1, Fibrosis Inducing E3 Ligase 1) behaves distinctly in cells. First, only FIEL1 overexpression significantly decreased PIAS4 protein levels (Figure 3C). Compared to AREL1, solely FIEL1 interacted with PIAS4 protein via co-immunoprecipitation (Figure 3D). Moreover, overexpressed FIEL1 in murine lung epithelial (MLE), HeLa, and 293T cells co-migrated with the endogenous protein upon FIEL1 immunoblotting, which suggested that FIEL1 is the predominant *KIAA0317* isoform in all of these cell lines (data not shown). FIEL1 is sufficient for PIAS4 ubiquitination *in vitro* (Figure 3E). FIEL1 expression selectively decreased PIAS4, compared to other PIAS family members in MLE cells (Figure 3F). A randomly selected HECT E3 ligase, UBE3B, was also tested as a negative control (Figure 3F). FIEL1 expression in HeLa and 293T cells also decreased PIAS4 protein levels (data not shown). Conditional expression of FIEL1 in MLE cells using a doxycycline-inducible plasmid resulted in PIAS4 protein degradation (data not shown). Further, FIEL1 expression significantly decreased PIAS4 protein levels, whereas FIEL1 knockdown using shRNA stabilized

PIAS4 by extending its half-life (Figure 3G-H). FIEL1 also regulates PIAS4 protein levels in human fetal lung primary fibroblast MRC5 cells. As shown in Figure 3I and J, expression of FIEL1 reduced PIAS4 protein levels in a dose dependent manner, whereas other proteins such as TGFβR1, TGFβR2, SMURF1, and SMAD7 levels were unchanged. Moreover, FIEL1 expression did not reduce PIAS4 mRNA levels (Figure 3K). TGFβ treatment increased FIEL1 protein and decreased PIAS4 protein in MRC5 cells while also increased the association of PIAS4 and FIEL1 (Figure 3L). Last, TGFβ treatment drastically increased FIEL1 mRNA levels (data not shown). We also determined that K31 is the ubiquitin acceptor site within PIAS4 (Figure 4A-C). We measured FIEL1 and PIAS4 protein levels in lung tissues from five control subjects and five subjects with IPF. Subjects with IPF had significantly less PIAS4 protein and more immunoreactive FIEL1 protein in their lungs versus control subjects (Figure 3M). We also tested this pathway in bleomycin-induced murine lung fibrosis (165, 166). Bleomycin challenge significantly increased FIEL1 protein level and decreased PIAS4 protein level in mice lungs with a maximum effect at day 14 (Figure 3N). These results suggest that the FIEL1-PIAS4 pathway is functional and important in individuals with IPF.
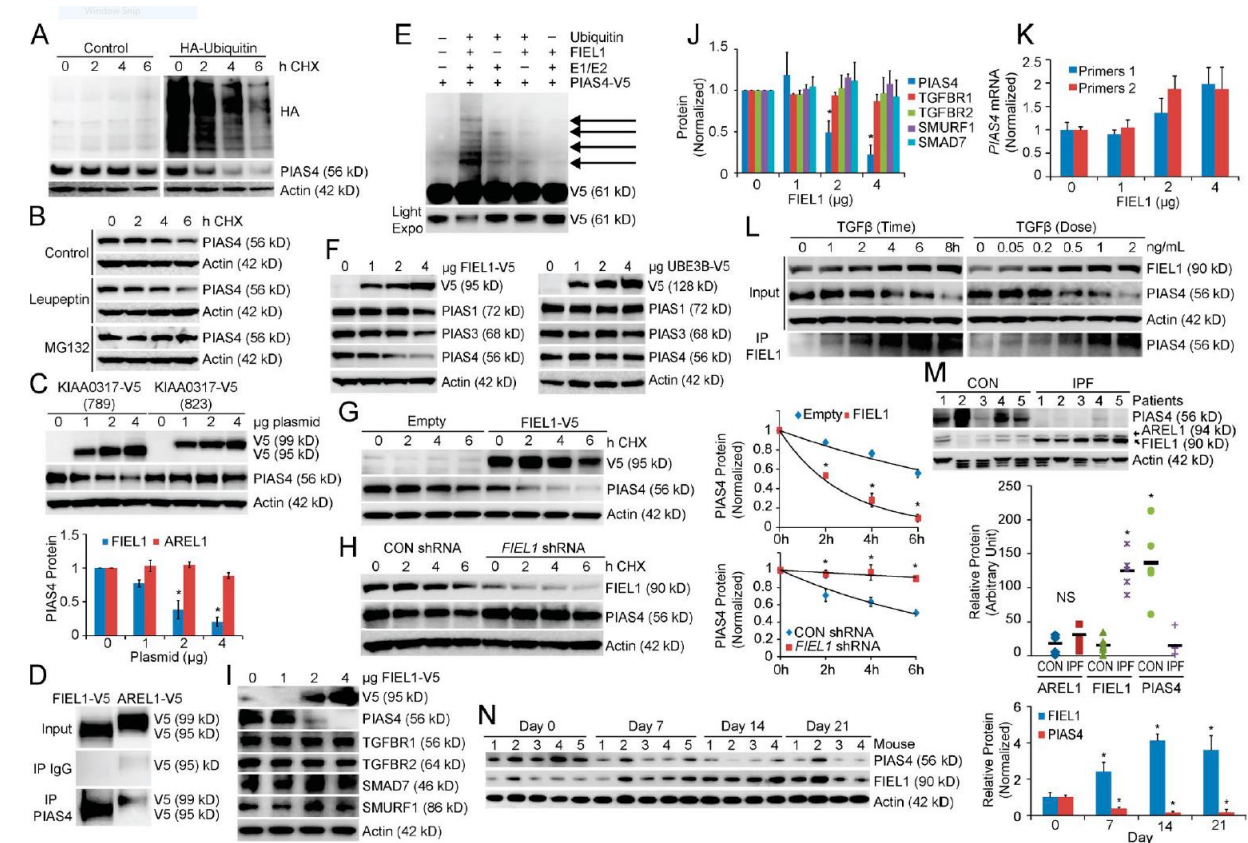
Figure 3 FIEL1–PIAS4 pathway in pulmonary fibrosis

(A) PIAS4 protein half-life determination in MLE cells transfected with empty plasmid or ubiquitin plasmid (n = 2). (B) PIAS4 protein half-life determination with MG132 or leupeptin treatment (n = 3). (C) Immunoblots (top) showing levels of PIAS4 protein and V5 after KIAA0317 (823 aa, AREL1) and (789 aa, FIEL1) plasmid expression. PIAS4 protein quantification was normalized and graphed (bottom). Data represent mean values ± SEM (n = 3 independent experiments; *, P < 0.05 compared with 0 µg plasmid, Student's t test). (D) PIAS4 protein was immunoprecipitated from cell lysate using a PIAS4 antibody and coupled to protein A/G beads. PIAS4 beads were then incubated with in vitro–synthesized products expressing HIS-V5-FIEL1 (789 aa) or HIS-V5-AREL1 (823 aa). After washing, proteins were eluted and processed for V5 immunoblotting (n = 2). (E) In vitro ubiquitination assay. Purified E1 and E2 components were incubated with V5-PIAS4 and FIEL1. The full complement of ubiquitination reaction components (second lane) showed polyubiquitinated PIAS4 proteins (n = 3). (F) Immunoblots showing levels of PIAS proteins and V5 after ectopic FIEL1 or UBE3B expression. (G and H) PIAS4protein half-life determination in MLE cells with empty plasmid or FIEL1 expression (G); PIAS4 protein half-life determination with CON shRNA or FIEL1 shRNA expression (H). Data represent mean values ± SEM (n = 3 independent experiments; *, P < 0.05 compared with Empty or to Control, Student's t test). (I–J) Immunoblots (I) showing levels of PIAS4, TGFBR1, TGFBR2, SMAD7, Smurf1, and V5 after FIEL1 expression. Protein quantification was graphed (J). Data represent mean values ± SEM (n = 3 independent experiments; *, P < 0.05 compared with 0 µg FIEL1, Student's t test). (K) mRNA levels of PIAS4 upon FIEL1 expression was measured using two sets of PIAS4 RT-PCR primers. Data represent mean values ± SEM (n = 3 independent experiments). (L) MRC5 cells were treated with TGFβ in a time- or dose-dependent manner; cells were collected and immunoblotted for FIEL1 and PIAS4. Endogenous FIEL1 was also immunoprecipitated and immunoblotted for PIAS4 (n = 3). (M) PIAS4 and FIEL1 immunoblotting from lung tissues samples from five control and five IPF patients. PIAS4 and both the shorter and longer forms of KIAA0317 were quantified using ImageJ and graphed. Data represent mean values (n = 5 patients; NS, not significant *, P < 0.05 compared with CON, Student's t test). (N) C57BL/6J mice were treated i.t. with bleomycin (0.02 U) for up to 21 d. Mice were then euthanized, and lungs were isolated and assayed for PIAS4 and FIEL1 immunoblotting. Bands corresponding to each protein on

23

immunoblots were quantified using ImageJ software, and the results are displayed graphically. Data represent mean values ± SEM (n = 4–5 mice per group; *, P < 0.05 compared with day 0, Student's t test).
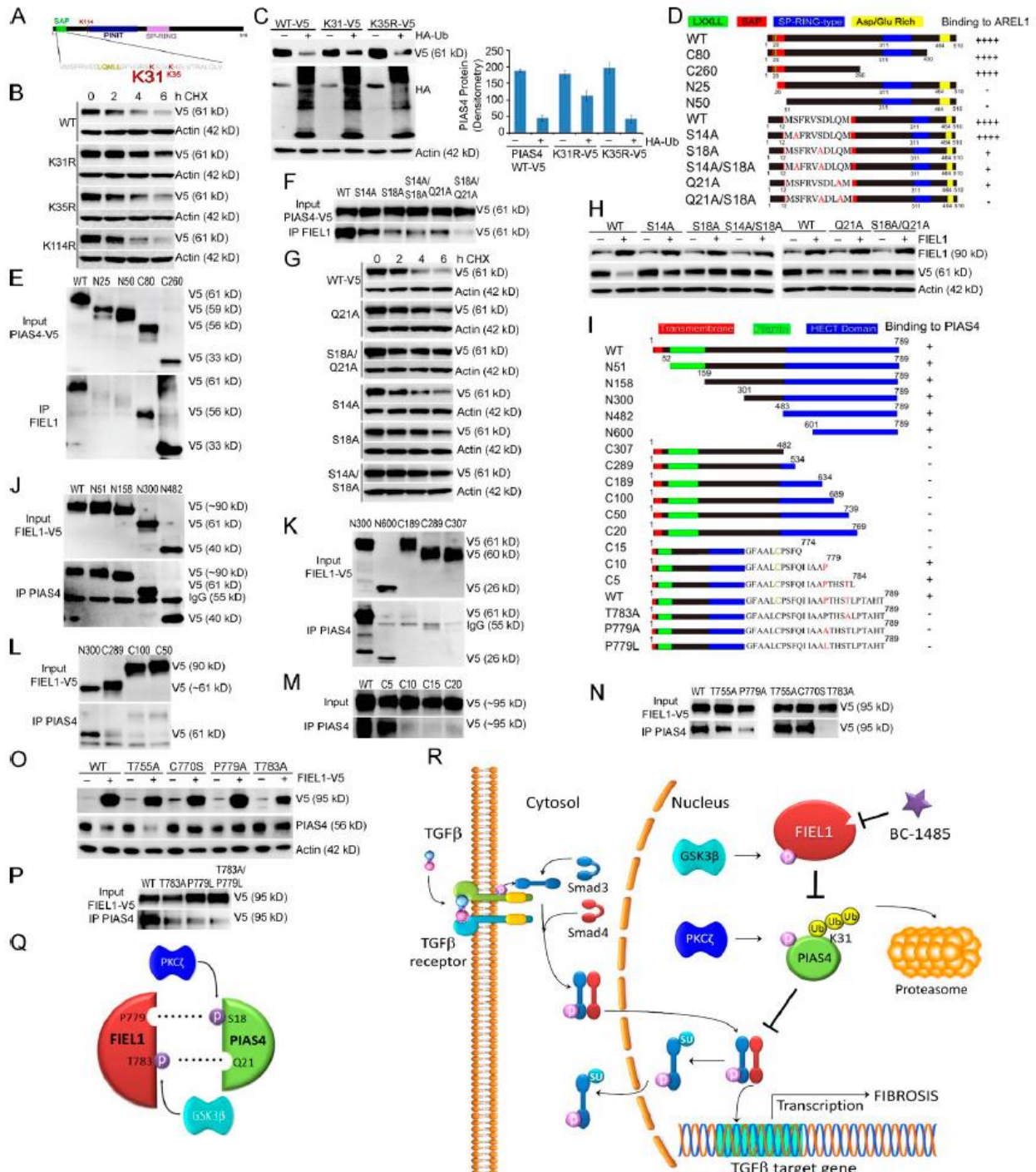
Figure 4 Mapping Study of FIEL1 and PIAS4 interaction

A. Several point mutants of PIAS4 were designed and cloned into a pcDNA3.1D/V5-HIS vector. B. Half-life study of WT, K31R, K35R, and K114R PIAS4 in MLE cells. C. MLE cells were co-transfected with WT or PIAS4 lysine

mutants with or without HA-Ubiquitin. Cells were then collected and immunoblotted. PIAS4 protein levels were quantified and graphed. Data represent mean values ± SEM (n=3 independent experiments; NS, not significant, *, p<0.05 compared to without HA-Ubiquitin, Student's t-test). D. Several deletional mutants of PIAS4 were designed and cloned into a pcDNA3.1D/V5-HIS vector. E-F. FIEL1 protein was immunoprecipitated from cell lysates using a FIEL1 antibody and coupled to protein A/G beads. FIEL1 beads were then incubated with in vitro synthesized products expressing HIS-V5-PIAS4 mutants. After washing, proteins were eluted and processed for V5-PIAS4 immunoblotting. G. Half-life study of WT, Q21A, S14A, S18A, S18A/Q21A, and S14A/S18A PIAS4 in MLE cells. H. MLE cells were co-transfected with WT or PIAS4 mutants with or without FIEL1. Cells were then collected and immunoblotted. I. Several deletional mutants of FIEL1 were designed and cloned into a pcDNA3.1D/V5-HIS vector. J-N, P. PIAS4 protein was immunoprecipitated from cell lysate using a PIAS4 antibody and coupled to protein A/G beads. PIAS4 beads were then incubated with in vitro synthesized products expressing HIS-V5-FIEL1 mutants. After washing, proteins were eluted and processed for V5-FIEL1 immunoblotting. O. MLE cells were transfected with WT or FIEL1 mutants. Cells were then collected and immunoblotted for PIAS4 protein. Q. The cartoon illustrates the "double locking" molecular interplay between PIAS4 and FIEL1. Specifically, both the P779 and GSK3β phosphorylated T783 residues within FIEL1 are required for PIAS4 binding; both the Q21 and PKCζ phosphorylated S18 residues within PIAS4 are required for FIEL1 binding. R. PIAS4 suppresses the TGFβ pathway, in part, by sumoylating SMAD3 and causing SMAD3 nuclear exportation. FIEL1 serves as a bona-fide E3 ligase and triggers the site-directed ubiquitination of PIAS4. TGFβ hijacks FIEL1 protein to ubiquitinate PIAS4 and promote fibrosis. PKCζ phosphorylates PIAS4 and regulates its stability. Moreover, GSK3β serves as another regulator of PIAS4 protein stability through the phosphorylation of FIEL1. A small-molecule FIEL1 inhibitor, BC-1485, lowers tissue fibrosis by antagonizing the actions of FIEL1 on PIAS4-TGFβ signaling.

2.1.4 FIEL1 promotes TGFβ signaling

Using a SMAD reporter assay (Qiagen), we determined that FIEL1 overexpression increased SMAD promoter driven luciferase activity upon TGFβ stimulation (Figure 5A). By decreasing PIAS4 protein, expression of FIEL1 also decreased SMAD3 sumoylation (Figure 5B) as previously described (22, 163) and further promoted SMAD3 nuclear concentration (Figure 5C). FIEL1 ectopic expression did not change SMAD3 phosphorylation. FIEL1 expression increased the expression of fibrotic proteins Fibronectin (FN) and alpha smooth muscle actin (α-SMA) in MRC5 cells (Figure 5 FIEL1 promotes TGFβ signalingFigure 5D). When we knock down FIEL1 using several shRNAs, we observed a significantly reduced SMAD driven luciferase activity, with shRNA 3 serving as a negative control (Figure 5E). FIEL1 knockdown increased PIAS4 protein, increased SMAD3 sumoylation (Figure 5F), and further decreased SMAD3 nuclear concentration (Figure 5G). FIEL1 knockdown also decreased the expression of fibrotic proteins Fibronectin (FN) and alpha smooth muscle actin (α-SMA) in MRC5 cells (Figure 5H). To

complement the biochemistry approach, we also performed immunostaining on MRC5 cells, and we observed that FIEL1 knockdown also reduced nuclear localization of SMAD3 upon TGFβ treatment (Figure 5I).
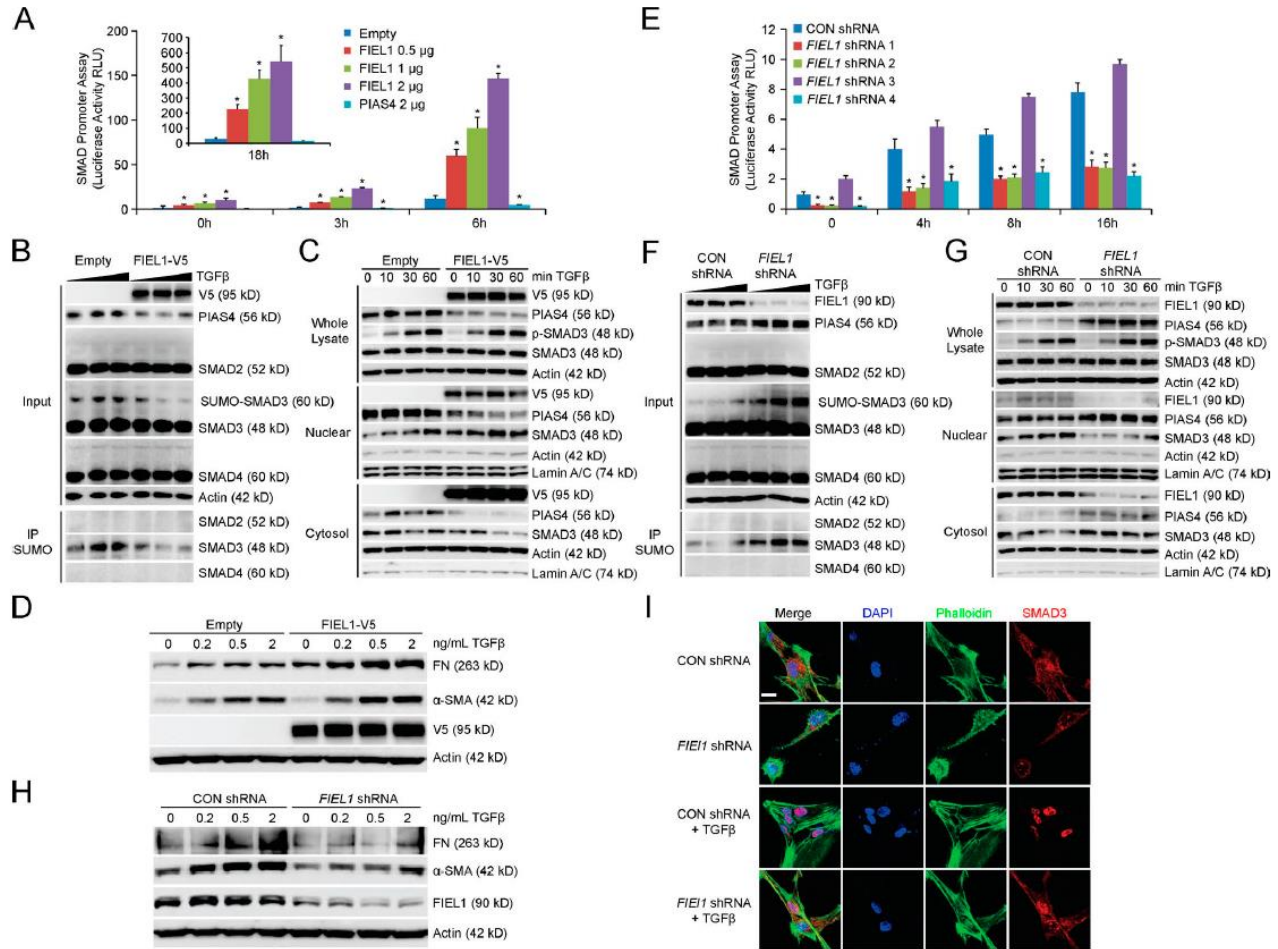
Figure 5 FIEL1 promotes TGFβ signaling

(A and E) SMAD reporter assays. 293T cells were cotransfected with Cignal SMAD dual luciferase reporter plasmids along with empty, FIEL1, Con shRNA, or FIEL1 shRNA. 24 h later, cells were treated with TGFβ for 2–16 h. Cells were collected and assayed for luciferase activity to evaluate SMAD promoter activity. Data represent mean values ± SEM (n = 3; *, P < 0.05 compared with empty, Student's t test). (B and F) 293T cells were transfected with empty, FIEL1, CON shRNA, or FIEL1 shRNA for 48 h before TGFβ treatment (0–2 ng/ml) for 1 h. Cells were then collected and immunoblotted. Cell lysates were immunoprecipitated using SUMO antibody before SMAD2, 3, and 4 immunoblotting (n = 2). (C and G) 293T cells were transfected with empty, FIEL1, CON shRNA, or FIEL1 shRNA for 48 h before TGFβ treatment (2 ng/ml) for up to 1 h. Cells were then collected and nuclear/ cytosol fractions were isolated prior to immunoblotting. (D and H) MRC5 cells were transfected with empty, FIEL1, CON shRNA, or FIEL1 shRNA for 48 h before TGFβ dose course treatment for an additional 18 h. Cells were then collected and immunoblotted (n = 2). (I) MRC5 cells were seeded in 35-mm glass bottom dishes before being transfected with CON shRNA or FIEL1 shRNA for 48 h before TGFβ treatment for an additional 30 min. Cells were then fixed and immunostained with α-SMAD3.The nucleus was counterstained with DAPI and F-actin was counterstained with phalloidin (n = 3). Bar, 10 μm.

2.1.5 PIAS4 phosphorylation by PKCζ is required for FIEL1 binding

We next investigated the FIEL1 binding site within PIAS4. We determined that PIAS4 S18 and Q21 are both important for FIEL1 interaction (Figure 4D-F). We performed a kinase screen and determined that PKCζ interacts with PIAS4 via Co-IP (Figure 6A). PKCζ expression also decreased PIAS4 protein level, whereas JNK1 expression was unable to achieve such an effect (Figure 6B). Moreover, PKCζ knockdown using shRNA drastically stabilized PIAS4 protein in a $t_{1/2}$ study (Figure 6C), whereas PKCζ expression decreased PIAS4 $t_{1/2}$ to about 2h (Figure 6D). TGFβ stimulation also drastically increased PIAS4 serine phosphorylation and PKCζ association, but not PKCα association (Figure 6E-F). PKCζ directly phosphorylated PIAS4 in a kinase assay (Figure 6G). PKCζ knockdown also protected PIAS4 from phosphorylation and degradation during TGFβ treatment (Figure 6H). Compared to WT PIAS4, S18A and S14/S18A double mutant exhibited a dramatic decrease in phosphorylation and offered resistance to degradation during TGFβ treatment (Figure 6I). PIAS4 S18A, Q21A, and S18/Q21A double mutants also exhibited much longer half-lives (Figure 4G) and resisted degradation from FIEL1 co-expression (Figure 4H). Last, we performed a peptide binding experiment (Figure 6J). The peptide with S18 phosphorylation (P2) showed the strongest binding to FIEL1; the peptide with both S18 phosphorylation and Q21 mutation (P3) offered drastically decreased FIEL1 interaction. These experiments suggested that PKCζ is an authentic regulator of PIAS4 protein stability; Q21 and phosphorylated S18 of PIAS4 are both required for FIEL1 interaction.
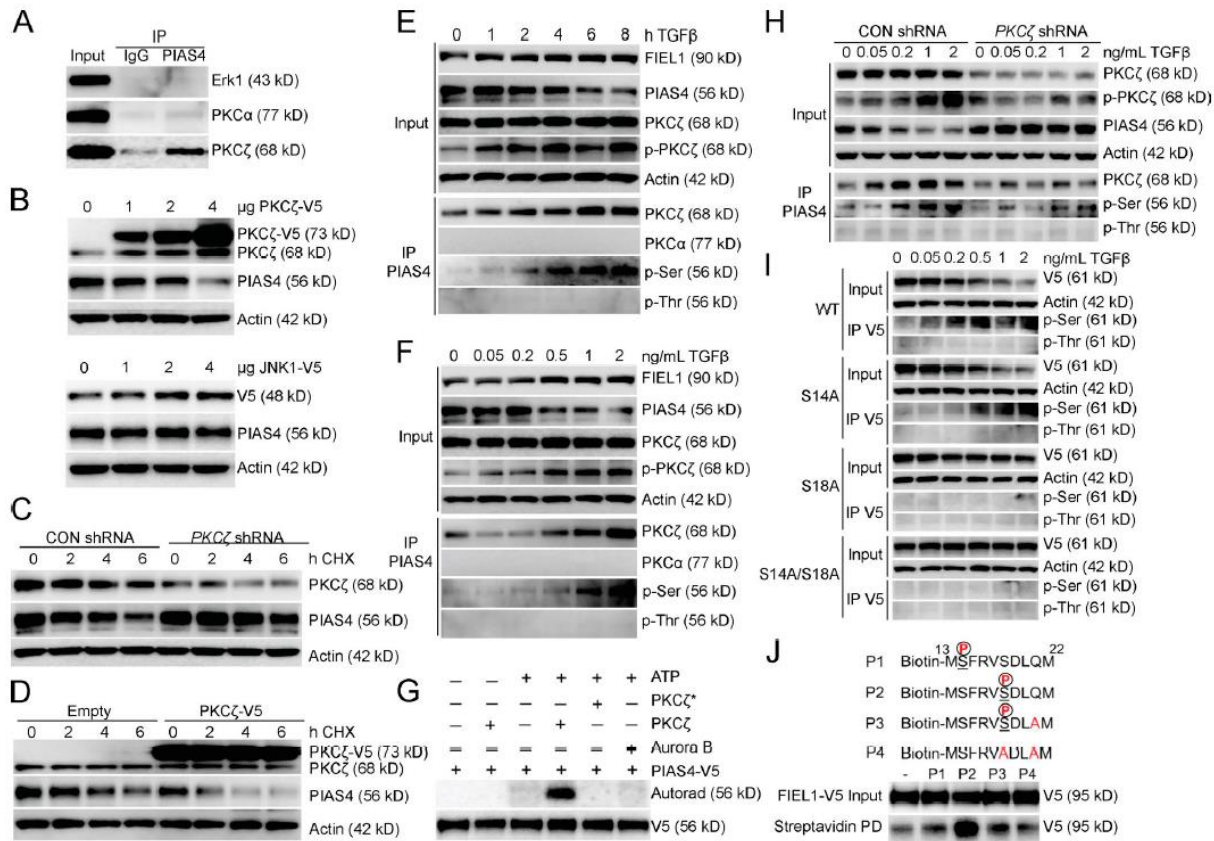
Figure 6 PIAS4 phosphorylation by PKCζ is required for FIEL1 binding

(A) Endogenous PIAS4 was immunoprecipitated and immunoblotted for Erk1, PKCα, and PKCζ (n = 2). (B) MLE cells were transfected with increasing amounts of PKCζ or JNK1 plasmids for 18 h before PIAS4 immunoblotting (n = 2). (C) PIAS4 protein half-life determination with CON shRNA or PKCζ shRNA expression (n = 3). (D) PIAS4 protein half-life determination with Empty or PKCζ plasmid overexpression (n = 3). (E and F) MRC5 cells were treated with TGFβ in a time or dose-dependent manner; cells were collected and immunoblotted for FIEL1, PIAS4, PKCζ, and p-PKCζ (Thr410). Endogenous PIAS4 was also immunoprecipitated and followed by PKCζ, PKCα, phosphoserine, and phosphothreonine immunoblotting (n = 2). (G) In vitro PKCζ kinase assay. Recombinant PKCζ (Enzo) was used as the kinase, and V5-tagged PIAS4 was synthesized via TnT in vitro kits (Promega), purified by HIS pulldown, and used as the substrate. The kinase reactions were incubated at 37°C for 2 h, and products were resolved by SDS-PAGE and processed for autoradiography either by using Personal Molecular Imager (Bio-Rad Laboratories) or immunoblotting for V5 to visualize the substrate input. *, heat inactivated PKCζ (n = 2). (H) Immunoblots showing levels of FIEL1, PKCζ, p-PKCζ (Thr410), and PIAS4 protein in 293T cells transfected with either CON shRNA or PKCζ shRNA, followed by a TGFβ dose treatment. Endogenous PIAS4 was also immunoprecipitated and followed by PKCζ, phosphoserine, and phosphothreonine immunoblotting. (I) 293T cells were transfected with WT, S14A, S18A, or S14/18A PIAS4 before being treated with a dose course of TGFβ. Cells were then collected and assayed for V5-PIAS4 immunoblotting. Overexpressed V5-PIAS4 was also immunoprecipitated using a V5 antibody and followed by phosphoserine immunoblotting (n = 2). (J) Four biotin-labeled PIAS4 peptides were bound to streptavidin and served as the bait for FIEL1 binding. After washing, proteins were eluted and immunoblotted for FIEL1-V5 (n = 2).

28

2.1.6 GSK3β phosphorylation of FIEL1 is required for PIAS4 targeting

We next investigated the PIAS4 binding site within FIEL1. A mapping study was conducted similarly to Figure 4D and we determined that both P779 and T783 are important for PIAS4 interaction (Figure 4I-N). Compared with WT FIEL1, neither P779A nor T783A mutant expression decreased PIAS4 protein levels (Figure 4O). We also determined that C770 is a potential active site of FIEL1 as the C770S mutant also failed to decrease PIAS4 protein level (Figure 4O). SNP database analysis indicated a naturally occurring polymorphism (rs371610162) within FIEL1 (P779L). We further tested this mutation in a binding assay and showed that T783A, P779L, and P779L/T783A double mutants all lost interaction with PIAS4 (Figure 4P). We performed a kinase screen and determined that GSK3β interacts with FIEL1 via Co-IP (Figure 7A). WT GSK3β overexpression decreased PIAS4 protein levels in a dose dependent manner, and PIAS4 protein levels decreased more dramatically when we transfected cells with a constitutively activated GSK3β hyper mutant plasmid (Figure 7B). Moreover, a CHX $t_{1/2}$ study suggested that WT GSK3β ectopic expression decreased PIAS4 $t_{1/2}$ to about 4h, whereas the more potent GSK3β hyper mutant further decreased PIAS4 $t_{1/2}$ to about 2 h (Figure 7C). TGFβ stimulation drastically increased FIEL1 threonine phosphorylation (Figure 7D), and GSK3β knockdown drastically stabilized PIAS4 in a $t_{1/2}$ study (Figure 7E). Moreover, GSK3β knockdown also prevented FIEL1 threonine phosphorylation and protected PIAS4 from degradation with TGFβ treatment (Figure 7F).

Using the lung lysates from Figure 3M, we performed a Co-IP experiment and observed a positive and significant association between PIAS4 and phospho-threonine signal, which suggested that FIEL1 threonine phosphorylation is essential for PIAS4 binding (Figure 7G). We

further studied the role of FIEL1 T783 in regulating PIAS4 protein stability. FIEL1 T783A mutant overexpression completely failed to decrease PIAS4 protein level. However, in phosphorylation mimic T783D mutant, FIEL1 expression decreased PIAS4 protein level more dramatically compared to WT FIEL1 expression (Figure 8A). Moreover, a $t_{1/2}$ study suggested that WT FIEL1 expression decreased PIAS4 $t_{1/2}$ to about 4h, whereas the more potent phosphorylation mimic T783D further decreased PIAS4 $t_{1/2}$ to about 2 h (Figure 8B). The FIEL1 T783A mutant was resistant to GSK3β phosphorylation *in vitro* (Figure 8C) and in cells (Figure 8D). We also performed a peptide binding experiment (Figure 8E). Peptide with phosphorylation at T783 (P2) showed the strongest binding to PIAS4; peptide with no phosphorylation (P1) or T783A mutant (P4) offered drastically decreased PIAS4 interaction. FIEL1 T783A and P779L expression both failed to decrease PIAS4 protein level (Figure 8F) or half-lives (Figure 8G). FIEL1 T783A/P779L double mutant expression showed a dominant negative phenotype by increasing PIAS4 protein levels (Figure 8F). We further used PIAS4 peptide 2 with S18 phosphorylation (Figure 6J) as bait and determined that both P779L and T783A FIEL1 drastically lost binding with PIAS4 (Figure 8H), which is similar to Figure 4P. Similarly, FIEL1 Peptide 2 with phosphorylation at T783 (P2) (Figure 8E) was used to reconfirm the importance of S18 phosphorylation and Q21 within PIAS4 for FIEL1 interaction (Figure 8I), which is similar to Figure 4F. Last, FIEL1 T783A/P779L dominant negative mutant overexpression protected PIAS4 from TGFβ treatment (Figure 8J). These experiments suggested that GSK3β phosphorylation of FIEL1 is required for PIAS4 targeting, and FIEL1 residues P779 and phosphorylated T783 are both required for PIAS4 interaction (Figure 4Q).
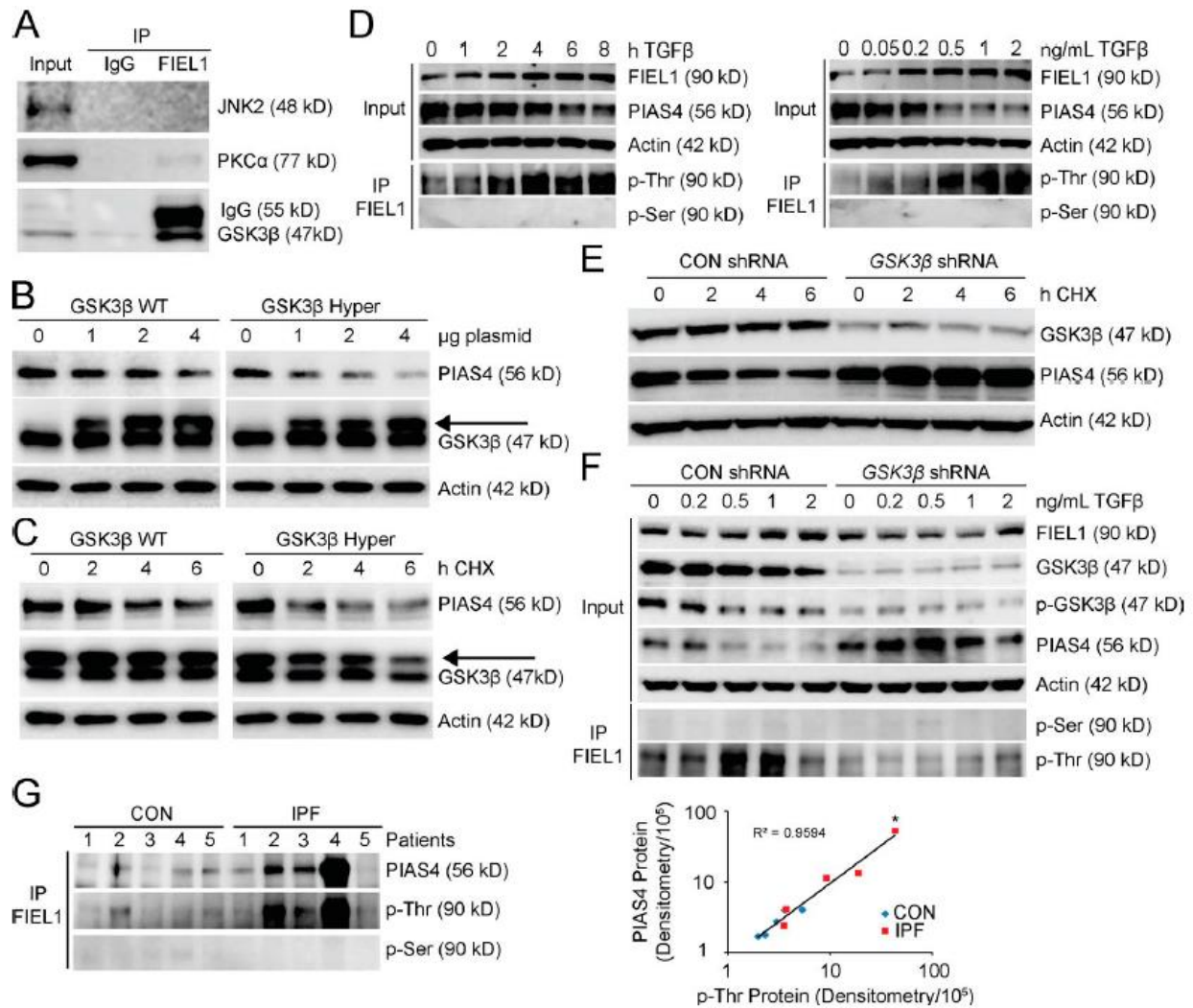
Figure 7 GSK3β regulates PIAS4 protein stability through FIEL1

(A) Endogenous FIEL1 was immunoprecipitated and followed by JNK2, PKCα, and GSK3β immunoblotting (n = 2). (B) MLE cells were transfected with increasing amounts of WT or constitutively activated GSK3β hyper mutant plasmids for 18 h before PIAS4 immunoblotting. The arrow indicates the overexpressed GSK3β (n = 2). (C) PIAS4 protein half-life determination with WT GSK3β or hyperactive GSK3β plasmid overexpression. The arrow indicates the overexpressed GSK3β (n = 2). (D) MRC5 cells were treated with TGFβ in a time or dose-dependent manner; cells were then collected and immunoblotted for FIEL1 and PIAS4. Endogenous FIEL1 was also immunoprecipitated and followed by phosphoserine and phosphothreonine immunoblotting (n = 2). (E) PIAS4 protein half-life determination with CON shRNA or GSK3β shRNA expression (n = 2). (F) Immunoblots showing levels of GSK3β, phospho-GSK3β (Ser9), PIAS4, and FIEL1 protein in 293T cells transfected with either CON shRNA or GSK3β shRNA followed by a TGFβ dose treatment. Endogenous FIEL1 was also immunoprecipitated, followed by phosphoserine and phosphothreonine immunoblotting. (G) Lung samples from Figure 3J were subjected to FIEL1 immunoprecipitation, followed by PIAS4, phosphothreonine, and phosphoserine immunoblotting. PIAS4 protein abundance was plotted as a function of p-Thr protein (n = 5 patients per group; *, P <0.01, Pearson correlation).
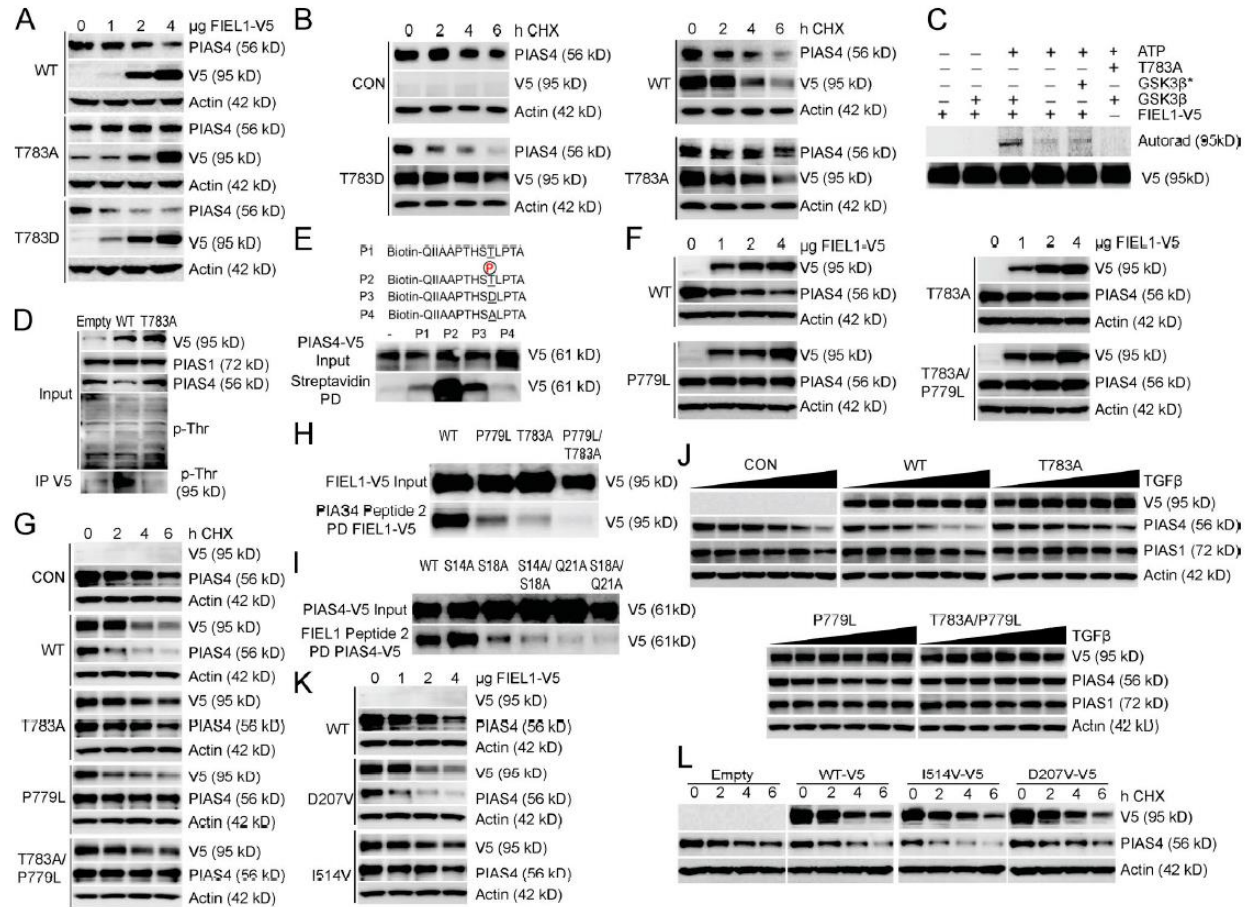
Figure 8 GSK3β phosphorylation of FIEL1 is required for PIAS4 targeting

(A) MLE cells were transfected with increasing amounts of WT, T783A, or T783D mutant FIEL1 plasmids for 18 h before PIAS4 immunoblotting (n = 2). (B) PIAS4 protein half-life determination with WT, T783A, or T783D mutant FIEL1 (n = 2). (C) In vitro GSK3β kinase assay. Recombinant GSK3β (Enzo) was used as the kinase, and V5-tagged FIEL1 were synthesized via TnT in vitro kits (Promega), purified by HIS pulldown, and used as the substrate. The kinase reactions were incubated at 37°C for 2 h, and products were resolved by SDS-PAGE and processed for autoradiography either by using Personal Molecular Imager (Bio-Rad Laboratories) or immunoblotting for V5 to visualize the substrate input. *heat inactivated GSK3β (n = 2). (D) 293T cells were transfected with empty, WT, or T783A FIEL1 for 24h. Cells were then collected and immunoblotted for V5-FIEL1 and PIAS4. Overexpressed V5-FIEL1 was also immunoprecipitated using V5 antibody and followed by phosphothreonine immunoblotting (n = 2). (E) Four biotin-labeled FIEL1 peptides were prebound to streptavidin and served as the bait for PIAS4 binding. After washing, proteins were eluted and processed for PIAS4 immunoblotting (n = 2). (F) MLE cells were transfected with increasing amounts of WT, T783A, P779L, or T783A/P779L double mutant FIEL1 plasmids for 18 h before PIAS4 immunoblotting. (G) PIAS4 protein half-life determination with WT, T783A, P779L, or T783A/P779L double mutant FIEL1 (n = 2). (H) PIAS4 peptide 2 (Biotin-MSF RVS(p)DLQM) was prebound to streptavidin and served as the bait for FIEL1 binding. After washing, proteins were eluted and processed for V5-FIEL1 immunoblotting (n = 2). (I) FIEL1 peptide 2 (Biotin-QII AAP THST(p)LPTA) was bound to streptavidin and served as the bait for PIAS4 binding. After washing, proteins were eluted and processed for V5-PIAS4 immunoblotting (n = 2). (J) 293T cells were transfected with WT, T783A, P779L, or T783A/P779L double mutant FIEL1 before being treated with TGFβ. Cells were then collected and assayed for PIAS4 immunoblotting. (K) MLE cells were transfected with increasing amounts of WT, I514V, or D207V mutant FIEL1 plasmids for 18 h before PIAS4 immunoblotting. (L) PIAS4 protein half-life determination with WT, I514V, or D207V mutant FIEL1 expression.

32

2.1.7 Gene transfer of FIEL1 exacerbates bleomycin induced lung injury in vivo

So far, our *in vitro* studies suggest that FIEL1 promotes TGFβ signaling *in vitro*. As exacerbated TGFβ signaling partakes in fibrotic formation, the results raise the possibility that expression of FIEL1 *in vivo* might alter host inflammatory responses and induce fibrotic lung injury. To extend the above observations *in vivo*, mice were infected with an empty lentivirus or lentivirus encoding FIEL1 for 144 h (10^7 cfu/mouse, intratracheally [i.t.]). Mice were then challenged with bleomycin (0.02U i.t.) for an additional 1-21 days (Figure 9A). Mice were euthanized to analyze parameters of fibrotic lung injury. Bleomycin injury is one of the most widely studied models of pulmonary fibrosis (18, 158, 165, 166). As shown in Figure 9B, the increased BAL total protein concentration that occurs after bleomycin injury in control mice was significantly higher in mice overexpressing FIEL1. Total inflammatory cells and Chemokine CXCL1 levels in BALs were also significantly increased in mice overexpressing FIEL1 (Figure 9C-D). Specifically, the differential cell counts of the BALs revealed that the total increase in inflammatory cells was mostly due to neutrophils and lymphocytes, with the exception of macrophages on day 7 (Figure 9E-G). FIEL1 expression in mice also significantly reduced survival (Figure 9H). Bleomycin challenge also showed changes consistent with peribronchiolar and parenchymal fibrosis in a time-dependent manner (Figure 9I-J). Elevated lung collagen deposition visualized by Masson Trichrome staining also suggested that FIEL1 expression exacerbates bleomycin-induced lung fibrosis (Figure 9J-K).We observed a marked increase in lung fibrosis in mice overexpressing FIEL1 as demonstrated by significantly increased hydroxyproline content (Figure 9L). The extent of these changes present in FIEL1 expression mice was substantially increased compared to the empty control (Figure 9I-L). Last, we analyzed FIEL1/PIAS4 protein

levels in murine lung samples and observed that lentiviral FIEL1 expression completely depleted

PIAS4 protein in the lung (Figure 9Figure 9M).
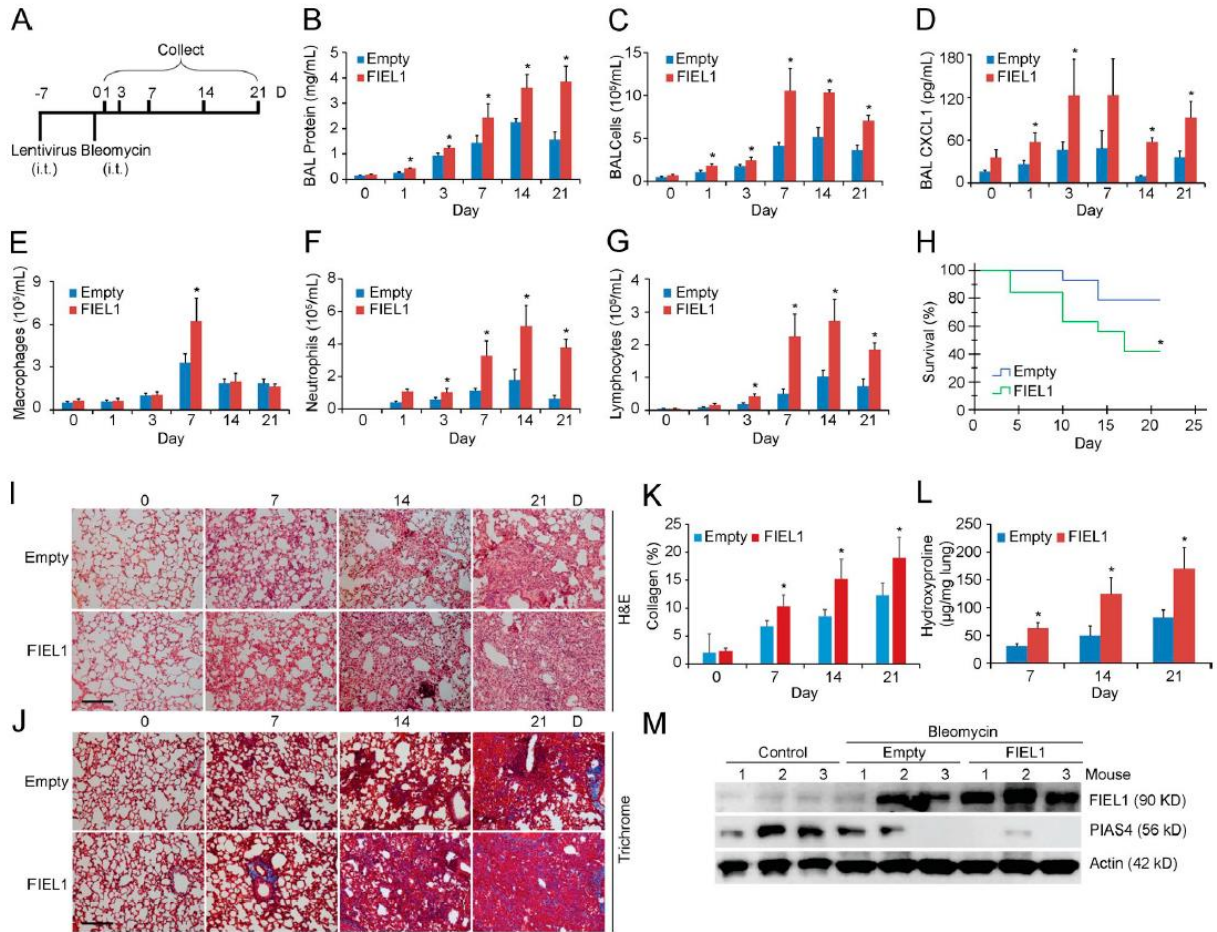
Figure 9 Gene transfer of FIEL1 exacerbates bleomycin-induced lung injury in vivo

(A)C57BL/6J mice weretreated i.t. with Lenti-Empty or Lenti-FIEL1 (107 PFU/mouse) for 144 h; mice were then treated i.t. with bleomycin (0.02 U). Mice were euthanized over the next 1–21 d, and lungs were lavaged with saline, harvested, and then homogenized. (B–D) Lavage protein, total cells, and CXCL1 concentrations were measured. Data represent mean values ± SEM (n = 4–6 mice per group, data are from one of the two experiments performed; *, P < 0.05 compared with empty, Student's t test). (E–G) Lavage cells were then processed for Wright-Giemsa stain; lavage macrophages, neutrophils, and lymphocytes were counted and graphed. Data represent mean values ±SEM (n = 4–6 mice per group, *, P < 0.05 compared with empty, Student's t test). (H) Survival studies of mice that were given bleomycin. Mice were carefully monitored over time; moribund, preterminal animals were immediately euthanized and recorded as deceased. Kaplan-Meier survival curves were generated using SPSS software (n = 9–11 mice per group; *, P < 0.05 compared with Empty, Log-rank test). Empty: n = 9, FIEL1: n = 11. (I and J) Hematoxylin and eosin (H&E) and Trichrome staining were performed on lung samples. Bars, 100 μm. (K) Collagen percentage quantification from Trichrome staining. Data represent mean values ± SEM (n = 4–6 mice per group, *, P < 0.05 compared with empty, Student's t test). (L) Hydroxyproline content was measured in lungs from 7, 14, and 21 d after

bleomycin challenge. Data represent mean values ± SEM (n = 4–6 mice per group, *, P < 0.05 compared with empty, Student's t test). (M) Mice lungs were isolated and assayed for PIAS4 and FIEL1 immunoblotting.

2.1.8 FIEL1 knockdown ameliorates bleomycin-induced lung injury in vivo

To further confirm the role of FIEL1 in lung fibrosis and inflammation, we pursued *in vivo* knockdown studies. Mice were first infected with lentivirus encoding CON shRNA or *FIEL1* shRNA for 144h (10^7CFU/mouse, i.t) and then challenged with bleomycin (0.05U i.t.) for an additional 1-21 days (Figure 10A). FIEL1 knockdown significantly decreased BAL protein concentrations, total cell counts, and chemokine CXCL1 levels (Figure 10B-D). Specifically, the differential cell counts of BALs revealed that the total decrease in inflammatory cells was mostly due to neutrophils and lymphocytes, with the exception of macrophages on day 3 and 21 (Figure 10E-G). FIEL1 knockdown in mice also significantly improved survival (Figure 10H). Peribronchiolar and parenchymal fibrosis were also substantially decreased in FIEL1 knockdown mice (Figure 10I-J) suggesting that FIEL1 knockdown ameliorates bleomycin-induced lung injury. Elevated lung collagen deposition visualized by Masson Trichrome staining also suggested that FIEL1 expression exacerbates bleomycin-induced lung fibrosis (Figure 10J-K). We observed a marked decrease in lung fibrosis in FIEL1 knockdown mice as demonstrated by a significant decrease in hydroxyproline content (Figure 10L). Last, we analyzed FIEL1 and PIAS4 protein levels in murine lung samples and showed that lentiviral FIEL1 knockdown reversed bleomycin induced FIEL1 increase and rescued PIAS4 protein levels in the lung (Figure 10M).
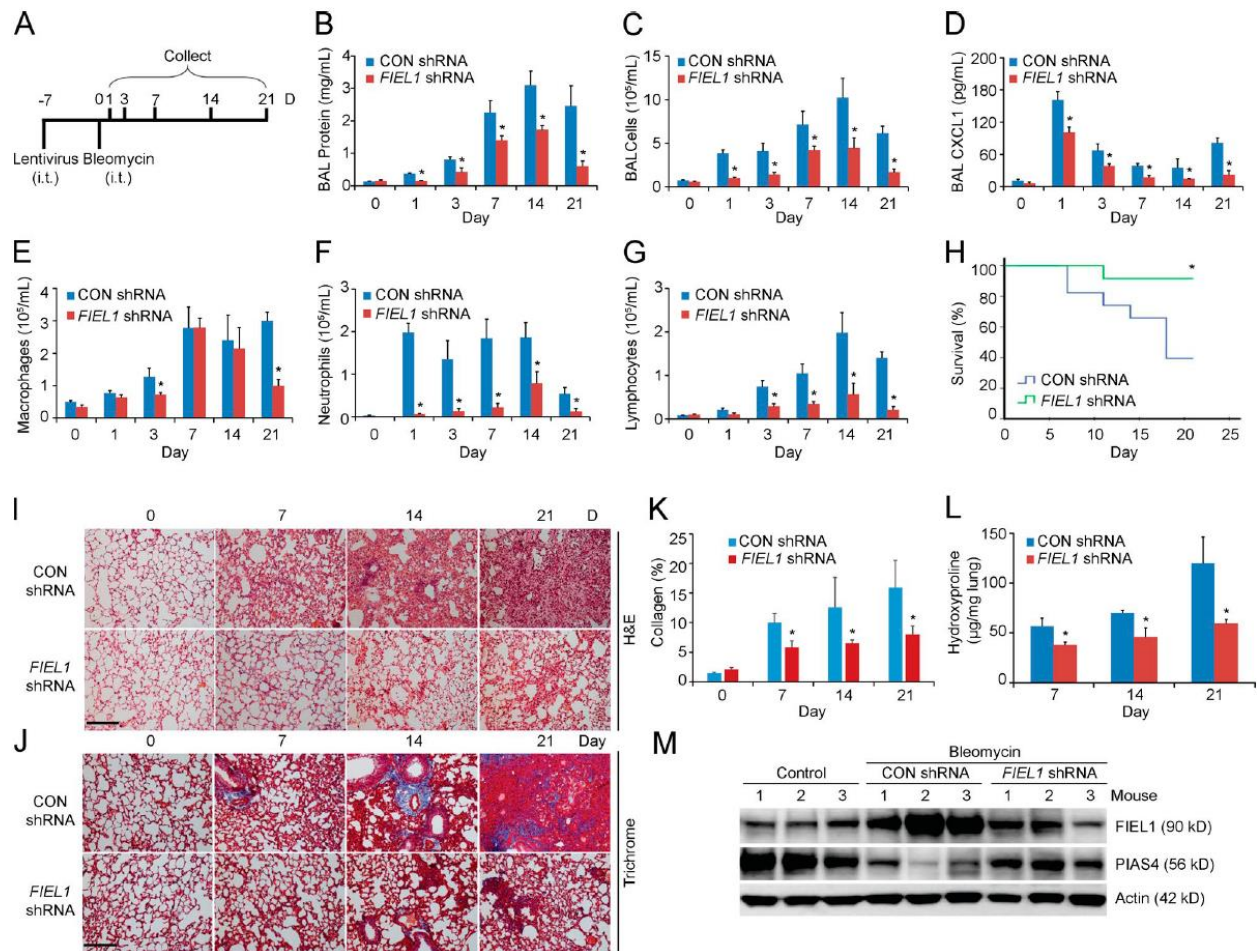
Figure 10 FIEL1 knockdown ameliorates bleomycin-induced lung injury in vivo

(A) C57BL/6J mice were treated i.t. with Lenti-CON shRNA or Lenti-FIEL1 shRNA (107 PFU/mouse) for 144 h; mice were then treated i.t. with bleomycin (0.05 U). Mice were euthanized over the next 1–21 d, and lungs were lavaged with saline, harvested, and then homogenized. (B–D) Lavage protein, total cells, and CXCL1 concentrations were measured. Data represent mean values ± SEM (n = 4–6 mice per group, data are from one of the two experiments performed; *, P < 0.05 compared with Control, Student's t test). (E–G) Lavage cells were then processed for Wright-Giemsa stain; lavage macrophages, neutrophils, and lymphocytes were counted and graphed. Data represent mean values ± SEM (n = 4–6 mice per group, *, P < 0.05 compared with Control, Student's t test). (H) Survival studies of mice that were given bleomycin. Mice were carefully monitored over time; moribund, preterminal animals were immediately euthanized and recorded as deceased. Kaplan-Meier survival curves were generated using SPSS software (n = 8 mice per group; *, P < 0.05 compared with Control, Log-rank test P < 0.05). Empty: n = 8, FIEL1: n = 8. (I and J) H&E and Trichrome staining was performed on lung samples. Bar indicates 100 μm. (K) Collagen percentage quantification from Trichrome staining. Data represent mean values ± SEM (n = 4–6 mice per group, *, P < 0.05 compared with Control, Student's t test). (L) Hydroxyproline content was measured in lungs from 7, 14, and 21 d after bleomycin challenge. Data represent mean values ± SEM (n = 4–6 mice per group; *, P < 0.05 compared with Control, Student's t test). (M) Mice lungs were isolated and assayed for PIAS4 and FIEL1 immunoblotting.

2.1.9 Anti-fibrotic activity of a FIEL1 small molecule inhibitor

We first constructed a FIEL1 HECT domain homology model using the NEDD4 HECT domain structure (167, 168) (Protein Database 2XBF.pdb) (Figure 11A). We observed a major cavity within the C-terminal of the FIEL1 HECT domain that is also required for PIAS4 binding (Figure 11A). Through the LibDock program from Discovery Studio 3.5, we were able to screen potential ligands for the FIEL1 cavity. We selected BC-1480 as a backbone to further develop new small-molecule inhibitors (Figure 11B). BC-1485 was synthesized by reacting alaninamide with BC-1480 (data not shown). BC-1485 fits in the FIEL1 cavity fairly well by having several electrostatic interactions with GLN 774, HIS 788, ILE 776, and THR 783 (Figure 11C-D)

2.1.9.1 In vitro

We next sought to investigate the effect of FIEL1 small molecule inhibitors *in vitro*. Compared to BC-1480, BC-1485 exhibited >100 fold activity in disrupting the FIEL1/PIAS4 interaction (Figure 11E). BC-1485 also exhibited potent activity towards disrupting FIEL1 directed PIAS4 ubiquitination (Figure 11F). Finally, we tested BC-1485 in cells and observed a drastic dose-dependent increase in PIAS4 protein levels (Figure 11G). BC-1485 also decreased the expression of α-SMA in MRC5 cells (data not shown). BC-1485 also stabilized PIAS4 by extending its half-life (Figure 11H) without altering its mRNA level (Figure 11I).
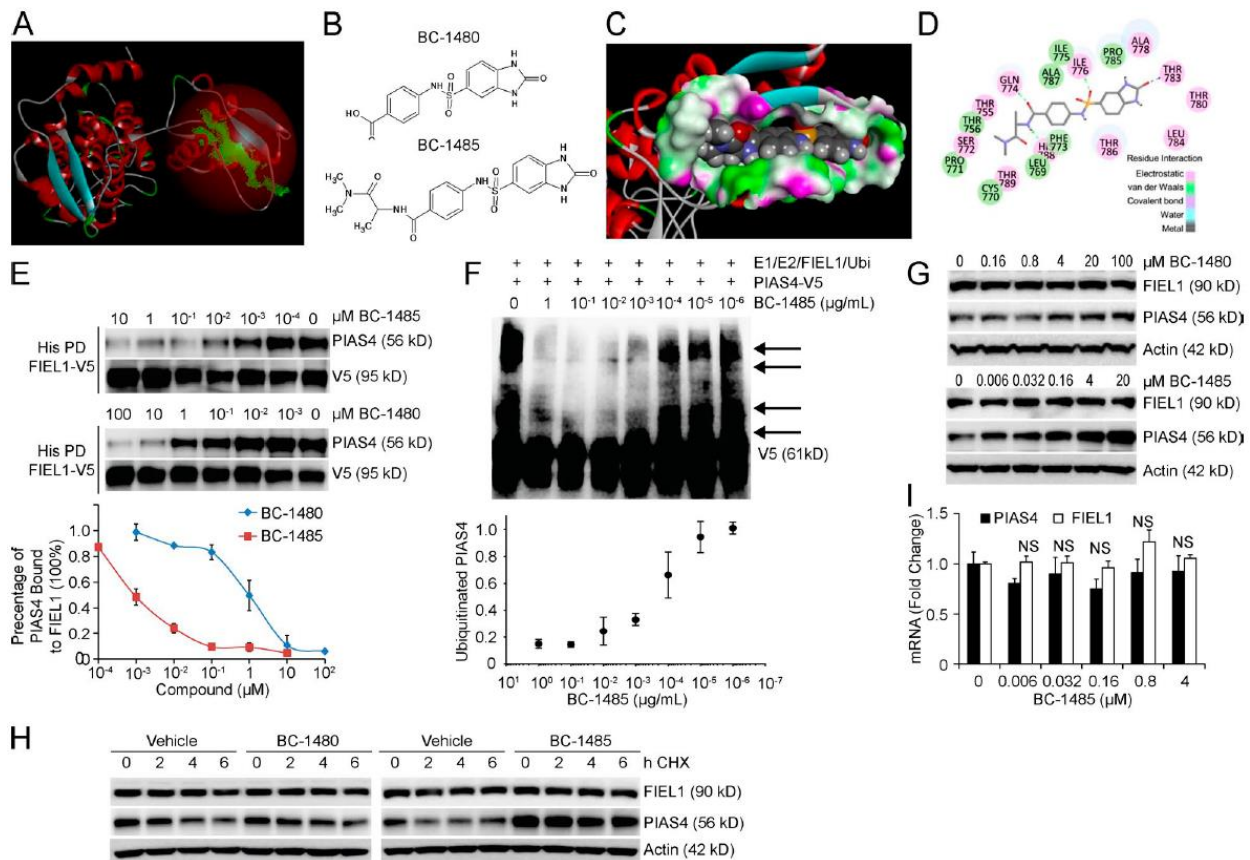
Figure 11 Antifibrotic activity of a FIEL1 small molecule inhibitor in vitro

(A) Structural analysis of the FIEL1 HECT domain revealed a major cavity within the C terminus of the HECT domain. (B) Structures of the BC-1480 backbone (4-(2-Oxo-2,3-dihydro-1H-benzoimidazole-5-sulfonylamino)-benzoic acid) and lead compound BC-1485. (C and D) Docking studies of the lead compound, BC-1485, interacting with the FIEL1-HECT domain. (E) FIEL1 protein was HIS-purified from FIEL1 expression in 293T cells using cobalt beads. Beads were then extensively washed before exposure to BC-1480 or BC-1485 at different concentrations (10^{-4} to 100 μM). Purified PIAS4 protein was then incubated with drug-bound FIEL1 beads overnight. Beads were washed, and proteins were eluted and resolved on SDS-PAGE. The relative amounts of PIAS4 detected in the pull-downs was normalized to loading and quantified (n =2). (F) In vitro ubiquitination assay. Purified FIEL1, E1, and E2 protein were incubated with purified V5-PIAS4, and the full complement of ubiquitination reaction components with increased concentrations of BC-1485 showed decreased levels of polyubiquitinated PIAS4 (arrows). (bottom) Levels of ubiquitinated PIAS4 as a function of BC-1485 concentration (n = 2). (G) MLE cells were exposed to BC-1480 or BC-1485 at various concentrations for 18 h. Cells were then collected and immunoblotted (n = 3). (H) PIAS4 protein half-life determination after BC-1480 or BC-1485 treatment at 5 μM for 18 h. (I) PIAS4 and FIEL1 mRNA analysis after BC-1485 treatment for 18 h. Data represent mean values ± SEM (n = 3 independent experiments; NS, not significant compared with 0 μM condition, Student's t test).

2.1.9.2 In vivo

To further assess the kinetics of the anti-fibrotic activity of BC-1485, we first tested it *in vivo* following bleomycin injury. Briefly, mice were challenged with bleomycin (0.05U i.t.); BC-

1485 and control compound BC-1480 were given in the drinking water (~5mg/kg/d) for an additional 7-21 days (Figure 12A). BC-1485 significantly decreased BAL protein concentrations and CXCL1 levels (Figure 12B-C,). BC-1485 also significantly decreased BAL total cell counts, specifically neutrophils and lymphocytes (Figure 12D-G), and significantly improved survival (Figure 12H). Peribronchiolar and parenchymal fibrosis were also substantially decreased by BC-1485 (Figure 12I). Decreased lung collagen visualized by Trichrome staining also suggested that BC-1485 ameliorates bleomycin-induced lung injury (Figure 12I and K). We observed a marked decrease in lung fibrosis in mice treated with the BC-1485 as demonstrated by a significant decrease in hydroxyproline content (Figure 12I-J). We further tested BC-1485 in a dose dependent manner using a bleomycin model. This time, mice were challenged with bleomycin (0.05U i.t.) for 10 days before being treated with BC-1485 (2 and 10mg/kg/d in drinking water) for an additional 10 days prior to sacrifice (Figure 13A). BC-1485 significantly decreased BAL protein concentrations and cell counts compared to vehicles (Figure 13B-C). Specifically, BC-1485 dose-dependently decreased macrophages, neutrophils, and lymphocytes (Figure 13D) and significantly improved survival (Figure 13E). We observed a marked decrease in lung fibrosis in mice treated with BC-1485 as demonstrated by a significant decrease in hydroxyproline content (Figure 13F). Peribronchiolar and parenchymal fibrosis were also substantially decreased by BC-1485 (Figure 13G). Decreased lung collagen visualized by Trichrome staining also suggested that BC-1485 ameliorates bleomycin-induced lung injury (Figure 13G-H). Lastly, BC-1485 rescued PIAS4 protein levels in bleomycin treated lungs (Figure 13I). Hence, small-molecule targeting of the FIEL1/PIAS4 pathway reduced the severity of fibrosis in a preclinical model (Figure 4R).

39
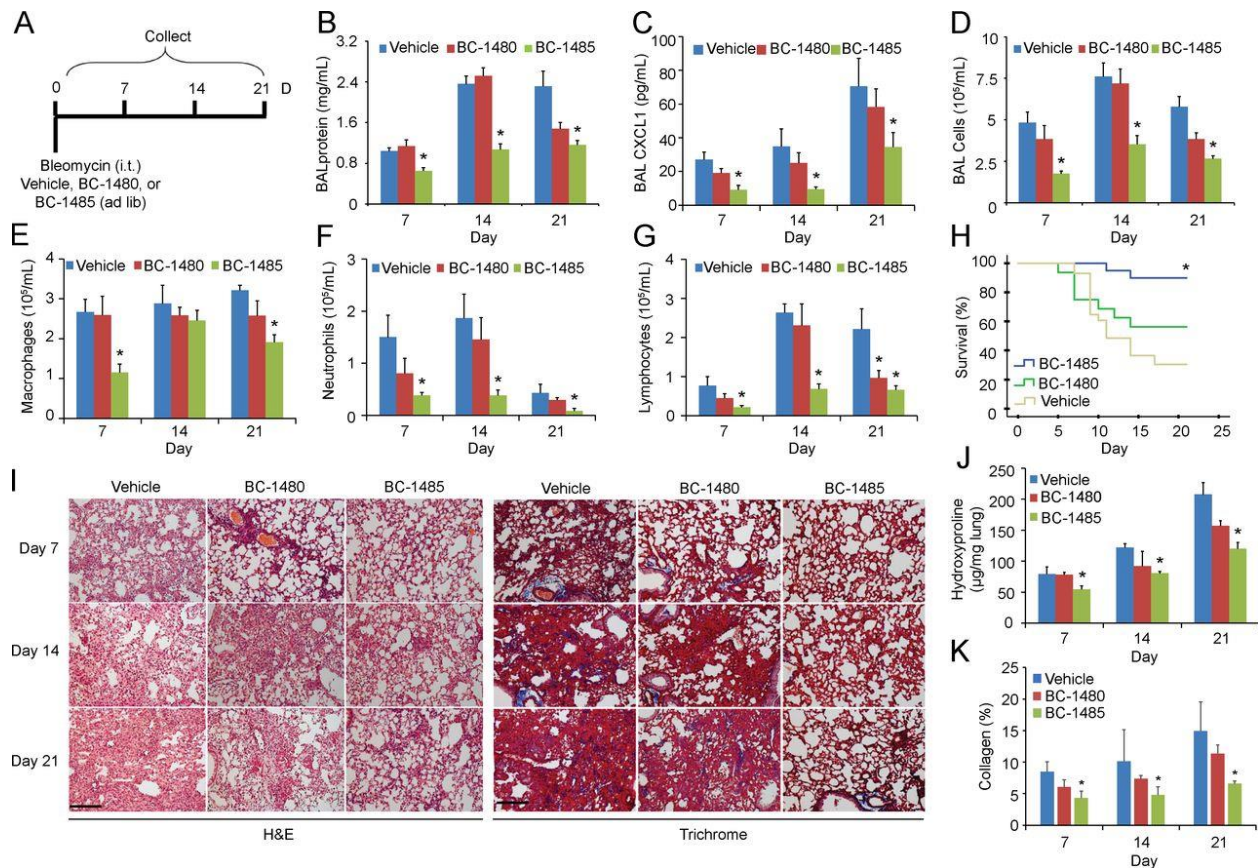
Figure 12 Anti-fibrotic activity of a FIEL1 small molecule inhibitor in vivo

A. C57BL/6J mice were administered i.t. with bleomycin (0.05U). Compounds BC-1480 and BC-1485 were given to mice at the same time through drinking water with an estimated dose of 5mg/kg/d. Mice were euthanized over next 1-21 days, and lungs were lavaged with saline, harvested, and then homogenized. B-D. Lavage proteins, CXCL1, and total cell count were measured. Data represent mean values ± SEM (n=4-8 mice per group, data are from one of two experiments performed; *, $p<0.05$ compared to Vehicle, Student's t-test). E-G. Lavage cells were also processed for Wright-Giemsa stain; Lavage macrophages, neutrophils, and lymphocytes were counted and graphed. Data represent mean values ± SEM (n=4-8 mice per group, *, $p<0.05$ compared to Vehicle, Student's t-test). H. Survival studies of mice that were given bleomycin and compound treatments. Mice were carefully monitored over time; moribund, preterminal animals were immediately euthanized and recorded as deceased. Kaplan-Meier survival curves were generated using SPSS software (n = 12-24 mice per group; *, $p<0.05$ compared to Vehicle, Log Rank test $p<0.05$). Vehicle: n=24, BC-1480: n=13, BC-1485: n=12. I. H&E and Trichrome staining was performed on lung samples. Original magnification, x20. Bar indicates 100 μm. J. Hydroxyproline content were measured in lungs from 7, 14, and 21d after bleomycin challenge. Data represent mean values ± SEM (n=4-8 mice per group, *, $p<0.05$ compared to Vehicle, Student's t-test). K. Collagen percent quantification from Trichrome staining. Data represent mean values ± SEM (n=4-8 mice per group, *, $p<0.05$ compared to Vehicle, Student's t-test).
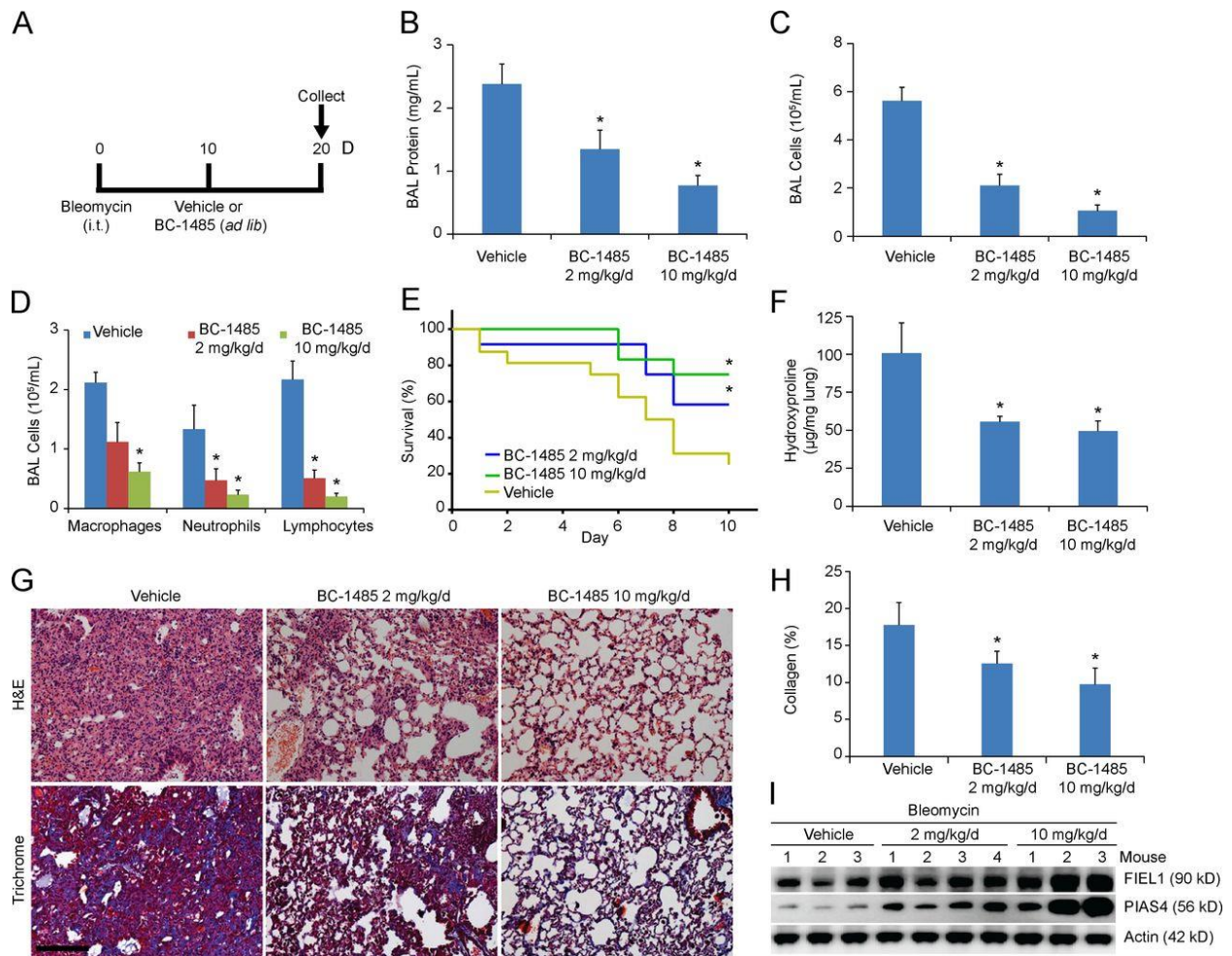
Figure 13 Anti-fibrotic activity of a FIEL1 small molecule inhibitor in vivo

A. C57BL/6J mice were administered i.t. with bleomycin (0.05U). 10 days later, compound BC-1485 was given to mice through the drinking water with an estimated dose of 2 or 10mg/kg/d. Mice were euthanized an additional 10 days later, and lungs were lavaged with saline, harvested, and then homogenized. B-C. Lavage proteins and total cell count were measured. Data represent mean values ± SEM (n=6-9 mice per group, *, p<0.05 compared to Vehicle, Student's t-test). D. Lavage cells were also processed for Wright-Giemsa stain; Lavage macrophages, neutrophils, and lymphocytes were counted and graphed. Data represent mean values ± SEM (n=6-9 mice per group, *, p<0.05 compared to Vehicle, Student's t-test). E. Survival studies of mice that were given bleomycin and compound treatments. Mice were carefully monitored over time; moribund, pre-terminal animals were immediately euthanized and recorded as deceased. Kaplan-Meier survival curves were generated using SPSS software (n = 12-16 mice per group; *, p<0.05 compared to Vehicle, Log Rank test p<0.05). Vehicle: n=16, BC-1485 (2mg/kg/d): n=12, BC-1485 (10mg/kg/d): n=12. F. Hydroxyproline content were measured in lungs from 10d after bleomycin challenge. Data represent mean values ± SEM (n=6-9 mice per group, *, p<0.05 compared to Vehicle, Student's t-test). G. H&E and Trichrome staining were performed on lung samples from A. Original magnification, x20. Bar indicates 100 μm. H. Collagen percent quantification from Trichrome staining. Data represent mean values ± SEM (n=6-9 mice per group, *, p<0.05 compared to Vehicle, Student's t-test). I. Mice lungs were isolated and assayed for PIAS4 and FIEL1 immunoblotting.

2.1.10 Discussion

TGFβ signaling plays a key role in the pathogenesis of tissue fibrosis (169). PIAS4 suppresses the TGFβ pathway, in part, by SUMOylating SMAD3 and causing its nuclear export (22, 23, 161). Here we show that FIEL1 appears to promote TGFβ signaling and fibrosis by destabilizing PIAS4. Our data not only authenticate FIEL1 as a *bona-fide* E3 ligase, but also show that it triggers the site-directed ubiquitination and degradation of PIAS4 leading to exacerbated fibrotic signaling. One evidence to support that FIEL1 regulates PIAS4 protein stability is that MRC5 cells ectopically expressing FIEL1 increased PIAS4 mRNA level (Figure 3K). This is a common compensatory mechanism used by cells to rescue protein loss. As an E3 ligase, it is quite possible that FIEL1 targets many other proteins for ubiquitination and degradation. We measured protein abundance of several pro-TGFβ and anti-TGFβ proteins such as TGFβR1, TGFβR2, SMAD7, and SMURF1 in cell lysates with ectopically expressing FIEL1 (Figure 3I). However, the absence of any difference in their protein levels suggests that it is plausible that FIEL1 regulates SMAD signaling through PIAS4. However, we do not rule out the possibility that other proteins could also play a role linking FIEL1 to the SMAD pathway, given that all E3 ligases are known to target many substrates at the same time. We believe that the FIEL1/PIAS4 pathway is relevant in both epithelial cells and fibroblasts as we have tested this pathway in both cell types (Figure 3C, I, L, Figure 5B-I), which matches the current understanding that both epithelial cells and fibroblasts may be involved in the formation of fibrosis (143, 158, 170, 171). However, future studies are needed to identify which cell type is more involved in the FIEL1/PIAS4 pathway.

We found that PKCζ is a regulator of PIAS4 protein stability and described a mechanism of PIAS4 basal protein turnover controlled constitutively by FIEL1. This provides an internal

checkpoint for the cell to shut off the anti-fibrotic pathway, a mechanism that TGFβ hijacks to shut down PIAS4 and promote fibrosis. Moreover, we found that GSK3β is another regulator of PIAS4 protein stability through the phosphorylation of FIEL1. There appears to be a new "double locking" molecular interplay between FIEL1 and PIAS4. Specifically, both the P779 and GSK3β phosphorylated T783 residues within FIEL1 are required for PIAS4 binding; both the Q21 and PKCζ phosphorylated S18 residues within PIAS4 are required for FIEL1 binding. We believe that the FIEL1/PIAS4 molecular interplay is based on two pairs of interactions between pT783-Q21 and P779-pS18 (Figure 4Q-R). In this model, both PKCζ and GSK3β up-regulate TGFβ signaling, which correlates well with several previous studies (172-174).

We observed a naturally occurring amino acid variant in FIEL1 (P779L). This hypomorphic polymorphism exhibited a significant decrease in PIAS4 interaction. Thus, its expression did not decrease PIAS4 protein levels or half-life. We further characterized a naturally occurring amino acid variant (rs113140862) in FIEL1 (I514V). This polymorphism, conversely, exhibited hypermorphism as shown by accelerated PIAS4 degradation and shortened protein half-life (Figure 8K-L). FIEL1[P779L] may be an important and protective polymorphism in IPF, while FIEL1[I514V] may be a susceptible polymorphism in IPF via exacerbated TGFβ signaling. Further prospective studies in large IPF cohorts are required in order to validate this observation.

The FIEL1 HECT domain served as the mechanistic centerpiece and structural basis for designing first-in-class FIEL1 inhibitors. We had previously used a similar approach to design the inhibitors for the pro-inflammatory protein FBXO3 (175, 176). Since the FIEL1 inhibitor also docks at the same region within the HECT domain as the substrate PIAS4, the inhibitor works by disrupting the FIEL1/PIAS4 interaction. By adding an alaninamide group to the BC-1480 backbone we generated BC-1485, which improved its activity >100 fold. BC-1485 optimally

interacts with FIEL1, exerts robust anti-fibrotic activity by stabilizing PIAS4, and inhibits TGFβ signaling in both human MRC5 cells and a murine model of pulmonary fibrosis. The effectiveness of this inhibitor underscores the physiological importance of the FIEL1/PIAS4 pathway in regulating TGFβ signaling. Currently, there is no cure for IPF, despite extensive research. Many failed clinical trials suggest the complexity of TGFβ signaling and lack of an "authentic" drug target (177-180). Our study may be highly clinically relevant because subjects with IPF exhibited a significant increase in FIEL1 and decrease in PIAS4 protein. Further, FIEL1 threonine phosphorylation is also significantly increased in IPF lung tissue, which is positively associated with PIAS4 binding (Figure 7G). Interestingly, only the shorter isoform of *KIAA0317* (789aa, FIEL1) is significantly increased in IPF lung tissue; our FIEL1 inhibitor design was also based on the cavity within FIEL1. The longer form of KIAA0317 lacks the drug binding cavity which renders FIEL1 inhibitor ineffective (data not shown). Moreover, in all of the cell lines (MLE, 293T, and HeLa) and tissues tested here, we found very little, if any, longer isoform of KIAA0317 protein present (Figure 3M, data not shown). Thus, FIEL1 may be physiologically relevant in TGFβ signaling and IPF. Indeed, both FIEL1 knockdown and inhibition significantly ameliorates tissue fibrosis coupled with a very dramatic decrease in collagen level in a bleomycin model (Figure 10K, Figure 12K, Figure 13H). These results suggest that FIEL1 may be a promising new therapeutic target for fibrotic diseases such as IPF.

2.1.11 Acknowledgements

2.1.12 Materials and Methods

2.1.12.1 Materials

Sources of the murine lung epithelial (MLE) and 293T cell lines were described previously (181, 182). MRC5 cells were from ATCC. Purified ubiquitin, E1, E2, MG132, Leupeptin, and cyclohexamide (CHX) were purchased from Calbiochem. Mouse monoclonal V5 antibody, the pcDNA3.1D cloning kit, *E. coli* Top10 One Shot competent cells, the pENTR Directional TOPO cloning kits, and Gateway mammalian expression system were from Invitrogen. The HECT domain E3 ligase cDNA, scramble shRNA, *FIEL1*, *PKCζ*, and *GSK3β* shRNA sets were purchased from OpenBiosystems. Nucleofector transfection kits were from Amaxa. The lentiviral packaging system and cobalt beads were from Clontech. Immobilized protein A/G beads were from Pierce. *In vitro* transcription and translation (TnT) kits were from Promega. Cignal SMAD Reporter luciferase Kit (CCS-017L) and mRNA isolation kit were from Qiagen. Complete protease inhibitors were from Roche. KIAA0317 antibodies were from Sigma, Antibody Verify, and Santa Cruz. PIAS and GSK3β antibodies were from Cell Signaling and Santa Cruz. CXCL1 and IL6 mouse ELISA kits and TGFβ protein were from R&D Systems. Peptides were custom synthesized from CHI Scientific. DNA sequencing was performed at Genewiz. All small molecule compound analysis was performed by the University of Pittsburgh Mass Spectrometry and NMR facility.

2.1.12.2 Human Samples

This study was approved by the University of Pittsburgh Institutional Review Board. Lung tissues were from the University of Pittsburgh lung transplant tissue bank. Lung tissues from IPF patients were obtained from excess pathologic tissues after lung transplantation under a protocol approved by the University of Pittsburgh Institutional Review Board. Normal lung tissues were obtained from donor lungs that were not suitable for patient use and provided by the Center for Organ Recovery and Education (CORE). The CORE lungs were only used if there were no considerable lung abnormalities based on high resolution CT scan. Multiple small sections of the parenchyma were collected and immediately frozen at -80ºC for future use. Tissue lysates were used for the western blot analysis.

2.1.12.3 Cell culture

MLE cells were cultured in Dulbecco's Modified Eagle Medium-F12 (Gibco) supplemented with 10% fetal bovine serum (DMEM-F12-10). 293T cells were cultured in Dulbecco's Modified Eagle Medium (Gibco) supplemented with 10% fetal bovine serum (DMEM-10). MRC5 cells were cultured in Eagle's Minimum Essential Medium (Gibco) supplemented with 10% fetal bovine serum (EMEM-10). For protein expression in MLE cells, nucleofection was used following Amaxa's protocol. For protein overexpression in 293T cells, Fugene6HD transfection reagents were used following the manufacturer's protocol. For protein expression in MRC5 cells, MRC-5 Cell Avalanche™ Transfection Reagent was used following the manufacturer's protocol. Cells were treated with TGFβ at 0-2 ng/ml for 0-18h. For FIEL1, PKCζ, or GSK3β knockdown studies in cells, scramble shRNA, *FIEL1*, *PKCζ,* or *GSK3β* shRNA were used to transfect cells for 48h. For drug treatment, compounds were solubilized in DMSO before being added to the cells

for up to 18 h. Cell lysates were prepared by brief sonication in 150 mM NaCl, 50 mM Tris, 1.0 mM EDTA, 2 mM dithiothreitol, 0.025% sodium azide, and 1 mM phenylmethylsulfonyl fluoride (Buffer A) at 4°C. For half-life study, MLE cells were exposed to cycloheximide (40µg/ml) in a time dependent manner for up to 8h. Cells were then collected and immunoblotted.

2.1.12.4 In vitro protein binding assays

PIAS4 protein was immunoprecipitated from 1mg cell lysate using PIAS4 antibody (goat) and coupled to protein A/G agarose resin. PIAS4 beads were then incubated with *in vitro* synthesized products (50µl) expressing V5-FIEL1 mutants. After washing, the proteins were eluted and processed for V5-FIEL1 immunoblotting. Similarly, FIEL1 was immunoprecipitated from 1mg cell lysate using FIEL1 antibody (rabbit) and coupled to protein A/G agarose resin. FIEL1 beads were then incubated with *in vitro* synthesized products (50µL) expressing V5-PIAS4 mutants. After washing, the proteins were eluted and processed for V5-PIAS4 immunoblotting.

2.1.12.5 In vitro peptide binding assays

Biotin labeled peptides were first coupled to streptavidin agarose beads for 1h. Beads were then incubated with *in vitro* synthesized FIEL1 or PIAS4 for 18h. After washing, proteins were eluted and processed for FIEL1 or PIAS4 immunoblotting.

2.1.12.6 In vitro drug binding assays

FIEL1 protein was HIS-purified from FIEL1 expressed in 293T cells using Talon metal affinity resin. Resins were then extensively washed prior to exposure to BC-1480 or BC-1485 at different concentrations (10^{-4} to 100 µM). Purified recombinant PIAS4 protein was then incubated with drug-bound FIEL1 resins overnight. Resins were washed, and proteins were eluted and

resolved on SDS-PAGE. The relative amounts of PIAS4 detected in the pull-downs were normalized to loading and quantified.

2.1.12.7 In vitro ubiquitin conjugation assays

The assay was performed in a volume of 20 µl containing 50 mM Tris pH 7.6, 5 mM $MgCl_2$, 0.6 mM DTT, 2 mM ATP, 400 µM MG132, 50 nM Ubiquitin activating enzyme, 0.5 µM M UbcH5, 0.5 µM UbcH7, 2 µM ubiquitin, and 1 µM ubiquitin aldehyde. TnT Coupled Reticulocyte *in vitro* synthesized FIEL1-V5 and PIAS4-V5 proteins were purified via Talon metal affinity resin, and reaction products were processed for V5 immunoblotting.

2.1.12.8 In vitro kinase assays

The assays were performed by combining 50 mM Tris pH 7.6, 100 mM $MgCl_2$, 25 mM β-Glycerolphosphate, and 5 mg/mL BSA, bringing them to a total volume of 25 µL using combinations of 0.5 mM ATP, 0.2 µCi γ-32P ATP (Perkin Elmer), 500 nM recombinant Aurora B (Calbiochem), either 500 nM of recombinant PKCζ (Enzo) or 500 nM of recombinant GSK3β (Enzo), and V5-tagged PIAS4 or V5-tagged FIEL1 synthesized via TnT *in vitro* kits (Promega) and purifying them by HIS pulldown. Reaction products were incubated at 37°C for 2 hours, resolved by SDS-PAGE, and processed for autoradiography either by using Personal Molecular Imager (BioRad) or immunoblotting for V5 to visualize substrate input.

2.1.12.9 Hydroxyproline Assay

Murine lungs were dried and weighed prior to digestion with HCl. Hydroxyproline concentrations were measured using previously described methods (183, 184). Hydroxyproline content was normalized to dry lung weight.

2.1.12.10 SMAD reporter assay

Cignal SMAD Reporter luciferase plasmids were co-transfected with Empty, FIEL1, PIAS4, CON shRNA, or *FIEL1* shRNA for 24-48h before TGFβ treatment for an additional 2-18h. Cells were then collected and assayed for firefly and renilla luciferase activity. SMAD transcription activity was normalized by a firefly and renilla luciferase activity ratio.

2.1.12.11 Immunostaining

MRC5 cells were seeded in 35mm MatTek glassbottom dishes before the plasmid transfection, inhibitor, and TGFβ treatment. Cells were washed with PBS and fixed with 4% paraformaldehyde for 20 min, then exposed to 2% BSA, 1:500 mouse α-SMA, goat FN or SMAD antibodies, and 1:1000 Alexa 488 or Alexa 567 labeled goat anti rabbit, chicken anti-mouse or donkey anti-goat secondary antibodies sequentially for immunostaining. The nucleus was counterstained with DAPI and F-actin was counterstained with Alexa 488-Phalloidin. Immunofluorescent cell imaging was performed on a Nikon A1 confocal microscope using 405 nm, 488 nm, or 567 nm wavelengths. All experiments were done with a 60 x oil differential interference contrast objective lens.

2.1.12.12 Molecular docking studies and compound design

The docking experiments were carried out using software from Discovery Studio 3.5. A library containing 500,000 approved or experimental drugs was first used to screen potential ligands for FIEL1. FIEL1-HECT domain structural analysis revealed a major drug binding cavity within the c-terminal of the HECT domain. The binding cavity was adopted into the LibDock algorithm to screen for the optimum inhibitor. Based on the docking and best-fit analysis of suitable ligands, BC-1480 was used as the backbone to synthesize other compounds.

2.1.12.13 BC-1485 synthesis

A mixture of 4-(2-oxo-2,3-dihydro-1*H*-benzo[d]imidazole-5-sulfonamido)benzoic acid
(66 mg, 0.2 mmol), *N*-(3-Dimethylaminopropyl)-N-ethylcarbodiimide hydrochloride (38.3 mg,
0.2 mmol), and 1-Hydroxybenzotriazole hydrate (30.6 mg, 0.2 mmol) in DMF (3 mL) was stirred
at room temperature for 10 minutes followed by the addition of 2-amino-*N,N*-
dimethylpropanamide hydrochloride (37 mg, 0.24 mmol), and triethylamine (24.3 mg, 0.24
mmol). The reaction was stirred at room temperature under nitrogen overnight and concentrated
under vacuum. The residue was dissolved in dichloromethane (1 mL) and purified by flash
chromatography (silica gel, toluene/2-propanol/ammonia hydroxide=80/20/1, v/v/v) to obtain a
sticky white solid. It was suspended in 2N HCl (2 mL), sonicated for 10 min, and filtered. The
wet cake was washed with water several times and then dried by vacuum suction to obtain the
desired product as a white powder (30 mg, 35% yield)): ^{1}H NMR (400 MHz, DMSO-d_6) δ 11.10
(s, 1H), 10.97 (s, 1H), 10.47 (s, 1H), 8.38 (d, *J* = 8.0 Hz, 1H), 7.72 (d, *J* = 8.4 Hz, 2H), 7.41 (d, *J*
= 9.2 Hz, 1H),7.28 (s, 1H), 7.12 (d, *J* = 8.4 Hz, 2H), 7.01 (d, *J* = 8.4 Hz, 1H), 4.84 (m, 1H), 3.01
(s, 3H), 2.81 (s, 3H), 1.22 (d, *J* = 6.8 Hz, 3H); ^{13}C NMR (100 MHz, DMSO-d_6) δ 172.30 (C=O),
165.45 (C = O), 155.66 (C =O), 141.26, 133.95, 131.45, 130.10, 129.26, 129.13, 120.83, 118.62,
108.74, 107.02, 45.55, 36.89, 35.71, 17.42; HRMS (ESI) calculated for $C_{19}H_{21}N_5O_5S$: 431.12634,
found: 432.13353 $[M+H]^+$.

2.1.12.14 RT–qPCR, cloning, and mutagenesis

Total RNA was isolated and reverse transcription was performed followed by real-time
quantitative PCR with SYBR Green qPCR mixture as described (185). All mutant *PIAS4* and
FIEL1 plasmid constructs were generated using PCR-based approaches and appropriate primers
and subcloned into a pcDNA3.1D/V5-HIS vector.

2.1.12.15 Lentivirus construction

To generate lentivirus encoding FIEL1, Lenti-Plvx-FIEL1 plasmid was co-transfected with Lenti-X HTX packaging plasmids (Clontech) into 293T cells following the manufacturer's instructions. 72 h later, virus was collected and concentrated using Lenti-X concentrator (Clontech).

2.1.12.16 Animal studies

All procedures were approved by the University of Pittsburgh Institutional Animal Care and Use Committee. For fibrosis studies, male C57BL/6J mice were deeply anesthetized using a ketamine/xylazine mixture, and the larynx was well visualized under a fiber optic light source before endotracheal intubation with a 3/400 24-gauge plastic catheter. 10^7 CFU of lentivirus encoding genes for Empty (E), FIEL1, CON shRNA, or *FIEL1* shRNA was given i.t. for 144 h before administration of bleomycin (0.02U~0.05U i.t.) for up to 21 days. Animals were euthanized and assayed for BAL protein, cell count, cytokines, and lung infiltrates. Survival studies were performed on mice that were given bleomycin (0.02U~0.05U i.t.). Mice were carefully monitored over time; moribund, preterminal animals were immediately euthanized and recorded as deceased. For time course drug studies, mice were deeply anesthetized as above. Bleomycin (0.05U i.t.) was given i.t. before BC-1480 or BC-1485 (~5mg/kg/d) was administered to the mice through their drinking water. 7-21d later, animals were euthanized and analyzed as above. For dose course drug studies, mice were deeply anesthetized as above. Bleomycin (0.05U i.t.) was given i.t. 10 days before BC-1485 (~2-10mg/kg/d) was administered to the mice through their drinking water. Another 10 days later, animals were euthanized and analyzed as above.

2.1.12.17 Tissue Staining

Murine lung samples were fixed in 10% neutral buffered formalin and embedded in paraffin and sectioned as previous described (18). Sections were stained with eosin and hematoxylin or Masson's Trichrome. Images were acquired from 20X lens from random fields from each section. Fibrotic areas (blue channel) were isolated and determined by pixel area using ImageJ.

2.1.12.18 Statistical Analysis

Statistical comparisons were performed through SPSS (IBM) with $p<0.05$ indicative of significance. Survival curves were generated through SPSS (IBM).

2.2 Kelch-like Protein 42 is a Pro-Fibrotic Ubiquitin E3 Ligase in Systemic Sclerosis

The second part of aim one utilizes high-throughput techniques to screen for ubiquitin E3 ligases affecting TGF-β signaling in systemic sclerosis. Some E3 ligase sub-families are comprised of 20 or fewer members, which makes ectopic over-expression and blotting a feasible screening technique (187). However, this method is inherently biased and may fail to capture more biologically relevant regulatory relationships from other un-screened E3 ligases. In the goal of fully capturing the mechanistic network of protein degradation underlying our disease model, we undertook unbiased high throughput screening assays, in which RNAi libraries targeted against ubiquitin E3 ligases were transfected to cells and assayed for their effect on the biology. In this study we investigated E3 ligases controlling TGF-β-dependent fibrotic signaling in SSc primary cells using automated microscopy of SMAD protein translocation as our high throughput screening.

2.2.1 Study Overview

Systemic scleroderma (SSc) is an autoimmune disease that affects over 2.5 million people globally. SSc results in dysfunctional connective tissues with excessive pro-fibrotic signaling, affecting skin, cardiovascular, and particularly lung tissue. Over three-quarters of individuals with SSc develop pulmonary fibrosis within 5 years, the main cause of SSc mortality. No approved

medicines to manage lung SSc currently exist. Recent research suggests that pro-fibrotic signaling by transforming growth factor β (TGF-β) is directly tied to SSc. Previous studies have also shown that ubiquitin E3 ligases potently control TGF-β signaling through the targeted degradation of key regulatory proteins; however, the roles of these ligases in SSc–TGF-β signaling remain unclear. Here, we utilized primary SSc patient lung cells for high-throughput screening of TGF-β signaling via high-content imaging of nuclear translocation of the pro-fibrotic transcription factor SMAD family member 2/3 (SMAD2/3). We screened an RNAi library targeting ubiquitin E3 ligases and observed that knockdown of the E3 ligase Kelch-like protein 42 (KLHL42) impairs TGF-β–dependent pro-fibrotic signaling. KLHL42 knockdown reduced fibrotic tissue production and decreased TGF-β–mediated SMAD activation. Using unbiased ubiquitin proteomics, we identified phosphatase 2 regulatory subunit B'epsilon (PPP2R5e) as a KLHL42 substrate. Mechanistic experiments validated the ubiquitin-mediated control of PPP2R5e stability through KLHL42. PPP2R5e knockdown exacerbated TGF-β–mediated pro-fibrotic signaling, indicating a role for PPP2R5e in SSc. Our findings indicate that the KLHL42–PPP2R5e axis controls pro-fibrotic signaling in SSc lung fibroblasts. We propose that future studies could investigate whether chemical inhibition of KLHL42 may ameliorate pro-fibrotic signaling in SSc.

2.2.2 Introduction

Pulmonary fibrosis also manifests as a secondary feature of other diseases. Systemic sclerosis (SSc) or scleroderma is an auto-immune rheumatic disease affecting numerous tissue and organ systems and is characterized by the hardening and fibrosis of connective tissues. SSc displays prominently in the skin, through skin thickening or increased inflammation, but afflicts numerous organs including the lung, through SSc-associated interstitial lung disease (SSc-ILD)

54

2.2.2.1 Scleroderma and Lung Fibrosis

Due to the resulting pulmonary fibrosis and respiratory failure, SSc-ILD is the primary cause of mortality for SSc patients (188, 189). Over three-quarters of SSc patients develop lung fibrosis within five years of diagnosis, with a subset developing progressive fibrotic disease (190). SSc-ILD is characterized by decreased respiratory function due to excessive hardening and fibrotic scarring due to extra-cellular matrix deposition in the lung. In combination with increased inflammatory response, epithelial injury, and cellular fibrotic transition, the fibrous production and collagen deposition in the lung interstitium leads to respiratory failure (191, 192). While new therapeutics are under evaluation, current treatment options that target the underlying pathophysiology are limited (193). Pro-fibrotic cellular signaling pathways are associated with the pathological remodeling of the lung leading to SSc-ILD, particularly that of the transforming growth factor beta pathway (TGF-β) (191). Research has shown TGF-β cytokine and downstream signaling to have stark causal effects on SSc disease models (194).

2.2.2.2 Ubiquitin-based Regulation of TGF-β signaling and a role within SSc-ILD

TGF-β signaling proceeds through cellular recognition of the TGF-β cytokine by receptor complexes, and activation of the SMAD transcription factors (19). In canonical TGF-β/SMAD signal transduction, receptor-regulated SMAD2/3 protein is phosphorylated, complexed with co-SMAD protein SMAD4, and shuttled to the nucleus whereupon pro-fibrotic transcription programs are activated (150). Nuclear localization and activating phosphorylation of SMAD transcription factors is essential for their signaling transduction, as numerous studies have shown inhibition of TGF-β signaling upon SMAD inactivation or nuclear exclusion (195-199). SMAD-dependent TGF-β signaling is tightly regulated through a variety of mechanisms, including post-translational protein degradation pathways (200, 201).

Protein degradation is an evolutionarily conserved process for regulating cellular protein longevity. Dysfunctional or aberrant protein degradation lay at the heart of many diseases, including fibrotic signaling in the lung. Ubiquitination is a crucial mechanism to regulate homeostasis in TGF-β signaling, as E3 ligase mediated degradation of the TGF-β receptors, and of the SMAD2/3 transcription factors help to dampen signaling (202, 203). However, ubiquitination is associated with pathologic fibrotic signaling; we and other groups have observed ubiquitination proteins affected multiple facets of fibrotic signaling in the lung, including the TGF-β pathway (200, 204-206). Further, pro-fibrotic E3 ligases have also shown promise as targets for chemical inhibition to reduce deleterious fibrotic signaling (11, 141, 207, 208). To uncover new ubiquitin E3 ligases regulators of SSc fibrotic signaling, we utilized a high throughput imaging system to screen an RNAi library targeting E3 ligases for their effect on SMAD2/3 translocation in SSc lung fibroblasts

Here we report the development of SSc lung fibroblasts as a screening tool for TGF-β activation based on SMAD2/3 nuclear translocation. We identified the ubiquitin E3 ligase KLHL42 as a pro-fibrotic mediator of TGF-β-SSc fibrotic signaling. KLHL42 was also shown to be a regulator of the stability of the Protein phosphatase 2A regulatory subunit PPP2R5e, and may regulate fibrotic signaling through the PP2A pathway. This study provides a new model of E3 ligase control for fibrotic signaling in SSc lung disease.

2.2.3 Development of SMAD2/3 translocation ratio screening assay

The Systemic Sclerosis Center of Research Translation at the University of Pittsburgh works with the University of Pittsburgh Medical Center in the collection of tissue and explant samples from SSc patients for research. Through this Center, we utilized primary SSc patient lung

fibroblasts in culture as the basis for the HCS assay. Previous research demonstrated SSc cell cultures have increased TGF-β/SMAD signaling, and exhibit a strongly pro-fibrotic phenotype, which would make them ideal for RNAi loss-of-function screening (194, 209, 210).

We first sought to validate SSc cells as a proper tool for high-content screening in 384-well plate format. Immunofluorescent studies of SSc lung fibroblasts (SSc cells) show responsiveness to TGF-β1 stimulation, leading to increased SMAD2/3 fluorescent signal in the nucleus (Figure 14A). As a surrogate for overall fibrotic activity, we calculated a *translocation ratio* metric based on the nuclear SMAD2/3 immunostaining relative to cytoplasmic SMAD2/3. As SMAD transcription factors are shuttled to the nucleus for fibrotic signaling, we hypothesized that increased translocation ratio represented a more fibrotic response. The translocation ratio metric showed robust results through a titration of primary and secondary antibody for both baseline and TGF-β1-stimulated treatments (Figure 14B). We calculated a Z'-factor of 0.39 for this assay; this signal window proved adequate for screening (Figure 14C) (211). Silencing of an essential protein for the TGF-β/SMAD signaling process would result in a decreased translocation ratio (Figure 14D). We then proceeded to screen for key ubiquitin e3 ligase modulators.
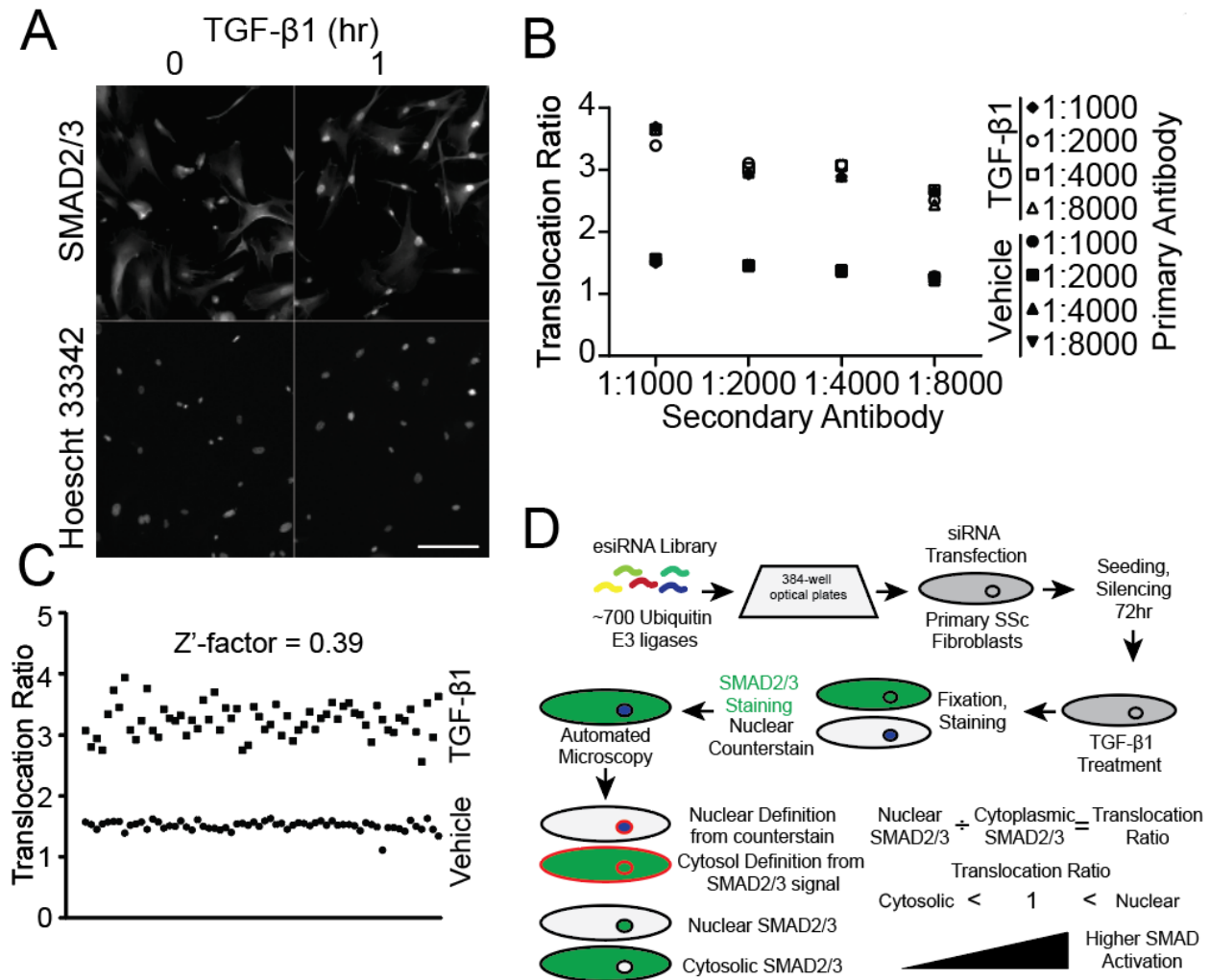
Figure 14 Assay development for Scleroderma lung fibroblasts

(A) Immunofluorescence analysis of SSc lung fibroblasts for SMAD2/3 localization without and with short-term TGF-β1 stimulation. (B) Optimization of assay conditions. Translocation ratios were calculated for titrations of primary and secondary antibody without and with TGF-β1 treatment. (C) Z'-factor calculation of SMAD2/3 translocation ratio with vehicle or TGF-β1 treatment (n = 64 wells per treatment). (D) Schematic of high-content assay to measure SMAD translocation assay with RNAi screen. SSc cells were treated with siRNA library in 384-well glass plates prior to TGF-β1 treatment, fixation and staining for SMAD2/3 and the nucleus. The nucleus was segmented based on nuclear counterstain signal, and the cytosolic region was defined through expansion of the nuclear segment to the threshold of SMAD2/3 fluorescent signal. The translocation ratio was defined as the ratio of nuclear to cytosolic signal, with higher signal suggestive of greater SMAD activation. Translocation Ratios were calculated with either Gen5 software (BioTek) or CellProfiler (65). Scale bar = 200µm (A).

2.2.4 The E3 ligase KLHL42 affects fibrotic signaling and SMAD activation in SSc

With the validation of SSc fibroblasts as potential screening tool we sought to screen an esiRNA library (Sigma) against ubiquitination proteins for their effect on SMAD2/3 localization. Following siRNA knockdown and TGF-β1 stimulation, we collected and immunostained SSc fibroblasts for SMAD2/3 protein, conducted automated microscopy, and calculated a translocation ratio for each esiRNA (Figure 15A). We observed that most siRNA had little effect on changing translocation ratio relative to control esiRNA, but we observed hits whose silencing reduced the SMAD2/3 translocation ratio (Figure 15B). Given that knockdown of these targets resulted in a reduced translocation ratio (less nuclear SMAD2/3 protein), we hypothesized these ubiquitination proteins functioned as *pro-fibrotic* mediators. Of these hits, we observed the Kelch-like protein 42 (KLHL42) to be a relatively under-characterized E3 ligase. Previous studies suggest KLHL42 functioned as part of the Cullin-3 E3 ligase complex, in which KLHL42 functions as the key substrate-engaging protein to facilitate substrate ubiquitination (212, 213). However, the effect of KLHL42 on fibrotic signaling is unclear. We validated the initial screening data through confocal microscopy, as *KLHL42* knockdown resulted in decreased SMAD2 activation upon TGF-β1. Knockdown of the TGF-βR1 receptor was used as a positive control, as loss of a major membrane receptor for TGF-β1 would impede TGF-β1-mediated activation of SMAD signaling (20) (Figure 15C). *KLHL42* knockdown significantly reduced production of fibrotic proteins such as fibronectin (Figure 15D-E). Further, we observed through immunoblot assay that *KLHL42* knockdown affects SMAD2 activation (Serine-465/467 phosphorylation), without changing total SMAD2 protein level suggesting the effect of KLHL42 occurs upstream in the signaling process and not through the degradation of SMAD2 protein (Figure 15F-G). These initial studies suggest KLHL42 may be a pro-fibrotic E3 ligase.
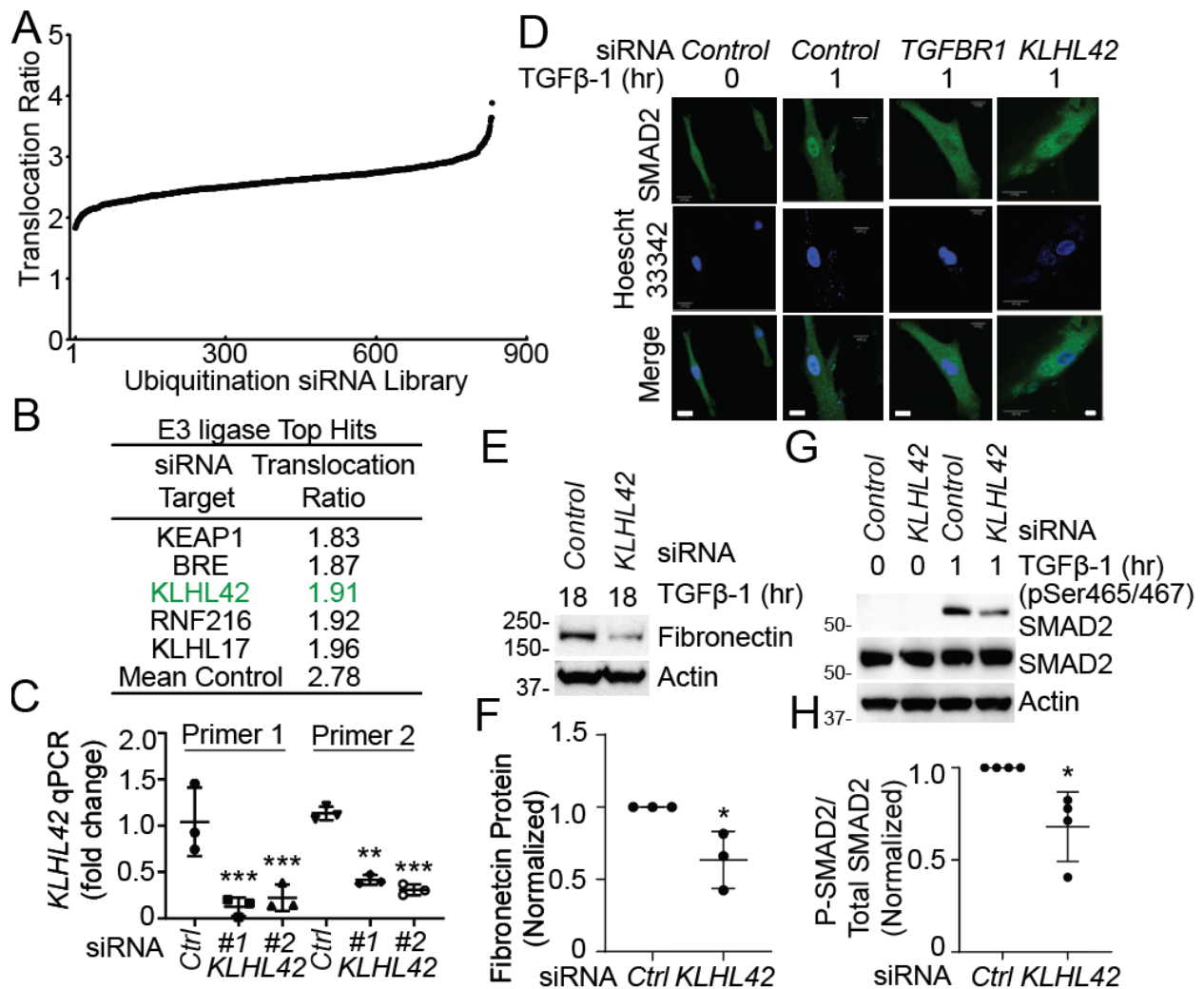
Figure 15. Depletion of Ubiquitin E3 ligase KLHL42 impairs TGF-β1-mediated fibrotic signaling

(A) Screening of SSc fibroblasts with an esiRNA library targeted against ubiquitination proteins and E3 ligases by their effect on SMAD2/3 translocation ratio. (B) KLHL42 is a top hit from the SSc fibroblast translocation ratio screen. (C) qPCR analysis of KLHL42 knockdown by RNAi in SSc cells. Data and means ± SD of 3 independent experiments. (D) Knockdown of *KLHL42* impairs SMAD2 nuclear translocation upon TGF-β1 treatment. (E) Immunoblot analysis of fibrotic products following *KLHL42* Knockdown and prolonged TGF-β1 treatment. (F) Quantification of Fibronectin signal from (D), data and means ± SD of 3 independent experiments. (G) Immunoblot analysis of SMAD2 activation following *KLHL42* Knockdown and TGF-β1 treatment. (H) Quantification of phosphorylated SMAD2 (Ser465/467) to total SMAD2 signal from (F), data and means ± SD of 4 independent experiments, *P < 0.05, **P < 0.01, ***P < 0.001, relative to controls or as indicated by one-way ANOVA with Tukey's test of multiple comparisons (C) or two-tailed Student's t-test (F, H). Scale bar = 20µm (D).

60

2.2.5 Unbiased determination of PPP2R5e as a putative KLHL42 substrate

Ubiquitin E3 ligases primarily exert biologic function through the targeted ubiquitination and degradation of substrate proteins. To uncover the putative KLHL42 substrate we conducted unbiased ubiquitin proteomics mass spectrometry. We utilized LifeSensors *Tandem Ubiquitin Binding Entities* (TUBE) technology to purify ubiquitinated proteins from *Control* or *KLHL42* siRNA-treated SSc fibroblasts prior to mass spectrometry(214, 215) (Figure 16A). This technology uses multiple ubiquitin binding moieties linked to resin to affinity purify poly-ubiquitinated proteins from the lysate. Our hypothesis was that the putative KLHL42 substrate protein would be less ubiquitinated in *KLHL42* siRNA-treated cells (KLHL42-depleted) relative to control. Less ubiquitinated substrate would prevent its precipitation with the TUBE pull-down and thus the candidate substrate would be less represented in the proteomics study. The study detected 2486 total proteins, among which 155 were detected to be directly ubiquitinated (Figure 16B). Among the detected proteins, 291 unique proteins were detected in solely the *KLHL42* knockdown, 464 found only in the control sample, and 1731 were found in both samples (Figure 16C). We focused our analysis on proteins disproportionately represented on the *Control* siRNA treatment relative to *KLHL42* siRNA, (464 proteins) as these proteins may have been less ubiquitinated when *KLHL42* was silenced.

We analyzed the sub-set of interest for any gene ontology terms that would be enriched relative to the total dataset using *Gene Ontology enRIchment anaLysis and visuaLizAtion tool* (216). We observed that several ontologies terms were significantly enriched in the *Control* siRNA treatment group relative to the total dataset (Figure 16D), including Protein Phosphorylation. This suggests that proteins disproportionately represented in the Control siRNA group (and potential KLHL42 substrates) may be involved with protein phosphorylation. Next, we investigated the set

of proteins detected to be directly ubiquitinated and only found in the *Control* siRNA treatment

group for their relevance to the enriched gene ontologies (49 proteins). Of these proteins, the

Protein phosphatase 2A regulatory subunit epsilon (PPP2R5e) was one of the proteins to be

detected as directly ubiquitinated and is related to the process of protein phosphorylation. PPP2R5e

functions as a regulatory subunit for Protein phosphatase 2A (PP2A)(217, 218). Intriguingly, PP2A

has been implicated in regulation of fibrotic and TGF-β signaling, including SSc patient samples,

suggesting PPP2R5e might function through this pathway in SSc and be a candidate substrate of

KLHL42 (219-221).
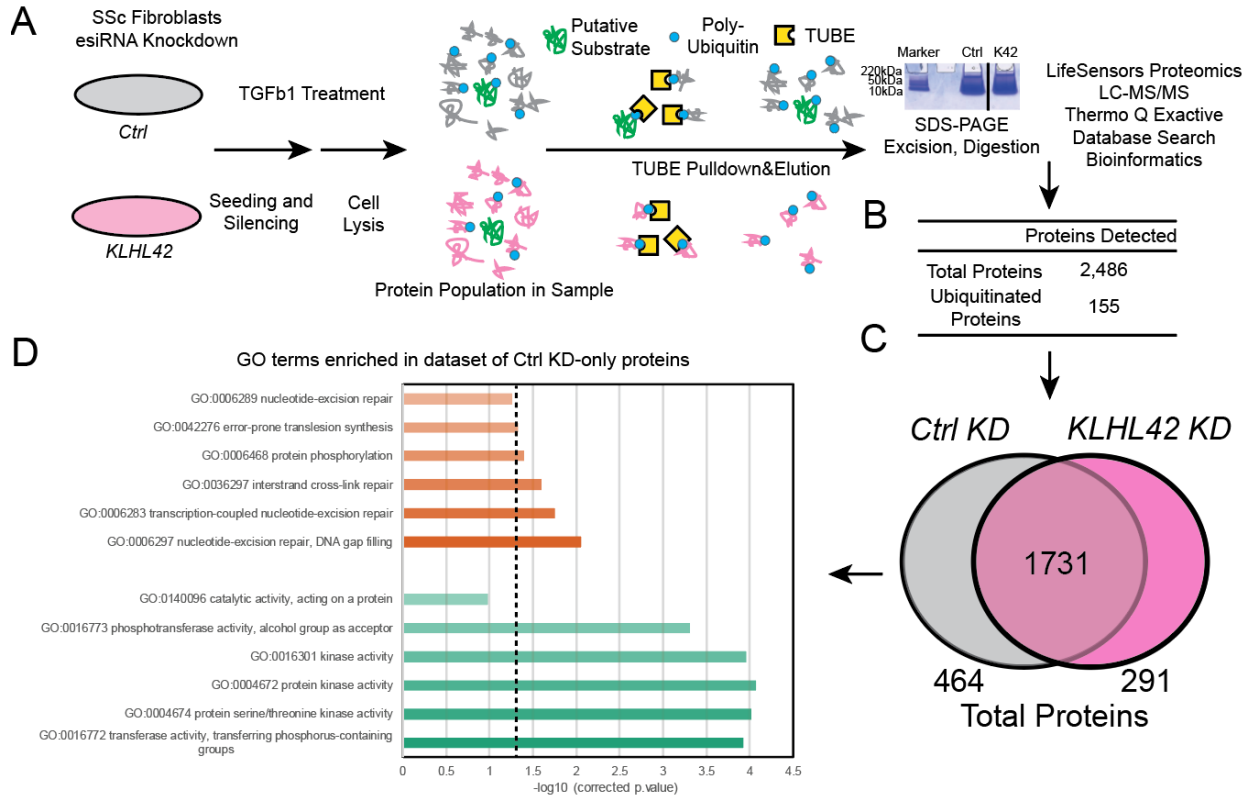
Figure 16 Ubiquitin Proteomics Screen Uncovers PPP2R5e as a potential KLHL42 substrate

(A) Schematic of ubiquitin proteomics experiment to find KLHL42 substrates. SSc cells were treated with control or *KLHL42* siRNA, treated with TGF-β1 prior to lysis and precipitation of ubiquitinated proteins with TUBE technology. Precipitated proteins were then subjected to mass spectrometry analysis _more needed. (B) Total proteins detected from ubiquitin proteomics. 155 unique proteins were detected to be directly ubiquitinated. (C) Overlap of unique proteins detected between control and *KLHL42* siRNA treatments. Proteins in the *Control* KD-only set were considered potential substrates of KLHL42. (D) Proteins detected in the *Control* KD-only set were queried for gene ontology (GO) terms significantly enriched relative to the total dataset – several phosphorylation related terms were

significantly enriched. The protein phosphatase 2A regulatory subunit PPP2R5e was detected in the *Control* KD-only set and directly detected to be ubiquitinated, and is a candidate substrate of KLHL42.

2.2.6 Detected PPP2R5e ubiquitination on Lysine-84 controls protein stability

The ubiquitin proteomics assay on SSc fibroblasts detected that PPP2R5e was directly ubiquitinated, with the highest probability on lysine 84 (Figure 17A). Given the proximity of two other lysine residues to Lys-84, (Lys-86, Lys-89), there was a chance the detected ubiquitination was on these Lys site instead of Lys-84. Initial data analysis used a minimum localization probability of 0.75 to remove ambiguous sites. Previous proteomic studies have detected PPP2R5e to be ubiquitinated, with several other lysines corroborated by multiple studies (Lys-41, -346, -449, -456)(222) (Figure 17B). To validate PPP2R5e as a ubiquitinated substrate from the proteomics assay, and to understand the ubiquitination mechanism on PPP2R5e, we constructed Lys to Arg mutants point mutants corresponding to detected ubiquitin conjugation sites and the results of our analysis (Lys-84, -86, -89). These constructs were expressed in cells and subjected to cycloheximide (CHX) chases to assay PPP2R5e protein stability (Figure 17C-F). We observed wild-type (WT) PPP2R5e showed instability by 8 hours of treatment, as did other lysine→arginine mutants except for K84R. The persistence of this mutant suggests K84 is a critical ubiquitination site for PPP2R5e stability.
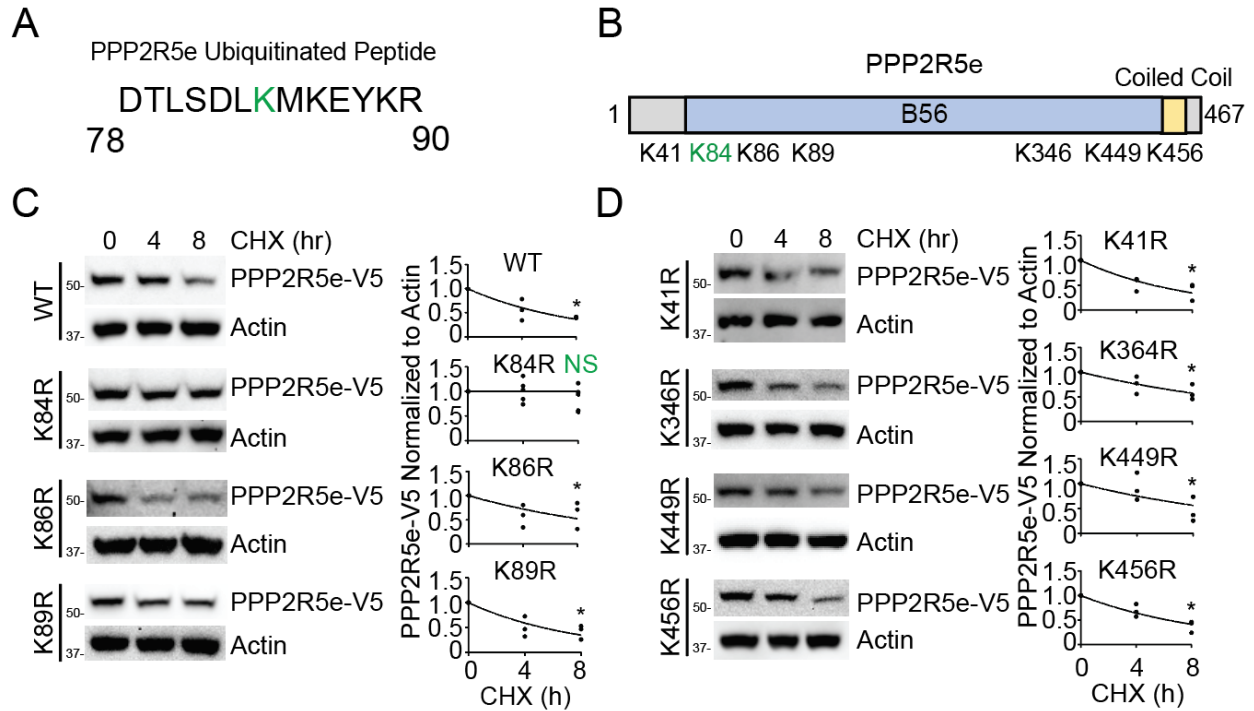
Figure 17 Lysine 84 is a candidate ubiquitin acceptor site within PPP2R5e

(A) PPP2R5e peptide identified by ubiquitin proteomics spectrometry, with high probability of ubiquitin remnant on Lys-84. (B) Schematic of detected ubiquitin modifications of PPP2R5e from post-translational modifications database (Phosphosite). Potentially modified lysine sites from this study (Lys-84, 86, 89) are included. (C) Immunoblot analysis of PPP2R5e-V5 protein and Lys-Arg mutants of suspected Lys sites from this study following cycloheximide (CHX) time course. Data of 3-5 independent experiments. (D) Immunoblot analysis of PPP2R5e-V5 protein and Lys-Arg mutants of Lys sites from other studies following cycloheximide (CHX) time course. Data of 3 independent experiments. *P $<$ 0.05; NS P$>$0.05, by F-test comparisons of nonlinear regression (one-phase decay), with the null hypothesis that rate constant k = 0 (C-D).

2.2.7 KLHL42 binds PPP2R5e and facilitates in poly-ubiquitination and degradation

Finally, to validate PPP2R5e as a bona-fide substrate of KLHL42, we investigated the mechanism of ubiquitination. Endogenous PPP2R5e immunoprecipitated from KLHL42 siRNA-treated SSc fibroblasts showed less ubiquitination relative to control (Figure 18A). As an orthogonal approach, we ectopically expressed KLHL42-HA with HIS-tagged PPP2R5e prior to HIS pull-down and ubiquitin blotting. We observed that KLHL42 co-expression enhanced the poly-ubiquitin signal detected upon PPP2R5e precipitation (Figure 18B). As substrate poly-

ubiquitination often signals for degradation, we probed if KLHL42 depletion affected PPP2R5e protein level, and observed *KLHL42* knockdown led to significantly increased PPP2R5e signal relative to control (Figure 18C-D). We utilized other airway cells, BEAS-2B to ectopically express KLHL42, and we observed a significant dose-dependent decrease in PPP2R5e protein level (Figure 18E). Further, the critical lysine site PPP2R5e mutant, K84R, proved resistant to co-expression with KLHL42 (Figure 18F-lane 4), relative to wild-type PPP2R5e (Figure 18F-lane 2), suggesting KLHL42 mediates the protein stability of PPP2R5e through Lys-84. These data suggest KLHL42 regulates PPP2R5e ubiquitination and protein stability. Finally, we investigated the role of PPP2R5e on fibrotic signaling in SSc cells (Figure 18G-I). We observed significantly decreased PPP2R5e protein upon siRNA treatment (Figure 18G-I). PPP2R5e KD resulted increased fibrotic production upon TGF-β1 treatment as measured by fibronectin protein relative to control siRNA (Figure 18G, H). These data suggest a role for the KLHL42-PPP2R5e degradation axis in fibrotic SSc signaling, as KLHL42 functions as a pro-fibrotic mediator degrading the PP2A-enhacing subunit PPP2R5e and resulting in increased fibrotic signaling (Figure 18G).
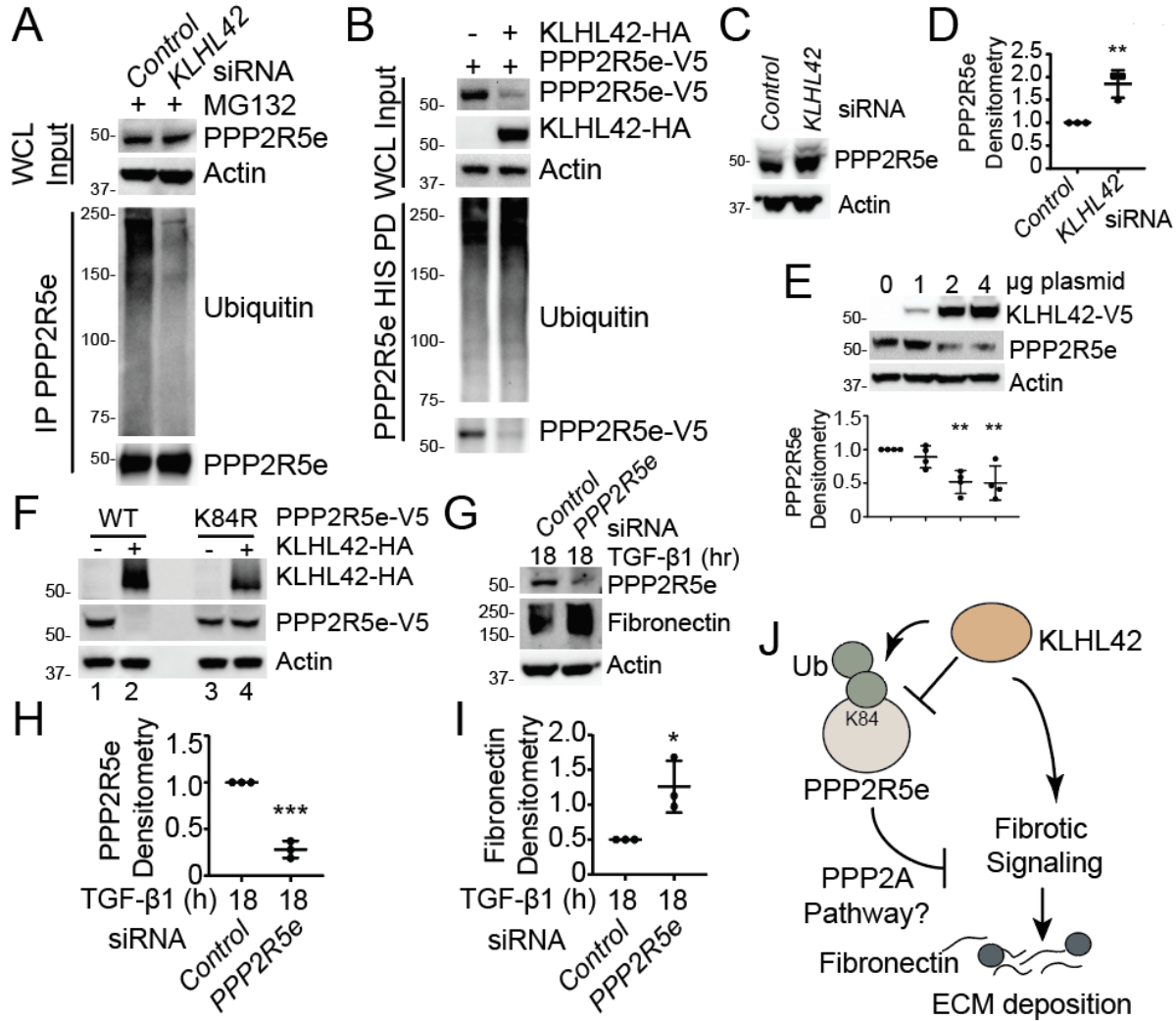
Figure 18 PPP2R5e is a KLHL42 substrate, and PPP2R5e affects TGF-β signaling in SSc

(A) Immunoblot validation of ubiquitin proteomics assay; PPP2R5e protein was immunoprecipitated from SSc cells with control or KLHL42 siRNA treatments. (B) Immunoblot analysis of in vivo ubiquitination assay in SSc cells, as PPP2R5e-V5-HIS protein pull down was subjected to ubiquitin immunoblotting. (C) Immunoblot analysis of PPP2R5e level protein following control or KLHL42 siRNA treatments. (D) Densitometry of (C). Data and means ± SD of 3 independent experiments. (E) Immunoblot analysis of PPP2R5e protein following dose OE of KLHL42-V5 plasmid. Data and means ± SD of 4 independent experiments. (F) Wild-type or K84R mutant PPP2R5e-V5 was expressed without or with co-expression of KLHL42-HA prior to blotting. (G) SSc cells were treated with PPP2R5e siRNA prior to 18hr TGF-β1 treatment and immunoblotting. (H-I) Densitometry of PPP2R5e (H) and Fibronectin (I) Protein without and with PPP2R5e knockdown and 18hr TGF-β1 treatment. Data and means ± SD of 3 independent experiments. (J) Schematic of proposed model, in which KLHL42 controls the ubiquitination and stability of PPP2R5e. PPP2R5e affects PP2A anti-fibrotic activity and downstream fibrotic signaling, leading KLHL42 to be a pro-fibrotic regulator in SSc. *P < 0.05, ***P < 0.001, by two-tailed Student's t-test (D, H, I). **P < 0.01, by ANOVA, with Dunnett's test for multiple comparisons (E).

2.2.8 Discussion

This study demonstrated SMAD2/3 immunostaining and automated microscopy as a screening tool for SSc cells. We calculated a *translocation ratio* of SMAD signal, as a surrogate for TGF-β pathway activity. This assay system is robust and shows good assay parameters with a Z-factor of 0.38. We observed that the knockdown of the e3 ligase Kelch-like protein 42 (KLHL42) acutely affects SMAD localization and affects downstream TGF-β/fibrotic signaling, suggesting KLHL42 is a pro-fibrotic E3 ligase. To uncover potential KLHL42 substrates, we conducted unbiased mass spectrometry ubiquitin proteomics. Through bioinformatic analysis, the Protein phosphatase 2A regulatory subunit epsilon (PPP2R5e) emerged as a putative substrate, and we confirmed Lysine 84 as a critical site for PPP2R5e stability through unbiased proteomics and mutagenesis assay. Finally, we demonstrated that KLHL42 facilitates the poly-ubiquitination of PPP2R5e leading to its degradation, and that knockdown of PPP2R5e increases fibrotic protein production, potentially through the PP2A pathway.

Phosphatase control of TGF-β signaling is a major mechanism in SSc. PP2A has been shown to play a direct role in regulating fibrotic signaling in primary SSc disease models. TGF-β treatment was observed to affect PP2A modulation of ERK1/2 activation in SSc fibroblast-autocrine signaling (223). ERK activation has been directly implicated in dysfunction mechanics from SSc fibroblasts, and has been observed to be constitutively activated in fibroblasts (224, 225). Further, TGF-β treatment to dermal fibroblasts causes PP2A decrease in transcript/protein levels (220). The regulatory subunit PPP2R5e belongs to the B56/B' family and modulates overall PP2A activity(217). PPP2R5e expression directly leads to more de-phosphorylation of PP2a substrates, suggesting PPP2R5e is an enhancer of PP2a activity (218). This is in line with our functional observations, as we observed PPP2R5e knockdown led to increased fibrotic signaling. Most

research has emphasized the role of PPP2R5e in neoplasia; this is the first study to suggest a function in SSc-ILD fibrotic signaling. More study is needed to characterize the exact molecular mechanisms of KLHL42 control of PPP2R5e and PP2A signaling.

E3 ligases may play an important role in SSc-ILD signaling. Our previous studies have shown E3 ligases can potently control fibrotic signaling through the targeted degradation of key signal transduction (141). There is evidence that this paradigm can be extended to SSc-ILD fibrotic signaling as well (226, 227). Further, therapeutic targeting of ubiquitination may show promise in lung fibrotic diseases. Recent studies have shown inhibition of the E3 ligase Skp2 ameliorates fibrotic phenotypes in mice (228), and pharmacological inactivation of Cullin-type E3 ligases was protective in experimental pulmonary fibrosis models (207). Current therapeutic options in SSc-ILD are limited, and ubiquitin E3 ligases may prove new targets for intervention.

In conclusion, we utilized two unbiased approaches (siRNA screen and proteomics) to discover the ubiquitin e3 ligase KLHL42 as a mediator of fibrotic signaling in SSc-ILD, through the regulation of PPP2R5e ubiquitination and stability.

2.2.9 Experimental procedures

2.2.9.1 Materials

PPP2R5e cDNA was from DNASU HsCD00735088 (229). QuikChange II XL Site-Directed Mutagenesis Kit (200521) was from Agilent. BEAS-2B (CRL-9609) were from ATCC. Anti-HA-Tag (6E2) (2367S), -Ubiquitin (P4D1) (3936,), -Phospho-Smad2 (Ser465/467) (138D4) (3108), and -Smad2/3 (D7G7) (8685) were from Cell Signaling Technology. 384-well glass bottom tissue culture plates (P384-1.5H-N) were from Cellvis. Antibiotic-Antimycotic Supplement (15240062), DMEM media (10569044), DMEM-F12 (11330057), FBS (26140079),

Pen-Strep (15140122) were from Gibco. Lullaby siRNA transfection reagent (LL7) was from OzBiosciences. hTGF-β1 (100-21) was from PeproTech. Anti-PPP2R5e (NBP1-79638,) was from Novus. TnT T7 Quick Coupled Transcription/Translation (L1170) was from Promega. Anti-Fibronectin (EP5) (sc-8422,) and -PPP2R5e (A-11) (sc-376176) were from Santa Cruz. His-Tag Dynabeads (10103D) and Hoescht 33342 (H3570) were from Invitrogen. Anti-beta-Actin(AC-15)(A5441) was from Sigma-Aldrich. Anti-Rabbit IgG, Alexa Fluor 488 (A-11008), anti-V5 Tag (R960), Protein A/G Magnetic Beads (88802), pcDNA3.1D TOPO Kit (K490001), were from Thermo Fisher. Primers for cloning and dsiRNA were from IDT. Custom siRNA library was from SigmaAldrich. Anti-Mouse IgG HRP (18-8817-30) and -Rabbit IgG HRP (18-8816-31) were from Rockland Immunochemicals. MG-132 (F1101) was from UBP BIO. Cytation5 was from BioTek.

2.2.9.2 Cell Culture

Primary SSc patient lung fibroblasts were cultured in DMEM (Gibco) according to previous technique (209, 230). Beas-2b cells were from ATCC and cultured in HITES media supplemented with 10% FBS. Cells were treated with cycloheximide (100μg/mL). Cells were transfected with Nucleofector 2b (Amaxa), XtremeGene HP Plasmid reagent (Roche), XtremeGene siRNA reagent (Roche) or Lullaby siRNA reagent (OzBiosciences). TGF-β1 (Peprotech) was treated at 2ng/mL for indicated times in DMEM without FBS supplement.

2.2.9.3 siRNA Transfection

Cells were seeded to a confluency of 50% before siRNA transfection. siRNA was transfected using Lullaby siRNA reagent (OzBiosciences). 1µg of siRNA was mixed with 10uL

of Lullaby reagent in 1/10th of final cell volume for 25min and added dropwise to cells. Knockdown proceeded for 48-72hr prior to cell collection and analysis. Sequences of dsiRNA used:

KLHL42 siRNA 1:

5'rCrUrUrArUrCrArGrUrGrUrCrCrUrUrGrArCrArArGrCrATT3'

5'rArArUrGrCrUrUrGrUrCrArArGrGrArCrArCrUrGrArUrArArGrArA3

KLHL42 siRNA 2:

5'rArCrUrCrUrGrArArArUrUrArUrCrUrGrArUrArUrUrUrUGT-3'

5'rArCrArArArArUrArUrCrArGrArUrArArUrUrUrCrArGrArGrUrGrU-3'

PPP2R5e siRNA:

5'rCrArGrCrUrArArUrUrArUrGrGrArUrArUrUrGrUrCrArUCT-3'

5'rArGrArUrGrArCrArArUrArUrCrCrArUrArArUrUrArGrCrUrGrArC-3'

TGFBR1 siRNA:

5'rGrUrUrUrGrArArUrArUrUrCrUrCrArCrArUrCrArArGrCTT-3'

5'rArArGrCrUrUrGrArUrGrUrGrArGrArArUrArUrUrCrArArArCrArU-3'

2.2.9.4 Immunoprecipitation and Immunoblotting

Cells were lysed in immunoprecipitation (IP) buffer (50 mM Tris HCl pH 7.6, 150 mM NaCl, 0.25 % v/v Triton-X-100) for two hours at +4C with 1:100 dilution of immunoprecipitating antibody. Antibody was captured with Protein A/G beads (ThermoFisher) for an additional two hours. Immunoprecipitate was washed 3 times with IP buffer, and eluted in 1x Laemmli buffer at 88°C for five minutes prior to immunoblotting analysis. Immunoprecipitated samples were blotted with Anti-Mouse or Anti-Rabbit TrueBlot (Rockland).

2.2.9.5 Cloning

Recombinant DNA constructs were prepared through PCR cloning techniques and cloned into pcDNA3.1D vector (ThermoFisher) unless otherwise noted. Point mutants were generated with QuickChange XL 2 site-directed mutagenesis kit (Aglient). All constructs were validated by DNA sequencing (Genewiz).

2.2.9.6 Ubiquitination siRNA SMAD translocation Screen

Primary SSc patient lung fibroblast cells were seeded in 384-well glass-bottom plates (Cellvis) (5,000 cells per well) and were transfected with MISSION esiRNA targeting ubiquitination proteins (E1, E2, E3 ligases etc.) (Sigma-Aldrich) using XtremeGene siRNA transfection reagent (Roche). Knockdown proceeded for 72 hours prior to TGF-β1 (Peprotech) (2ng/mL) stimulation for 1 hour. Cells were then fixed (4% paraformaldehyde), permeabilized (0.5% Triton-X-100) and stained for endogenous SMAD2/3 (Cell Signaling) followed by Goat anti-Rabbit Alexa Fluor 488 or 647 (Invitrogen) and nuclear counterstain with Hoescht 33342 (Invitrogen). Fluorescent signal was imaged using Cytation5 (BioTek) or Image Express (Molecular Devices). SMAD2/3 Translocation Ratio (Nuclear to Cytosolic signal) was calculated and analyzed by either cell profiler (231) or Gen5 software (BioTek).

2.2.9.7 Ubiquitin Proteomics

Ubiquitin proteomics and TUBE experiment were conducted at *LifeSensors* (Malvern, USA). Experimental and Control samples were analyzed using biological duplicates. Usage of biological replicates allowed for better accounting of variability among each step of the mass spectrometry workflow (cell culture, sample preparation, analysis).

Samples were spun down, and duplicate 22 ul volumes of each sample were mixed with SDS loading buffer. Samples were heated at 90°C for 5 min, and run on SDS-PAGE prior to Coomassie Blue staining. Remaining sample was run on a different gel, resulting in each sample being run on a total of 3 gel lanes. The lanes were excised, reduced with TCEP, alkylated with iodoacetamide, and digested with trypsin. Tryptic digests were analyzed using a 150 min LC run on a Thermo Q Exactive HF mass spectrometer. A 30 min blank was run between samples.

Ubiquitin proteomics resulted in 4 RAW files, two each for KLHL42 siRNA treatment and control siRNA treatment. MaxQuant 1.6.2.3 was used to query MS data against the Uniprot human database (2018_10_01); 196,371 entries were specifically searched. First search peptide mass tolerance was set at 20ppm; main search peptide tolerance was set at 4.5 ppm. Fragment ion mass tolerance was set at 20ppm. Protein, peptide and site false discovery rate was set at 1%. Full trypsin specificity was used to generate peptides, with a maximum of 3 missed cleavages permitted. Carabimidomethyl (C) was set as a fixed modification, with Acetyl (Protein N-term), Oxidation (M), and GlyGly (K) considered as variable modifications.

Protein quantification was performed using Razor + unique peptides. Razor peptides are shared (non-unique) peptides assigned to the protein group with the most other peptides (Occam's razor principle). Quantitation was based on the sum of the peptide MS peak areas for the protein (Intensity), due to its increased accuracy compared to MS/MS count. To account that larger

proteins will generate more peptides, the intensity values were adjusted by normalizing against the number of theoretical peptides for each protein (iBAQ intensity). We then sorted (largest to smallest order) on the iBAQ values to determine which proteins are more abundant in a sample. Data were then analyzed via Gene Ontology enRIchment anaLysis and visuaLizAtion tool, querying the 464 proteins identified solely in the control siRNA treatments (and thus may have lost ubiquitination when KLHL42 was knocked-down) for their gene ontologies as previously described(216). The set of proteins detected to be directly ubiquitinated and only found in the Control siRNA treatment group (49 proteins) were manually inspected based on their relevance to the enriched gene ontologies, leading to the uncovering of PPP2R5e.

2.2.9.8 Confocal Microscopy

SSc cells were seeded in 35-mm MatTek glass bottom dishes before siRNA knockdown and TGF-β1 treatment. Cells were washed with 1xPBS prior to fixation with 4% paraformaldehyde and permeabilization with 0.5% Triton-x100. Following blocking with 2%BSA in PBS, cells were exposed to SMAD2 primary antibody (1:500) overnight, and then 1:1,000 Alexa Fluor 488– secondary antibodies for immunostaining. The nucleus was counterstained with Hoescht 33342. Cells were visualized with a Nikon A1 confocal microscope using 405 nm, 488 nm, or 567 nm wavelengths. All experiments were done with a 60× oil differential interference contrast objective lens.

2.2.9.9 Statistics

All statistical tests were calculating using Graphpad Prism 8. $P < 0.05$ was used to indicate significance. Densitometry was calculated using ImageJ (NIH).

2.2.10 Acknowledgements

2.2.11 Data Availability

Ubiquitin proteomics data has been uploaded through the MassIVE repository, ID: MSV000084800 (ftp://massive.ucsd.edu/MSV000084800/), The MSViewer Data can be accessed at http://msviewer.ucsf.edu/prospector/cgi-bin/mssearch.cgi?report_title=MS-Viewer&search_key=axtpvumdao&search_name=msviewer; the key is axtpvumdao.

2.2.12 Conflict of interest

The authors acknowledge no conflicts of interest with the contents of this article

3.0 Ubiquitination in Innate Immunity and Inflammation

Innate immunity is a critical mechanism for lung homeostasis and for host defense against infection. During respiratory infection, the pathogens are recognized, pro-inflammatory signaling is initiated, cytokine and other immune stimulated species are released, and cells extravasate into the alveolar space. In some cases, the inflammatory and immunological response is hyperactive, causing damage to the alveolar space itself, and often resulting in catastrophic loss of respiratory function. In this aim we explored the role of protein degradation along multiple steps of the inflammatory process during lung infection, inflammation, and injury, with the goal of identifying new molecular mechanism and new potential targets for chemical targeting.

3.1 RING Finger E3 Ligase PPP1R11 Regulates TLR2 Signaling and Innate Immunity

Adapted from: McKelvey, Lear, Dunn et al, RING Finger E3 Ligase PPP1R11 Regulates TLR2 Signaling and Innate Immunity. *eLife* 2016;5:e18496 DOI: 10.7554/eLife.18496, (232)

In our first sub-aim, we explored the proteolytic regulation of the pattern-recognition receptor, Toll-Like Receptor 2 (TLR2). Lower respiratory infection into the alveolar space results in the accumulation of pathogen-specific molecular patterns, known as PAMPs. These signatures are detected by pulmonary cells through Pattern Recognition Receptors such as TLR2. Receptors then initiate pro-inflammatory signaling to spur an immune response in response to the pathogen invasion. This project investigated the degradation of TLR2 by the RING E3 ligase PPP1R11, and

its effect on the ability to mount an inflammatory response during Gram positive bacterial infection.

3.1.1 Study Overview

Toll-like receptor 2 (TLR2) is a pattern recognition receptor that recognizes many types of PAMPs that originate from gram-positive bacteria. Here we describe a novel mechanism regulating TLR2 protein expression and subsequent cytokine release through the ubiquitination and degradation of the receptor in response to ligand stimulation. We show a new mechanism in which an uncharacterized RING finger E3 ligase, PPP1R11, directly ubiquitinates TLR2 both *in vitro* and *in vivo*, which leads to TLR2 degradation and disruption of the signaling cascade. Lentiviral gene transfer or knockdown of PPP1R11 in mouse lungs significantly affects lung inflammation and clearance of *Staphylococcus aureus*. There is a negative correlation between PPP1R11 and TLR2 levels in white blood cell samples isolated from patients with *Staphylococcus aureus* infections. These results suggest that PPP1R11 plays an important role in regulating innate immunity and gram-positive bacterial clearance by functioning, in part, through the ubiquitination and degradation of TLR2.

3.1.2 Toll-Like Receptors in Innate Immunity

The human toll-like receptor (TLR) family consists of ten family members (TLR1-TLR10)(233). TLRs are single transmembrane pattern recognition receptors that recognize molecules derived from various pathogens, referred to as pathogen-associated molecular patterns (PAMPs)(234-238) . TLRs are highly conserved from invertebrates to mammals, and are essential

for mediating innate immunity and the production of cytokines in response to infectious agents (239). All TLRs share common structural features, including multiple leucine-rich repeats (LRR), a transmembrane domain, and a conserved cytoplasmic Toll−interleukin 1 receptor (IL-1R) domain (TIR domain)(233). Specifically, LRR motifs from individual TLRs provide ligand binding sites for diverse PAMPs, whereas the TIR domain interacts with several intracellular proteins such as MyD88, which is essential for the transduction of downstream signaling (240, 241).

3.1.2.1 The Biologic Role of TLR2

Within the TLR family, TLR2 possesses the unique ability to recognize glycolipids, lipopeptides, lipoproteins, and lipoteichoic acids from gram-positive bacteria. Thus, TLR2 is the key element of innate immunity that defends against gram-positive bacteria (242). TLR2 is expressed not only in immune cells, but is also present in pulmonary alveoli and airway epithelial cells, suggesting that it plays a role in mucosal innate immunity and infection-induced lung injury (171, 243-245). Interestingly, TLR2 deficient mice are highly susceptible to *S. aureus* infection (246), and in humans, a loss-of-function TLR2 mutation has been linked to susceptibility to infectious and inflammatory diseases, faster disease progression, and a more severe course of sepsis in critically ill patients (247-250). These studies illustrate the protective role of TLR2 in response to inflammatory insults and infectious diseases. Therefore, TLR2 augmentation may be a novel therapeutic strategy in the fight against gram-positive infection.

In this study, we characterize a previously undescribed RING finger E3 ligase family member, PPP1R11, and identify its role in regulating cytokine secretion through targeted TLR2 protein ubiquitination and degradation. These studies describe a new molecular mechanism contributing to mucosal innate immunity.

3.1.3 TLR2 polyubiquitination is regulated by RING E3 ligase PPP1R11

We first investigated TLR2 protein degradation using a transformed murine lung epithelial (MLE) cell line. MLE cells express high levels of TLR2 protein (Data not shown). Cells were stimulated with the TLR2 ligand, Pam3CSK4, and TLR2 protein levels decreased after 4 hours. However, co-treatment with the proteasomal inhibitor MG-132 preserved TLR2 protein levels, while treatment with the lysosomal inhibitor leupeptin did not. Further, cell lysates from these treatments were subjected to TLR2 immunoprecipitation and Ubiquitin immunoblotting. High molecular weight ubiquitin signals in TLR2 immunoprecipitate were detected only in cell lysates treated with MG-132 (Figure 19A). Taken together, this suggests that the TLR2 ligand, Pam3CSK4, induces the polyubiquitination and subsequent degradation of TLR2 via the proteasome. We also investigated the type of ubiquitin linkage on TLR2 using a UbiCRest (Ubiquitin Chain Restriction Analysis) assay (114). Polyubiquitinated TLR2 was subjected to several deubiquitinating enzymes (DUB) that target specific ubiquitin linkages (Figure 20A). As shown in Figure 19, USP2, a DUB that non-specifically targets all ubiquitin linkages, completely reduced polyubiquitinated TLR2. We also observed a drastic decrease in TLR2 ubiquitination in the OTUB1 treated sample, which suggests that TLR2 ubiquitination is regulated in part through K48 ubiquitin linkage. We also observed K48-specific ubiquitin linkage of TLR2 following TLR2 immunoprecipitation and immunoblotting (Figure 20B). MG-132 dramatically increased the half-life of TLR2 (Figure 20C) and Ubiquitin overexpression drastically reduced TLR2 protein levels and half-life (Figure 20D, Figure 19C). These studies suggest that TLR2 protein degradation occurs in a ubiquitin-dependent manner.

Next, we tested over fifty E3 ligases that might be involved in TLR2 degradation (Data not shown) and found that overexpression of PPP1R11 decreased TLR2 levels (Figure 21A). Ectopic

expression of PPP1R11 triggered TLR2 degradation in a dose dependent manner (Figure 19D) without affecting its mRNA levels (Figure 21B). Furthermore, ectopic PPP1R11 expression significantly decreased the half-life of TLR2 (Figure 19E), whereas PPP1R11 knockdown markedly increased its lifespan (Figure 19F, Figure 21C). Conversely, we observed no effect on TLR2 decay with the expression and silencing of fellow RING E3 ligase PCGF1 (Figure 21D-E). To confirm PPP1R11 as an authentic TLR2 target, we performed an *in vitro* ubiquitination assay using TLR2 as the substrate and observed polyubiquitination of TLR2 (Figure 19G).

To investigate the *in vivo* relevance of the PPP1R11/TLR2 pathway, we assayed white blood cell (WBC) pellets for PPP1R11 and TLR2 expression in control and S. aureus-infected patients from our Acute Lung Injury Registry and Biospecimen Repository(251). Control patients were mechanically ventilated patients intubated for airway protection without clinical evidence of or risk factors for ARDS (Acute Respiratory Distress Syndrome), while *S. aureus*-infected patients had evidence of *S. aureus* in tracheal aspirates, blood, or both, and had evidence of or risk factors for ARDS. In control patients, we observed no correlation between PPP1R11 and TLR2 levels, but observed a significantly negative PPP1R11/TLR2 correlation in *S. aureus*-infected patients. We interpret these data to suggest that during *S. aureus* infection, TLR2 levels may be attenuated in part by PPP1R11 expression. This study suggests that the PPP1R11/TLR2 pathway may be relevant in the innate immune response to *S. aureus* infection in patients (Figure 21F).

RING finger E3 ligases utilize several unique residues, such as cysteine and histidine, to interact with zinc and form the two RING finger domains required for E3 ligase activity (252). They are characterized by the unique property of auto-ubiquitination (253, 254). We confirmed that PPP1R11 is an authentic ring finger E3 ligase by showing its ability to auto-ubiquitinate in the presence of ubiquitin, E1, and several different E2 conjugating enzymes (Figure 19H). We also

showed that several E2 conjugating enzymes such as UBE2R1 and UBE2D2 preferably interact

with PPP1R11 *in vitro* (Figure 19I). Lastly, we showed that PPP1R11 interacts with endogenous

UBE2D2 through cellular co-immunoprecipitation (Figure 19J). We also selectively mutated

several key residues of PPP1R11 putative RING finger (Figure 22A) and showed their loss-of-

function in inducing TLR2 degradation (Figure 22B). H126 was chosen as negative control since

it is outside of the RING finger domains. The effect of PPP1R11 was specific to TLR2, as ectopic

expression of PPP1R11 did not alter TLR3, TLR7, TLR8, or TLR9 protein levels (Figure 23).

These experiments suggest that PPP1R11 is an authentic RING finger E3 ligase that specifically

induces TLR2 ubiquitination and degradation.
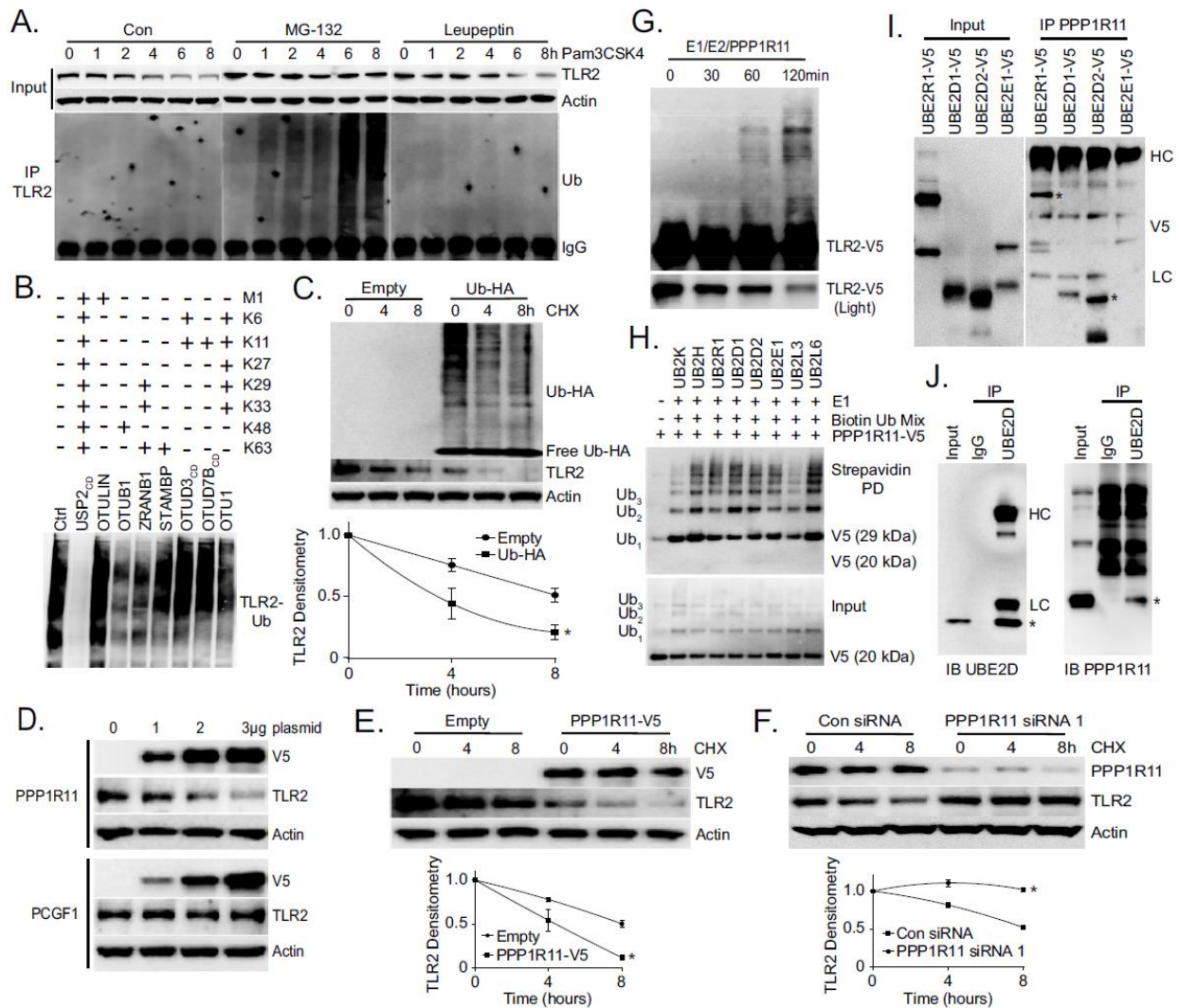
Figure 19 TLR2 polyubiquitination is regulated by PPP1R11

A. Murine lung epithelial (MLE) cells were treated with Pam3CSK4 with or without MG-132 or Leupeptin in a time-dependent manner. Cells were collected and immunoblotted for TLR2 and Actin. Endogenous TLR2 was also immunoprecipitated and followed by Ubiquitin immunoblotting. **B.** MLE cells were pretreated with MG-132 for 18h to induce accumulation of polyubiquitinated TLR2 protein. Endogenous TLR2 was immunoprecipitated using TLR2 antibody and protein A/G beads. After washing, TLR2 beads were then incubated with different DUBs before being assayed for ubiquitin immunoblotting. **C.** TLR2 protein half-life determination in MLE cells transfected with Empty plasmid or Ubiquitin plasmid. Cells were collected and immunoblotted for TLR2, HA, and Actin. Below the panel levels of each protein on immunoblots were quantified densitometrically (Normalized to time zero) and shown graphically. Data represent mean values ± SEM (n=3); *, $p < 0.05$, significant compared to Control, Student's t-test. **D.** Immunoblots showing levels of TLR2 proteins, V5, and Actin after PPP1R11 or PCGF1 plasmid dose over-expression. **E-F.** TLR2 protein half-life determination in MLE cells with empty or PPP1R11 plasmid expression (E); TLR2 protein half-life determination with Control or *PPP1R11 siRNA* expression (F). Below each panel levels of each protein on immunoblots were quantified densitometrically (Normalized to time zero) and shown graphically. Data represent mean values ± SEM (n=3); *, $p < 0.05$, significant compared to Control, Student's t-test. **G.** *In vitro* ubiquitination assay. Purified E1 and E2 components were incubated with TLR2-V5, PPP1R11, and the full complement of ubiquitination reaction components for different lengths of time. **H.** *In vitro* ubiquitination assay. PPP1R11-V5 was incubated with purified E1, varying E2s, biotinylated ubiquitin, and the full complement of

ubiquitination reaction components. The reaction mixture was subjected to streptavidin pulldown prior to V5 immunoblotting. **I.** PPP1R11 protein was immunoprecipitated from cell lysate using a PPP1R11 antibody and coupled to protein A/G beads. PPP1R11 beads were then incubated with *in vitro* synthesized products expressing V5-tagged E2 conjugating enzymes. After washing, proteins were eluted and processed for V5 immunoblotting. **J.** Endogenous PPP1R11 was also immunoprecipitated and immunoblotted for UBE2D.
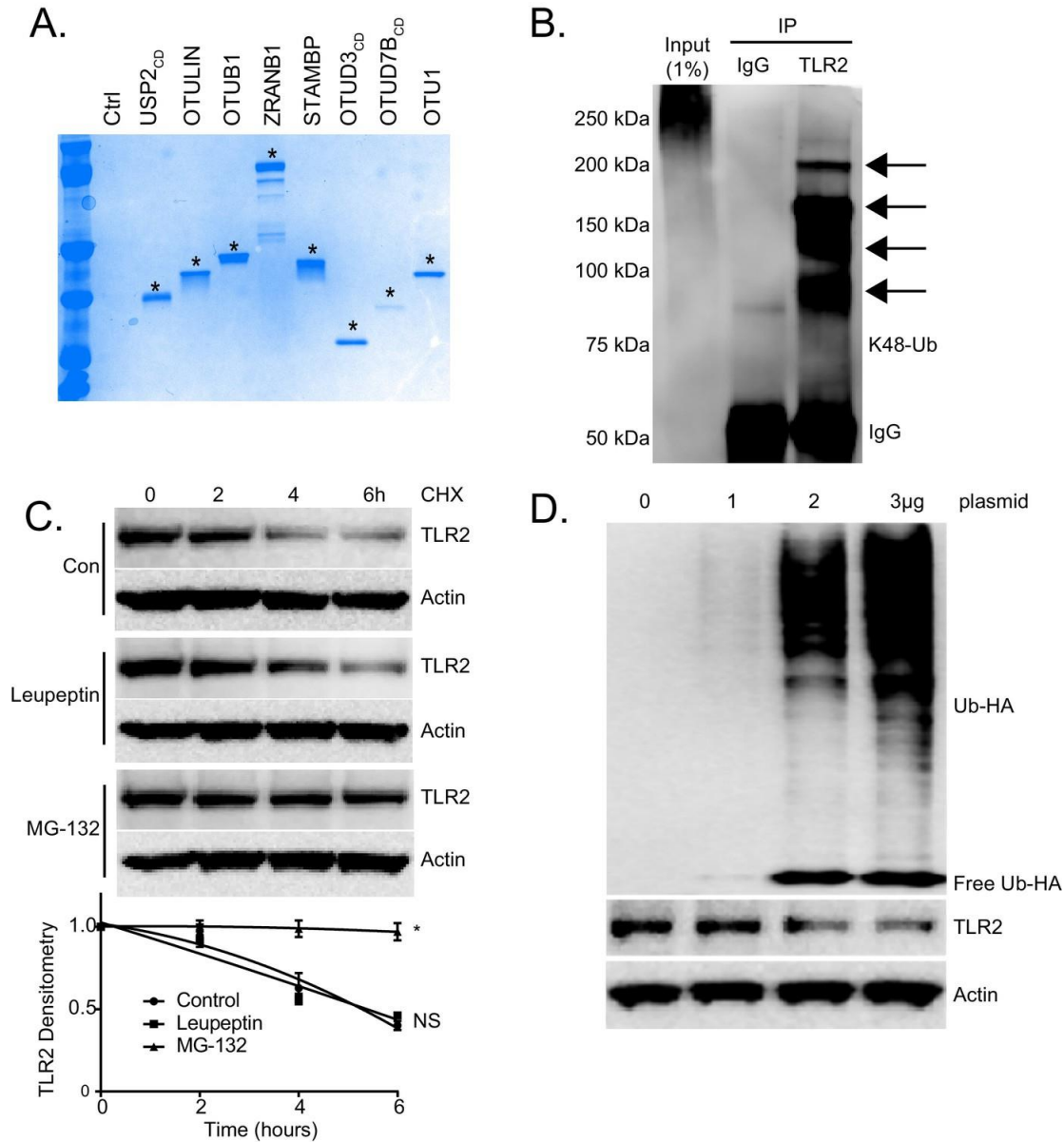
Figure 20 TLR2 is regulated by Ubiquitination

(A) Coomassie blue staining of UBICrest supernatant following DuB assay. Stars represent indicated Dub signal (Figure 1B). (B) TLR2 immunoprecipitation from MLE cells prior to immunoblotting for K48-specific ubiquitin linkages. (C) TLR2 protein half-life study with MG132 or Leupeptin. Below the panel levels of each protein on immunoblots were quantified densitometrically and shown graphically. Data represent mean values ± SEM (n = 3);

*p<0.05, significant compared to Control, Student's t-test. (D) Immunoblots showing levels of TLR2 proteins and HA-Ubiquitin after ectopic Ubiquitin plasmid expression.
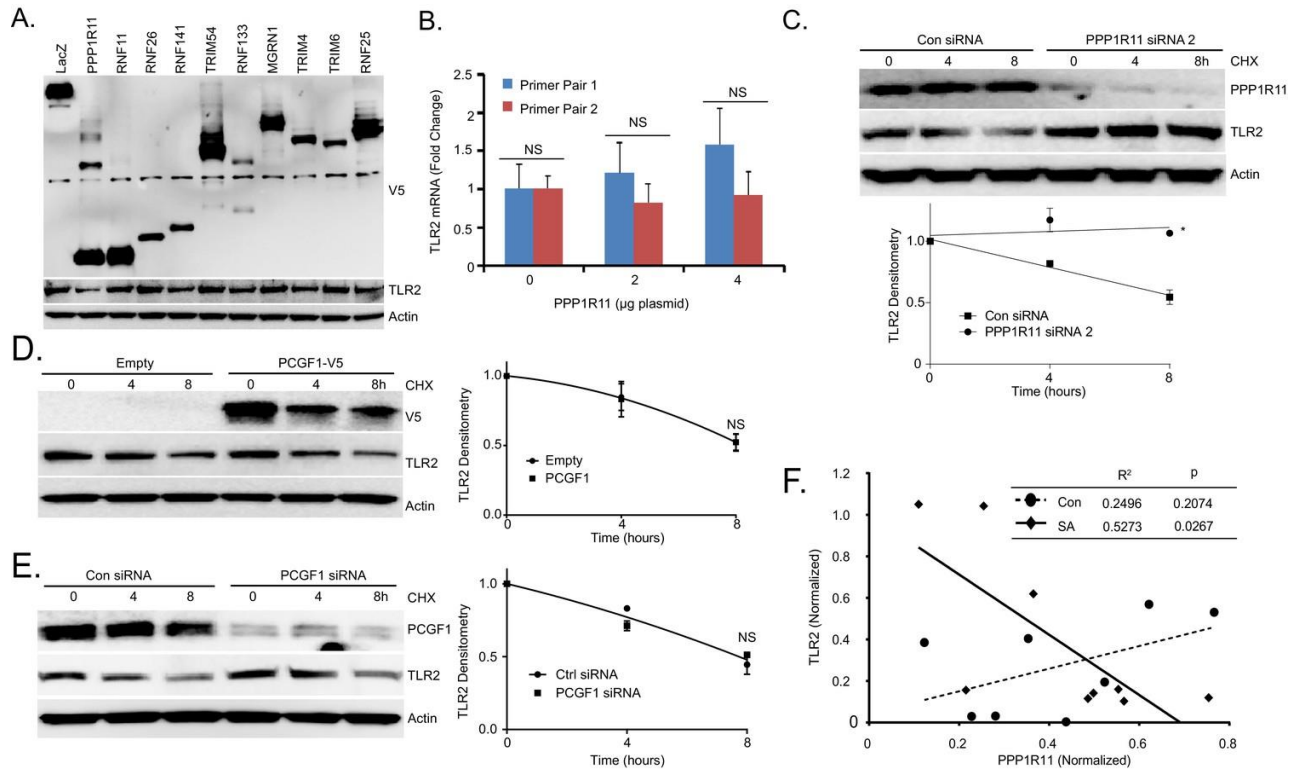
Figure 21 The RING E3 ligase PPP1R11 regulates TLR2 stability

(A) MLE cells were transfected with LacZ or one of the other 10 randomly selected Ring-finger E3 ligases. 18 hr later, cells were collected and immunobloted. (B) TLR2 mRNA levels from MLE cells transfected with increasing amounts of PPP1R11. (C) TLR2 protein half-life determination with CON siRNA or PPP1R11 siRNA expression. Next to the panel levels of each protein on immunoblots were quantified densitometrically (Normalized to Time zero) and shown graphically. The data represent mean values ± SEM (n = 3); *p<0.05, significant compared to Control, Student's t-test (D) Half-life determination with PCGF1 expression and (E) PCGF1 silencing in MLE cells. Next to the panel levels of each protein on immunoblots were quantified densitometrically (Normalized to Time zero) and shown graphically. The data represent mean values ± SEM (n = 3); NS, p>0.05, not significant compared to Control, Student's t-test (F) Correlation between TLR2 and PPP1R11 levels in white blood cell samples from control patients (n = 8) compared to S. aureus-infected patients (n = 9).
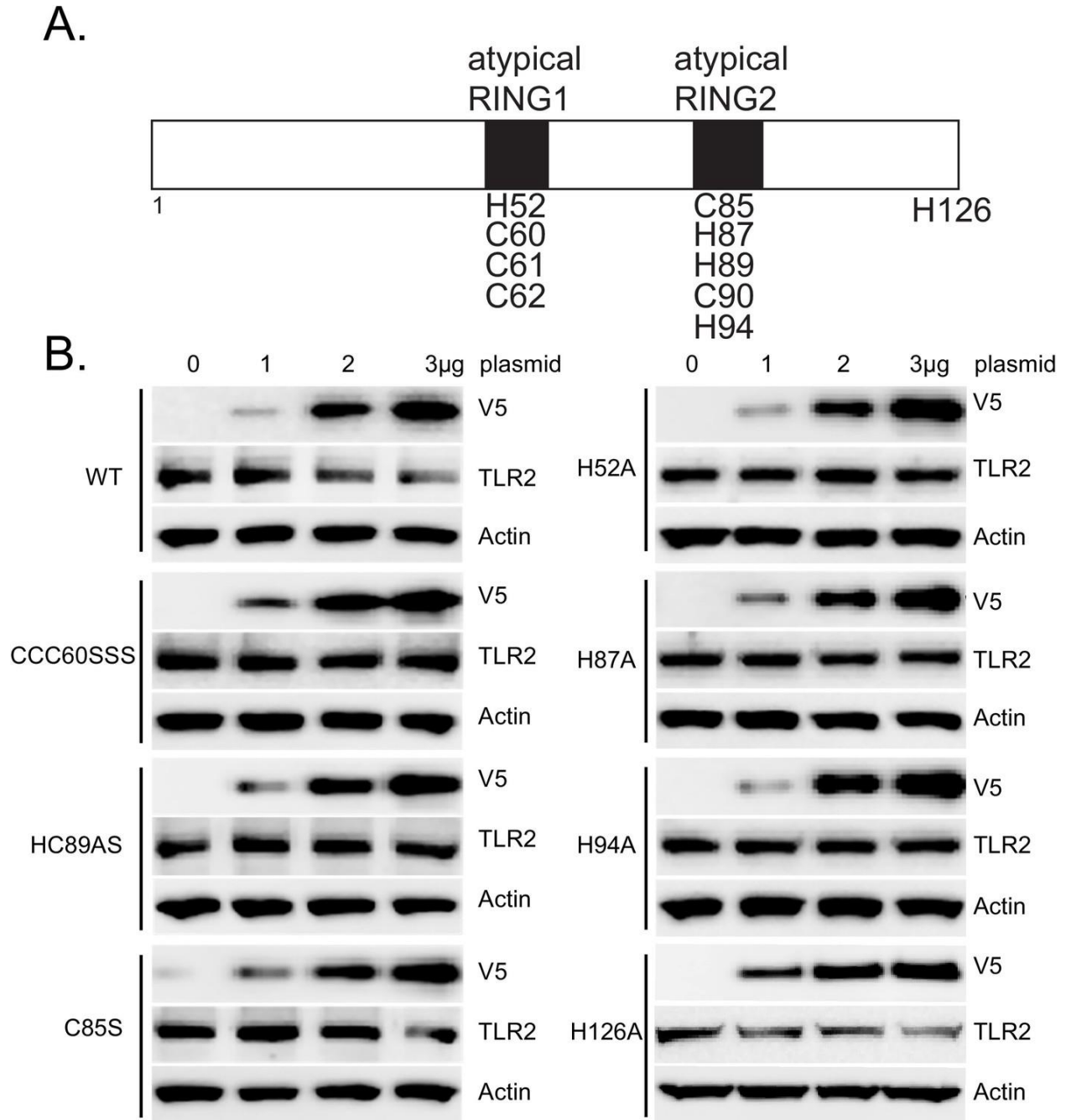
Figure 22 PPP1R11 is a non-canonical RING E3 ligase

(A) Schematic of putative atypical RING domains within PPP1R11. Candidate cysteine and histidine residues are listed, as well as a non-candidate H126. (B) MLE cells were transfected with increasing amounts of plasmid encoding WT or mutant PPP1R11. 18 hr later, cells were collected and immunoblotted for TLR2.
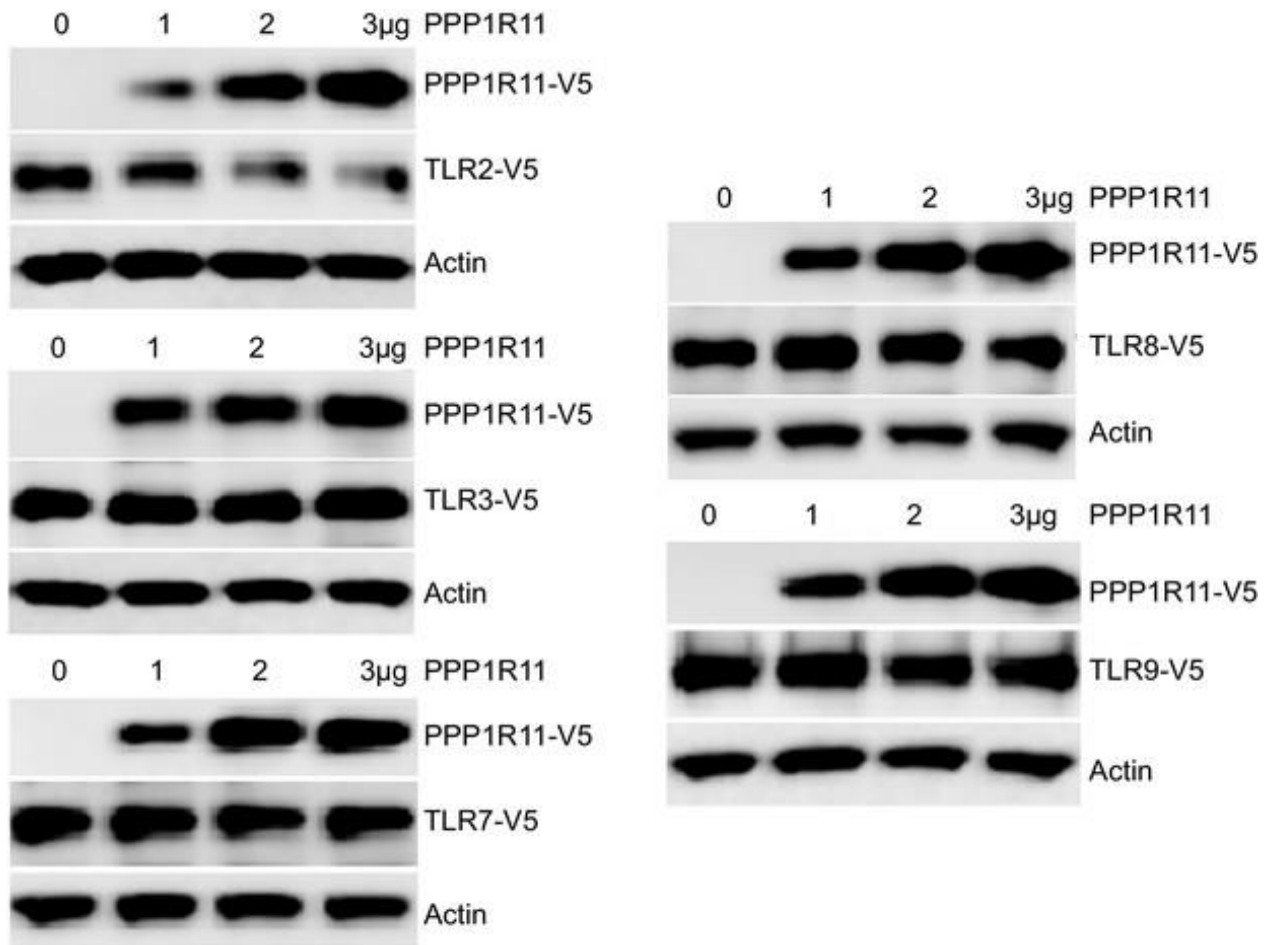
Figure 23 PPP1R11 does not regulate the stability of other TLR receptors

MLE cells were co-transfected with V5 tagged TLRs and increasing amounts of plasmid encoding PPP1R11. 18 hr later, cells were collected and immunoblotted for V5.

3.1.4 PPP1R11 regulates Pam3CSK4-induced TLR2 protein degradation and inflammation

To further elucidate the PPP1R11/TLR2 pathway in cells, we treated MLE cells with the TLR2 ligand, Pam3CSK4. We observed a time-dependent increase in PPP1R11 protein levels and decrease in TLR2 protein levels with this treatment (Figure 24A). Further, cell lysates from these conditions were subjected to TLR2 immunoprecipitation, and high levels of PPP1R11 protein were detected in cells treated with Pam3CSK4 for 4 and 6 hours. PPP1R11/TLR2 association at these time points also reflects the highest degree of TLR2 protein loss (Figure 24A). We also examined the role of PPP1R11 in Pam3CSK4-induced TLR2 protein degradation, and upon ectopic expression of PPP1R11, we observed an accelerated decay of TLR2 protein with Pam3CSK4 treatment (Figure 24B). Last, we performed PPP1R11 knockdown in MLE cells, and we observed stabilized TLR2 protein levels as well as less ubiquitination upon Pam3CSK4 treatment as compared to control siRNA (Figure 24C). TLR2 immunoprecipitation also showed protein ubiquitination beginning at 1 hour post Pam3CSK4 treatment, which is consistent with increased PPP1R11/TLR2 association (Figure 24A). These studies suggest that the TLR2 ligand, Pam3CSK4, induces TLR2 degradation, in part, through the ubiquitination of TLR2 by the E3 ligase PPP1R11.

We also generated a series of TLR2 lysine mutants to further characterize the mechanism of ubiquitin transfer to TLR2. Mutation of lysine 754 to arginine (K754R) within TLR2 resulted in its highest level of stability, a much extended half-life (Figure 25A), and resistance to Pam3CSK4-induced degradation (Figure 25B). K754R TLR2 is also resistant to *in vitro* ubiquitination and degradation during PPP1R11 co-expression (Figure 25C-D). We confirmed that the K754R mutant TLR2 is expressed and localized normally in cells (Figure 25E). This suggests that the extended stability of the TLR2 K754R mutant is due to its inability to be ubiquitinated by

86

PPP1R11 and that K754 is a potential PPP1R11 ubiquitination site within TLR2. Since Pam3CSK4 induces the TLR2 signaling pathway that leads to cytokine release, we hypothesized that by ubiquitinating TLR2, the E3 ligase PPP1R11 is able to suppress the TLR2 signaling pathway. Indeed, ectopic expression of PPP1R11 reduces both IL-6 and CXCL1 cytokines by 40-50% upon Pam3CSK4 treatment (Figure 24D-E), whereas PPP1R11 knockdown significantly increased both IL-6 and CXCL1 cytokine release in MLE cells (Figure 24F-G). Cytokine release upon overexpression and knockdown of fellow RING E3 ligase Trim52 resulted in no significant difference relative to controls (Figure 25F-G). Finally, we embarked on gene editing experiments to confirm the regulatory role of PPP1R11 on TLR2 and cytokine release. Utilizing CRISPR-Cas9 technology, we generated a 2 bp deletion in the first exon of *Ppp1r11* in MLE cells leading to an immediate pre-mature stop codon. Following colony expansion, we assayed protein half-life and observed stabilized TLR2 half-life in the *Ppp1r11* KO cells relative to control (Figure 26A). We also challenged PPP1R11 KO cells with PAM3CSK4, and observed increased IL-6 and CXCL1 cytokine release relative to control cells (Figure 26B-C). From these observations we believe PPP1R11 suppresses TLR2-linked inflammatory signaling.
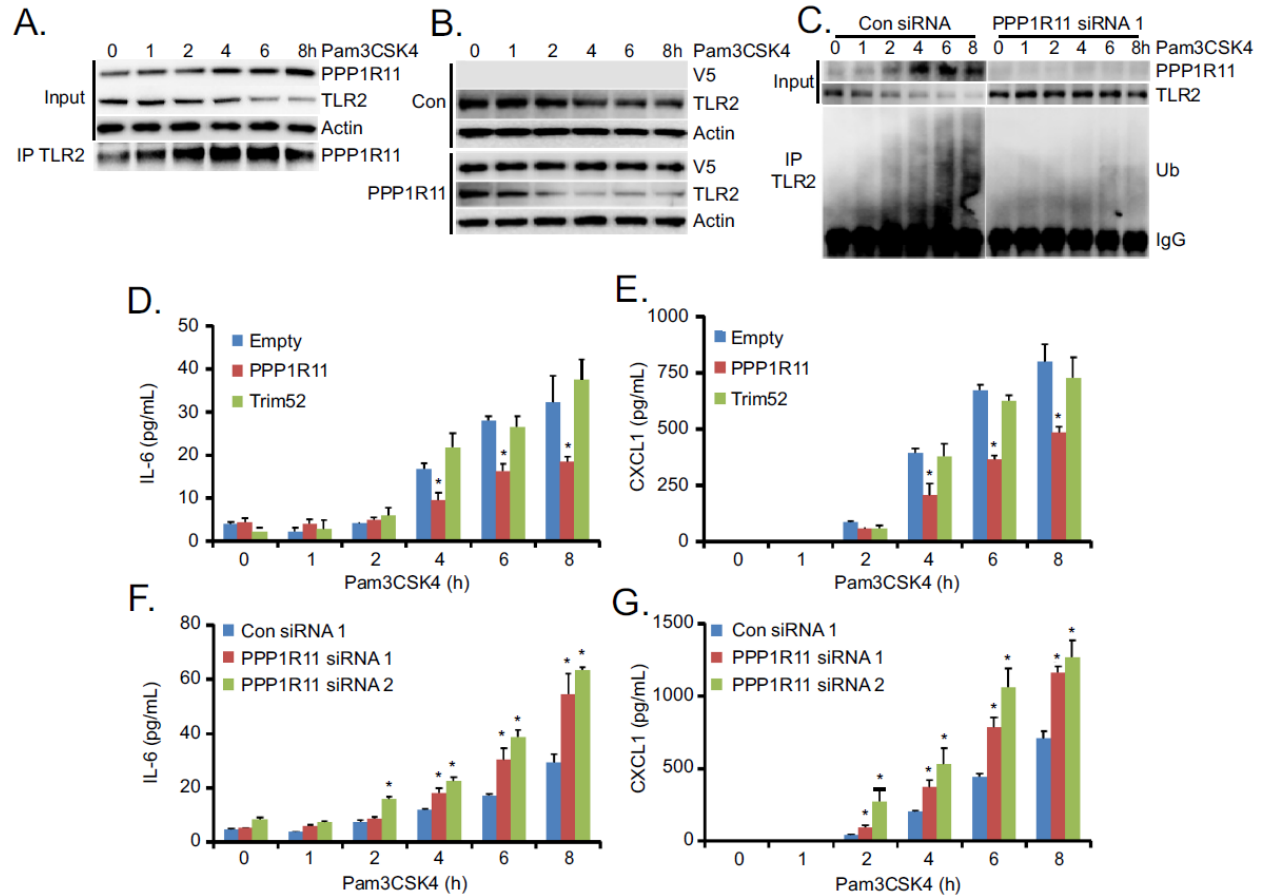
Figure 24 PPP1R11 regulates Pam3CSK4-induced TLR2 protein degradation and inflammation

A. MLE cells were treated with Pam3CSK4 in a time-dependent manner. Cells were collected and immunoblotted for PPP1R11, TLR2, and Actin. Endogenous TLR2 was also immunoprecipitated and immunoblotted for PPP1R11. B. MLE cells were transfected with either empty or PPP1R11 plasmid. 24h later, cells were exposed to Pam3CSK4 in a time-dependent manner. Cells were collected and immunoblotted for V5, TLR2, and Actin. C. MLE cells were transfected with either control or PPP1R11 siRNA. 48h later, cells were exposed to Pam3CSK4 in a time-dependent manner. Cells were collected and immunoblotted for V5, TLR2, and Actin. Endogenous TLR2 was also immunoprecipitated and followed by ubiquitin immunoblotting. D-E. MLE cells were transfected with either empty, PPP1R11, or TRIM52 plasmid. 24h later, cells were exposed to Pam3CSK4 in a time-dependent manner. Cell media was then collected and assayed for IL-6 and CXCL1 (Data represent mean values ± SEM n=4; *, $p < 0.05$, significant compared to Control, Student's t-test). F-G. MLE cells were transfected with either control or *PPP1R11 siRNA*. 48h later, cells were exposed to Pam3CSK4 in a time-dependent manner. Cell media was then collected and assayed for IL-6 and CXCL1 (Data represent mean values ± SEM n=4; *, $p < 0.05$, significant compared to Control, Student's t-test).
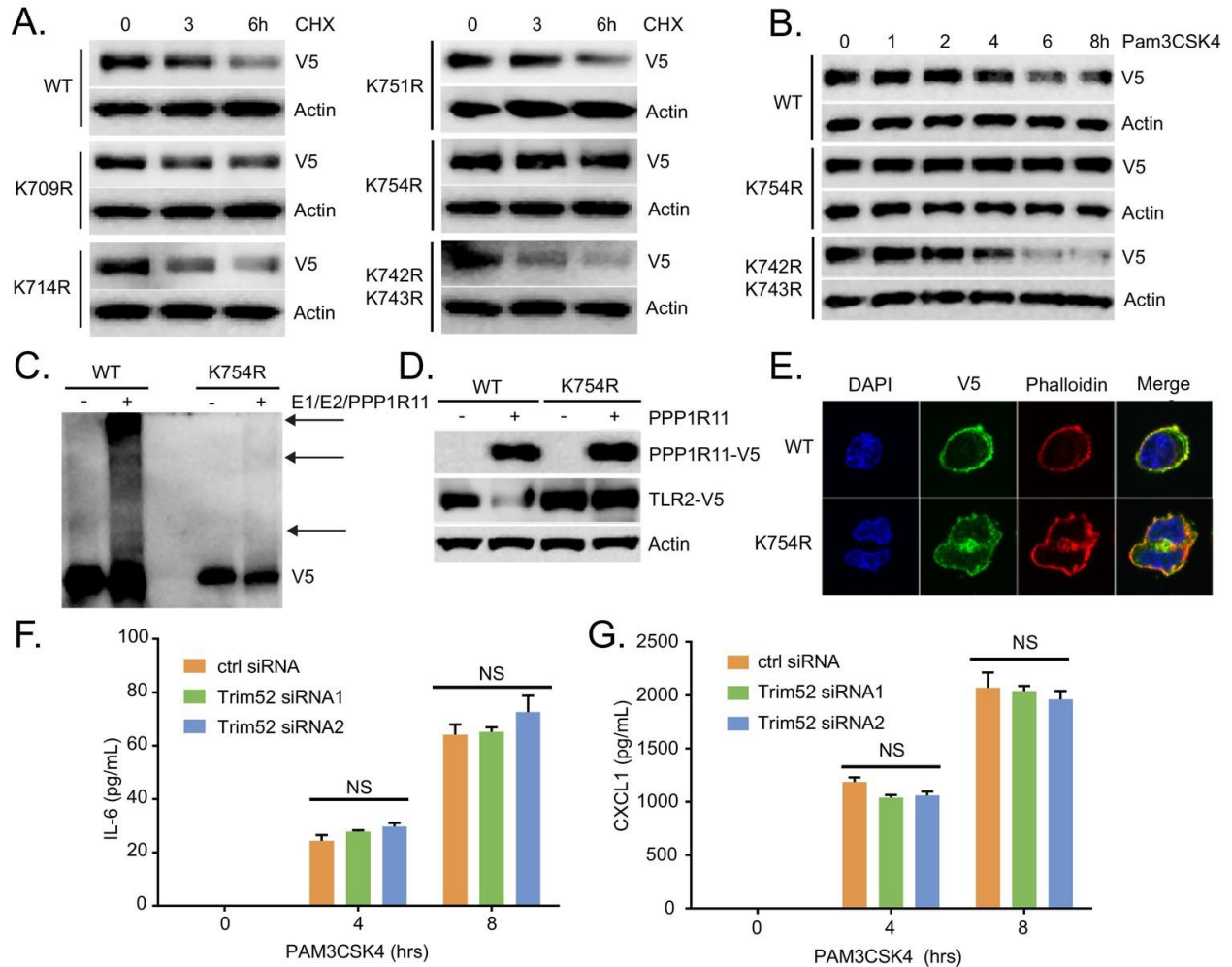
Figure 25 TLR2 ubquitination is regulated through Lysine 754

(A) Half-life study of WT and lysine mutant TLR2 in MLE cells. (B) MLE cells were transfected with WT or mutant TLR2 before Pam3CSK4 treatment. Cells were then immunoblotted for V5-TLR2. (C) In vitro ubiquitination assay using WT or K754R TLR2 as the substrate. (D) MLE cells were co-transfected with WT or TLR2 lysine mutants with or without PPP1R11. Cells were then collected and assayed for immunoblotting. (E) V5 tagged WT and K754R TLR2 were transfected in MLE cells. 18 hr later, cells were fixed, permeabilized, immunostained for V5 (Green). The nucleus was counterstained with DAPI, and F-actin was counterstained with Alexa 488-Phalloidin. (F–G) MLE cells were transfected with either control or Trim52 siRNA. 72 hr later, cells were exposed to Pam3CSK4 in a time-dependent manner. Cell media was then collected and assayed for IL-6 and CXCL1 (Data represent mean values ± SEM n = 3; NS, p>0.05, not significant compared to Control, Student's t-test).
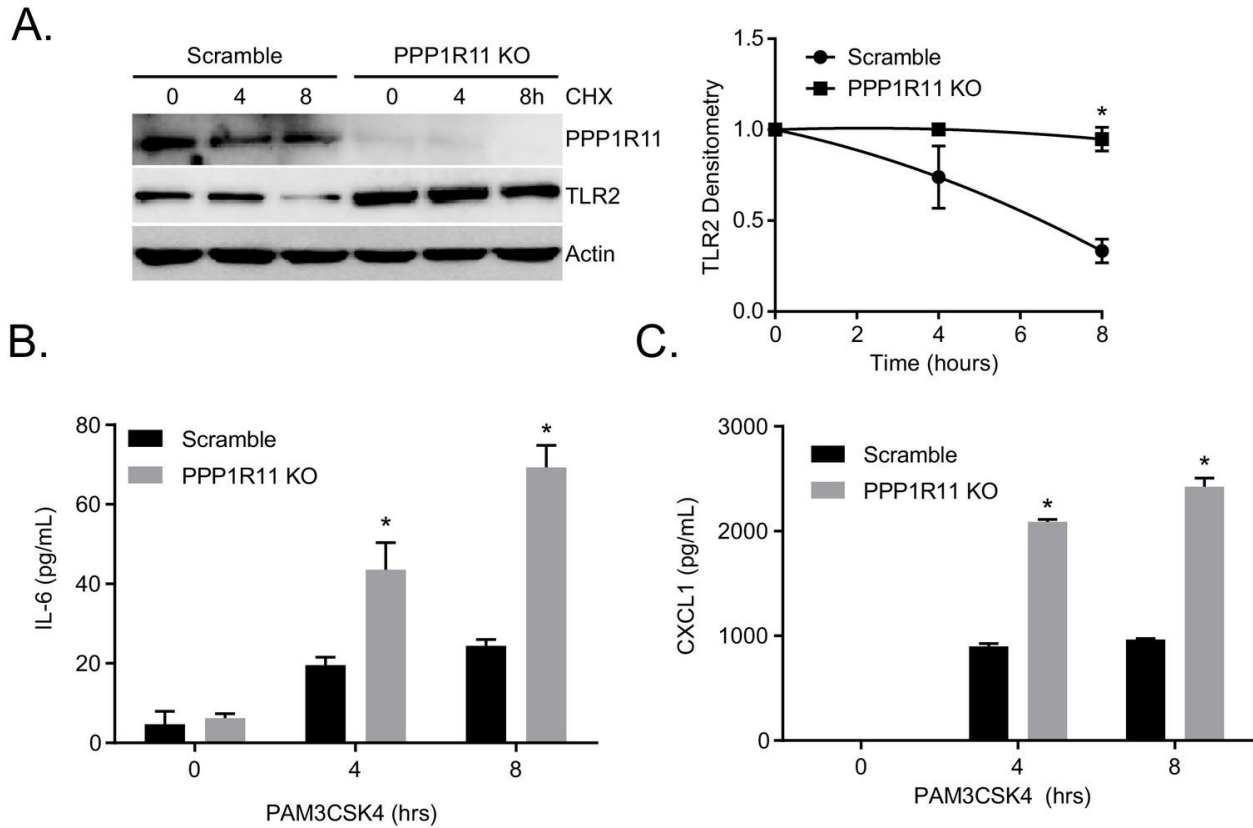
Figure 26 Ppp1r11 KO cells rescue TLR2 stability and function

(A) Half-life study of TLR2 in Ppp1r11 CRISPR KO MLE cells and Ctrl MLE cells. The levels of each protein on immunoblots were quantified densitometrically (Normalized to Time zero) and shown graphically. The data represent mean values ± SEM (n = 3); *p<0.05, significant compared to Control, Student's t-test. (B–C) Ppp1r11 KO and control cells were exposed to Pam3CSK4 in a time-dependent manner. Cell media was then collected and assayed for IL-6 and CXCL1 (Data represent mean values ± SEM n = 3; *p<0.05, significant compared to Control, Student's t-test).

3.1.5 PPP1R11 gene transfer reduces lung inflammation and decreases bacterial clearance

To further characterize the role of PPP1R11 in TLR2-mediated infection, mice were infected with an empty lentivirus or lentivirus encoding PPP1R11. Mice were then challenged with *Staphylococcus aureus* (intratracheally, 10^8 CFU). *S. aureus*, a gram-positive bacterium, is a significant contributor to nosocomial pneumonia, sepsis-associated acute lung injury (ALI), and acute respiratory distress syndrome (ARDS)(46, 255). Mice were euthanized before analysis of lung inflammation and systemic bacterial loads. PPP1R11 gene transfer significantly reduced lung inflammation shown by reduced lavage cytokines, protein concentrations, cell counts, and cell infiltrates (Figure 27A, B, C, D, E, and L). However, there were significantly higher bacterial loads in the lung, lavage fluid, blood, and liver (Figure 27F, G, H, and I), and there was a trend towards an increase in the spleen and kidney (Figure 27J and K). We also showed that in mice infected with *S. aureus*, PPP1R11 expression in the lung effectively reduced TLR2 protein levels (Figure 27M).
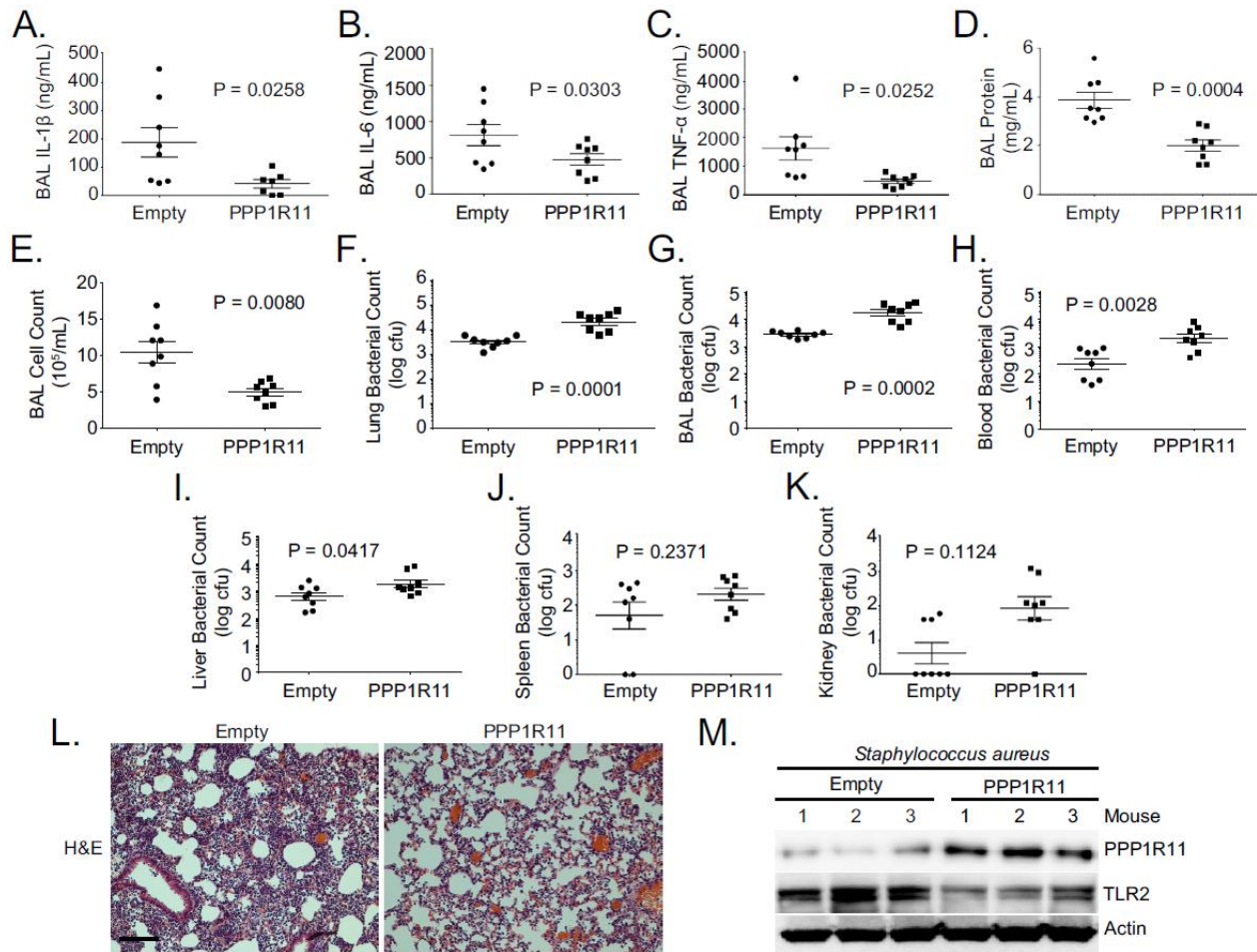
Figure 27 PPP1R11 gene transfer in the lung reduces lung inflammation and decreases bacterial clearance

Lenti-Empty or Lenti-PPP1R11 (10^7 PFU/mouse) was administered i.t. to C57BL/6J mice for 144h; mice were then infected i.t. with *S. aureus* (10^8 CFU). Mice were euthanized after 18h, and lungs were lavaged with saline, harvested, and then homogenized. Blood, liver, spleen, and kidney were also harvested and homogenized. A-E and G. Lavage cytokines, BAL protein, BAL cell counts, and BAL bacterial counts were measured. Data represent mean values ± SEM (n=8 mice per group; p < 0.05, significant compared to Control, Student's *t*-test). F and H-K. Lung, blood, liver, spleen, and kidney bacterial counts were measured. Data represent mean values ± SEM (n=8 mice per group; p < 0.05, significant compared to Control, Student's *t*-test). L. H&E staining was performed on lung samples. Original magnification, 20X. Bar indicates 100 μm. M. Mice lungs were isolated and assayed for TLR2, PPP1R11, and Actin immunoblotting.

3.1.6 PPP1R11 knockdown induces lung inflammation and increases bacterial clearance

To further confirm that PPP1R11 suppresses an inflammatory response through TLR2 *in vivo*, mice were first infected with lentivirus encoding control shRNA or *Ppp1r11* shRNA and then challenged with *S. aureus* (intratracheally, 2.5*10^7 CFU). PPP1R11 knockdown significantly increased lavage cytokines, protein concentrations, cell counts, and cell infiltrates (Figure 28A, B, C, D, E, and J). Interestingly, increased lung inflammation further cleared bacterial loads in the lavage fluids, lung, and blood (Figure 28F, G, and H), and there was a trend towards decreased bacterial loads in the liver (Figure 28I). We also showed that in mice infected with *S. aureus,* PPP1R11 knockdown effectively increased TLR2 protein levels in lung (Figure 28K). Taken together, these results suggest that PPP1R11 is a negative regulator of TLR2 signaling and inflammatory cytokine release, which mediates the clearance of *S. aureus* after acute infection.
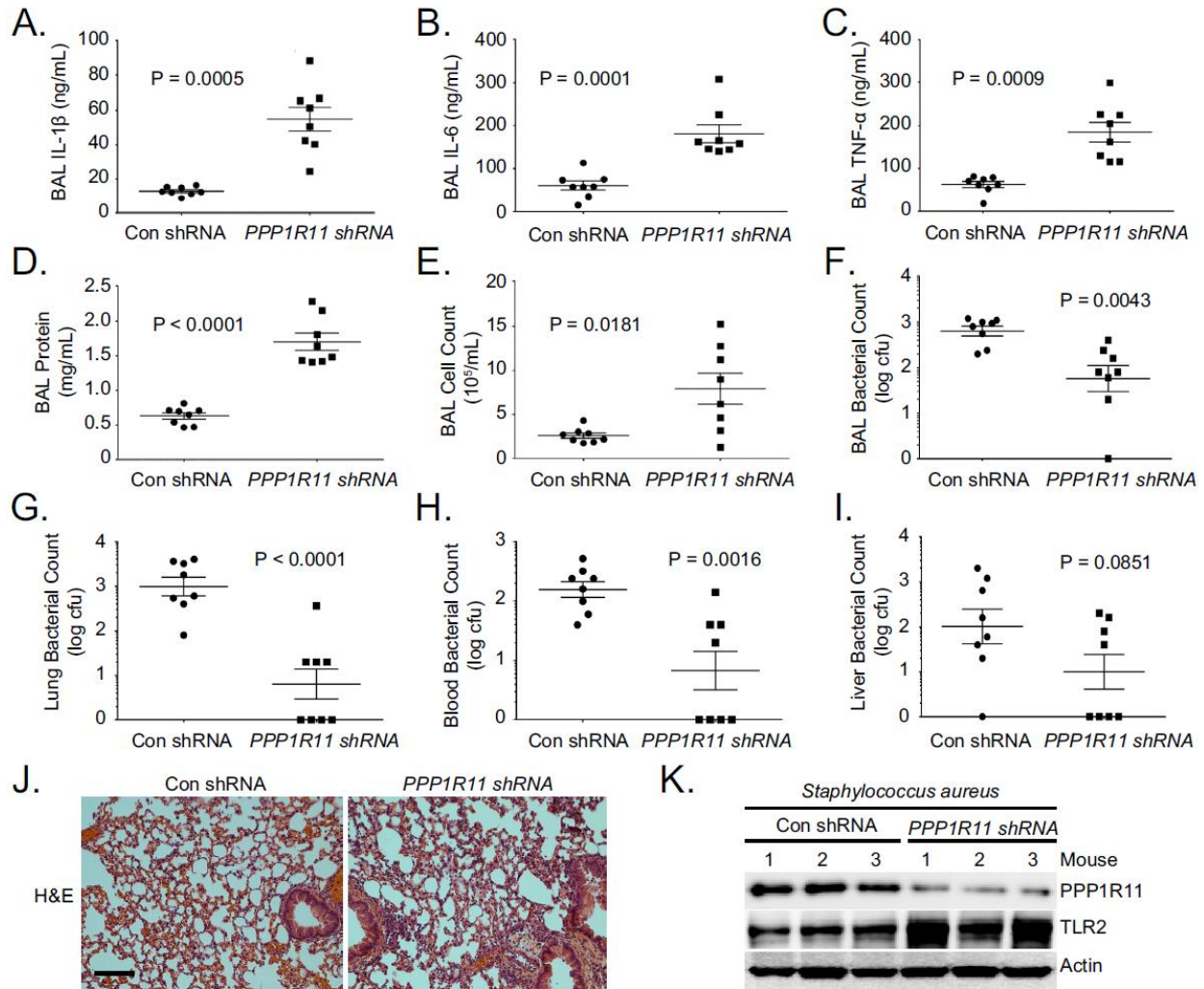
Figure 28 PPP1R11 knockdown induces lung inflammation and increases bacterial clearance

Lenti-control shRNA or Lenti-*PPP1R11* shRNA (10^7 PFU/mouse) was administered i.t. to C57BL/6J mice for 144h; mice were then infected i.t. with *S. aureus* ($2.5*10^7$ CFU). Mice were euthanized after 18h, and lungs were lavaged with saline, harvested, and then homogenized. Blood, liver, spleen, and kidney were also harvested and homogenized. A-F. Lavage cytokines, BAL protein, BAL cell counts, and BAL bacterial counts were measured. Data represent mean values ± SEM (n=8 mice per group; p < 0.05, significant compared to Control, Student's *t*-test). G-I. Lung, blood, and liver bacterial counts were measured. Data represent mean values ± SEM (n=8 mice per group; p < 0.05, significant compared to Control, Student's *t*-test). J. H&E staining was performed on lung samples. Original magnification, 20X. Bar indicates 100 μm. K. Mice lungs were isolated and assayed for TLR2, PPP1R11, and Actin immunoblotting.

3.1.7 Discussion

Pattern recognition receptors play a critical role in mucosal immunity by sensing PAMPs from invading pathogens and initiating cellular responses to eliminate those pathogens. Here we

94

show a novel mechanism by which the previously unrecognized RING finger E3 ligase, PPP1R11, attenuates TLR2 signaling in response to *S. aureus* infection by targeting TLR2 for proteasomal degradation. PPP1R11 (Protein Phosphatase 1 Regulatory Subunit 11) was originally described to interact with and inhibit protein phosphatase 1 activity (256) . It also has another name, TcTex5 (T-Complex-Associated-Testis-Expressed 5), and it was implied that mutation of TcTex5 is associated with a mouse sperm motility abnormality in sterile t-haplotype mutant mice (257, 258). However, its E3 ligase activity has never been described. Canonical RING finger domains contain the consensus sequence $C-X_2-C-X_{[9-39]}-C-X_{[1-3]}-H-X_{[2-3]}-C-X_2-C-X_{[4-48]}-C-X_2-C$, where both cysteine and histidine residues are involved in zinc coordination(113). However, we believe that PPP1R11 has a non-canonical RING finger domain with all the characteristics of a Ring finger E3 ligase (Figure 19G, H, I, Figure 22A). We show relative specificity of TLR2 targeting by PPP1R11, as none of the other TLRs tested were degraded by PPP1R11 expression (Figure 23). However, it is possible that other E3 ligases target TLR2 for ubiquitination as this phenomenon has been well described with other substrates, e.g. SCF E3 ligase subunits Fbxw1, Fbxw7, Fbxw8, Fbxl1, Fbxo4, and Fbxo31 are all capable of ubiquitinating cyclin D1(259). We do not rule out other RING finger E3 ligase or even other E3 ligase family members to potentially target TLR2 for ubiquitination, however, our data suggest that PPP1R11 targets TLR2 for proteasomal degradation via ubiquitination.

Targeted TLR2 degradation by PPP1R11 may act as a negative feedback mechanism in the lung to prevent a harmful, excessive inflammatory response that causes severe lung injury. We have observed similar function of other E3 ligase proteins such as Fbxl19 in acute lung injury and pneumonia (260). Indeed, we showed that treatment of MLE cells with TLR2 ligand, Pam3CSK4, up-regulates PPP1R11 protein levels and gradually reduces TLR2 protein levels at about 4-6hr

(Figure 24A). We also showed that ectopic expression of PPP1R11 in MLE cells significantly reduced Pam3CSK4-induced cytokine release, and gene editing of PPP1R11 significantly increases ligand-induced cytokine release (Figure 24D-E; Figure 26B-C). This evidence suggests that PPP1R11 could be a natural inflammatory suppressor in cells, and this pathway could be utilized to target multiple types of stimuli-induced inflammation. While targeted degradation of TLR2 may restrain excessive inflammatory responses, activation of this pathway is also critical for pathogen clearance. By manipulating levels of TLR2 in murine lungs through PPP1R11, we showed effects in downstream inflammation and *S. aureus* bacterial clearance (Figure 27 and Figure 28). These results are in line with previous studies showing TLR2 deficient mice were more susceptible to *S. aureus* infection (246). Specifically, higher inflammation in the lung might lead to lung injury, but also proved to be more efficient at clearing bacteria (Figure 28), whereas reduced inflammation in the lung is tissue-protective but fails to clear bacteria, which leads to systemic bacteremia (Figure 27). One approach to potentially control the balance between the beneficial effects of the inflammatory pathway and the harmful and excessive responses to pathogens is to manipulate PPP1R11. These results suggest that PPP1R11 inhibition might confer a protective phenotype against *S. aureus* pneumonia by augmenting TLR2 signaling, which is critical for bacterial clearance. As a proof-of-concept investigation, we observed a negative correlation between TLR2 and PPP1R11 protein levels in WBC pellets from *S. aureus*-infected patients. Interestingly, no correlation between PPP1R11 and TLR2 levels was observed in control patients (Figure 21). This experiment suggests that the PPP1R11/TLR2 pathway is only active during *S. aureus* infection. It is likely that other regulators such as kinases are also involved in PPP1R11-driven TLR2 ubiquitination, which is common in E3 ligase substrate targeting (176,

261). Further studies are warranted to investigate regulators that influence PPP1R11 expression and activity.

In conclusion, we show that the previously uncharacterized RING E3 Ligase, PPP1R11, is up-regulated in response to the TLR2 ligand, Pam3CSK4, and subsequently targets TLR2 for proteasomal degradation by ubiquitinating it at lysine 754. Down-regulation of TLR2 levels by PPP1R11 reduces pro-inflammatory cytokine secretion but impairs bacterial clearance in response to *S. aureus*. Taken together, this study characterizes a novel innate immune regulatory mechanism involving PPP1R11-targeted degradation of the pattern recognition receptor TLR2.

3.1.8 Acknowledgements

3.1.9 Materials and Methods

3.1.9.1 Materials

Sources of the murine lung epithelial (MLE) cell line was described previously(181, 182). QuikChange II XL Site-Directed Mutagenesis Kit (200522) was from Aglient Technologies. Nucleofector 2b and nucleofection kits (AAB-1001) were from Amaxa. High capacity RNA-to-cDNA kits (4387406) were from Applied Biosystems. HEK293T cells (CRL-3216) were from ATCC. Thermal Cycler Life ECO (BYQ6078) was from BIOER Technology. Secondary antibodies (170-515/6) and CFX96 Touch Real-Time qPCR (1855196) were from BioRad.

UbiCRest assay kit (K-400) was from Boston Biochem. Anti-TLR2 (12276), anti-Ubiquitin (3936, RRID:AB_331292), and anti-HA (3724, RRID:AB_1549585) antibodies were from Cell Signaling. Lenti-X Packaging System (631276) was from Clontech. Murine IL-1b (88-7261) and murine IL-6 (88-7064, RRID:AB_2574986) ELISA kits were from eBioscience. Ubiquitin E1, E2s, biotinylated ubiquitin (BML-UW0400) and cycloheximide (BML-GR310) were from Enzo. FBS (100-106) was from Gemini. DNA sequencing was performed at Genewiz. Dulbecco's Modified Eagle Medium-F12 (11965-092) was from Gibco. Anti-V5 antibody (R960, RRID:AB_159298) was from Invitrogen. PAM3CSK4 (tlrl-pms) was from InvivoGen. C57BL/6J mice (000664, RRID:IMSR_JAX:000664) were from Jackson Laboratory. SYBR Select Master Mix (4472918) was from Life Technologies. 35mm Glass Bottom MakTek dishes (P35GCOL-0-10-C) were from MatTek. Alexa Fluor 488 Phalloidin (A12379, RRID:AB_2315147), Hoechst 33342 (H3570), Alexa Fluor 488 conjugate Donkey anti-Mouse IgG (R3711), Alexa Fluor 568 conjugate Goat anti-Mouse IgG (H+L) (A-11004), Normal Goat Serum (50197Z) were from Molecular Probes. TnT® T7 Quick Coupled Transcription/Translation System (L1170) was from Promega. Murine CXCL1 (DY453) and Murine TNF-a (DY410) ELISA kits were from R&D Systems. PPP1R11 CRISPR/Cas9 KO plasmid (SC-429347), Anti PPP1R11 antibody (SC-135427, RRID:AB_10840420), Anti UBE2D (SC-166278, RRID:AB_2210152), Anti UBE2H (SC-100620, RRID:AB_2210469) were from Santa Cruz Biotechnology. Anti Actin antibody (A5441, RRID:AB_476744), leupeptin (L2884), TSB (22092), and Agar (A5306) were from Sigma Aldrich. PureLink RNA Mini kit (12183020), Strepavidin agarose resin (20349), and pcDNA3.1D V5/HIS/TOPO kit (K490040) were from Thermo Fisher Scientific. MG-132 (F1100) was from UBPBio.

3.1.9.2 Cell culture

Murine Lung Epithelial 12 cells (MLE) were from ATCC (CRL-2110) and cultured according to manufacturer's instructions. The identity of the cell lines was monitored by microscope based morphology analysis and immunoblotting with multiple markers. The cell lines were checked for mycoplasma contamination using MycoAlert™ Mycoplasma Detection Kit (Lonza, Switzerland). MLE cells were cultured in Dulbecco's Modified Eagle Medium-F12 (Gibco) supplemented with 10% fetal bovine serum (DMEM-F12-10). For PPP1R11 overexpression in MLE cells, an Amaxa nucleofection kit was used following manufacturer's protocol. 24h later, cells were treated with doses of Pam3CSK4 up to 10μg/ml. For PPP1R11 knockdown studies in MLE cells, scramble siRNA and PPP1R11 siRNA were used to transfect cells for 48h using electroporation. Cell lysates were prepared by brief sonication in 150 mM NaCl, 50 mM Tris, 1.0 mM EDTA, 2 mM dithiothreitol, 0.025% sodium azide, and 1 mM phenylmethylsulfonyl fluoride (Buffer A) at 4 °C. For half-life study, MLE cells were exposed to cycloheximide (40mg/ml) in a time dependent manner for up to 6h. Cells were then collected and immunoblotted. Protein densitometry was quantified through ImageJ and normalized to the zero time point for each set of condition.

3.1.9.3 UbiCRest assay

TLR2 protein was analyzed for ubiquitin linkage specificity via the UbiCRest method and following manufacturer's protocol (262). MLE cells were treated with MG-132 (20 μM) for 18 hours prior to immunoprecipitation of endogenous TLR2 protein. TLR2 bound antibodies were conjugated to Protein A/G agarose resin and distributed among nine tubes. The TLR2-resins were incubated with deubiquitinases with varying specificities to the eight ubiquitin linkages. The deubiqutinases used and their working concentrations were USP2 (0.5 μM), OTULIN (0.5 μM),

OTUB1 (0.5 μM), ZRANB1 (0.5 μM), STAMBP (0.5 μM), OTUD3 (0.5 μM), OTUD7A (0.1 μM), and OTU1 (0.5 μM). Following the reaction, TLR2 protein was eluted from resin and subjected to ubiquitin immunoblotting.

3.1.9.4 In vitro ubiquitin conjugation assays

The assay was performed in a volume of 25ml containing 50 mM Tris pH 7.6, 5 mM $MgCl_2$, 0.6 mM DTT, 2 mM ATP, 1.5 ng/ml E1, 10 ng/ml Ubiquitin E2 conjugating enzymes, 1mg/ml ubiquitin (Calbiochem), 1 mM ubiquitin aldehyde, and *in vitro* synthesized V5-TLR2 and PPP1R11. Reaction products were immunoblotted for V5.

3.1.9.5 In vitro protein binding assays

PPP1R11 protein was immunoprecipitated from 1mg MLE cell lysate using PPP1R11 antibody (rabbit) and coupled to protein A/G agarose resin. PPP1R11 beads were then incubated with *in vitro* synthesized products (50ul) expressing V5-E2 conjugating enzymes. After washing, the proteins were eluted and processed for V5 immunoblotting.

3.1.9.6 RT–qPCR, cloning, and mutagenesis

Total RNA was isolated and reverse transcription was performed followed by real-time quantitative PCR with SYBR Green qPCR mixture as described (185). All mutant PPP1R11 and TLR plasmid constructs were generated using PCR-based approaches using appropriate primers and subcloned into a pcDNA3.1D/V5-His vector.

3.1.9.7 Immunostaining

MLE cells were seeded in 35mm MatTek glass-bottom dishes before the plasmid transfection. Cells were washed with PBS and fixed with 4% paraformaldehyde for 20 min, then exposed to 2% BSA, 1:500 mouse V5 antibody and 1:1000 Alexa 568nm chicken anti-mouse antibody sequentially for immunostaining. The nucleus was counterstained with DAPI and F-actin was counterstained with Alexa 488-Phalloidin. Immunofluorescent cell imaging was performed on a Nikon A1 confocal microscope using 405 nm, 488 nm, or 567 nm wavelengths. All experiments were done with a 60x oil differential interference contrast objective lens.

3.1.9.8 Lentivirus construction

To generate lentivirus encoding PPP1R11, Plvx-PPP1R11 plasmid was co-transfected with Lenti-X HTX packaging plasmids (Clontech) into 293FT cells following the manufacturer's instructions. 72 h later, virus was collected and concentrated using Lenti-X concentrator.

3.1.9.9 Gene Editing

CRISPR guide RNAs (gRNA) were generated by *Santa Cruz Biotechnologies* specific to the first exon of *Ppp1r11* (TTGTAGGACGCCGTCCTTTG). MLE cells were transfected with 5 ug of plasmid. Transfection efficiency was confirmed via GFP expression. Cells were diluted and seeding to single-cell concentrations and sequence confirmed prior to half-life and cytokine studies.

3.1.9.10 Animal studies

All procedures were approved by the University of Pittsburgh Institutional Animal Care and Use Committee. For pneumonia studies, C57BL6 mice were deeply anesthetized using a

ketamine/xylazine mixture, and the larynx was well visualized under a fiber optic light source before endotracheal intubation with a 3/400 24-gauge plastic catheter. 10^7 CFU of lentivirus encoding genes for PPP1R11 or PPP1R11 shRNA was instilled i.t. for 144 h before the administration of S. aureus (strain 29213, 2.5*1e7-1e8CFU/mouse, i.t.) for 18 h, after which animals were euthanized and assayed for BAL protein, cell count, cytokines, lung infiltrates, and tissue bacterial count (175, 176, 251, 260).

3.1.9.11 Human Samples

This study was approved by the University of Pittsburgh Institutional Review Board. As part of an ongoing Acute Lung Injury Biospecimen Repository, blood was collected from critically ill, mechanically-ventilated patients admitted to the University of Pittsburgh Medical Center Presbyterian Hospital Medical Intensive Care Unit. Whole blood was treated with red blood cell lysis solution, and leukocytes were washed once with PBS prior to pelleting. Groups were separated into "control" and "injury" cohorts based on clinical evidence of or risk factors for Acute Respiratory Distress Syndrome (ARDS) as determined by an expert clinical panel. Control patients were mechanically ventilated without clinical evidence of or risk factors for Acute Respiratory Distress Syndrome (ARDS), while the injury cohort had clinical evidence of or risk factor for ARDS. For this study, samples were analyzed from a group of randomly selected control cohort patients (without *S. aureus* infection), as well as from patients with evidence of *S. aureus* infection (BAL, blood, or both) in the injury cohort. The Biospecimen Repository provided de-identified samples to this laboratory, and cell pellets were assayed for TLR2 and PPP1R11 proteins by immunoblotting, quantified using ImageJ software, and graphed in GraphPad. All data acquisition and densitometry was performed blinded prior to revealing cohort groups.

3.1.9.12 Statistical Analysis

Statistical comparisons were performed with mean ± standard error of the mean (SEM) for continuous variables. All data were statistically analyzed by unpaired 2 sample t-test with $p<0.05$ indicative of statistical significance. All analyses were performed using GraphPad Prism 6.

3.2 KIAA0317 Regulates Pulmonary Inflammation Through SOCS2 Degradation

Adapted from: Lear and McKelvey et al., KIAA0317 regulates pulmonary inflammation through SOCS2 degradation. *JCI Insight*. 2019;4(19):e129110. https://doi.org/10.1172/jci.insight.129110., (263)

Lung inflammation can be deleterious for humans, even in the context of infection. Exuberant inflammatory responses lead to extensive damage of the alveolar space, causing denudation of the basement membrane, edema formation, necrosis of pulmonary epithelial, and aberrant fibrotic response in an attempt to repair the damage (43). Together, these responses create conditions of acute lung injury leading to respiratory failure. Acute Respiratory Distress Syndrome is one example of this condition, in which runaway inflammatory signaling leads to respiratory failure in critical care patients (264). In this study we investigated a potent anti-inflammatory protein, SOCS2, and its regulation by the ubiquitin E3 ligase KIAA0317 in pulmonary epithelial cells. In the course of the lung's response to insult, pulmonary epithelial cells initiate the inflammatory response(265). The hypothesis was that SOCS2 anti-inflammatory activity may be an early step in the process, and intervention in its KIAA0317-mediated degradation may be an avenue to halt deleterious inflammation before the runaway cycle begins.

3.2.1 Overview

Dysregulated pro-inflammatory cytokine release has been implicated the pathogenesis of several life-threatening acute lung illnesses such as pneumonia, sepsis, and acute respiratory distress syndrome. The suppressor of cytokine signaling proteins, particularly SOCS2, have

recently been described as anti-inflammatory mediators. However, the regulation of SOCS2 protein has not been described. Here we describe a novel mechanism of SOCS2 regulation, by the action of the ubiquitin E3 ligase KIAA0317. KIAA0317-mediated degradation of SOCS2 exacerbates inflammation in vitro and depletion of KIAA0317 in vivo ameliorates pulmonary inflammation. KIAA0317 knockout mice exhibit resistance to LPS-induced pulmonary inflammation, while KIAA03017 re-expression mitigates this effect. We uncovered a small molecule inhibitor of KIAA0317 protein (BC-1365), which prevents SOCS2 degradation and attenuates LPS- and *P. aeruginosa*- induced lung inflammation in vivo. These studies show KIAA0317 to be a critical mediator of pulmonary inflammation through its degradation of SOCS2, and a potential candidate target for therapeutic inhibition.

3.2.2 Introduction

The inflammatory response in the lung is a critical response to infection, and in maintaining pulmonary homeostasis. Pathogen sensing by the host initiates inflammation via cytokine signaling cascades(266), which facilitates the activation of the immune system and recruitment of leukocytes to the afflicted area. However, uncontrolled pulmonary inflammation can be deleterious as several acute pathologies including acute respiratory distress syndrome (ARDS), are associated with high pro-inflammatory cytokine levels(44). In the case of ARDS, dysregulated pulmonary inflammation results in capillary damage, disruption of the alveolar epithelium, alveolar damage caused by leukocytes, and the influx of edema fluid rich in connective tissue and protein (267). ARDS affects almost 0.25 million patients annually, whom suffer over 40% mortality (264, 267, 268). Pulmonary inflammation is directly associated with pro-inflammatory cytokines such as IL-1, -6, and TNF (48, 269). Alveolar macrophages from ARDS patients show more activated nuclear

105

factor-kappa B (NF-κB) (49), and subsequent research has shown that the NF-κB signaling pathway promotes the transcription of cytokines involved in ARDS pathogenesis (49, 52, 270, 271).

3.2.2.1 SOCS proteins in anti-inflammatory signaling

Several families of proteins are tasked with suppressing cytokine signal transduction, including the suppressor of cytokine signaling (SOCS) proteins (272, 273) . The protein SOCS2 regulates the fate of many key signal transduction proteins, such as the protein kinases FLT3 and p38, the growth hormone receptor, and even other SOCS proteins (274-277). Research suggests that SOCS2 suppresses the NF-κB pathway, similar to other SOCS family members such as SOCS1 and SOCS3 (278). Further, SOCS2 was observed to mediate the degradation of the kinase STK38, which is known to enhance the activity of NF-κB signaling (279). Indeed, SOCS2 expression directly blunted NF-κB transactivation(280). In addition, SOCS2 was observed to regulate the stability of TRAF6, leading to inhibition of NF-kB pathways (281). Deletion of SOCS2 in mice leads to rampant systemic pro-inflammatory cytokine production following challenge with *T. gondii* or LPS (282). Despite these studies, there is little research into the role of SOCS2 in pulmonary inflammation and injury. Previous research suggests the stability of key proteins that regulate pulmonary inflammation influences lung pathology, such as the ubiquitin-proteasome-dependent degradation of TLR2, PIAS1, and FBXL2 (60, 232, 283). To better understand the role of SOCS2 in pulmonary inflammation, we investigated the regulation of SOCS2 protein stability and its effects on pulmonary inflammation.

3.2.2.2 The Regulation of SOCS2 through KIAA0317

Here we report the ubiquitin-mediated degradation of SOCS2 protein and its effect on pulmonary inflammation. We characterized SOCS2 ubiquitination, which was dependent on Protein Kinase C-alpha (PKCa)-mediated phosphorylation and stimulated by LPS exposure, leading to SOCS2 protein degradation through the proteasome. Through affinity mass spectrometry, we identified the ubiquitin E3 ligase KIAA0317 (also known as AREL1) as an interacting partner with SOCS2 and elucidated a mechanism by which KIAA0317 potently regulated SOCS2 protein stability and signaling. *Kiaa0317* knockdown in vivo increased SOCS2 protein level and lessened the severity of bacterially-induced lung inflammation. Subsequently, we developed CRISPR-Cas9 *Kiaa0317* knockout mice, which were resistant to LPS-induced pulmonary inflammation. Lentivirus rescue experiments with *Kiaa0317* knockout mice ablated their protection from LPS-induced inflammation, which supported this putative mechanism. Finally, we screened and developed a small-molecule inhibitor of KIAA0317 which showed efficacy in vitro and in vivo in preserving SOCS2 protein and ameliorating pulmonary inflammation in both bacterial and LPS-driven models of lung inflammation. Taken together, these experiments describe a new mechanism controlling pulmonary inflammation and potential avenue for therapeutic intervention.

3.2.3 SOCS2 is downregulated during pulmonary distress

To test the in vivo significance of SOCS2 in pulmonary inflammation, we analyzed its protein expression by immunoblotting lysate from circulating white blood cells from seven control subjects and ten ARDS patients, as defined by Berlin criteria and agreed upon by a minimum of three members of an expert clinical panel (Table 1). De-identified human plasma samples were

107

obtained from the University of Pittsburgh Acute Lung Injury Biospecimen Repository (IRB number #PRO10110387). Following immunoblotting, we observed patients with ARDS had significantly less immunoreactive SOCS2 in leukocyte lysate versus control subjects, suggesting SOCS2 protein is depleted during pulmonary inflammation (Figure 29A). We next sought to explore the role of SOCS2 in lung tissue types. We conducted single-cell RNA sequencing of normal human tissue to characterize SOCS2 cellular expression. Normal control lung tissue was obtained from organ donors, after rejection of the lungs for transplant prior to processing for RNA sequencing (209). The University of Pittsburgh Institutional Review Board approved procedures involving human samples. We observed SOCS2 to be predominantly expressed in pulmonary epithelia cells, specifically type-ii pneumocytes (Figure 29B). Lung epithelia play a critical role in pathogen detection and the initiative of inflammation during lung infection and stress (34, 284). We hypothesized that SOCS2 protein may be decreased in these cells in response to inflammatory stimuli such as LPS. We observed SOCS2 protein has a half-life between 2 and 4hr in murine lung epithelial cells (MLE), which is prolonged with proteasomal inhibitor MG132 treatment (Figure 29C). Further, Socs2 protein showed a dose-dependent decrease upon expression of ubiquitin in MLE cells (Figure 29D) suggesting Socs2 protein stability is regulated via the ubiquitin-proteasome system. We performed UbiCREST analysis to characterize Socs2 ubiquitination and observed Socs2 predominantly assembled ubiquitin chains with lysine-48 linkages (Figure 29E). Further, we expressed several ubiquitin constructs with all lysines mutated except for a specific one, thus impairing linkage-specific poly-ubiquitin chains. We observed that ubiquitin with solely lysine-48 was the only construct sufficient to generate high-molecular weight Socs2 polyubiquitination protein signal (Figure 29F). Finally, treatment of MLE with LPS led to decreased Socs2 protein signal and an increase in poly-ubiquitinated Socs2, suggesting SOCS2

108

ubiquitination and degradation is stimulated by LPS (Figure 29G). LPS treatment of MLE cells

did not result in a significant change in *Socs2* mRNA (Figure 29H).

Table 1 Clinical Parameters of ARDS Patients

Age	Sex	Primary Etiology	WBC	Vasopressor Use	LIPS Score	FiO2	PEEP	Duration of Mechanical Ventilation (Days)	30-Day Mortality
71	Male	Pneumonia	15.1	Yes	6.5	80	12	25	No
43	Female	Aspiration	9.5	Yes	7	50	8	20	No
36	Female	Pneumonia	7.5	No	4.5	60	14	12	No
18	Female	Non-pulmonary sepsis	12.1	Yes	5	40	10	61	No
43	Female	Non-pulmonary sepsis	23.3	Yes	6	100	15	4	No
73	Male	Aspiration	19.1	Yes	7.5	60	5	3	Yes
45	Female	Pneumonia	15.1	Yes	6.5	40	5	9	No
72	Female	Pneumonia	10.2	No	3.5	90	14	36	No
51	Male	Pneumonia	10.8	Yes	7.5	50	8	15	No
59	Female	Pneumonia	13.9	Yes	7.5	60	10	25	No

Figure 29 SOCS2 protein is ubiquitinated and degraded during pulmonary inflammation

A. Immunoblot analysis of leukocyte pellets from ARDS patients or control serum samples. Data represent means ±SEM, (n = 7-10; ***, p < 0.001 compared with Control, Mann-Whitney U-Test). B. Cell type clustering results of control lung tissue cells from single-cell RNA-sequencing of SOCS2 transcript. C. Immunoblotting following cycloheximide (CHX, 50 μg/mL), MG132 (20 μM), or leupeptin (50 μg/mL) treatment for indicated times with ectopic expression of V5-tagged SOCS2 in MLE cells. D. Immunoblotting following overexpression of ubiquitin in MLE cells. E. UbiCREST analysis of SOCS2 ubiquitination following immunoprecipitation from MLE cells, digestion supernatant shown below with deubiquitinase enzymes indicated with (*). F. Immunoblot analysis following expression of SOCS2-V5 and Ubiquitin lysine-to-arginine mutants. G. Immunoblotting analysis of MLE cells following SOCS2-HIS and HA-Ubiquitin expression. Following HIS PD, eluate was immunoblotted for HA ubiquitin signal. H. qPCR analysis of MLE cells treated with LPS for indicated times. Data represent mean values ± SEM (n = 3; NS, p > 0.05 compared with 0hr, Student's two-tailed unpaired t-test). C-G. Data are representative of n=2-3 independent experiments.

3.2.4 KIAA0317 targets SOCS2 for ubiquitination

The process of substrate ubiquitination is facilitated by substrate-engaging ubiquitin E3 ligases. We utilized recombinant GST-tagged SOCS2 as bait during incubation with epithelial cell BEAS-2B lysate prior to SOCS2 pull-down (PD) (Figure 30A). Following pull-down, we subjected the eluate to mass spectrometry analysis through MS BioWorks services (Ann Arbor, USA). Analysis uncovered several differentially detected peptides among SOCS2 PD relative to control GST PD. Among these, we observed the protein KIAA0317 (79 peptides detected), which has been previously described as an Homologous to the E6-AP Carboxyl Terminus (HECT)-domain ubiquitin E3 ligase (141, 164, 285, 286). Expression of KIAA0317 in MLE cells accelerated SOCS2 degradation in half-life studies, while shRNA silencing of *Kiaa0317* prolonged SOCS2 stability (Figure 30B-E). KIAA0317 overexpression specifically decreased SOCS2 in a dose-dependent manner; a randomly selected HECT E3 ligase, UBE3B, was also tested as a negative control (Figure 30F-G). KIAA0317 enhanced SOCS2 poly-ubiquitination in an in vivo ubiquitination assay (Figure 30H), and this effect was also observed through in vitro ubiquitination assays (Figure 30I). Expression of HIS-tagged SOCS2 in addition to LPS exposure led to an increased poly-ubiquitination signal upon HIS-SOCS2 pulldown. This signal is enhanced upon co-expression of KIAA0317 (Figure 30J), suggesting LPS enhances KIAA0317 induced poly-ubiquitination of SOCS2. As SOCS2 is suggested to suppress NF-κB signaling (280), we tested the role of KIAA0317 in this signaling. Silencing *Kiaa0317* silencing significantly reduced NF-κB promoter activity following stimulation with LPS or TNF (Figure 30K-L). These data suggested KIAA0317 is a candidate E3 ligase regulating SOCS2 ubiquitination and degradation.
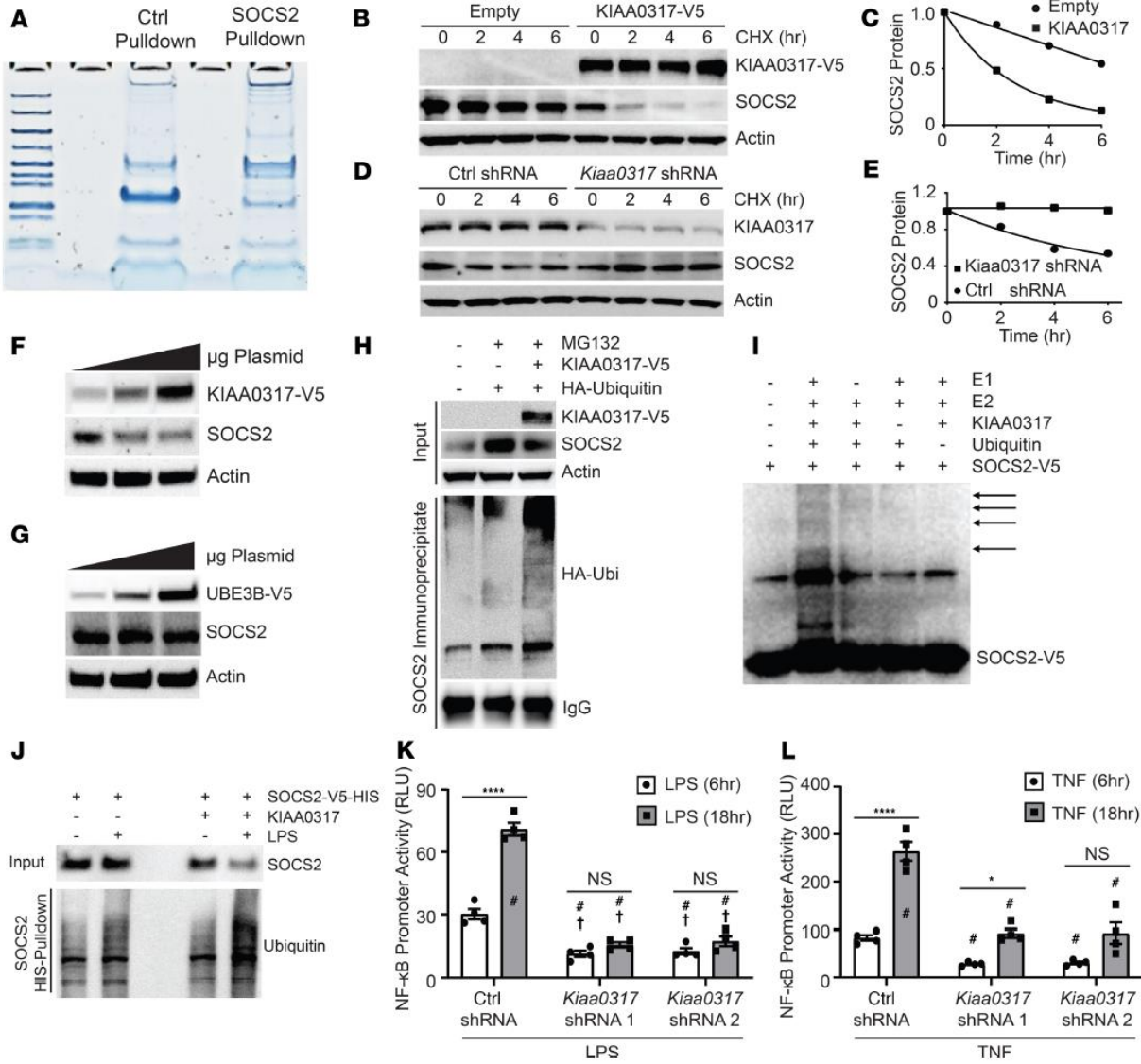
Figure 30 KIAA0317 Ubiquitinates and Degrades SOCS2 in Response to Bacterial Insult

A. Protein staining of eluate from Ctrl-GST and SOCS2-GST bait and capture of BEAS-2B lysate prior to mass spectrometry analysis. B. Immunoblotting following cycloheximide treatment (CHX, 50 μg/mL) for indicated times with ectopic expression of empty plasmid or V5-tagged KIAA0317 in MLE cells. C. SOCS2 protein densitometry (normalized to Actin) for B. (n=2). C. Immunoblotting following cycloheximide treatment (CHX, 50 μg/mL) for indicated times with ectopic expression of Ctrl shRNA or *Kiaa0317* shRNA in MLE cells. E. SOCS2 protein densitometry (normalized to Actin) for D. (n=2). F-G. SOCS2 Immunoblotting following F. KIAA0317 and G. UBE3B expression in MLE cells. H. in vivo ubiquitination assay and SOCS2 immunoprecipitation following co-expression with KIAA0317 and Ubiquitin. I. in vitro ubiquitination assay of SOCS2 protein. J. Immunoblot analysis of SOCS2 pull-down following KIAA0317 expression and LPS exposure. K.-L. NF-κB promoter activity assays in 293T cells transfected with control shRNA (CON) or *KIAA0317* shRNA and exposed to K. LPS (10μg/ml) or L. TNF (10ng/ml) for indicated times. Data represent mean values ± SEM (n = 4; *, p < 0.05; ****. <0.0001; NS, p > 0.05; compared to indicated treatment, to control shRNA 6hr treatment (^), or to control shRNA 18hr treatment (#), Two-way ANOVA with Bonferroni's multiple comparisons). F-J. Data are representative of n=2-3 independent experiments.

113

3.2.5 LPS stimulates site-specific SOCS2 phosphorylation and KIAA0317-mediated ubiquitination and degradation

Substrates are ubiquitinated often by conjugation to critical lysine sites. We mapped the putative ubiquitin acceptor site and the KIAA0317 binding site within SOCS2 (Figure 31A). To uncover the critical ubiquitin-acceptor site within SOCS2, we constructed several SOCS2 lysine to arginine mutants and assayed their protein half-lives (Figure 31B). Of the SOCS2 point mutants tested, only SOCS2 K173R exhibited an extended half-life (Figure 31B). We also probed the KIAA0317 binding site within SOCS2. KIAA0317 protein was first immunoprecipitated from cell lysates and coupled to protein A/G resin. We then incubated KIAA0317-resin with in vitro synthesized SOCS2-V5 mutants. After washing and elution, we analyzed via immunoblotting. We determined that KIAA0317 binds within the N-terminus of SOCS2 (Figure 31C).

We hypothesized this binding region within SOCS2 contained a critical moiety for recognition by KIAA0317. Ubiquitinated substrates are often post-translationally modified (e.g. phosphorylation), and these sites function as "degrons" for E3 ligase targeting (287). Thus, we set out to determine if there existed a key phospho-degron within SOCS2 for KIAA0317 recognition. Database analysis indicated that SOCS2 serine-52 is a candidate phosphorylation site within its N-terminus (NetPhos 2.0 software prediction, (288, 289)). Additionally, there is a naturally occurring missense polymorphism (S52N) (rs3741676) within this codon, and the SOCS2 S52N mutant exhibited an extended half-life (Figure 31D) and displayed lessened binding to KIAA0317 (Figure 31E). Finally, we observed that SOCS2 S52N as well as the K173R mutant was resistant to degradation when co-expressed with KIAA0317 (Figure 31F).

114
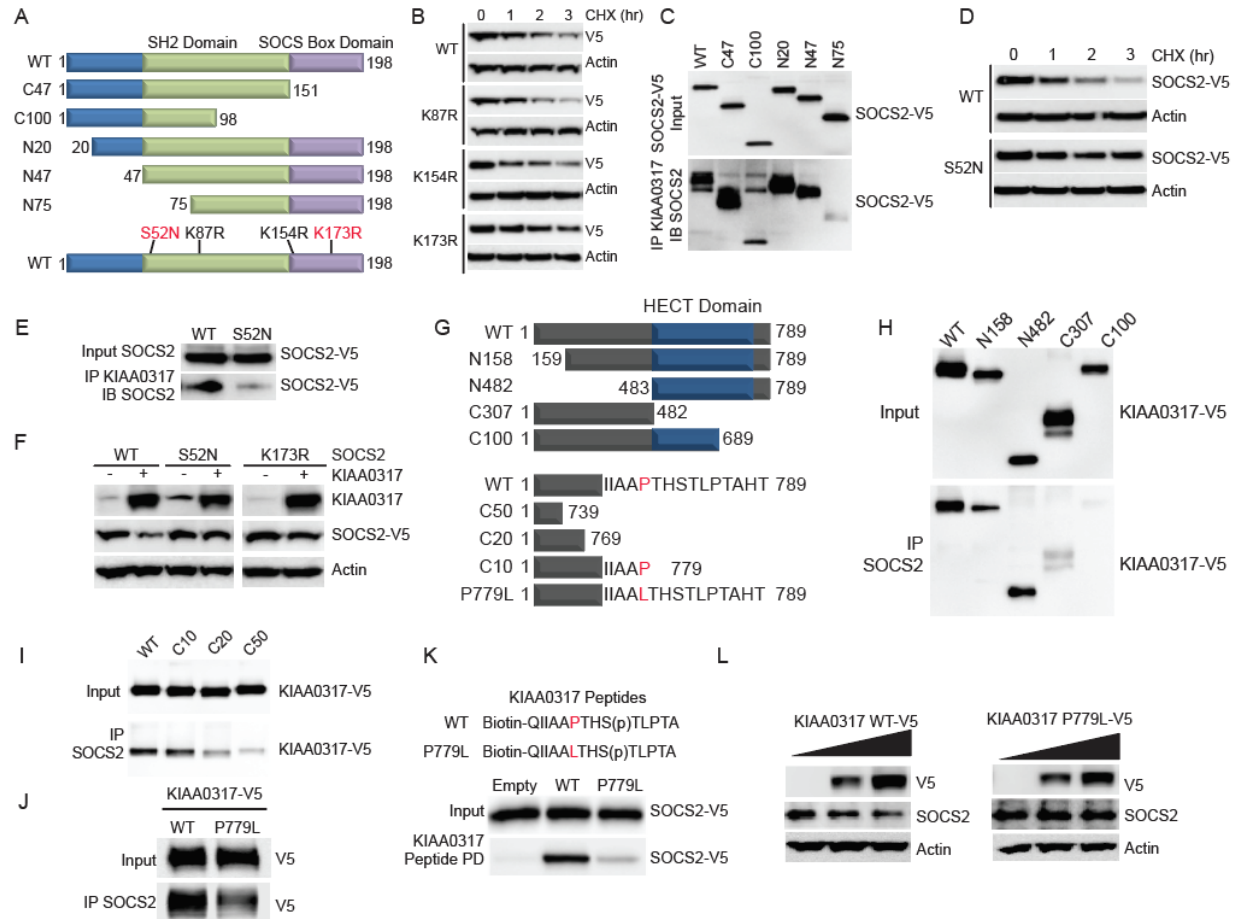
Figure 31 KIAA0317 targets SOCS2 phosphodegron for binding and ubiquitination

A. Schematic of SOCS2 deletional or point mutants used in mechanistic studies. B. Deletion mapping of SOCS2 site for binding KIAA0317. C. Immunoblot analysis of MLE cells expressing SOCS2 lysine mutants followed by cycloheximide (CHX, 50 μg/mL) treatment for the indicated times. D. Immunoblot analysis of MLE cells expressing SOCS2 S52N followed by cycloheximide (CHX, 50 μg/mL) treatment for the indicated times. E. Immunoblot analysis of SOCS2 S52N binding KIAA0317. F. Immunoblotting of MLE cells co-transfected with WT, SOCS2 S52N, or K173R mutant without or with KIAA0317. The lanes were run on the same gel but were noncontiguous. G. Schematic of KIAA0317 deletional or point mutants used in mechanistic studies. H-I. Deletion and point mapping of KIAA0317 site for binding SOCS2. J. KIAA0317 P779L binding assay with SOCS2. K. KIAA0317 Peptide binding assay. L. Immunoblot analysis of MLE cells expressing KIAA0317 WT and P779L at the increasing doses. WT (wild-type). B-F, H-L. Data are representative of n=2 independent experiments. IP: Immunoprecipitated, IB: Immunoblotted.

We sought out to determine the kinase responsible for SOCS2 phosphorylation at Serine 52. We screened for kinases via SOCS2 immunoprecipitation and immunoblot analysis. Of the kinases probed, only PKCA was detected in the SOCS2 immunoprecipitate (Figure 32A). We further observed that PKCA directly phosphorylated SOCS2 in an in vitro kinase assay (Figure

32B). PKCA affects SOCS2 protein stability, as PKCA expression decreased the protein half-life of SOCS2 in a cycloheximide chase (Figure 32C-D). Similarly, silencing of *Pkca* drastically stabilized SOCS2 protein (Figure 32E-F). LPS time and dose treatment promotes SOCS2 association with PKCA and KIAA0317, as well as the emergence of a phosphoserine signal corresponding to the predicted size of SOCS2 (~25kDa) (Figure 32G, H). This signal is reduced when *Pkca* is silenced (Figure 32I). Further, LPS increased KIAA0317 protein levels and decreased SOCS2 protein levels in both a time- and dose-dependent manner, as well as increasing the association between the two proteins (Figure 32G, H). To better understand the mechanism of KIAA0317 targeting of SOCS2, we embarked on a candidate mapping approach to identify the critical site within KIAA0317 for SOCS2 binding (Figure 31G). Through in vitro protein binding assays, we determined KIAA0317 binds to SOCS2 through the KIAA0317 C-terminus (Figure 31H-I). Interestingly, previous mapping studies have suggested KIAA0317 binds to substrates through specific C-terminal residues (such as proline-779) (141). Additionally, KIAA0317 P779 contains a naturally occurring polymorphism (rs371610162) resulting in P779L missense mutation. We observed that KIAA0317 P779L mutant protein has weakened binding with SOCS2 (Figure 31J), as does a peptide corresponding to the P779L sequence (Figure 31K). Finally, SOCS2 protein is insensitive to dose-dependent overexpression of P779L relative to WT (Figure 31L). Together, these results suggest that in response to LPS exposure, KIAA0317 facilitates the ubiquitination and degradation of SOCS2 protein, mediated by PKCA-mediated phosphorylation. This is consistent with the results of previous studies that suggested PKCA plays a role in inducing pro-inflammatory signaling, specifically through the NF-κB pathway (290-292). We hypothesized that this interaction plays a role in mechanisms of pulmonary inflammation.
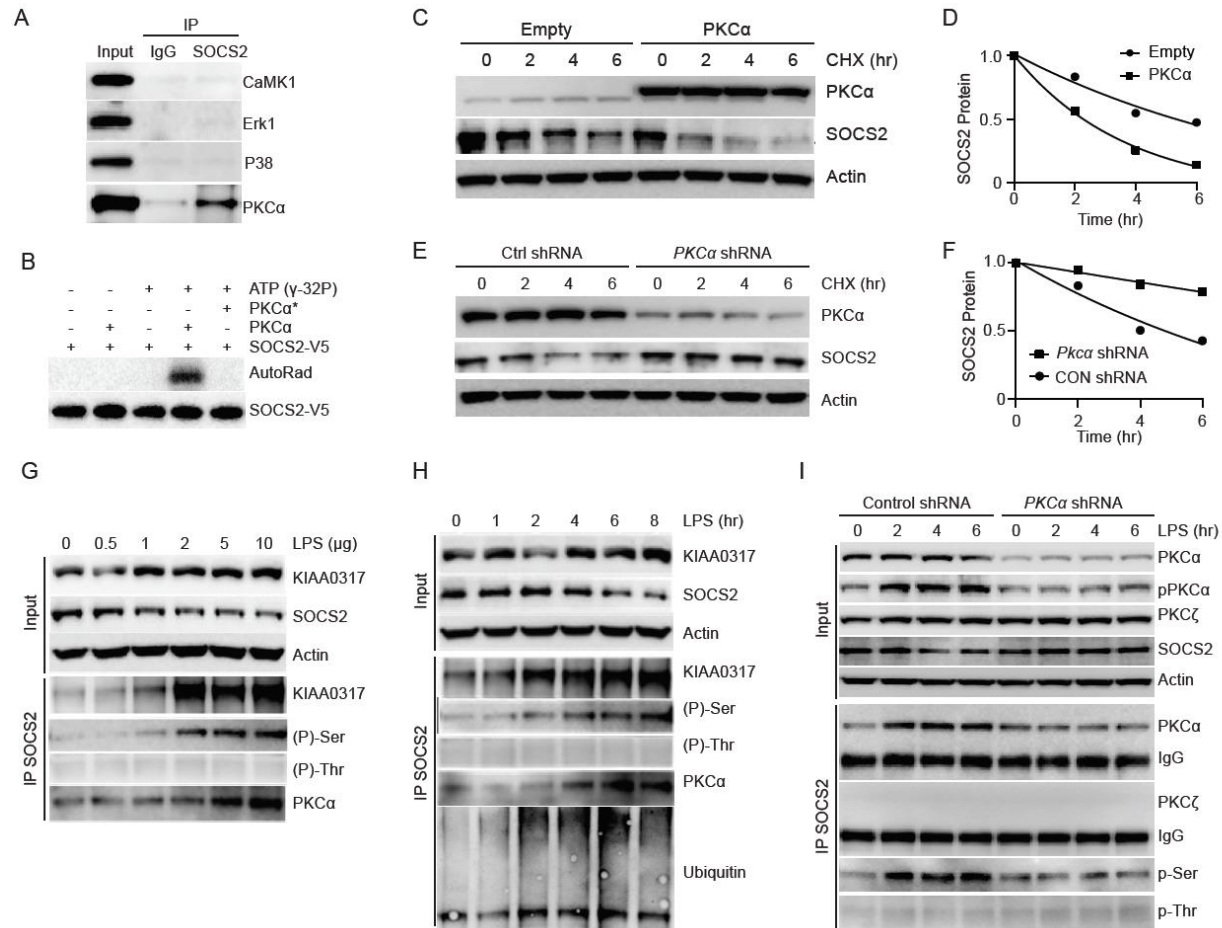
Figure 32 SOCS2 is phosphorylated by PKCA leading to its degradation

A. Endogenous SOCS2 immunoprecipitation from MLE cells and subsequent immunoblotting of several kinases (n=2). B. In vitro PKCA kinase assay. * indicates heat inactivated PKCA. C. Immunoblot analysis of MLE cells following expression of Empty or PKCA plasmids and exposure to CHX (100μg/mL) for the indicated times. D. SOCS2 protein densitometry (normalized to Actin) for C. (n=2). E. Immunoblot analysis of MLE cells following expression of CON shRNA or Pkca shRNA plasmids and exposure to CHX (100μg/mL) for the indicated times. F. SOCS2 protein densitometry (normalized to Actin) for E. (n=2). G. Immunoblot analysis of MLE cells exposed to LPS (8hr) for the indicated doses prior to endogenous SOCS2 immunoprecipitation. H. Immunoblotting of MLE cells exposed to LPS (10μg/mL) for the indicated times prior to endogenous SOCS2 immunoprecipitation. I. Silencing of Pkca and LPS time course prior to SOCS2 immunoprecipitation and immunoblot analysis in MLE cells. A-B, G-I. Data are representative of n=2 independent experiments.

117

3.2.6 Kiaa0317 knockdown ameliorates pseudomonas-induced lung injury in vivo

To explore the role of Kiaa0317 in pulmonary inflammation, we pursued in vivo knockdown studies. Mice were first infected with lentivirus encoding empty shRNA or *Kiaa0317* shRNA for 144h (1e7 PFU/mouse, i.t) and then challenged with PA103 (1e4 CFU/mouse, i.t.) for an additional 18h (Figure 33A). Mice were sacrificed and samples were processed for metrics of pulmonary inflammation. *Kiaa0317* knockdown significantly decreased lavage protein concentrations, lavage cell counts, and cell infiltrates without affecting bacterial load (Figure 33B, C, D, I). Further, *Kiaa0317* knockdown significantly decreased lavage cytokine levels of IL-6 and TNF (Figure 33E, F), and improved survival (Figure 33G). Pulmonary parenchymal tissue from *Kiaa0317*-silenced mice show higher SOCS2 protein (Figure 33H) and fewer inflammatory infiltrates (Figure 33I).
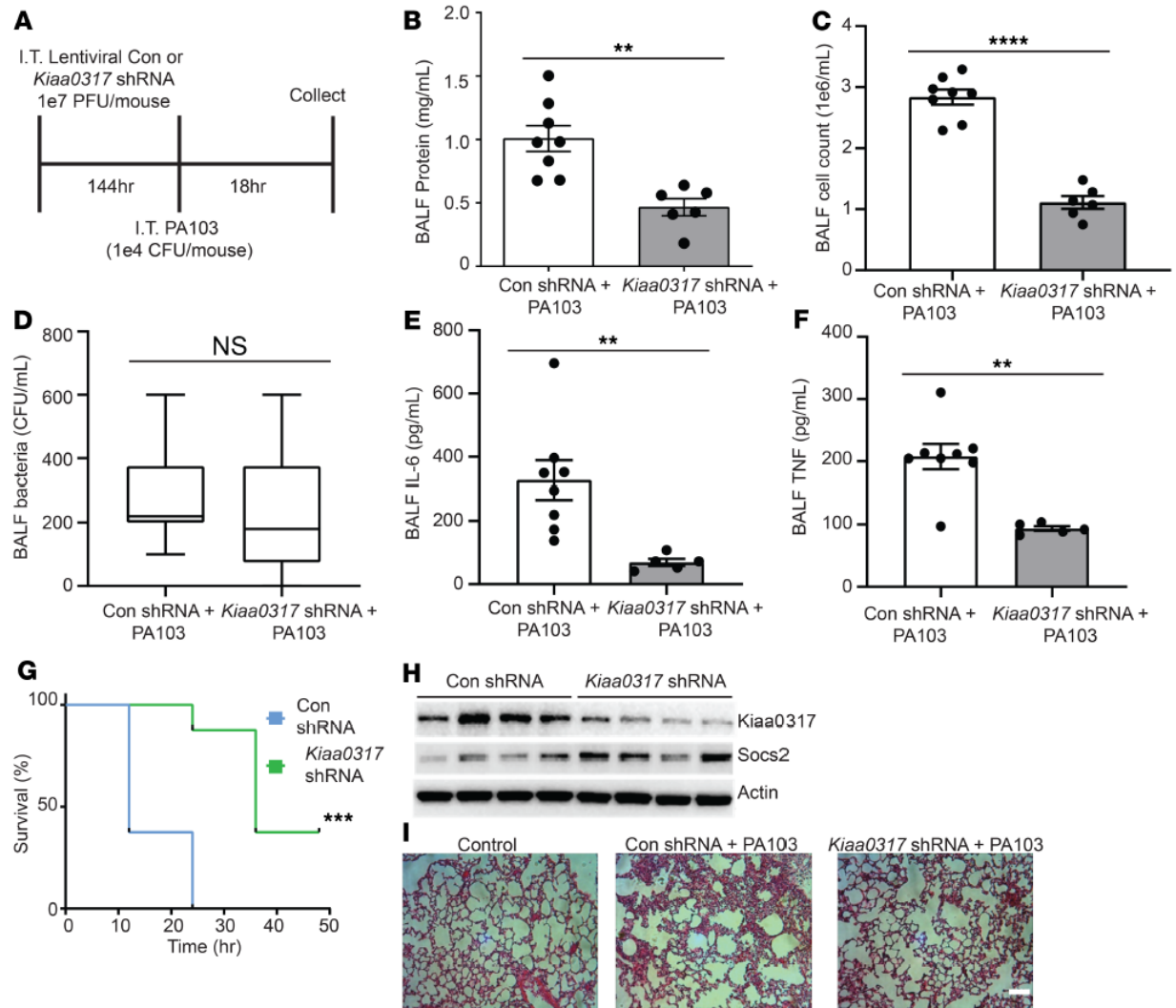
Figure 33 Kiaa0317 knockdown ameliorates pseudomonas-induced lung injury in vivo

A. Treatment strategy of lentiviral infection (1e7 PFU/mouse) and PA103 exposure (1e4 CFU/mouse). Mice were euthanized, and lungs were lavaged with saline and harvested. B-D. Protein concentration, cell count, and bacterial count measurements from bronchoalveolar lavage fluid (BALF) from treated mice, (n = 6-8 mice per group). D. Box represents the interquartile range, the line is the median, and the whiskers represent highest and lowest observations. E-F. ELISA analysis of BALF cytokines, E. IL-6, and F. TNF. G. Survival studies of mice exposed to PA103 (i.t. 1e5 CFU/mouse, n=8 mice per group). Mice were carefully monitored over time; moribund, preterminal animals were immediately euthanized and recorded as deceased. Kaplan-Meier survival curves were generated and compared; data represent mean values (n = 8 mice per group). H. Immunoblot analysis from representative murine lung homogenate, n=4 per group. I. Histology of murine lungs following H&E staining, bar indicates 100 μm. **, $p < 0.01$; ***, $p < 0.001$; ****, $p < 0.0001$; NS, $p > 0.05$; compared with control shRNA, two-tailed unpaired Student's t-test (B-F) or compared with control shRNA, log-rank (Mantel-Cox) test (G).

119

3.2.7 KIAA0317 -/- mice are resistant to LPS-induced lung inflammation

As transient silencing of KIAA0317 in C57BL6/J mice conferred a protective phenotype against PA103-induced pulmonary inflammation, we extended these studies by generating *Kiaa0317*-deficient mice. *Kiaa0317*-knockout mice were generated using CRISPR-Cas9 technology using previously described techniques (293). A sgRNA targeting exon 13 of KIAA0317 introduced a double stranded break, and subsequent NHEJ repair resulted in a 91 base pair deletion in the genomic DNA sequence, with no effects in mouse morphology or the predicted off-targeting regions (Figure 34A-D). Sequencing of the cDNA of the generated knockout revealed that the genomic DNA deletion produces a cDNA transcript missing exon 13. Splicing of exon 12 to 14 generates a frame-shift in exon 14 at amino acid 500 resulting in the introduction of a stop codon at position 503 of the knockout transcript (Figure 34A, B).

We next sought to explore the role of Kiaa0317 genetic deletion in experimental pulmonary inflammation. We observed decreased *Kiaa0317* transcript signal from *Kiaa0317*$^{+/-}$ mice, and transcript depletion in *Kiaa0317*$^{-/-}$ mice (Figure 35A-B). To test the role of *Kiaa0317* knockout in pulmonary inflammation, we challenged *Kiaa0317*$^{+/+}$, $^{+/-}$, and $^{-/-}$ mice with LPS (3 mg/kg) for 18 hours. Mice were euthanized prior to analysis of parameters of inflammatory injury. Relative to wild-type, *Kiaa0317*$^{+/-}$ and $^{-/-}$ mice showed significant and step-wise decreases in indicators of inflammatory injury, such as bronchoalveolar lavage fluid (BALF) protein concentration (Figure 35C), cell count (Figure 35D), as well as decreases in pro-inflammatory cytokine release (Figure 35E-G). Histological analysis revealed fewer inflammatory infiltrates among *Kiaa0317*$^{+/-}$ and $^{-/-}$ mice (Figure 35H). These data suggest *Kiaa0317* deletion confers protection against experimental pulmonary inflammation.

120
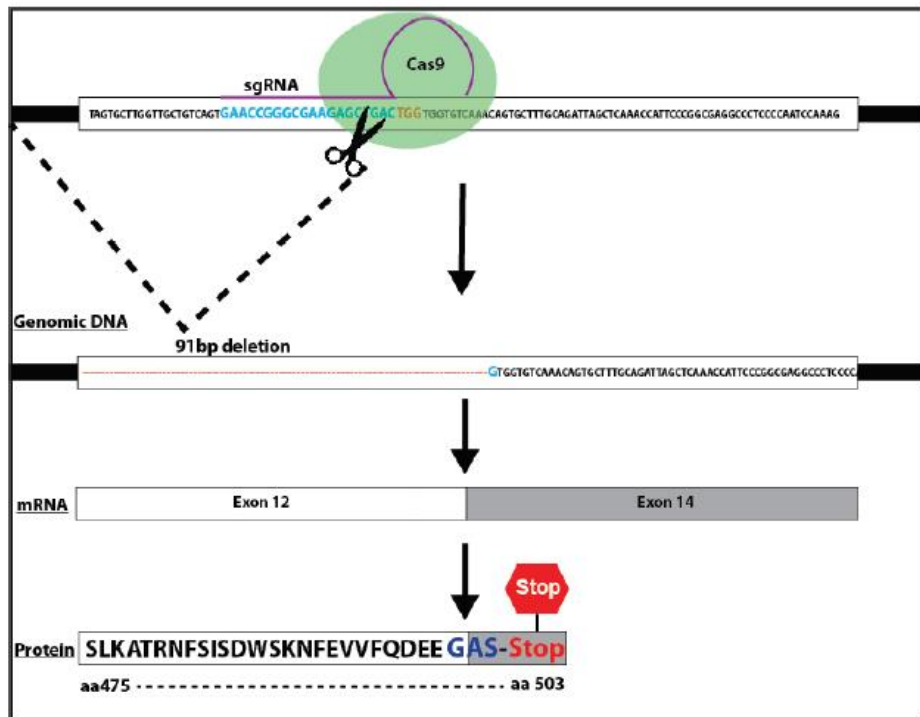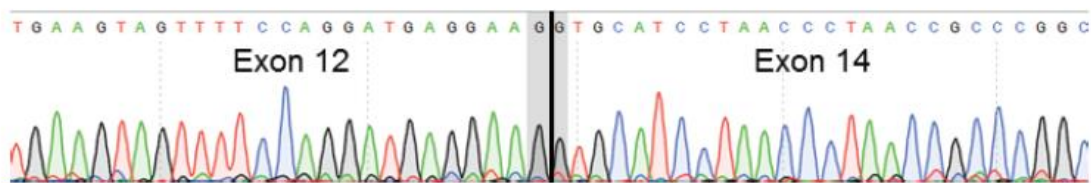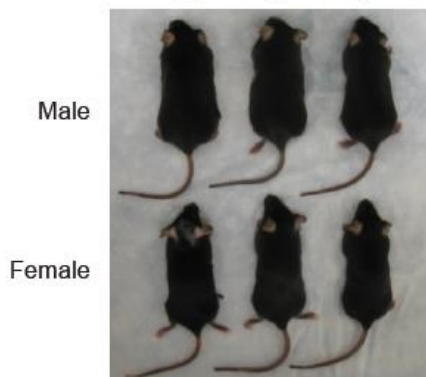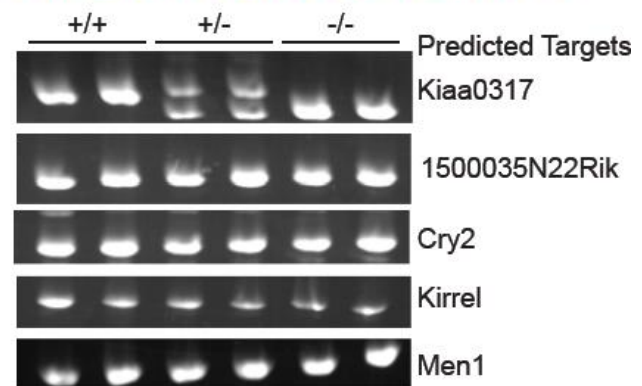
Figure 34 Generation of Kiaa0317-/- knockout mice

A-B. CRISPR-Cas9 gene editing of C57BL6/J mice. B. CRISPR editing resulted in 91bp deletion in exon 13. C. Female and Male Kiaa0317+/- and Kiaa0317-/- mice do not show morphological differences from WT. D. PCR amplification and sequencing detected no off-target effects in Kiaa0317-/- mice among top predicted targets, n=2 mice per genotype.
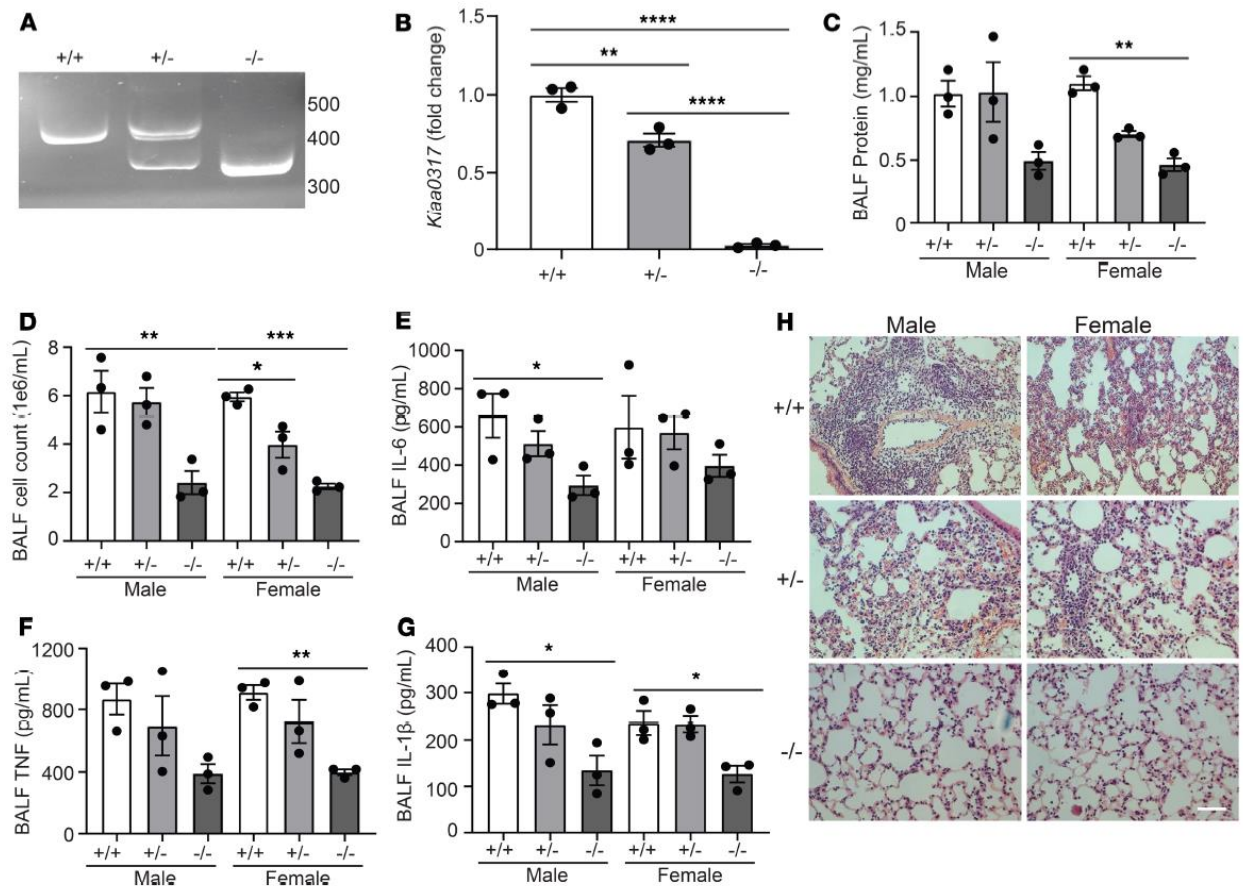
Figure 35 Kiaa0317 knockout confers protection from LPS-induced lung inflammation

A. sgRNA target site amplification from Kiaa0317+/+, +/-, and -/- mice. B. Kiaa0317 transcript levels among Kiaa0317+/+, +/-, and -/- mice. Data represent mean values ± SEM (n = 3 mice). C-G. Kiaa0317+/+, +/-, and -/- mice were intra-tracheally inoculated with LPS (3mg/kg) for 18h. Data represent mean values ± SEM (n = 3 mice per group). C-D. Cell count and protein concentration from bronchoalveolar lavage fluid (BALF). E. BALF TNF concentration. F. BALF IL-1 concentration. G. BALF IL-6 concentration. H. Histology of murine lungs following H&E staining, bar indicates 100 μm. *, $p < 0.05$; **, $p < 0.01$; ***, $p < 0.001$; ****, $p < 0.0001$; compared to indicated group or to sex-specific +/+ group, One-Way ANOVA with Tukey's multiple comparisons (B) or One-Way ANOVA with Dunnett's multiple comparisons (C-G).

3.2.8 KIAA0317 re-expression sensitizes Kiaa0317-/- to LPS-induced pulmonary inflammation

To further validate the role of *Kiaa0317* in pulmonary inflammation, we conducted a series

of lentiviral rescue experiments utilizing KIAA0317 WT and the binding-deficient P779L mutant,

122

and with LPS challenge (Figure 36). *Kiaa0317*$^{-/-}$ mice with empty lentivirus showed lower BALF protein concentration, cell counts, and cytokine release relative to *Kiaa0317*$^{+/+}$ mice (Figure 36A-E). However, an inflammatory phenotype was observed upon lentiviral expression of KIAA0317 WT in *Kiaa0317*$^{-/-}$ mice. Interestingly, KIAA0317 P779L *Kiaa0317*$^{-/-}$ mice phenocopied control *Kiaa0317*$^{-/-}$ mice. Further, the distinct effect of KIAA0317 WT and P779L expression was observed in BALF leukocyte differential counts (Figure 36F-H). BALF from both *Kiaa0317*$^{+/+}$ and $^{-/-}$ mice expressing KIAA0317 showed a large count and proportion of neutrophils. However, BALF from KIAA0317$^{-/-}$ mice expressing Empty or P779L-encoded lentivirus contained fewer leukocytes, and a smaller proportion of neutrophils (Figure 36G). Histological staining showed less inflammatory infiltration among *Kiaa0317*$^{-/-}$ mice expressing Empty and KIAA0317 P779L (Figure 36I). From these data, we conclude that the resistance to pulmonary inflammation by *Kiaa0317*$^{-/-}$ mice is due to KIAA0317.
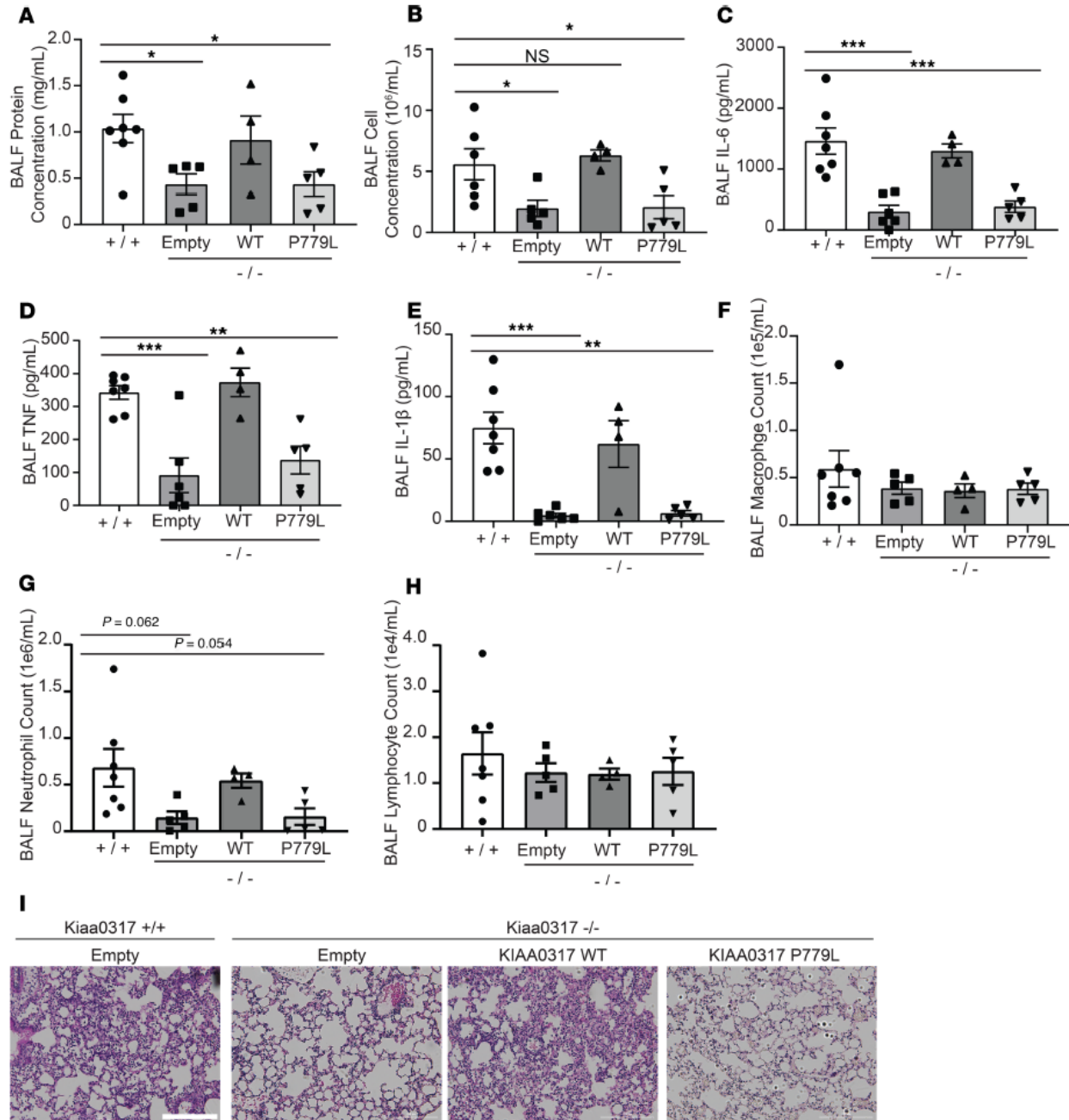
Figure 36 Re-expression of KIAA0317 in Kiaa0317-/- mice ablates resistance to inflammation

Mice were infected i.t. with lentivirus encoding empty, KIAA0317 WT, or KIAA0317 P779L (1e7 PFU/mouse) prior to LPS exposure (3 mg/kg). Following exposure, mice were euthanized, and lungs were lavaged with saline and harvested. A-B. Protein concentration and cell count measurements from bronchoalveolar lavage fluid (BALF). C-E. BALF cytokine concentrations. F-H. BALF leukocyte differential. A-H. Data represent mean values ± SEM (n = 4-7 mice; *, p < 0.05; **, p<0.01; ***, p<0.001; compared with *Kiaa0317$^{+/+}$* mice, One-Way ANOVA with Dunnett's Multiple Comparisons). I. Histology of murine lungs following H&E staining, bar indicates 200 μm. *, p < 0.05; **, p < 0.01; ***, p < 0.001; compared to *Kiaa0317$^{+/+}$* mice, One-Way ANOVA with Dunnett's multiple comparisons (A-H).

3.2.9 Kiaa0317-/- resistance to pulmonary inflammation is ablated upon depletion of SOCS2

Next, we wanted to explore the role of SOCS2 in *Kiaa0317*$^{-/-}$ mice. To study this, we conducted lentiviral SOCS2 silencing experiments and LPS challenge with *Kiaa0317*$^{+/+}$ and $^{-/-}$ mice (Figure 37). We recapitulated previous results showing the susceptibility of SOCS2-silenced WT (*Kiaa0317*$^{+/+}$) mice to LPS-induced inflammation, and extended these observations to a lung inflammation model (282). BALF from these SOCS2-silenced-*Kiaa0317*$^{+/+}$ mice showed higher protein and cell concentration, cytokine secretion, and leukocyte recruitment relative to control shRNA (Figure 37A-H). Similar to earlier observations above (Figure 35), control-*Kiaa0317*$^{-/-}$ mice showed resistance to LPS-induced pulmonary inflammation. However, SOCS2-silenced-*Kiaa0317*$^{-/-}$ mice phenocopied SOCS2-silenced WT (*Kiaa0317*$^{+/+}$) mice. We hypothesize that silencing of the putative substrate of KIAA0317, SOCS2, removes the protection of KIAA0317 knockout. Finally, histological analysis showed enhanced inflammatory infiltration among both SOCS2-silenced *Kiaa0317*$^{+/+}$ and $^{-/-}$ mice (Figure 37I). These rescue experiments suggest that *Kiaa0317* is both necessary and sufficient for LPS-induced pulmonary inflammation. Further, this inflammatory phenotype operates through a KIAA0317-SOCS2 axis, as depletion of SOCS2 enhances inflammation, even in the background of *Kiaa0317* genetic knockout. Collectively, the above studies suggest *Kiaa0317* plays an integral role in mediating cytokine-driven inflammation via the SOCS2-cytokine axis.
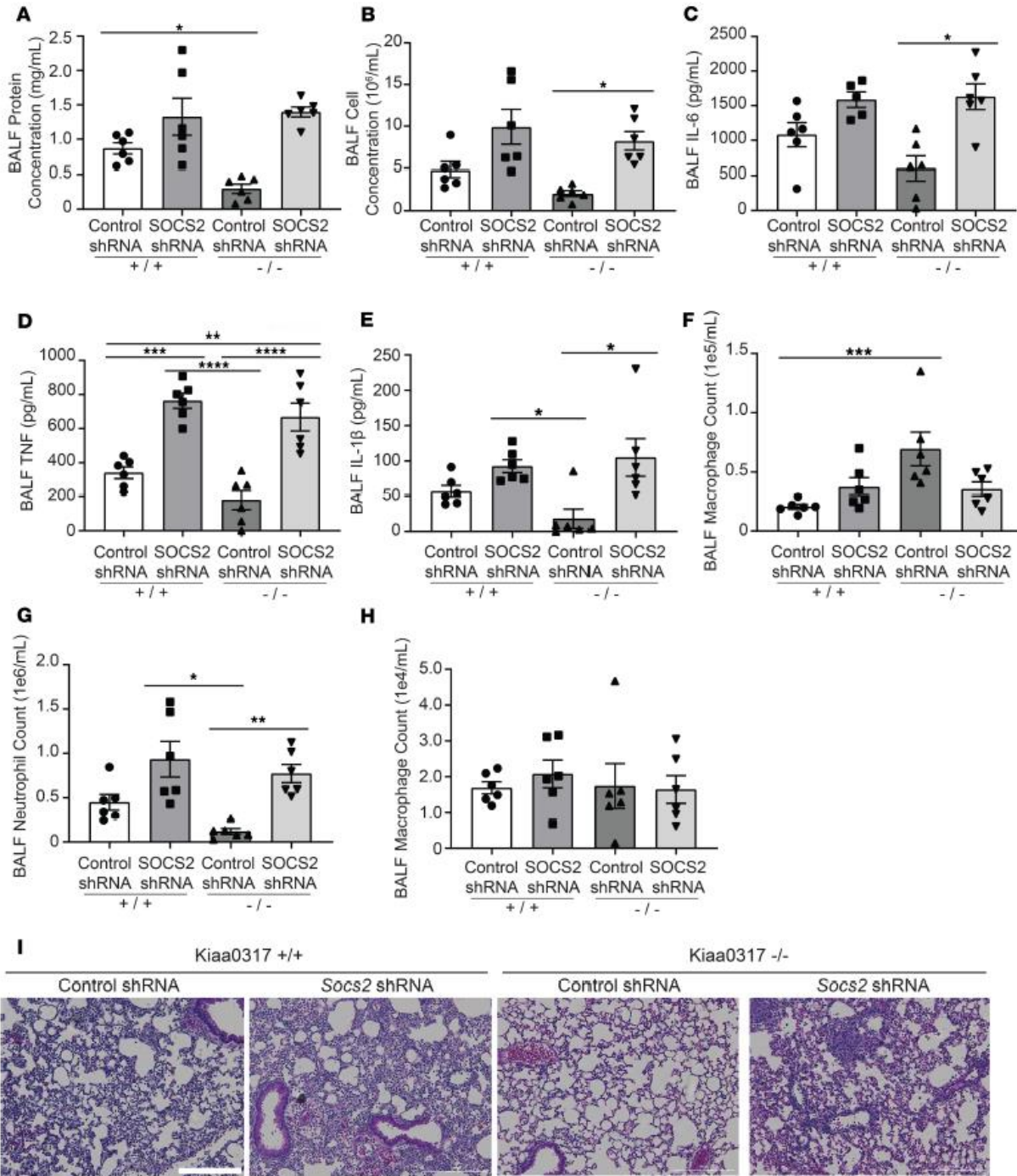
Figure 37 Protected phenotype of Kiaa0317-/- mice requires SOCS2

Mice were infected i.t. with lentivirus encoding empty, Control shRNA, or Socs2 shRNA (1e7 PFU/mouse) prior to LPS exposure (3 mg/kg). Following exposure, mice were euthanized, and lungs were lavaged with saline and harvested. A-B. Protein concentration and cell count measurements from bronchoalveolar lavage fluid (BALF). C-E. BALF cytokine concentrations. F-H. BALF leukocyte differential. A-H. Data represent mean values ± SEM (n = 5-6 mice) I. Histology of murine lungs following H&E staining, bar indicates 200 μm. *, p < 0.05; **, p<0.01; ***, p<0.001; ****, p<0.0001; compared with Control shRNA-Kiaa0317+/+ mice or as indicated, One-Way ANOVA with Tukey's Multiple Comparisons.

3.2.10 KIAA0317 domain analysis and inhibitor screening

KIAA0317 harbors a conserved HECT domain within its C-terminus (294, 295). Since the HECT domain carries out the E3 ligase activity of transferring ubiquitin to the substrate, we hypothesized that small molecule inhibition of the HECT domain would disrupt KIAA0317 substrate targeting. We constructed an *in silico* homology model using the NEDD4 HECT domain (296, 297) (2XBF.pdb) (Figure 38A) to assay potential ligands on the KIAA0317-HECT domain 3-D structure (Figure 38B). We used molecular docking analysis and score-ranking operations through the LibDock program (Discovery Studio 3.5) to virtually screen 5e5 small molecules. The top ten score-ranking molecules were selected and evaluated further using in vitro experiments (Data not shown). In this model, the inhibitors interact with distinct residues within the HECT domain (Figure 38C). We tested one of the selected compounds, termed BC-1365, in an in vitro binding assay, which resulted in potent inhibition of the KIAA0317/SOCS2 interaction (Figure 38D). We also tested this compound in MLE cells and observed increased SOCS2 protein levels while KIAA0317 protein was unaffected (Figure 38E). BC-1365 titration also did not alter mRNA levels of *Socs2* (Figure 38F). To probe the effect of BC-1365 on the activity of other HECT E3 ligases, we treated MLE and BEAS-2B cells with BC-1365 and immunoblotted for known HECT E3 ligase substrate protein levels (Table 2). We did not observe increase in any other HECT E3 ligase substrate relative to the increase in SOCS2 (Figure 39A-B). Additionally, we conducted target validation studies using RNAi knockdown of *Kiaa0317* prior to treatment with BC-1365 and LPS (Figure 39C-F). We observed that BC-1365 treatment of MLE cells increased SOCS2 protein level, but not to a higher extent in the background of *Kiaa0317* silencing (Figure 39C). We also tested the supernatant of these cells for pro-inflammatory cytokine release and observed decreased IL-6 and CXCL-1 during *Kiaa0317* depletion compared to control, however we

observed no difference upon BC-1365 treatment among *Kiaa0317* depleted cells (Figure 39D-E). Finally, we assayed the effect of BC-1365 on primary human PBMCs. We observed a dose-dependent effect of BC-1365 in decreasing the secretion of pro-inflammatory cytokines IL-6, TNF, and IL-1β from human primary PBMCs exposed to LPS (Figure 41A-C). These data suggest chemically inhibiting KIAA0317 protein prevents SOCS2 degradation and dampens pro-inflammatory signaling.
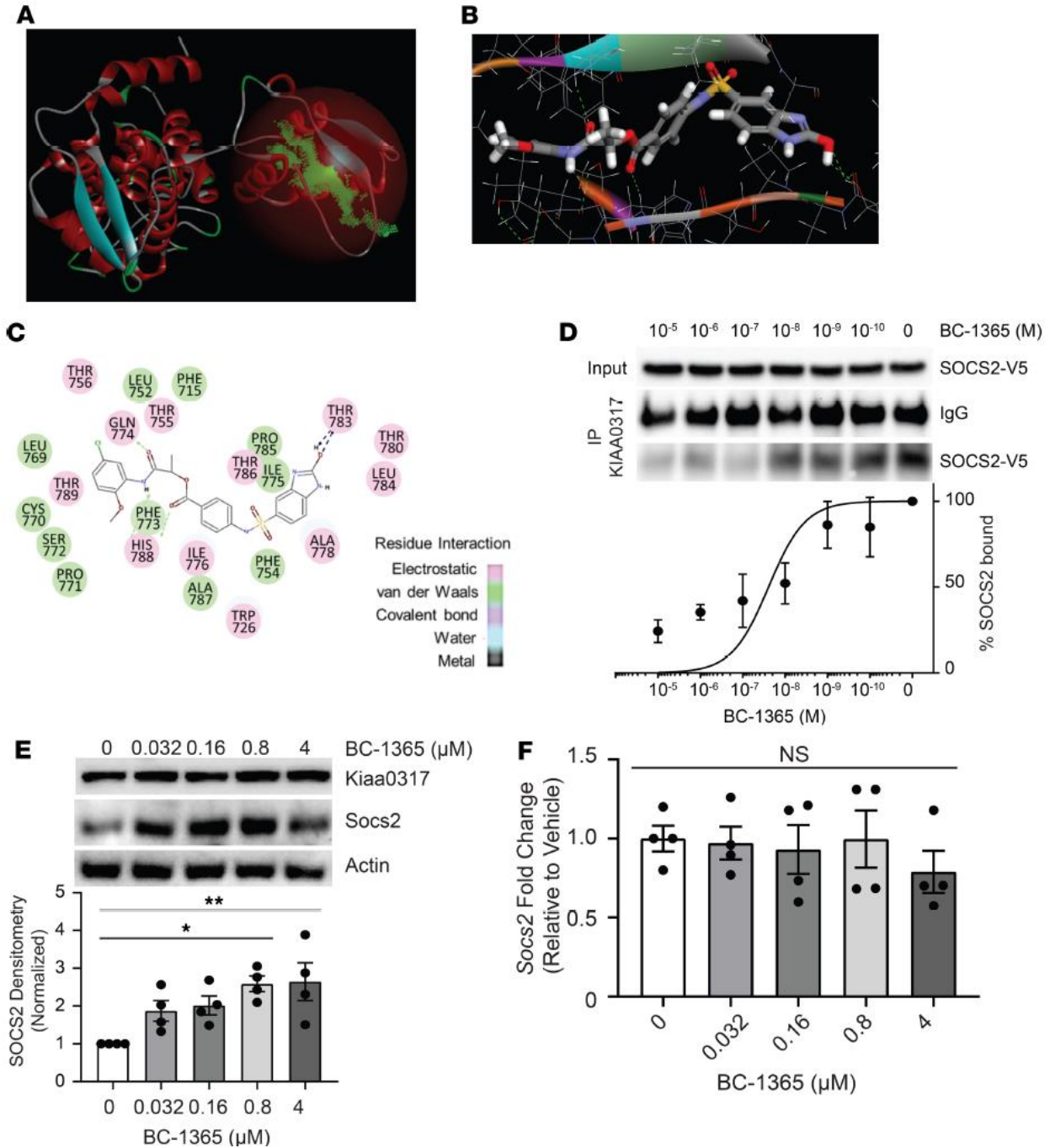
Figure 38 Chemical inhibition of KIAA0317 prevents SOCS2 degradation and inflammation in vitro

A. Structural analysis of the KIAA0317 HECT domain revealed a major cavity within the C-terminus of the HECT domain. B-C. Docking study of candidate inhibitor BC-1365 with the KIAA0317-HECT domain. D. BC-1365 Competition Assay. SOCS2 protein was incubated with KIAA0317-bound resin and a titration of BC-1365 prior to immunoblot analysis. The relative amounts of SOCS2 detected in the pull-downs was normalized to vehicle and quantified. Data represent mean values ± SEM (n=3). E. Immunoblot analysis of MLE cells following exposure to a titration of BC-1365, Data represent mean values ± SEM (n=4). F. MLE cells were exposed to a titration of BC-1365 for 18h before qPCR analysis, data represent mean values ± SEM (n = 4). NS, $p>0.05$; *, $p < 0.05$; **, $p<0.01$; compared with vehicle treatment, One-Way ANOVA with Dunnett's Multiple Comparisons (E-F)

129

Table 2 HECT E3 ligase Homology to KIAA0317

E3 Ligase	Homology Ranking	Characterized Substrate	Reference
KIAA0317/AREL1	0		
NEDD4L	1	SMAD2	(298)
NEDD4	2	GRB10	(299)
HACE1	3	Rac1 (1/2/3)	(300)
ITCH	4	CXCR4	(301)
WWP2	5	Oct-3/4	(302)
HUWE1	6	Mcl-1	(303)
HECW1	7	DVL	(304)
SMURF1	8	SMAD1	(305)
HECW2	9	Hp1a	(306)
SMURF2	10	SMAD2 (same as#2)	(307)
WWP1	11	TGFBR1	(308)
UBE3C	12	IRF-7	(309)
UBE3B	13	BCKDK	(310)
UBE3A	14	P27	(311)
HECTD2	15	PIAS1	(283)
HERC3	16	P65	(312)
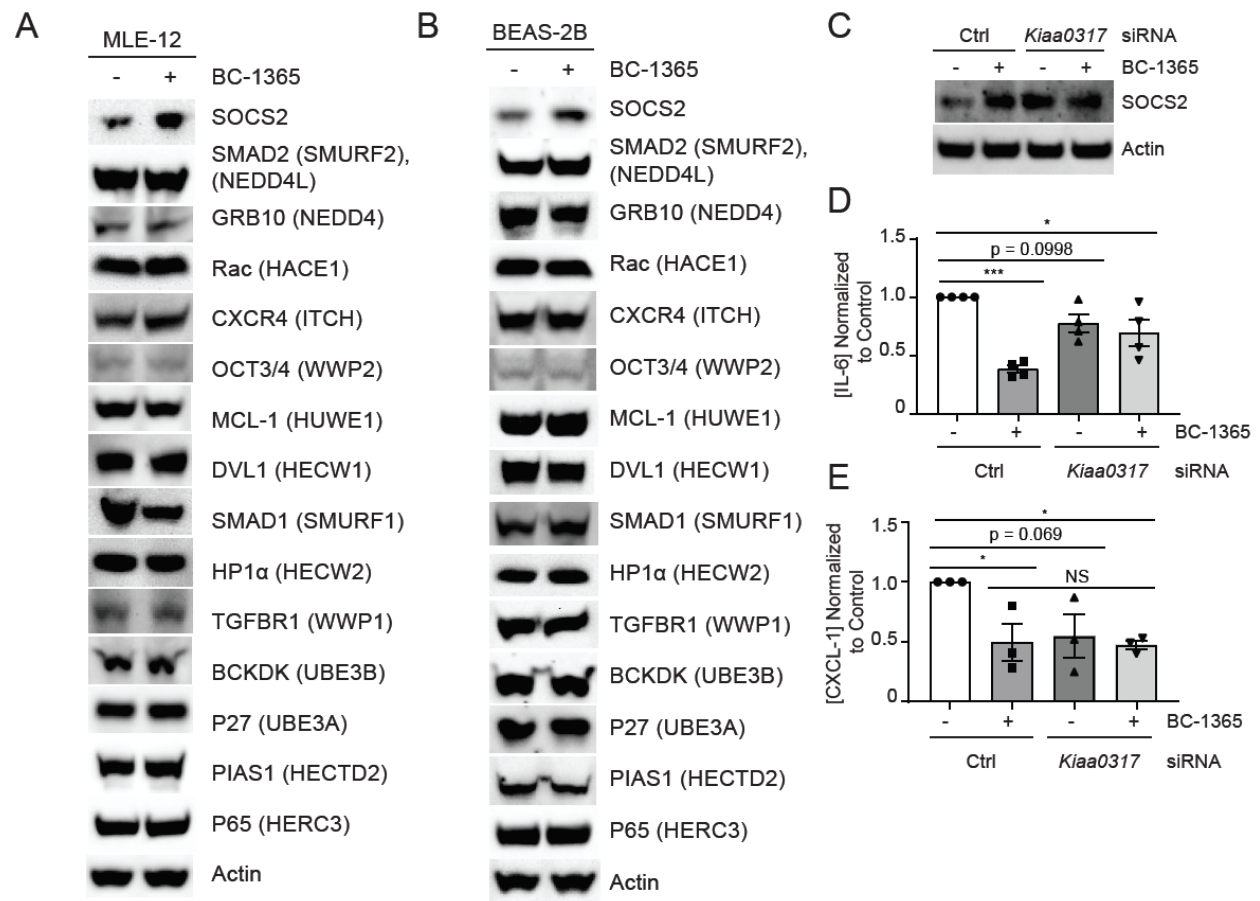
Figure 39 BC-1365 is specific to KIAA0317

A-B. Immunoblotting Analysis of known HECT-E3 Ligase substrates from MLE-12 and BEAS-2B cells treated with BC-1365. Parentheses after substrate name indicates HECT E3 ligase shown to regulate it (e.g. GRB10 targeted by NEDD4). C. SOCS2 blotting from MLE treated with Control or Kiaa0317 siRNA without or with BC-1365 treatment prior to LPS exposure. D-E. ELISA analysis of supernatant from cells treated in C. for inflammatory cytokines: D. IL-6 and E. CXCL1, data represent mean values ± SEM (n = 3-8). NS, p>0.05; *, p < 0.05; ***, p<0.001; compared with untreated Control, One-Way ANOVA with Tukey's Multiple Comparisons (D-E). A-C. Data are representative of n=2-3 independent experiments.

131

3.2.11 Anti-inflammatory activity of a KIAA0317 small molecule inhibitor in vivo

To assess in vivo anti-inflammatory activity of BC-1365, we exposed C57BL/6J mice to *P. aeruginosa* (PA103) and BC-1365. Briefly, PA103 was administered i.t. (1e4 CFU) immediately followed by BC-1365 delivery i.p. (10 mg/kg) for 18hr exposure. BC-1365 did not affect BALF bacterial counts (Figure 40A), however, BC-1365-treated mice displayed significantly decreased lavage protein concentrations, cell counts, and cell infiltrates relative to vehicle-treated (Figure 40B, C, I). Further, BC-1365 significantly decreased lavage cytokine levels (Figure 40D-F), increased SOCS2 protein levels (Figure 40H), and reduced histological infiltrates (Figure 40I). As an alternative approach, we tested BC-1365 in vivo using an LPS model (Figure 41D-H). Briefly, LPS (3mg/kg, i.t.) and BC-1365 (10 mg/kg, i.p.) were co-administered to C57BL/6J mice. Following 18 hours, mice were euthanized, and lungs were lavaged with saline. BC-1365 treatment led to significantly decreased lavage protein concentrations, cell counts, and cell infiltrates in LPS-stimulated mice (Figure 41D, E, H). Further, BC-1365 treatment significantly decreased lavage cytokine levels (Figure 41F-G). Hence, small molecule targeting of the KIAA0317-SOCS2 pathway reduces severity of cytokine-driven lung inflammation (Figure 42).
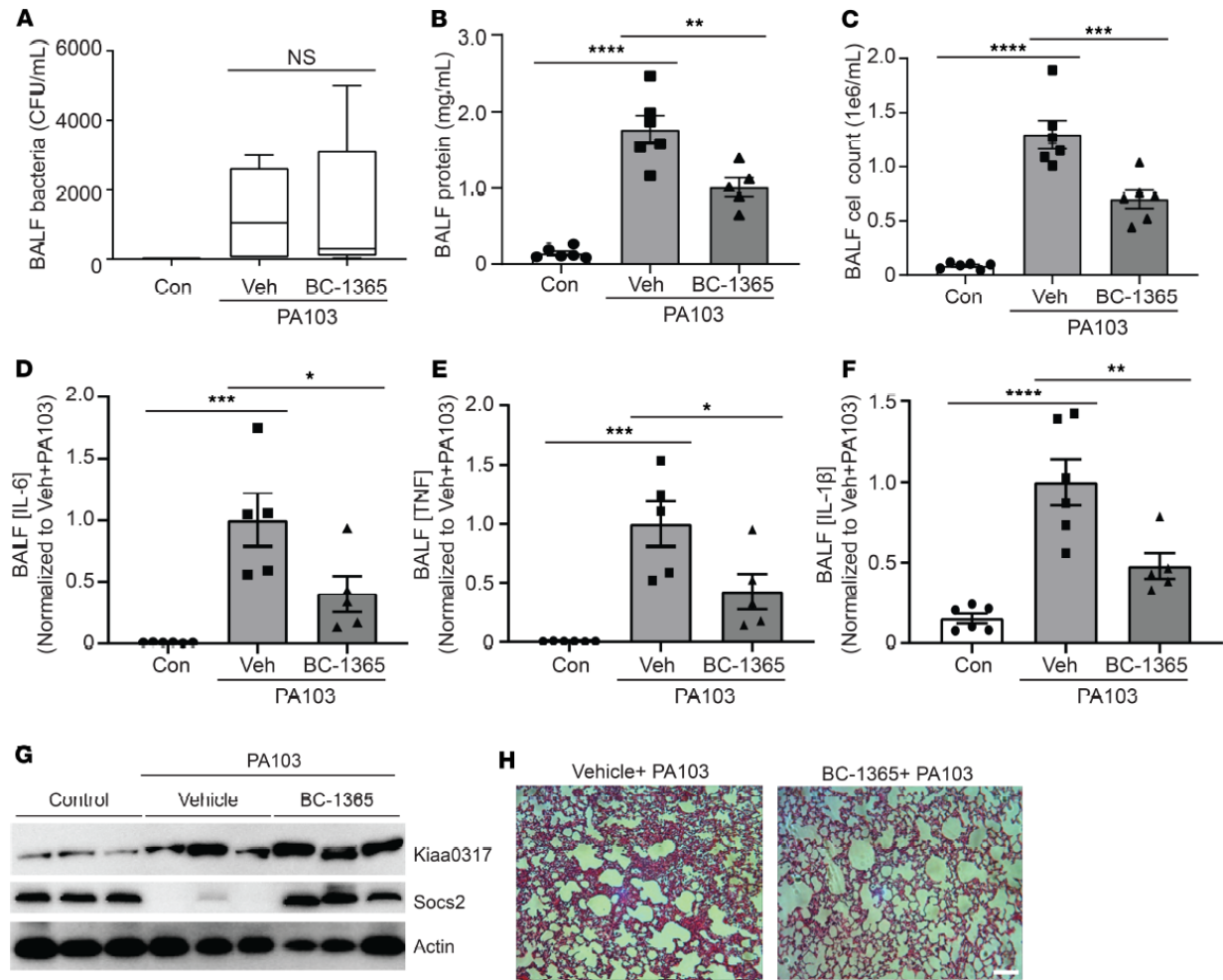
Figure 40 KIAA0317 small molecule inhibitor is anti-inflammatory in vivo

A-E. C57BL/6J mice were exposed to PA103 and treated with BC-1365 for 18hr. Following exposure, mice were sacrificed, and lungs were lavaged with saline and harvested. Box represents the interquartile range, line is the median, and the whiskers represent highest and lowest observations. A-C. Bacterial count, protein concentration, and cell count measurements from bronchoalveolar lavage fluid (BALF). D-F. BALF cytokine concentrations. A-F. Data represent mean values ± SEM (n = 4-8 mice; *, p < 0.05; **, p<0.01; ***, p<0.001; ****, p<0.0001; compared with Control mice or as indicated, One-Way ANOVA with Tukey's Multiple Comparisons). H. Immunoblotting of mouse lung homogenate for Kiaa0317 and Socs2 protein signal, n=3 mice per treatment. I. Representative histology of murine lungs following hematoxylin and eosin staining, bar indicates 100µm. NS, p>0.05; *, p < 0.05; **, p<0.01; ***, p<0.001; ****, p<0.0001; compared with control treatment or as indicated, One-Way ANOVA with Tukey's Multiple Comparisons (A-F).
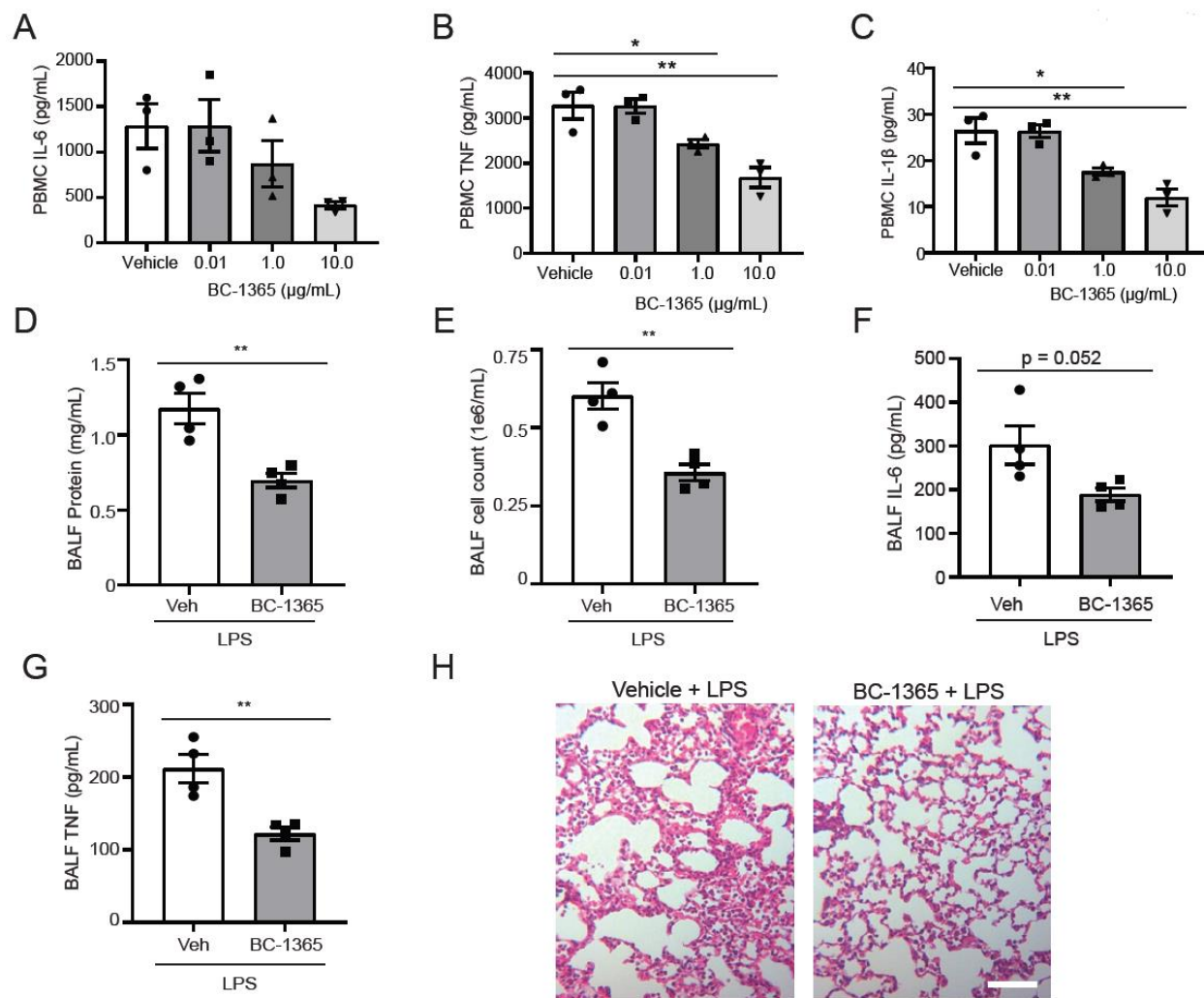
Figure 41 BC-1365 shows efficacy in cell and animal models of inflammation

A-C. ELISA analysis of cytokine release from LPS-treated PBMC co-treated with BC-1365 at indicated doses. Data represent mean values ± SEM (n = 3). D-H. C57BL/6J mice were intratracheally inoculated with LPS (3mg/kg) and intraperitoneal BC-1365 treatment (10mg/kg). 18h later, mice were sacrificed, and lungs were lavaged with saline and harvested. (D-E) Protein concentration and cell count measurements from bronchoalveolar lavage fluid (BALF). (F-G) BALF cytokine concentrations. D-G. Data represent mean values ± SEM (n = 4 mice). J. Histology of murine lungs following H&E staining, bar indicates 100µm. NS, p>0.05; *, p < 0.05; **, p<0.01; compared with Vehicle, One-Way ANOVA with Dunnett's Multiple Comparisons (A-C), or , two tailed unpaired Student's t-test (D-G).

3.2.12 Discussion

These studies have established a mechanism of SOCS2 protein regulation leading to the control of pulmonary inflammation. We showed the ubiquitin E3 ligase KIAA0317 targets SOCS2 for ubiquitination and degradation by the proteasome and modulating pro-inflammatory signaling. In mouse models of LPS and PA-103 exposure, KIAA0317 depletion and deletion reduced markers of pulmonary inflammation and rescued SOCS2 protein. Re-introduction of KIAA0317 protein into these models removed any protective phenotype; however, re-introduction of a binding deficient KIAA0317 mutant preserved the protection from experimental inflammation. We also uncovered a small molecule inhibitor of KIAA0317 activity, BC-1365, which preserved SOCS2 protein from degradation in vitro and lessened cytokine release from primary tissue samples. BC-1365-treated mice also displayed resistance to experimental pulmonary inflammation.

SOCS2 mediates the degradation of a variety of proteins and functions as a feedback inhibitor to cytokine signaling (57). While SOCS2 has been shown to regulate several cytokine related pathways (282, 313), recently SOCS2 has been observed to directly regulate NF-κB signaling (280, 281). Similarly, the silencing of KIAA0317 weakened LPS and TNF-induced NF-κB promoter activity in 293 cells (Figure 30K-L). LPS has been shown to induce cellular ubiquitination (314, 315), and we have previously observed E3 ligase induction and substrate-association by such insult (60, 283). We observed that LPS exposure promoted SOCS2 association with KIAA0317, and accelerated SOCS2 protein ubiquitination and degradation (Figure 32H, I). LPS also increased SOCS2 polyubiquitin signal, which was further increased by co-expression with KIAA0317 (Figure 30J). These data show that KIAA0317 functions as a pro-inflammatory E3 ligase.

135

Mapping studies elucidated the critical regions of SOCS2-KIAA0317 binding. We observed that SOCS2 requires serine-52 for binding with KIAA0317, potentially functioning as a phosphodegron Figure 31C-F). Interestingly, there exists a naturally occurring polymorphism causing a S52N mutation (rs3741676). S52N SOCS2 protein was unable to bind KIAA0317, and resisted KIAA0317-mediated degradation (Figure 31D-F). PKCA was found to associate with SOCS2, facilitate its phosphorylation, and regulate its protein stability (Figure 32). This finding is interesting given that previous research show that PKCA upregulates NF-κB signaling (292, 316), potentially through the regulation of SOCS2 protein stability. Further, we observed that the C-terminal region, and proline-779, within KIAA0317 is critical for SOCS2 binding (Figure 31G-L). This residue itself is part of a naturally occurring polymorphism resulting in P779L mutation (rs371610162). KIAA0317 with P779L mutation is unable to degrade SOCS2 protein (Figure 31L). Additionally, P779L-expressed $Kiaa0317^{-/-}$ mice were resistant to LPS-induced pulmonary inflammation, compared to WT KIAA0317-expressed $Kiaa0317^{-/-}$ mice (Figure 36). These data further underscore the protective phenotype conferred by P779L mutation, potentially through the inability to degrade SOCS2 protein. Studies into the prevalence of these polymorphisms among populations and among patient cohorts are needed to investigate the pathological implications in humans.

Inflammatory lung diseases such as ARDS are often triggered by opportunistic infection, including gram-negative bacteria such as *P. aeruginosa*, leading to runaway inflammation and cytokine storm. We showed that shRNA knockdown of *Kiaa0317* in a *P. aeruginosa* mouse model led to reduced lung inflammation and less cytokines and immune infiltrates compared to control, without changing *P. aeruginosa* bacteria levels in a mouse model. We further explored this relationship through CRISPR/Cas9-mediated deletion of *Kiaa0317* in C57BL/6 mice (Figure 35).

Kiaa0317^{+/-} and [-/-] mice showed increasing protection from pulmonary inflammation relative to wild-type. This effect could be due to the difference in effector protein abundance, as we observed depletion in *KIAA0317* transcript through qPCR analysis (Figure 35B). Cytokine signal transduction pathways related to inflammation and innate immunity undergo significant cross-talk and pleiotropy, which impairs the generalizability of reductionist studies. To address this, we re-expressed our deleted KIAA0317 protein in Kiaa0317-/- mice (Figure 36). As we observed a similar pro-inflammatory phenotype among KIAA0317 rescued mice compared to WT, we hypothesize that KIAA0317 protein is the driving effector in this model. Additionally, E3 ligases often regulate multiple substrates, specifically seen in fellow-HECT E3 ligase ITCH (317). To test the link between SOCS2 and KIAA0317, we silenced SOCS2 in Kiaa0317-/- mice, prior to LPS challenge (Figure 37). By silencing SOCS2 expression in the background of KIAA0317, we questioned if the protection conferred by KIAA0317 deletion occurred in the absence of SOCS2. However, SOCS2-silenced *Kiaa0317*^{-/-} mice were susceptible to LPS-induced pulmonary inflammation and phenocopied SOCS2-silenced WT mice. This shows that the protective effect of KIAA0317 silencing is dependent of SOCS2. This interplay suggests the criticality of the two proteins in experimental lung inflammation. We suspect this KIAA0317-SOCS2 axis plays an essential role in regulating pulmonary innate immunity.

There are limited therapeutic options for treating diseases of pulmonary inflammation. Previous efforts utilized systemic corticosteroids or inhibition of immune cell surface receptors or secreted cytokines (318-320). These broad-spectrum agents such as corticosteroids have shown adverse effects in clinical trials that outweigh any potential benefit (321). Chemical inhibition of ubiquitin E3 ligases has been shown to alleviate experimental lung inflammation (62, 283). We screened a chemical library *in silico* against the C-terminus of KIAA0317, and uncovered a

chemical, termed BC-1365 (Figure 38A-C). BC-1365 abrogated SOCS2-KIAA0317 binding in vitro, restored SOCS2 protein levels in cells (Figure 38D-F) and reduced the abundance of pro-inflammatory cytokines secreted from PBMCs (Figure 41A-C). Based on these data, we tested BC-1365 in both *P. aeruginosa*- and LPS-induced murine models of ARDS. BC-1365 was also effective in vivo as BAL protein concentrations, BAL cell counts, lavage cytokine levels, and histological evidence of lung injury were all decreased in both models upon BC-1365 treatment (Figure 40) Small molecule inhibition of the KIAA0317/SOCS2 interaction reduces the severity of NF-κB-driven, cytokine-induced lung inflammation by modifying the abundance of SOCS2. These results suggest that KIAA0317 may be a promising new therapeutic target in the treatment of pulmonary inflammation. Future studies focusing on evaluating the safety profile, distribution, elimination, and metabolism of this antagonist are needed to fully understand the effects of this treatment, but the discovery of a novel therapy specific to a critical mechanism of pulmonary inflammation would be a crucial advancement in this field.
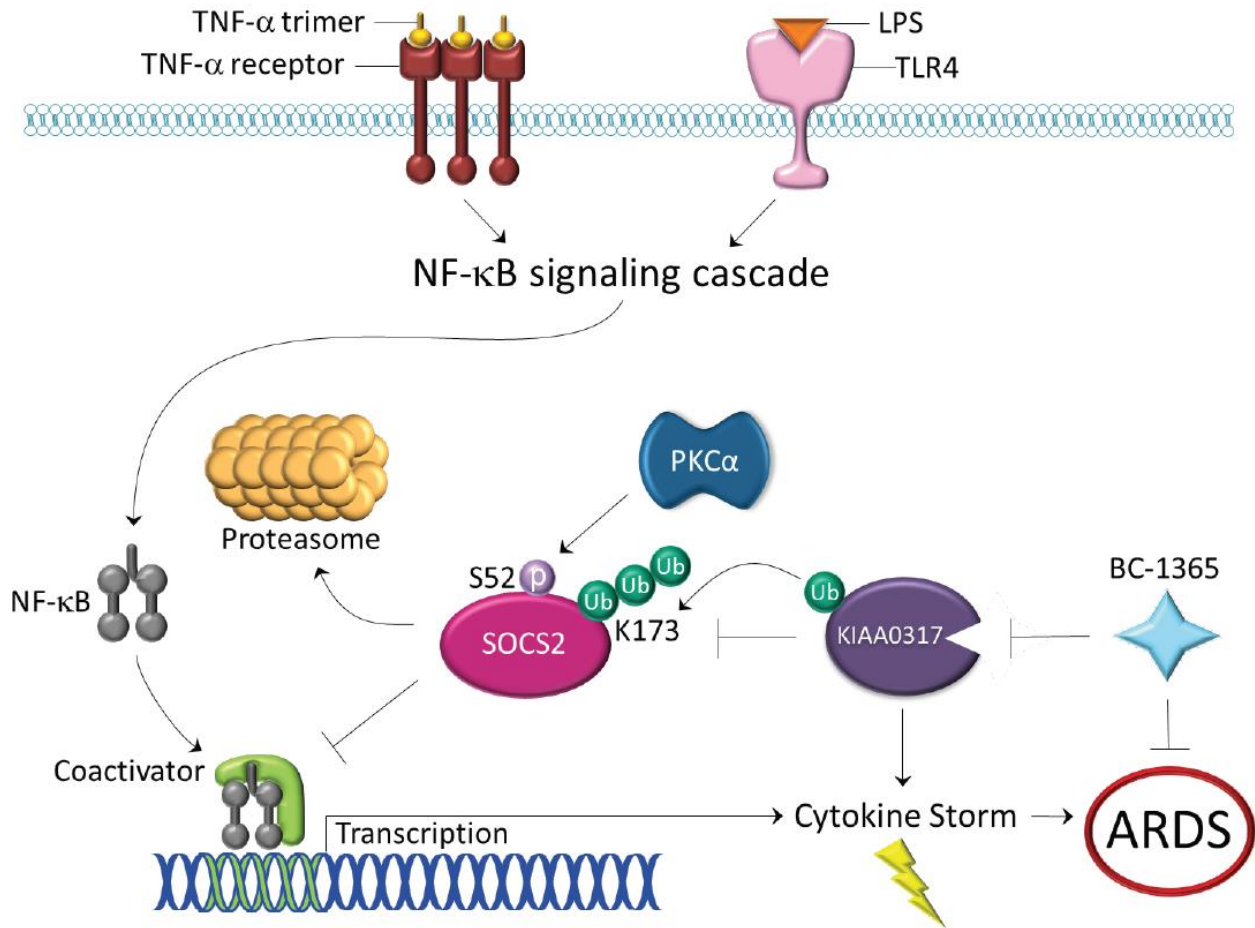
Figure 42 Proposed model of action

Microbial infection or stimuli robustly trigger inflammation by decreasing anti-inflammatory proteins such as SOCS2 in cells. Specifically, during microbial infection, KIAA0317 targets SOCS2 for its ubiquitination at Lys173; this process is facilitated by PKCA phosphorylation of SOCS2 at Ser52. A smallmolecule KIAA0317 inhibitor, BC-1365, lowered inflammation in the animal model of acute lung injury by antagonizing the actions of KIAA0317 on SOCS2-cytokine signaling.

3.2.13 Methods

3.2.13.1 Reagents and Materials

Rabbit Polyclonal anti-SOCS2 (Cat# ab3692, RRID:AB_304007) and recombinant human

PKC alpha protein(Cat# ab55672) were from Abcam. Recombinant Human SOCS-2 Protein (Cat#

H00008835-P01) was from Abnova. WesternBright Sirius HRP substrate (Cat# K-12043) was from Advansta. QuikChange II XL Site-Directed Mutagenesis Kit (Cat# 200521) was from Agilent Technologies. AnaSed (xylazine sterile solution) (Cat# 59399-110-20) was from Akorn. PureLink RNA Mini Kit (Cat# 12183025) was from Ambion. High-Capacity RNA-to-cDNA Kit (Cat# 4387406) and SYBR Select Master Mix for CFX (Cat# 4472942) were from Applied Biosystems PA-103 (Cat# 29260), MLE-12 (Cat# CRL-2110, RRID:CVCL_3751), Hek293T(Cat# CCL-2, RRID:CVCL_0030), and BEAS2-B (Cat# CRL-9609, RRID:CVCL_0168) were from ATCC. Life ECO Thermal Cycler (Cat# BYQ6078) was from BIOER. Goat anti-Rabbit HRP BioRad (Cat# 170-6515 RRID:AB_11125142), Goat anti-Mouse HRP (Cat# 170-6516 RRID:AB_11125547), Rabbit anti-Goat HRP (Cat# 172-1034 RRID:AB_11125144), DC Protein Assay Kit (Cat# 5000111), CFX96 Touch Real-Time PCR Detection System (Cat# 1855196), Personal Molecular Imager™ (PMI™) System(Cat# 1709400), ChemiDoc™ XRS+ System (Cat# 1708265), and TC20 Automated Cell Counter (Cat# 1450102) were from BioRad. Mouse Monoclonal anti-HA-Tag (clone 6E2) (Cat# 2367S RRID:AB_10691311), Rabbit Polyclonal anti-SOCS1 (clone A156) (Cat# 3950S RRID:AB_2192983), and Mouse Monoclonal anti-Phosphothreonine (Cat# 9386S RRID:AB_331239) were from Cell Signaling Technology. Lenti-X Packaging System (Cat# 631276) was from Clontech. Human TNF alpha Recombinant Protein (Cat# 14-8329-81) and Mouse IL-6 ELISA Ready-SET-Go! (Cat# 88-7064-22 RRID:AB_2574986) were from eBioscience. LPS, E. Coli O111:B4 (Cat# LPS25) was from EMD Millipore. Cycloheximide (Cat# BML-GR310) and Ubiquitinylation kit (Cat# BML-UW9920-0001) were from Enzo. TNF alpha Mouse ELISA Kit (Cat# BMS607-3TEN), IL-1 beta Mouse ELISA Kit Invitrogen (Cat# KMC0011), pcDNA3.1D-V5-HIS-TOPOInvitrogen(Cat# K490001), and pcDNA3.1D-V5-HIS-Empty Invitrogen (Cat# K490001) were from Invitrogen.

C57BL/6J Mus musculus (RRID:IMSR_JAX:000664) were from JAX. Mouse Monoclonal Anti-Ubiquitin (VU-1) (Cat# VU101) were from Life Sensors. ATP, [γ-32P]- 3000Ci/mmol 10mCi/ml (Cat# BLU002A) was from PerkinElmer. Pierce Streptavidin Magnetic Beads (Cat# 88816) were from Pierce. TnT T7 Quick Coupled Transcription/Translation (Cat# L1170) was from Promega. Cignal NFkB Pathway Reporter Assay Kit (LUC) (Cat# CCS-013L) was from Qiagen. X-tremeGENE 9 (XTG9-RO) (Cat# XTG9-RO) was from Roche. Rabbit Polyclonal anti-SOCS3 (clone H-103) (Cat# sc-9023 RRID:AB_2193305), Mouse Monoclonal anti-CaMKI (clone H-8) (Cat#sc-137225, RRID:AB_2069999), Rabbit Polyclonal anti-ERK1 (clone C-16) (Cat# sc-93 RRID:AB_631453), Rabbit Polyclonal anti-MAPK14 (p38α) (clone C-20) (Cat# sc-535 RRID:AB_632138), Mouse Monoclonal anti-PKC alpha (clone H-7) (Cat# sc-8393 RRID:AB_628142), Goat Polyclonal anti-p-PKCa (Ser 657) (Cat# sc-12356 RRID:AB_2168557), Mouse Monoclonal anti-Phosphoserine (Cat# sc-81516 RRID:AB_1128626), and Mouse Monoclonal anti-PKCz (Cat# sc-17781 RRID:AB_628148) were from Santa Cruz Biotechnology. Leupeptin (Cat# L2884), ATP (Cat# A2383), Mouse Monoclonal anti-beta-Actin (clone AC-15) (Cat# A5441 RRID:AB_476744), and Rabbit Polyclonal anti-KIAA0317 (Cat# SAB2108763) were from Sigma-Aldrich. Recombinant Glutathione S-Transferase Protein (Cat# 11213-HNAB) was from SinoBiological. Mouse Monoclonal anti-V5 Tag (Cat# R960-25 RRID:AB_2556564), Protein A/G Magnetic Beads (Cat# 88802), E. coli One Shot TOP10 (Cat# C404003), pcDNA3.1 Directional TOPO Expression Kit (Cat# K490001), were from Thermo Fisher Scientific. pRK5-HA-Ubiquitin-WT (Cat#17608, RRID:Addgene17608) Was a gift from Ted Dawson (322).

3.2.13.2 Contact for Reagent and Resource Sharing

Further information and requests for reagents may be directed to, and will be fulfilled by the corresponding author Bill B. Chen (chenb@upmc.edu)

3.2.13.3 Experimental Model and Subject Details

Human Studies (Acute Respiratory Distress Syndrome (ARDS)):

Adults aged 18-90 admitted to the Medical ICU in the UPMC Presbyterian Hospital with acute respiratory failure requiring mechanical ventilation via endotracheal tube were enrolled as patients if the onset of acute respiratory failure was associated with established risk factors for developing acute lung injury (sepsis, pneumonia, aspiration, blood transfusion, pancreatitis, or trauma) or if intubation was performed for airway protection in the setting of non-pulmonary critical illness. Enrollment took place within 48 h of the initiation of mechanical ventilation. After enrollment, patients were retrospectively sub-classified by an expert clinical panel into categories: 1) 'ARDS', as defined by Berlin criteria and agreed upon by a minimum of three members of an expert clinical panel, or 2) 'ventilated control,' as defined by intubation and mechanical ventilation for non-pulmonary critical illness without risk factor for ARDS. Cells were purified from whole blood and white cells were pelleted for further study.

Mouse experiments:

Mice were from Jackson Laboratories. For lentiviral studies, mice were confirmed as anesthetized prior to intratracheal instillation of 0.1 % (w/v) lysophosphatidylcholine (LysoPC) (specifically Palmitoyl:Stearoyl C16:C18) as an adjuvant. Following one hour, mice were intra-tracheally administered VSV-G pseudotyped lentivirus encoding Empty, KIAA0317 WT, or KIAA0317 P779L (pLVX); or Control shRNA or *Kiaa0317* shRNA (pLKO.1) (1e7 PFU/mouse). Plasmid expressed for 144 hours prior to subsequent treatment. Mice were intra-tracheally inoculated with LPS (3 mg/kg) or given *P. aeruginosa* (strain PA103, 1e4 CFU) for 18h. Following exposure, mice were euthanized, and lungs were lavaged with saline and harvested and subjected to analysis. Survival studies of mice were performed on mice that were given *P. aeruginosa* (strain

PA103, 1e5 CFU per mouse, intratracheally). For drug studies, mice were deeply anesthetized as above. PA103 (1e4 CFU) or LPS (3 mg/kg) was administered intratracheally before BC-1382 (10 mg/kg) was administered to the mice through an intraperitoneal injection. Eighteen hours later, animals were euthanized and analyzed as above.

3.2.13.4 Method Details

Plasmid Transfection— For protein overexpression in MLE-12 and BEAS-2B cells, cells were nucleofected using Nucleofector 2B (Amaxa), program T-13. For protein overexpression in HEK293T cells, XtremeGENE transfection reagents were used following the manufacturer's protocol. Expression was confirmed via western blotting.

Immunoblotting— Cell sample lysates were collected and digested in Buffer A (150 mM NaCl, 50 mM Tris, 1.0 mM EDTA, 2 mM dithiothreitol, 0.025% sodium azide, and 1 mM phenylmethylsulfonyl fluoride) on ice. Lysates were prepared by brief sonication at 4°C. Insoluble cellular debris were precipitated through centrifugation at 15,000x rcf for 10 min at 4°C. Lysate supernatant was normalized for protein concentration, and diluted in denaturing loading buffer, with a final 1X formulation of: 50 mM Tris HCl pH 6.8, 2% SDS, 10% Glycerol and 100 mM DTT. Protein concentration was determined by Lowry assay, and samples were normalized for content. Samples were resolved via SDS-PAGE prior to immunoblotting. Signal was detected via chemiluminescence on a Kodak Imaging Station.

Chemical and Compound treatment – MLE-12 and other cell lines were seeded to a density of 0.20×10^6 cells/mL in polystyrene 6-wells dishes treated by vacuum gas plasma in media supplemented with 2% FBS for 18h. LPS, MG-132 (10 µM), Leupeptin (10 µM), Cycloheximide

(50 μg/mL), or BC compound was added to cells at indicated doses for indicated time periods prior to subsequent analysis.

In vitro *ubiquitin conjugation assays*—The assay was performed in a volume of 20 µl containing 50 mM Tris, pH 7.6, 5 mM MgCl2, 0.6 mM DTT, 2 mM adenosine triphosphate (ATP), 400 µM MG132, 50 nM Ubiquitin activating enzyme, 0.5 µM UbcH5, 0.5 µM UbcH7, 2 µM ubiquitin, and 1 µM ubiquitin aldehyde. TnT coupled reticulocyte in vitro–synthesized tagless-KIAA0317 and SOCS2-V5 proteins were purified via HisPur Resin, and reaction products were processed for V5 immunoblotting.

Promoter Assays—HEK293 cells were co-transfected with Cignal NF-κB luciferase reporter assay plasmids and Empty, KIAA0317, SOCS2, CON shRNA, or *KIAA0317* shRNA for 24-48 h before exposure to LPS (10 µg/mL) and TNF (10 ng/mL) for an additional 6 or 18 h. Cells were then collected and assayed for luciferase activity according to manufacturer's instructions.

In vitro *protein binding assays*— KIAA0317 protein was immunoprecipitated from 1 mg MLE cell lysate using 1:100 dilution of KIAA0317 antibody (rabbit) for four hours at 25°C in IP buffer (50 mM Tris HCl pH 7.6, 150 mM NaCl, 0.25 % v/v Triton-X-100) and coupled to protein A/G agarose resin for an additional hour. V5-tagged SOCS2 deletion and point mutants (50 µl) were in vitro synthesized using TnT translation kits for 90 minutes at 30°C. KIAA0317-bound resin was then incubated with the in vitro synthesized bait protein for 18 hours at 4°C. Following binding, resin was washed with IP buffer, and eluted in 1X Laemmli buffer at 88°C for five minutes prior to immunoblotting analysis. Similarly, SOCS2 protein was immunoprecipitated from MLE

cell lysate subjected to binding against V5-tagged KIAA0317 mutants prior to immunoblotting analysis, as described above.

Immunoprecipitation Assays— MLE cells were cultured and treated as indicated prior to collection. Cell pellets were lysed with IP buffer (0.25% Triton-X-100 in 1x PBS, pH 7.6, 0.025% sodium azide, and 1 mM phenylmethylsulfonyl fluoride) on ice. Lysates were prepared by brief sonication at 4°C. Insoluble cellular debris were precipitated through centrifugation at 15,000x rcf for 10 min at 4°C. Lysate supernatant was normalized for protein concentration. Supernatants were exposed to a 1:50 dilution of the indicated antibody for three hours at 25°C. Immunoprecipitated protein was captured with 10 µL magnetic protein A/G resin per 1mL of lysate for 1 hour prior to two rounds of washing with IP buffer (1 mL). Protein was eluted by dilution in denaturing loading buffer, with a final 1X formulation of: 50 mM Tris HCl pH 6.8, 2% SDS, 10% Glycerol and 100 mM DTT and boiling for 5 minutes. Eluted samples were resolved via SDS-PAGE and subjected to immunoblotting.

shRNA Knockdown— For gene silencing studies in cells, shRNA were derived from the RNAi Consortium (TRC-Hs1.0, Human) and purchased from GE Dharmacon. pLKO.1 plasmids encoding control or gene-specific shRNA were transfected using plasmid transfection protocol above. Following 24 hours, media was exchanged for 0%-serum-containing media. After another 24 hours, cells were collected for subsequent analysis.

ELISA— Enzyme-linked immunosorbent assays were conducted on BALF samples from treated mice. BALF IL-1, IL-6, and TNF was detected by following manufacturer's instructions, and absorbance read using microplate reader.

Tissue staining—Murine lung samples were fixed in 10% neutral buffered formalin and embedded in paraffin and sectioned. Sections were stained with eosin and hematoxylin. Images were acquired from $20\times$ lens from random fields from each section.

Molecular docking studies— The docking experiments were carried out using Discovery Studio 3.5. KIAA0317 domain structural analysis revealed a major drug binding cavity within the c-terminal region. The binding cavity was adopted into the LibDock algorithm to screen for the optimum inhibitor. A library containing 3 million approved or experimental drugs was first used to screen potential ligands for KIAA0317. Based on the docking score and best-fit analysis of suitable ligands, ten compounds were selected and tested.

In vitro *drug-binding assays*—KIAA0317 protein was HIS-purified from KIAA0317 expressed in 293T cells using Talon metal affinity resin. Resins were then extensively washed before exposure to BC-1365 at indicated concentrations. Purified recombinant SOCS2 protein was then incubated with drug-bound KIAA0317 resins overnight. Resins were washed, and proteins were eluted and resolved on SDS-PAGE. The relative amounts of SOCS2 detected in the pull-downs were normalized to loading and quantified.

GST-Bait and Pull-down— Recombinant GST-SOCS2 protein was used as bait for BEAS-2B lysate incubation prior to pull-down and analysis, as previously described (323). Briefly, 1µg of GST-SOCS2 protein or recombinant GST protein was immobilized onto 0.5 mL of Glutathione Sepharose 4B resin in binding buffer (1x PBS + 0.2% v/v Triton X-100) for 2hr at +4C with agitation. Following capture, the bait and resin were incubated with 1mg of BEAS-2B cell lysate for 4hr at +4C. The resin was washed 5 times (1mL) with binding buffer prior to freezing of resin and shipment to MSBioWorks for analysis.

3.2.13.5 Quantification and Statistical Analysis

Protein Signal densitometry was quantified via ImageJ. Statistical comparisons were performed through Prism (GraphPad) utilizing two-tailed t-tests, Mann-Whitney U-Tets, one-way ANOVA with Tukey or Dunnett's multiple comparisons tests where described, and with $p<0.05$ indicative of significance.

3.2.13.6 Study Approval

The University of Pittsburgh Institutional Review Board approved procedures involving human samples. Normal control lung tissue was obtained from organ donors, after rejection of the lungs for transplant. All procedures were approved by the University of Pittsburgh Institutional Animal Care and Use Committee (Protocols 17030095 and 18114128). C57BL/6J males aged 8-10 weeks were acclimated to new housing for at least three days following shipping. Each house contained 4-5 mice with access to food and drink *ad libitum* in a room with a twelve-hour light/dark cycle. We confirmed mice were between 25 and 30g before any procedures. Mice were deeply anesthetized using a ketamine/xylazine mixture (80–100 mg/kg intraperitoneally (i.p.) prior to experimentation. Mice were carefully monitored over time; moribund, preterminal animals were

immediately euthanized and recorded as deceased. De-identified human plasma samples were obtained from the University of Pittsburgh Acute Lung Injury Biospecimen Repository (IRB number #PRO10110387). Informed consent was provided by all participants or their surrogates in accordance with the Declaration of Helsinki. Leukocyte was obtained from patient blood with a protocol approved by the University of Pittsburgh Investigational Review Board.

3.2.14 Acknowledgments

3.3 The RNFT2/IL-3Rα Axis Regulates IL-3 Signaling and Innate Immunity

Adapted from: Tong, Lear, and Evankovich et al., The RNFT2/IL-3Rα axis regulates IL-3 signaling and innate immunity. JCI Insight. 2020 Feb 13;5(3). pii: 133652. doi: 10.1172/jci.insight.133652. PMID: 31990690, (324)

Following the activation of inflammatory signaling in the lung, pulmonary epithelial cells release cytokines to begin the immune response to the distressed lung. Indeed, cytokines derived from the pulmonary epithelia can act in a paracrine or autocrine fashion to further stimulate

148

inflammatory signaling. In this study we investigate the proteolytic regulation of the interleukin-3 receptor subunit alpha in pulmonary epithelia, and its effect on inflammatory signaling. IL-3 treatment sensitized epithelial cells to LPS exposure, leading to an enhanced inflammatory response. While this study does not conclusively determine the source of IL-3 (we hypothesize it arises from the systemic vasculature), this study demonstrate a clear synergism between IL-3 and LPS/bacterial treatment in affecting inflammatory signaling, and presents the RING E3 ligase RNFT2 as a mediator of IL-3 signaling in the lung.

3.3.1 Overview

Interleukin-3 (IL-3) receptor α (IL-3Rα) is the α subunit of the ligand-specific IL-3R and initiates intracellular signaling in response to IL-3. IL-3 amplifies proinflammatory signaling and cytokine storm in murine sepsis models. Here we found that RNFT2 (RING finger transmembrane-domain containing protein 2, also TMEM118), a previously uncharacterized RING finger ubiquitin E3 ligase, negatively regulated IL-3-dependent cellular responses through IL-3Rα ubiquitination and degradation in the proteasome. In vitro, IL-3 stimulation promoted IL-3Rα proteasomal degradation dependent on RNFT2, and we identified IL-3Rα lysine 357 as a ubiquitin acceptor site. We determined that LPS priming reduces RNFT2 abundance, extends IL-3Rα half-life, and sensitizes cells to the effects of IL-3, acting synergistically to increase proinflammatory signaling. In vivo, IL-3 synergized with LPS to exacerbate lung inflammation in LPS and Pseudomonas aeruginosa-challenged mice; conversely, IL-3 neutralization reduced LPS-induced lung injury. Further, RNFT2 overexpression reduced lung inflammation and injury, whereas Rnft2 knockdown exacerbated inflammatory responses in LPS-induced murine lung injury. Last, we examined RNFT2 and IL-3Rα in human lung explants from patients with cystic fibrosis and also showed that

149

IL-3 is elevated in mechanically ventilated critically ill humans at risk for acute respiratory distress syndrome. These results identify RNFT2 as a negative regulator of IL-3Rα and show a potential role for the RNFT2/IL-3Rα/IL-3 axis in regulating innate immune responses in the lung.
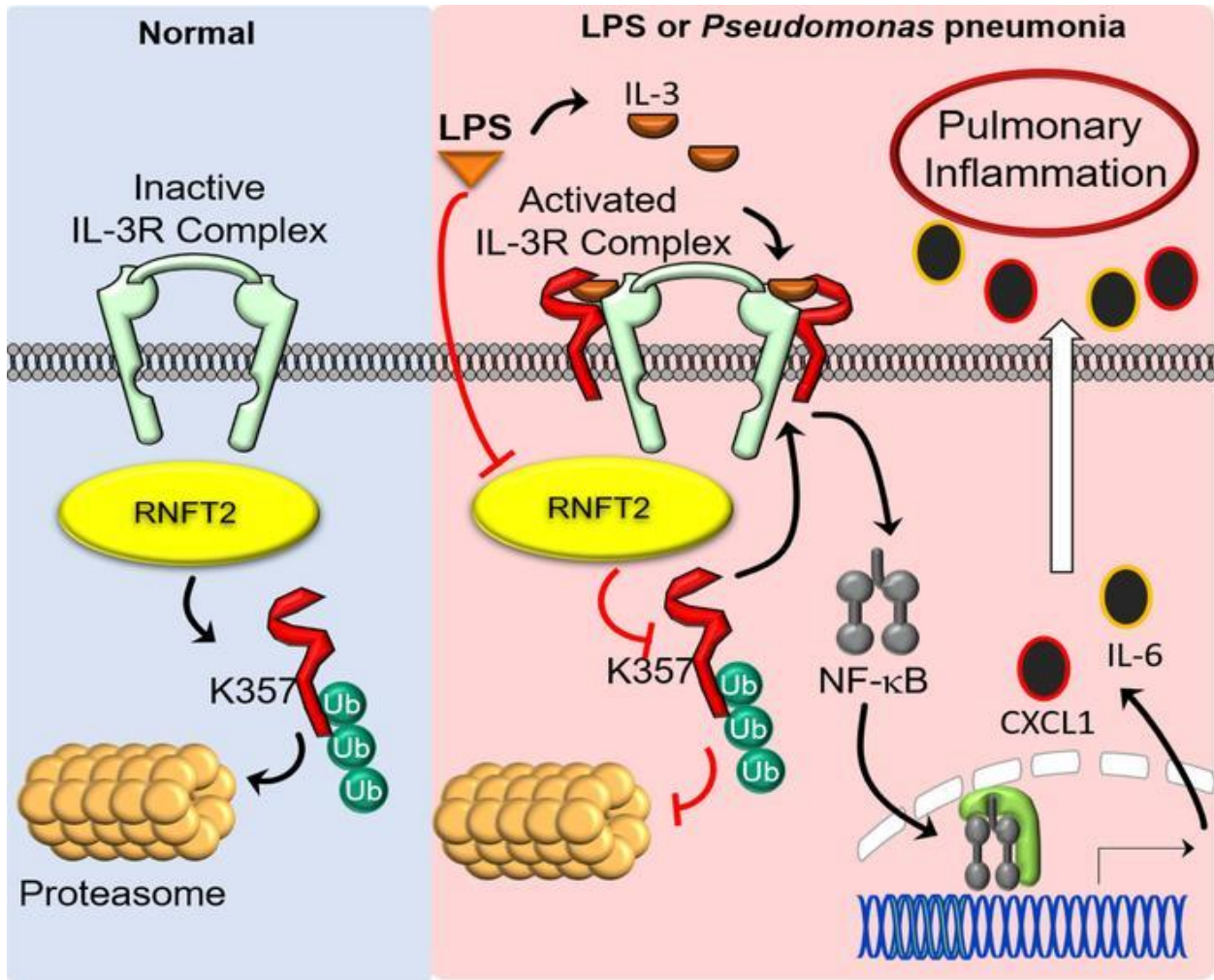
Figure 43 Graphical Abstract

Schematic of the RNFT2-IL3R model of activity. Under normal homeostatic conditions, IL3Rα is ubiquitinated by RNFT2 and proteolytically processed by the proteasome. During infection or acute lung inflammation, concurrent stimulation with LPS and exogenous IL3 leads to impaired RNFT2-mediated degradation of IL-3Ra and persistent pro-inflammatory signaling through NF-κB, leading to cytokine production, release, and increased inflammation.

150

3.3.2 Introduction – IL3 signaling in inflammation

Interleukin-3 (IL3), a cytokine that regulates hematopoiesis (325), also amplifies cytokine storm in murine sepsis(326), and in septic humans elevated circulating IL3 is associated with mortality (326). The downstream effects of IL3 are mediated by binding to its receptor, a complex that contains an alpha subunit (IL3Rα or CD123) and a beta subunit (IL3Rβ or CSF2RB) (327). IL3Rα neutralizing antibodies are protective in murine sepsis (326, 328) and IL3 predicts responsiveness to corticosteroid therapy in septic humans (329). Thus, the IL3/ IL3Rα axis may be a therapeutic target in sepsis and other acute inflammatory disorders. Here we show a previously uncharacterized mechanism regulating IL3Rα abundance through the ubiquitin/proteasome system (UPS), directed by the E3 ligase RING finger transmembrane-domain containing protein 2 (RNFT2).

3.3.2.1 Mechanism of IL-3 Signaling

IL3-initiated intracellular signaling is dependent on receptor subunits IL3Rα and IL3Rβ (325, 330). The beta subunit IL3Rβ, also known as the beta-common receptor (βc), is a shared receptor subunit that detects several colony-stimulating factor cytokines, including IL3, GM-CSF, and IL-5 (325, 327, 330). Depending on the stimulus (IL3, GM-CSF, or IL-5) and the cell type, several intracellular signaling pathways can be activated. The most well characterized signaling mechanisms include activation of the Janus kinase 2 (JAK2)/signal transducer and activator of transcription 5 (STAT5) pathway and the PI3 kinase pathway (331). Further, activation of the NF-κB pathway through TRAF6 recruitment to the beta subunit has been described (332). The consequences of these signaling pathways is diverse and context specific, as βc cytokines have

been implicated in several inflammatory diseases, including allergic asthma, inflammatory bowel disease, multiple sclerosis, and sepsis, among others(333). In murine sepsis, IL3 potentiates cytokine storm, a phenomenon associated with end-organ damage and mortality, and blockade of the IL3 receptor subunit IL3Rα protects against the deleterious effects of IL3 (326). Several E3 ligases have been shown to regulate innate immunity and inflammation in lung injury (141, 232, 334) (283, 335, 336), and here we characterize the E3 ligase RNFT2 as negative regulator of IL3Rα.

3.3.2.2 Post-Translational Regulation of IL3Rα

In this study, we show the IL3 receptor subunit IL3Rα is targeted for ubiquitination and degradation by the E3 ligase RNFT2 (RING finger transmembrane-domain containing protein 2, also TMEM118). We identify IL3Rα Lys357 as a critical residue regulating IL3Rα stability. In vitro, IL3 promotes RNFT2-dependent IL3Rα proteasomal degradation, an effect mitigated by LPS-priming. Using models of LPS and *Pseudomonas aeruginosa* (PA) murine lung injury in vivo, we show that while exogenous IL3 administration amplifies inflammation and organ damage, while IL3 neutralization is protective. Further, in LPS murine lung injury models, *RNFT2* over-expression conferred protection from the deleterious effects of IL3, while *Rnft2* knockdown augmented IL3-dependent effects and lung injury severity. Lastly, in humans we show IL3 is elevated in subjects with Acute Respiratory Distress Syndrome (ARDS), and that IL3Rα and RNFT2 abundance are inversely correlated in lung homogenates from lung explants in cystic fibrosis patients. These data show RNFT2 is a previously unrecognized regulator of IL3-dependent cellular effects by controlling IL3Rα stability.

3.3.3 IL3Rα is degraded in the proteasome in response to IL3

We sought out to determine IL3Rα protein stability. We confirmed IL3Rα expression in MLE-12 (MLE) cells and RAW cells (Figure 44A and Figure 45A). IL3Rα transcript was also present in RNA-Seq experiments from MLE cells (GEO accession GSE94680)(337). MLE cells were treated with cycloheximide (CHX) and IL3Rα half-life was observed to be ~ 6h; additionally, we found CHX-induced IL3Rα degradation was prevented by the proteasome inhibitor MG132, but not by the lysosomal inhibitor leupeptin (Figure 44A). We observed a similar half-life and preservation with MG132 treatment in RAW cells (Figure 45A). As IL3Rα protein is protected by proteasomal blockage, we hypothesized that IL3Rα degradation is regulated by the ubiquitin proteasome system. Indeed, expression of ubiquitin in MLE cells led to a dose-dependent decrease in IL3Rα protein (Figure 45B). Further, IL3Rα protein is retained following co-expression of ubiquitin and MG132 treatment (Figure 44B), an effect not seen with leupeptin treatment.

We next characterized the ubiquitination linkage type, as substrate ubiquitination controls several diverse cellular functions (97). We performed UbiCREST analysis, in which HIS-tagged IL3Rα was expressed in MLE cells prior to MG132 treatment, HIS-pulldown, and in vitro exposure to de-ubiquitinases (DuB) with differential activity to specific ubiquitin chain linkages (338). We observed digestion of IL3Rα polyubiquitination by DuBs with affinity for K48-, K27-, K29-, K33-, K11-, and K63-type linkages (Figure 45C). K48-linked polyubiquitination is a common linkage associated with proteasomal degradation (97, 339). As an orthogonal approach, we co-expressed IL3Rα and ubiquitin constructs with specific K→R mutations, prior to MG132 treatment and IL3Rα pull-down, followed by immunoblotting. We observed that the expression of several mutants, especially K48R and K63R mutants, resulted in reduced poly-ubiquitinated-IL3Rα compared to WT-Ubiquitin (Figure 45D). Taken together, these results suggest IL3Rα

ubiquitination is a signal for degradation. Ubiquitin is conjugated to substrate proteins at target lysine (K) residues, and we generated IL3Rα lysine-to-arginine (K→R) mutants to identify putative ubiquitin acceptor sites, as arginine (R) is unable to accept ubiquitin. We found the IL3Rα K357R mutant protein was resistant to degradation in CHX chase experiments (Figure 44C). Thus, K357 is a candidate ubiquitin acceptor site for IL3Rα. These experiments suggest that IL3Rα protein is regulated through ubiquitination leading to proteasomal degradation.

We examined whether IL3 stimulation would promote proteasomal degradation of IL3Rα and affect its downstream signaling. IL3Rα abundance decreased in a time- and dose-dependent manner following IL3 stimulation (Figure 44D), an effect that was mitigated by pre-treatment with MG132, but not leupeptin (Figure 44E). Additionally, IL3 stimulation reduced amounts of ectopic IL3Rα WT, but not IL3Rα K357R, in MLE cells (Figure 44F). These results suggest that IL3Rα undergoes ligand-induced degradation in the proteasome. Lastly, we examined if IL3Rα affected IL3 dependent downstream effects. TRAF6-dependent NF-κB activation has been shown as a cellular response to IL3(332) and we observed that IL3 stimulation of MLE cells increased TRAF6 abundance as well as RelB and phospho-P100, proteins involved in the NF-κB signaling cascade (Figure 44G). Further, over-expression of IL3Rα augmented these effects (Figure 44G).
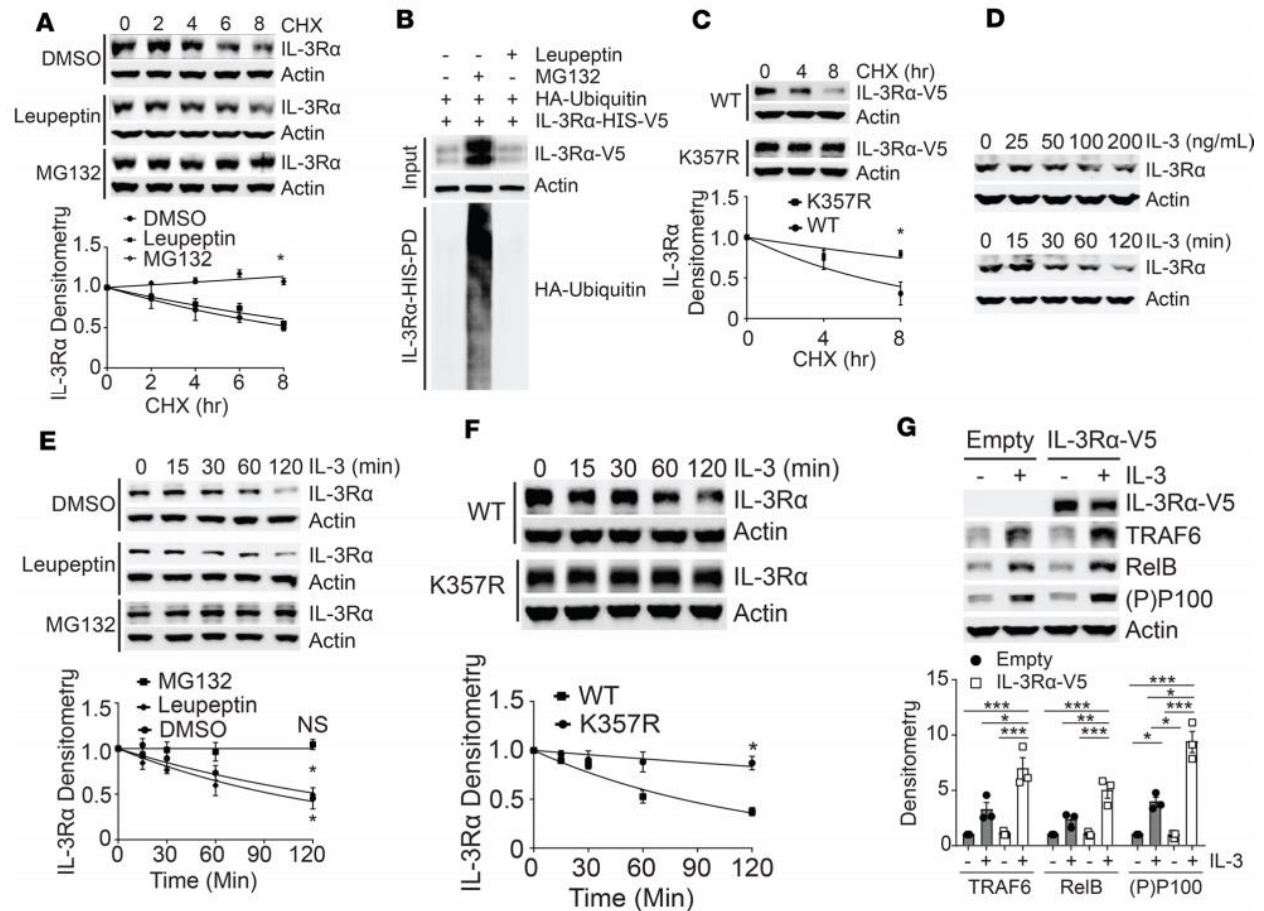
Figure 44 IL3Rα is degraded in the proteasome in response to IL3

(A) Immunoblot analysis of IL3Rα protein abundance in MLE cells treated with cycloheximide (CHX) with or without MG-132 or Leupeptin in a time-dependent manner, Data and means ± SEM of 3 independent experiments. (B) Immunoblotting of IL3Rα-V5 HIS pull-down (HIS PD) from MLE cells after co-expression of IL3Rα-V5 and HA-Ubiquitin, and treatment with MG132 or leupeptin. (C) Immunoblot analysis of MLE cells transfected with WT or lysine mutant (K357R) IL3Rα and treated with CHX. Data and means ± SEM of 3 independent experiments. (D) Immunoblotting of IL3Rα protein abundance from MLE cells treated with recombinant IL3 protein (rIL3) in a dose or time-dependent manner. (E) Immunoblot analysis of IL3Rα protein amount from MLE cells treated with rIL3 with or without MG-132 or Leupeptin in a time-dependent manner. Data and means ± SEM of 3 independent experiments. (F) Immunoblot analysis of IL3Rα-V5 protein amount from MLE transfected with WT or K357R mutant IL3Rα and treated with rIL3 treatment. Data and means ± SEM of 3 independent experiments. (G) Immunoblot analysis of MLE cells transfected with IL3Rα or empty plasmid, and then were challenged with or without rIL3. Data and means ± SEM of 3 independent experiments. *P $<$0.05, **P $<$0.01, ***P $<$0.001 by F-test (A, C, E, F), or by one-way ANOVA with Tukey's post hoc test (G).
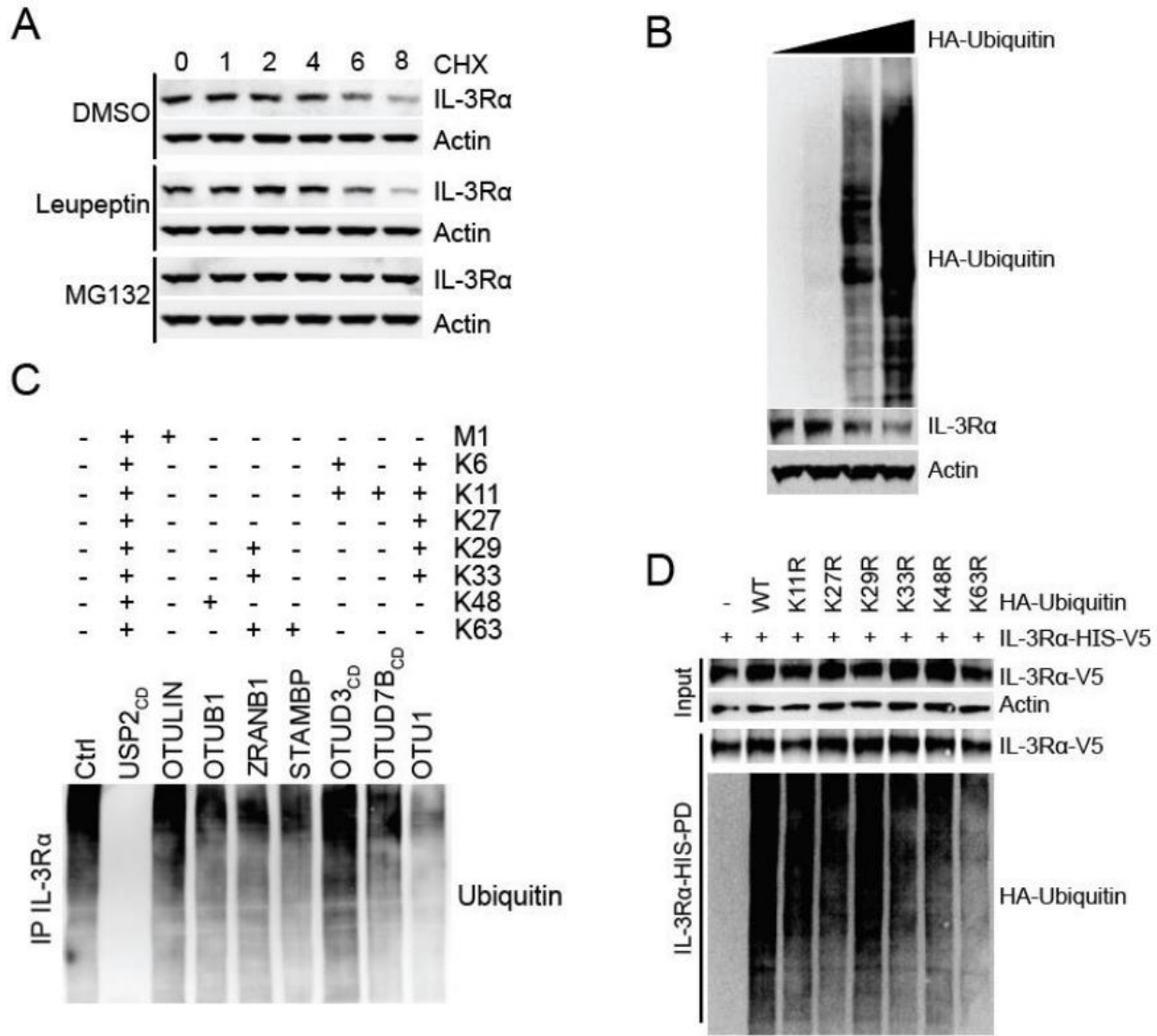
Figure 45 IL-3Rα is ubiquitinated and assembles specific poly-ubiquitin linkage types

(A) Western blot analysis of IL-3Rα abundance in lysates of RAW 264.7 cells treated with cycloheximide (CHX) with or without MG-132 or Leupeptin over time. Blots are representative of 2 independent experiments. (B) Western blot analysis of IL-3Rα abundance in lysates of MLE cells transfected with increasing amounts of a HA-Ubiquitin construct. Blots are representative of 2 independent experiments. (C) UbiCREST analysis of IL-3Rα immunoprecipitates from lysate of MLE cells after MG132 treatment. Blots are representative of 2 independent experiments. (D) Western blot analysis of IL-3Rα and Ubiquitin in IL-3Rα immunoprecipitates from lysate of MLE cells transfected with V5-IL-3Rα and HA-Ubiquitin K→R point mutants after MG132 treatment. Blots are representative of 2 independent experiments.

3.3.4 RING Finger E3 ligase RNFT2 regulates IL3Rα stability and signaling

We next investigated the mechanism involved in IL3Rα protein ubiquitination and degradation. We over-expressed E3 ligases in MLE cells(60, 141, 340, 341) and observed that the uncharacterized E3 ligase RNFT2 decreased IL3Rα protein amounts (Figure 46A), without affecting its mRNA expression (Figure 47A). Expression of RNFT2 led to a dose-dependent decrease of IL3Rα protein, but not that of IL3Rβ protein (Figure 46B). We observed that RNFT2 protein associated with IL3Rα in MLE cells by RNFT2 pull-down (Figure 46C). Thus, RNFT2 is a candidate E3 ligase targeting IL3Rα as a substrate for ubiquitination and degradation.

To confirm that RNFT2 functioned as an E3 ligase to ubiquitinate IL3Rα, we performed an in vitro ubiquitination assay. RNFT2 protein in addition to the full complement of ubiquitination machinery was sufficient to ubiquitinate IL3Rα in vitro (Figure 46D). As a complementary approach, we showed that co-expression of RNFT2 with HA-Ubiquitin and IL3Rα-HIS-V5 led to degradation of IL3Rα protein and increased the HA-ubiquitin signal upon IL3Rα-HIS pulldown as compared to control (Figure 46E). As a putative RING Finger E3 ligase, RNFT2 functions through its RING domain (Figure 47B). Mutation of critical residues within this region led to preservation of IL3Rα protein relative to WT (Figure 47C). To further confirm RNFT2 activity as an authentic ubiquitin E3 ligase, we performed in vitro binding assays and observed that RNFT2 indeed bound to several ubiquitin E2 enzymes (Figure 46F). We also confirmed the association of RNFT2 with endogenous UBE2D protein through cell-based pull-down assays (Figure 46G). Lastly, to demonstrate the specificity of RNFT2 to target IL3-Rα, we co-over-expressed RNFT2 with WT or K357R IL3-Rα. RNFT2 over-expression reduced amounts of IL3Rα WT, but not IL3Rα K357R (Figure 46H). Hence, we confirmed that RNFT2 is an authentic E3 ligase that targets IL3Rα as a substrate.

157
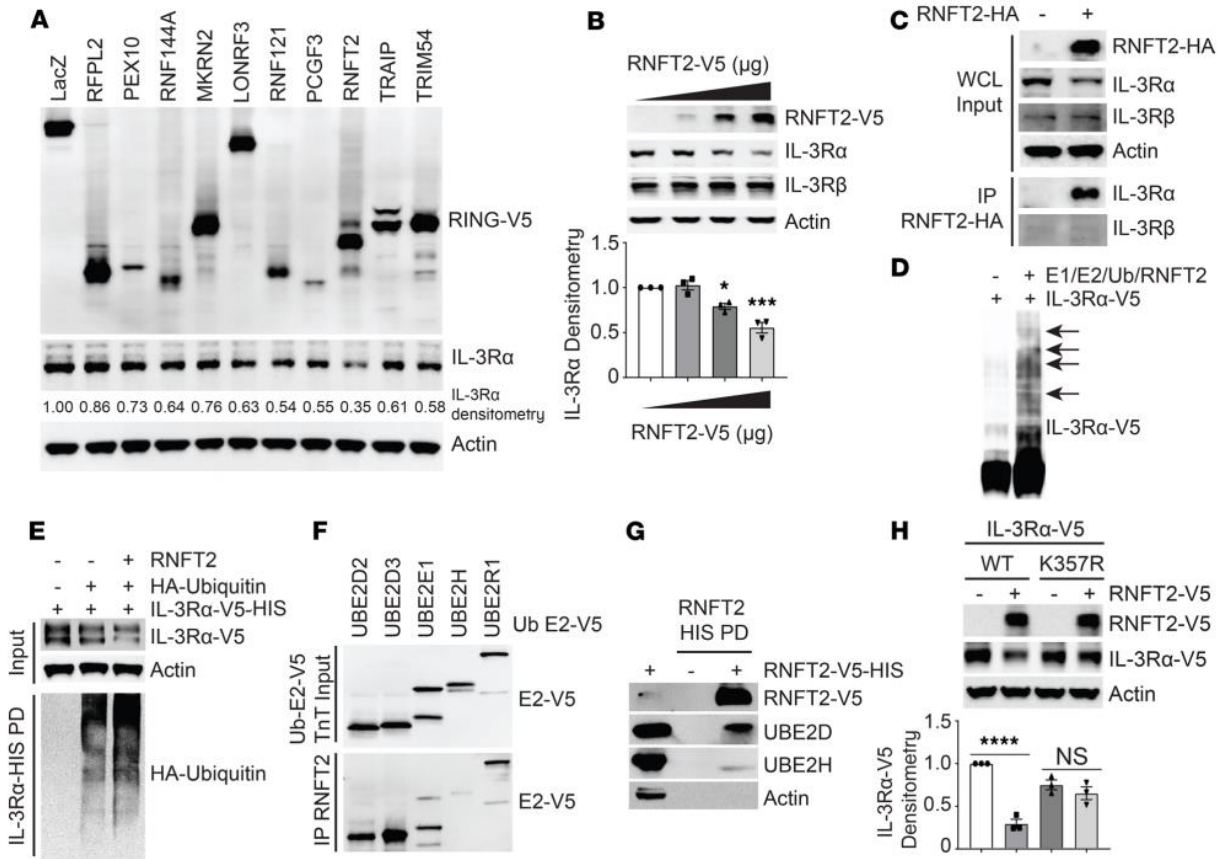
Figure 46 RING Finger E3 ligase RNFT2 regulates IL3Rα stability and IL3 signaling

(A) Immunoblot analysis of IL3Rα from MLE cells transfected with LacZ or one of the other 10 randomly selected Ring-finger E3 ligases. IL3Rα/Actin Densitometry normalized to LacZ treatment is shown belowF IL3Rα bands. (B) Immunoblotting of IL3Rα from MLE cells transfected with a dose course of RNFT2. Data and means ± SEM of 3 independent experiments. (C) Immunoblot analysis of MLE cells following expression of RNFT2-HA and immunoprecipitation (IP) of RNFT2-HA. (D) Immunoblotting of in vitro ubiquitination assay involving the full-complement of ubiquitination machinery (E1, E2, Ubiquitin, ATP, Mg++) and RNFT2 protein. (E) Immunoblot analysis of in vivo ubiquitination assay in MLE cells expressing IL3Rα-HIS-V5 with HA-Ubiquitin and RNFT2 prior to MG132 treatment and HIS-tag pulldown (HIS PD) of IL3Rα-HIS-V5. (F) Immunoblotting of in vitro protein binding assay between V5-tagged ubiquitin E2 enzymes (Ub E2) and immunoprecipitated RNFT2 protein (IP RNFT2). (G) Immunoblot analysis of MLE cells expressing RNFT2-HIS-V5 prior to HIS pulldown (HIS PD) of RNFT2. (H) Immunoblot analysis of MLE cells co-transfected with WT or K357R IL3Rα lysine mutants with or without RNFT2, Data and means ± SEM of 3 independent experiments. *P $<$ 0.05, ***P $<$ 0.001 by one-way ANOVA with Dunnett's post hoc test (B), or by one-way ANOVA with Tukey's post hoc test (H).
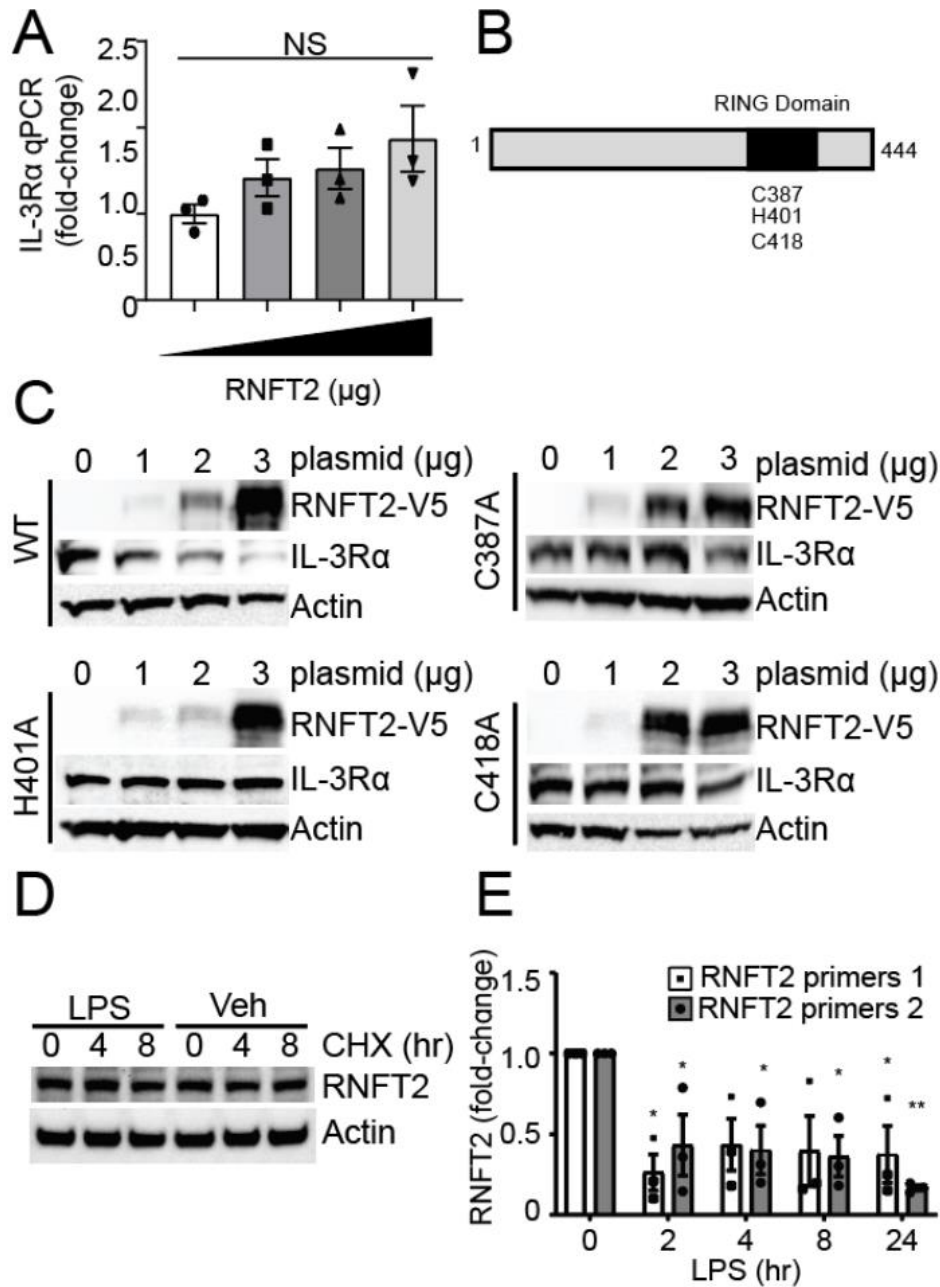
Figure 47 RNFT2 is a RING Ubiquitin E3 ligase and is transcriptionally down-regulated by LPS

(A) RT-qPCR analysis of IL-3Rα mRNA expression in MLE cells transfected with increasing amounts of RNFT2. Data are pooled from 3 independent experiments. (B) Schematic of RNFT2 sequence and critical residues within its predicted RING domain. (C) Western blot analysis of IL-3Rα abundance in lysates of MLE cells transfected with increasing amounts of RNFT2 WT and RING mutant constructs. (D) Immunoblot analysis of MLE cells treated with CHX time course without or with LPS co-treatment. (E) RT-qPCR analysis of RNFT2 mRNA expression in MLE cells treated with a time course of LPS and represented as fold change relative to 0hr time point. Blots are representative of 2-3 independent experiments. Data and means ± SEM of 3 independent experiments NS, $P > 0.05$, *$P < 0.05$, **$P < 0.01$; by one-way ANOVA with Dunnett's post hoc test (A, E).

Next, we investigated whether RNFT2 affected IL3Rα abundance and signaling in response to IL3. RNFT2 overexpression significantly enhanced rIL3-induced IL3Rα degradation (Figure 48A), whereas *Rnft2* knockdown markedly preserved IL3Rα protein with IL3 stimulation (Figure 48B). We found that ectopic expression of RNFT2 decreased TRAF6 protein amount in rIL3-stimulated MLE cells (Figure 48C), whereas *Rnft2* knockdown significantly increased TRAF6 protein abundance (Figure 48D).
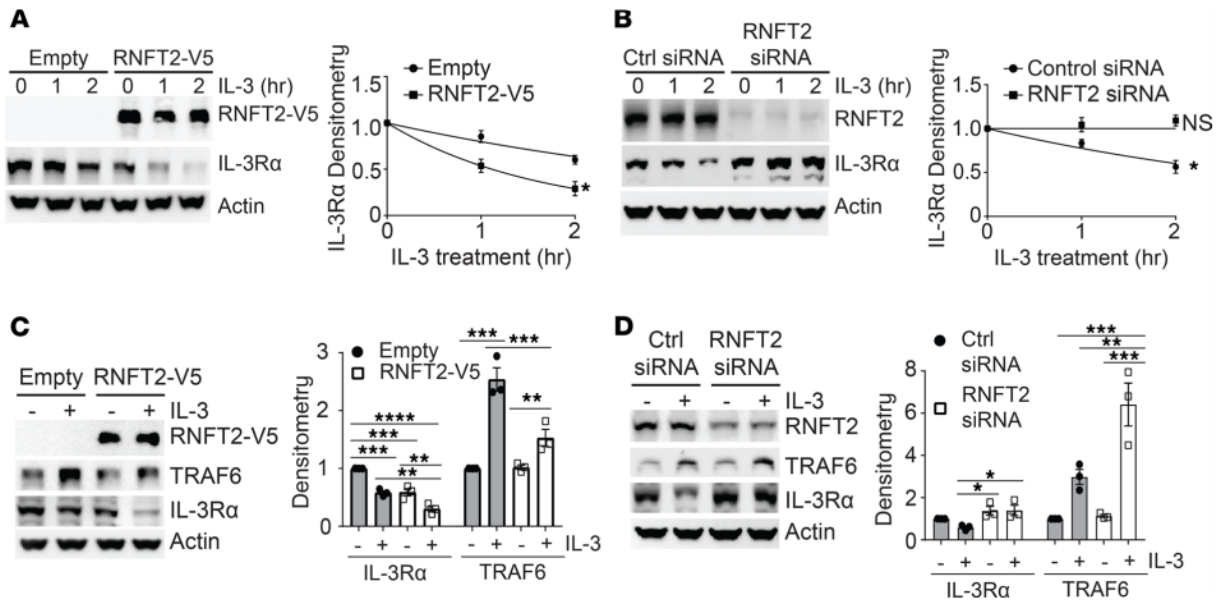
Figure 48 RNFT2 regulates IL3Rα protein levels and IL3Rα-dependent inflammatory signaling

(A) Immunoblotting of MLE cells transfected with empty or RNFT2 plasmid before IL3 treatment. Data and means ± SEM of 3 independent experiments. (B) Immunoblot analysis of MLE cells transfected with con-siRNA or Rnft2 siRNA before rIL3 treatment. Data and means ± SEM of 3 independent experiments. (C) Immunoblotting of MLE cells transfected with empty or RNFT2 plasmid and challenged with or without rIL3. Data and means ± SEM of 3 independent experiments. (D) Immunoblot analysis of MLE cells transfected with RNFT2 siRNA or control siRNA and were then challenged with or without rIL3. Data and means ± SEM of 3 independent experiments. *P ＜0.05, **P ＜0.01, ***P ＜0.001, ****P ＜0.0001 by F-test (A, B), or by one-way ANOVA with Tukey's post hoc test (C, D).

3.3.5 IL3 augments pro-inflammatory cellular responses to LPS through IL3Rα and RNFT2

IL3 exacerbates the pro-inflammatory effects of LPS(326). We hypothesized that this effect could be partially mediated through LPS-dependent modulation of IL3Rα stability. LPS treatment in MLE cells led to an increase in IL3Rα protein abundance and a concomitant decrease in RNFT2 protein levels (Figure 49A, B). While RNFT2 protein levels did not differ over an 8-hour CHX chase with or without LPS co-treatment, we observed that LPS treatment decreased R*nft2* gene transcription (Figure 47D, E). The LPS-mediated effect on IL3Rα protein levels was specific, as IL3Rβ protein levels were not affected by LPS (Figure 49C). Further, the increase in IL3Rα protein abundance was independent of changes in *IL3Rα* gene transcription (Figure 49D). We also found that in CHX chase experiments, LPS pre-treatment extended IL3Rα half-life (Figure 49E). Co-treatment of LPS with IL3 increased supernatant cytokine levels of IL-6 and CXCL-1 compared to LPS treatment alone, an effect further exacerbated with IL3Rα over-expression (Figure 49F, G).

We then examined the effect of RNFT2 over-expression or knockdown on cytokine secretion in MLE cells in response to LPS/IL3. RNFT2 over-expression mitigated the effect of LPS/IL3 co-treatment on CXCL-1 secretion (Figure 49H), while *Rnft2* knockdown exacerbated this effect (Figure 49I). Lastly, we co-over-expressed WT or K357R IL3Rα with an empty vector or RNFT2 and stimulated MLE cells with LPS/IL3. RNFT2 over-expression mitigated TRAF6 abundance as well as IL-6 and CXCL-1 cytokine secretion in cells co-overexpressed with WT IL3Rα; however, RNFT2 over-expression had no effect on TRAF6 abundance, or IL-6 and CXCL1 cytokine secretion in cells co-overexpressed with K357R IL3Rα (Figure 50A-C). Thus,

the degradation-resistant K357R IL3Rα mutant was not affected by RNFT2 over-expression.

Taken together, these data suggest that LPS sensitizes cells to IL3 through stabilization of IL3Rα.
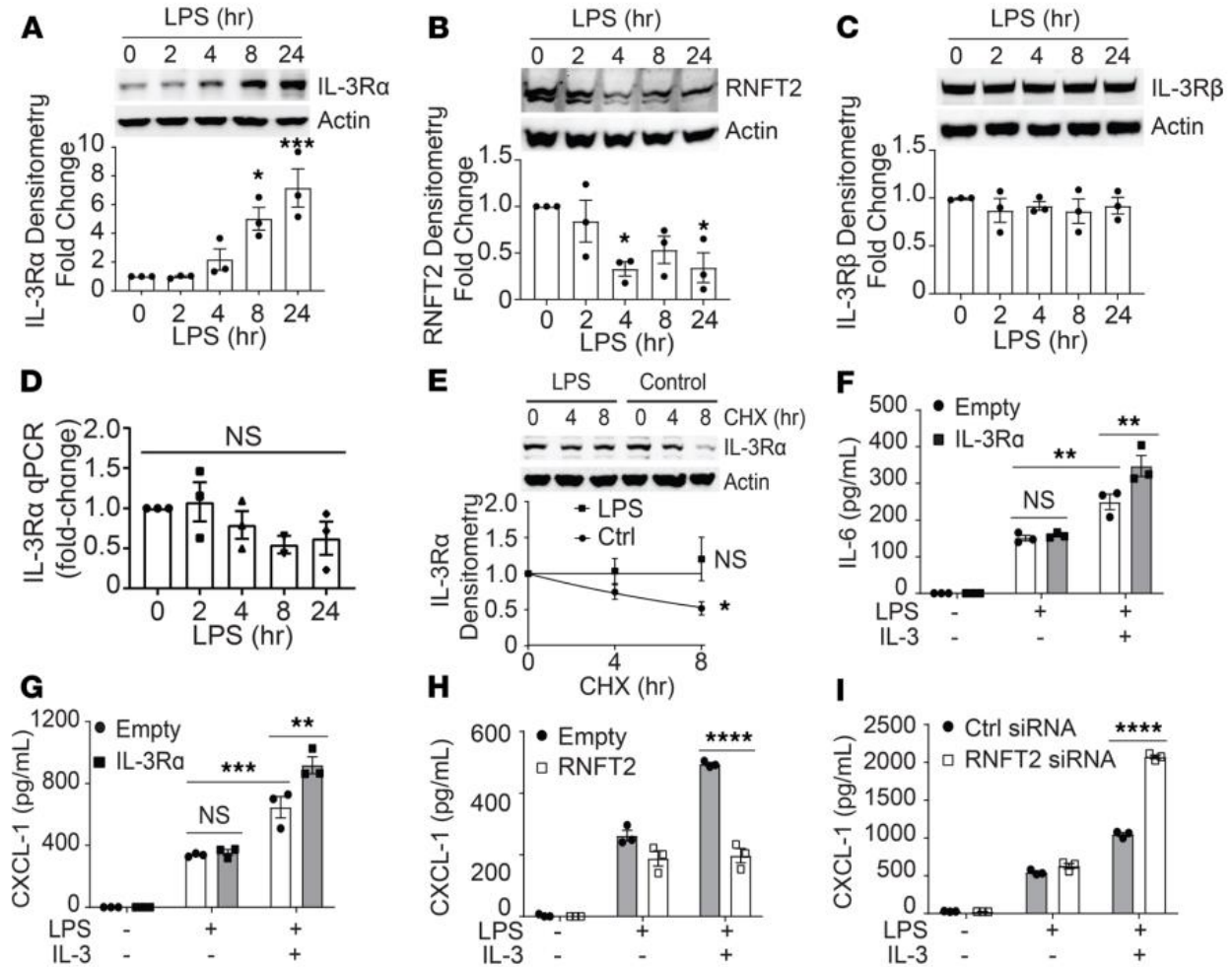
Figure 49 IL3 augments pro-inflammatory cellular responses to LPS through IL3Rα and RNFT2

(A-C) Immunoblot analysis of IL3Rα (A), RNFT2 (B), and IL3Rβ (C) protein abundances in Murine lung epithelial (MLE) cells treated with LPS at the indicated times. Blots (top) are representative of 3 independent experiments. Quantified data (lower) are means ± SEM from all experiments (n=3). (D) RT-qPCR analysis of IL3Rα mRNA expression in Murine lung epithelial (MLE) cells treated with LPS at the indicated times. Quantified data are means ± SEM from all experiments (n=3). (E) Immunoblot of IL3Rα in MLE cells treated with cycloheximide (CHX) and control (Con) or LPS, as indicated. Blots (top) are representative of 3 independent experiments. Quantified data (lower) are means ± SEM from all experiments (n=3). (F and G) ELISA analysis of IL-6 and CXCL-1 in supernatants from MLE cells transfected with IL3Rα or empty plasmid, and challenged with LPS and rIL3, as indicated. Data are means ± SEM from all experiments. (H) ELISA analysis of CXCL-1 in MLE cells transfected with RNFT2 or empty plasmid before treatment with LPS with or without rIL3. Data and means ± SEM of 3 independent experiments. (I) ELISA analysis of CXCL-1 in MLE cells transfected with con-siRNA or RNFT2 siRNA before treatment with LPS with or without rIL3. Data and means ± SEM of 3 independent experiments. *P $<$ 0.05, **P $<$ 0.01, ***P $<$ 0.001, ****P $<$ 0.0001 by F-test (E), by one-way ANOVA with Dunnett's post hoc test (A-D), by one-way ANOVA with Tukey's post hoc test (F-I).
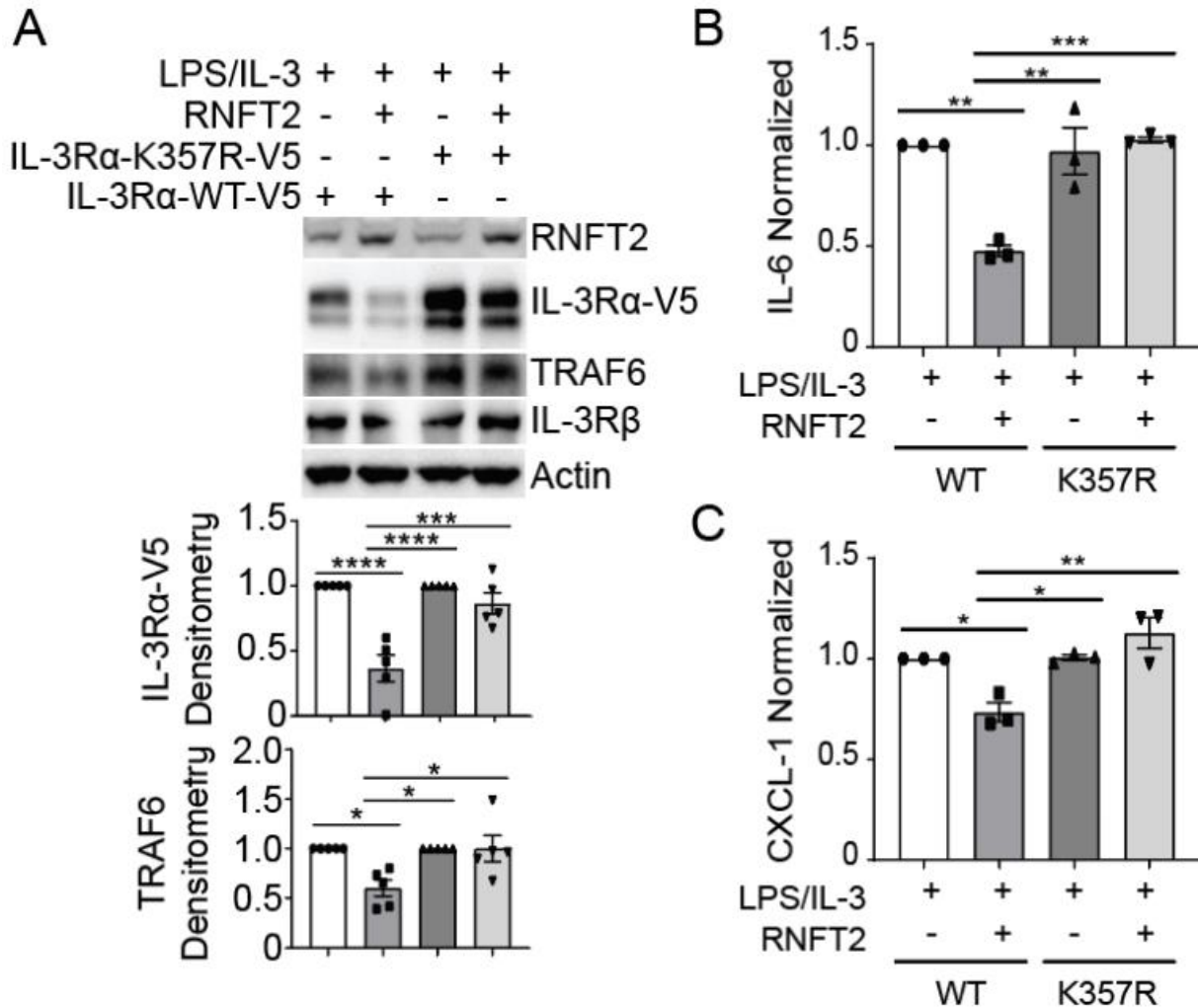
Figure 50 RNFT2 effect on inflammation proceeds through IL-3Rα

(A) Immunoblot analysis of IL3Rα, IL-3Rβ, and TRAF6 from MLE co-expressing WT or ubiquitin-resistant K357R mutant IL-3Rα and RNFT2 prior to LPS and IL-3 treatment. Data and means ± SEM of 5 independent experiments. (B-C) ELISA analysis of IL-6 and CXCL-1 abundances from MLE co-expressing WT or ubiquitin-resistant K357R mutant IL-3Rα and RNFT2 prior to LPS and IL-3 treatment. Data and means ± SEM of 3 independent experiments NS, P > 0.05, *P < 0.05, **P < 0.01, ***P < 0.001, ****P < 0.0001 by one-way ANOVA with Tukey's post hoc test (A-C).

3.3.6 IL3 augments LPS-induced murine lung injury

To determine whether IL3 contributed to the pathology of lung injury we used a clinically

relevant model for pneumonia and severe lung injury initiated by intratracheal administration of

LPS. After we treated mice with vehicle (PBS), LPS, recombinant IL3 (rIL3), or their combination intratracheally, we determined lung histology and protein concentration in Bronchoalveolar lavage fluid (BALF) were assayed 18 h later. LPS increased BALF protein amounts, and the abundance of the inflammatory cytokines IL-6, TNF-α, & IL-1β, and the DAMP HMGB1 in BALF. In contrast, IL3 treatment alone had only a modest effect on the same parameters. However, co-treatment of IL3 with LPS dramatically increased the amount of BALF protein, and abundance of the inflammatory cytokines IL-6, TNF-α, & IL-1β, and HMGB1 (Figure 51A-E) compared to LPS alone. BALF cell counts also displayed a similar pattern, with IL3/LPS co-treatment increasing BALF cell counts most dramatically among treatment groups (Figure 51F). Additionally, we observed increased numbers of BALF neutrophils and lymphocytes, but not macrophages, in mice co-treated with IL3 and LPS compared to PBS, LPS, or IL3 alone (Figure 51G-I). Lung histopathology was consistent in that IL3/LPS co-treatment caused the most severe lung injury compared to PBS, LPS, or IL3 alone (Figure 51J). Taken together, these results suggest that IL3 amplifies LPS-induced lung injury.
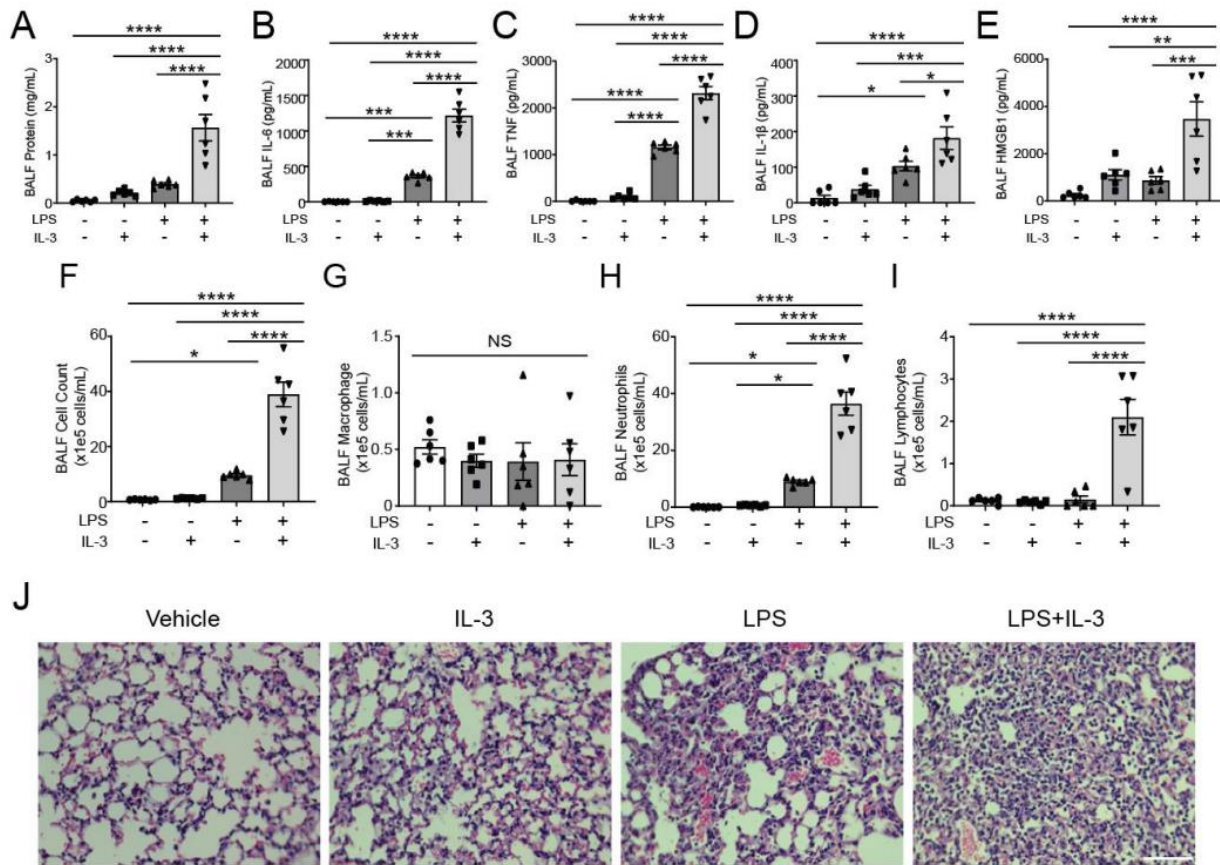
Figure 51 IL-3 aggravates LPS-induced lung injury in vivo

(A to E) ELISA analysis of total protein (A), IL-6 (B), TNF (C), IL-1β (D) and HMGB1 (E) concentration in BAL fluid from mice intratracheally treated with LPS and PBS or recombinant IL-3, as indicated. (F to I) Number of total cells (F), macrophages (G), neutrophils (H), and lymphocytes (I) in BAL fluid from mice treated intratracheally with LPS and PBS or recombinant IL-3, as indicated. Data are means ± SEM of 3 mice per group from 2 independent experiments. (J) Histological analysis of lung samples from mice treated as indicated. Images are representative of all independent experiments. Scale bar, 100 μm. *P < 0.05, **P < 0.01, ***P < 0.001, ****P < 0.0001, by one-way ANOVA with Tukey's post hoc test (A-I).

3.3.7 IL3 neutralization reduces inflammation in LPS-induced murine lung injury.

In separate experiments, we co-treated mice with LPS and either IgG (control) or a neutralizing antibody against IL3. We observed that BALF protein, and inflammatory cytokines IL-6, TNF-α, & IL-1β, and HMGB1 abundance were all significantly reduced in mice treated with

anti-IL3 compared to IgG-treated control mice (Figure 52 A-E). Further, blocking-IL3 treatment reduced BALF cell counts and neutrophils but had no effect on macrophage or lymphocyte counts (Figure 52F-I). Blocking IL3 antibody co-treatment reduced the severity of lung injury in histopathological sections (Figure 52J). Thus, IL3 may drive inflammation in LPS-induced lung injury.
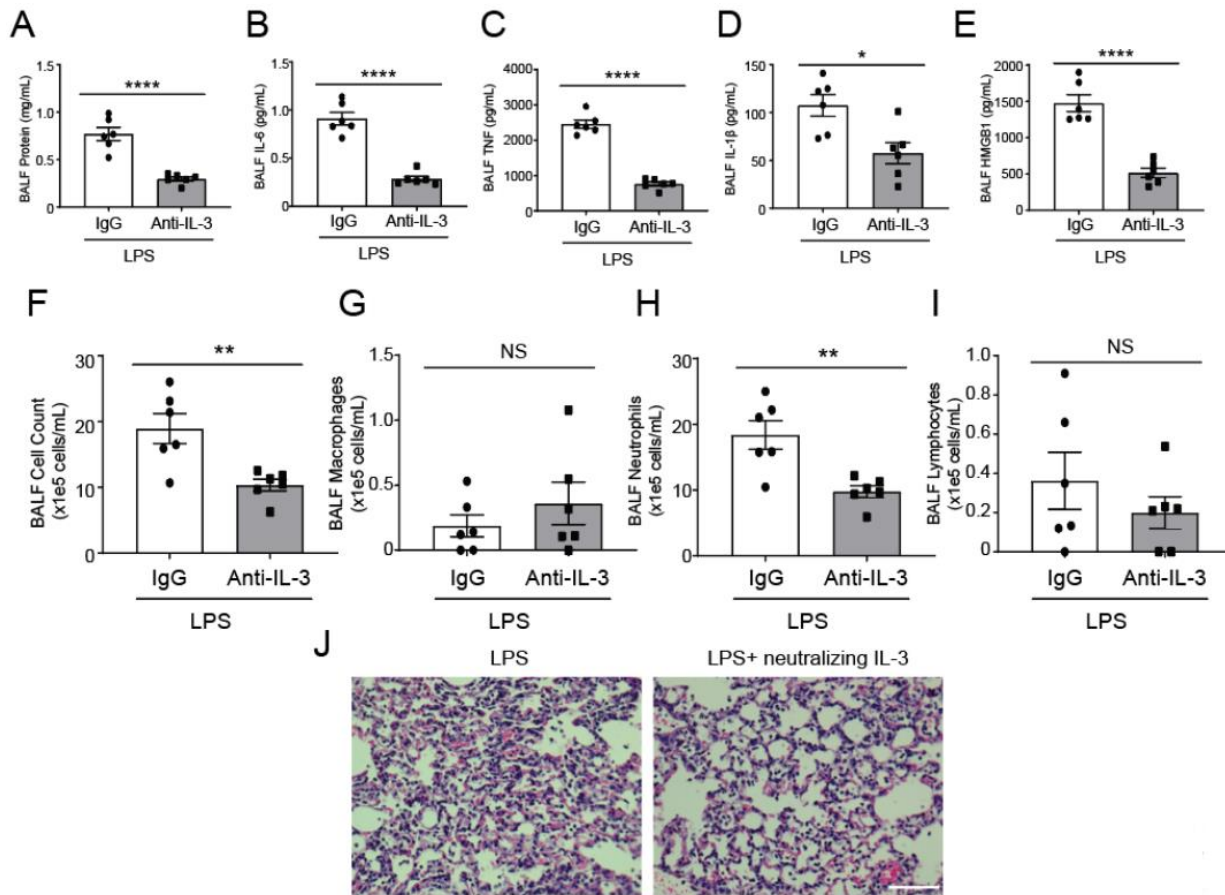
Figure 52 IL-3 blocking antibody attenuates LPS-induced lung injury

(A to E) ELISA analysis of total protein (A), IL-6 (B), TNF (C), IL-1β (D) and HMGB1 (E) concentration in BAL fluid from intratracheally treated with LPS and control or neutralizing IL-3 antibody, as indicated. Mice were euthanized after 18h, and lungs were lavaged with saline, and BALF were measured from mice. (F to I) Number of total cells (F), macrophages (G), neutrophils (H), and lymphocytes (I) in BAL fluid of mice treated intratracheally with LPS and control or neutralizing IL-3 antibody, as indicated. (J) Histological analysis of lung samples from mice treated as indicated. Images are representative of all independent experiments. Scale bar, 100 μm. Data are means ± SEM of 3 mice per group from 2 independent experiments. NS, P > 0.05, *P ＜0.05, **P ＜0.01, ***P ＜0.001, ****P ＜0.0001, by Student's t-test (AI).

3.3.8 The RNFT2/IL3Rα/IL3 axis regulates lung inflammation in vivo and in vitro

We next examined the role of RNFT2 during acute lung injury. RNFT2 is an uncharacterized E3 ligase. We first performed IHC on mouse lung sections and confirmed RNFT2 was expressed in the mouse lung (Figure 53A). We then measured RNFT2, IL3Rα, and IL3Rβ protein amounts in lung homogenates after intratracheal LPS and observed that RNFT2 abundance decreased, IL3Rα abundance increased, and IL3Rβ amounts were unchanged compared to control mice (Figure 54A, B). We also observed increased IL3 in the BALF of LPS-treated mice compared to controls (Figure 53B) To validate these observations in another infectious acute lung injury model, we treated mice with *Pseudomonas aeruginosa* (PA) and measured abundance of RNFT2, IL3Rα, and IL3Rβ and observed a similar pattern of protein signal, and of IL3 signal in murine BALF (Figure 53C-G).

To determine the role of RNFT2 in LPS/IL3-induced lung injury, we infected mice intratracheally with empty lentivirus or lentivirus encoding *Rnft2*, and subsequently challenged them with LPS with or without rIL3. *Rnft2* gene transfer significantly reduced lung inflammation and injury caused by LPS and rIL3 co-treatment as shown by decreased BALF cell counts, protein concentrations, cytokine release, and lung infiltrates (Figure 54C-G, K). Specifically, the BALF leukocyte differential revealed that the total decrease in inflammatory cells was mostly from neutrophils and lymphocytes, but not macrophages (Figure 55A-C).

Next, we administered lentivirus intratracheally encoding control shRNA or *Rnft2* shRNA and then exposed to LPS with or without rIL3. *Rnft2* knockdown significantly enhanced lung inflammation and injury caused by LPS and rIL3 treatment as shown by increased BALF cell counts, protein concentrations, cytokines release, and lung infiltrates (Figure 54H-J, L). Specifically, the differential cell counts of BALF revealed that the total increase in inflammatory

cells was mostly from neutrophils and lymphocytes, but not macrophages (Figure 55D-F). These

results suggest that RNFT2 modulates lung inflammation in vivo.
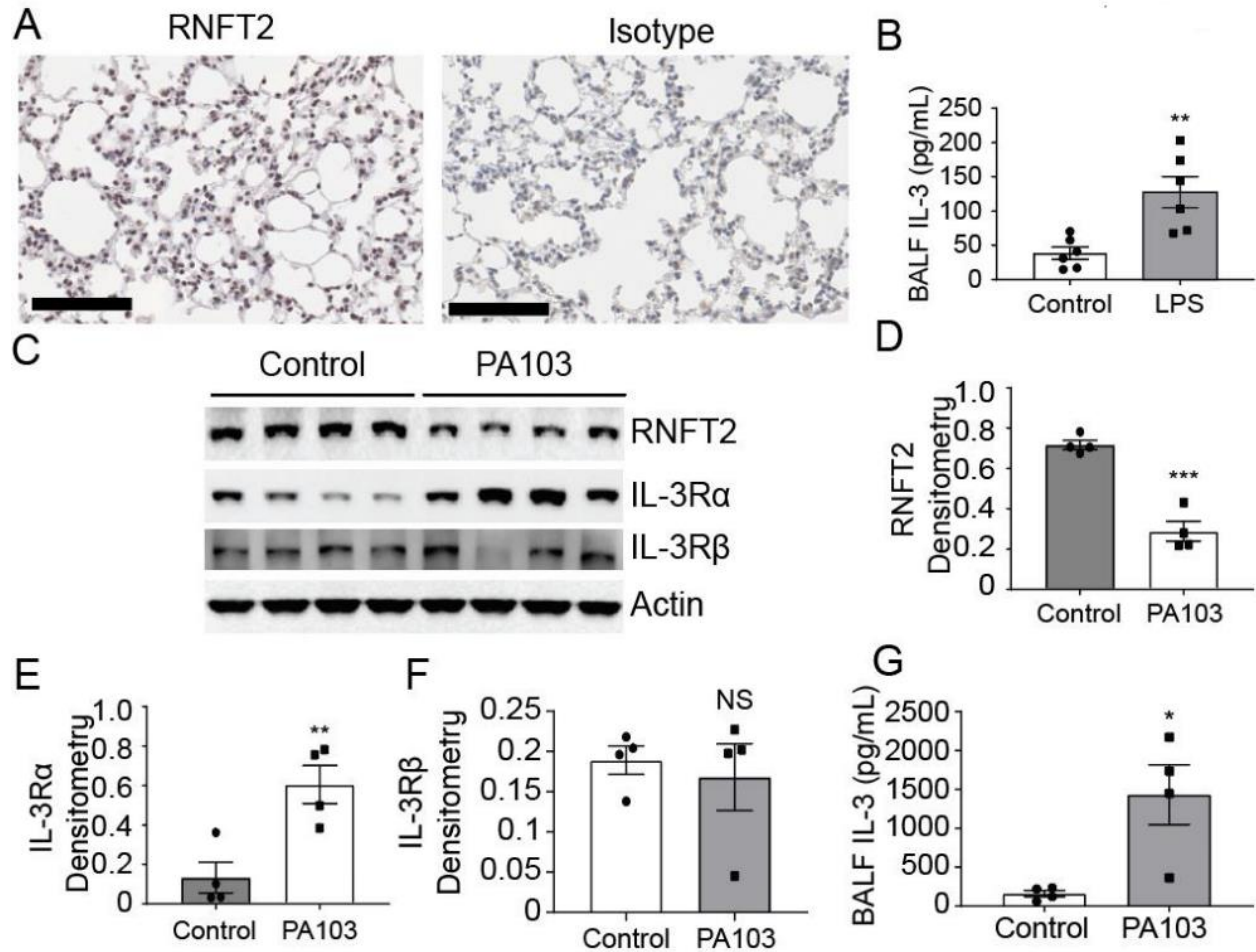
Figure 53 Bacterial infection influences Rnft2:Il3ra protein levels

(A) Immunohistochemical staining of Rnft2 in murine lung, scale bar = 100µm, Isotype control staining is also shown (B). ELISA analysis of Il3 in mouse BAL fluid treated intratracheally with LPS and PBS as indicated. Data are means ± SEM of 3 mice per group from 2 independent experiments. (C-F). Immunoblot analysis of mouse lung homogenate from Control or PA103-treated mice. (C). Protein densitometry analysis of RNFT2 (D), IL-3Rα (E), and IL-Rβ(F), from data in (C). (G). ELISA analysis of Il3 in mouse BAL fluid treated intratracheally with PA103 and PBS as indicated. Data are means ± SEM of 3 mice per group from 2 independent experiments. NS, $P > 0.05$, *P <0.05, **P <0.01, ***P <0.001, by Student's t-test (B, D, E-G).

168
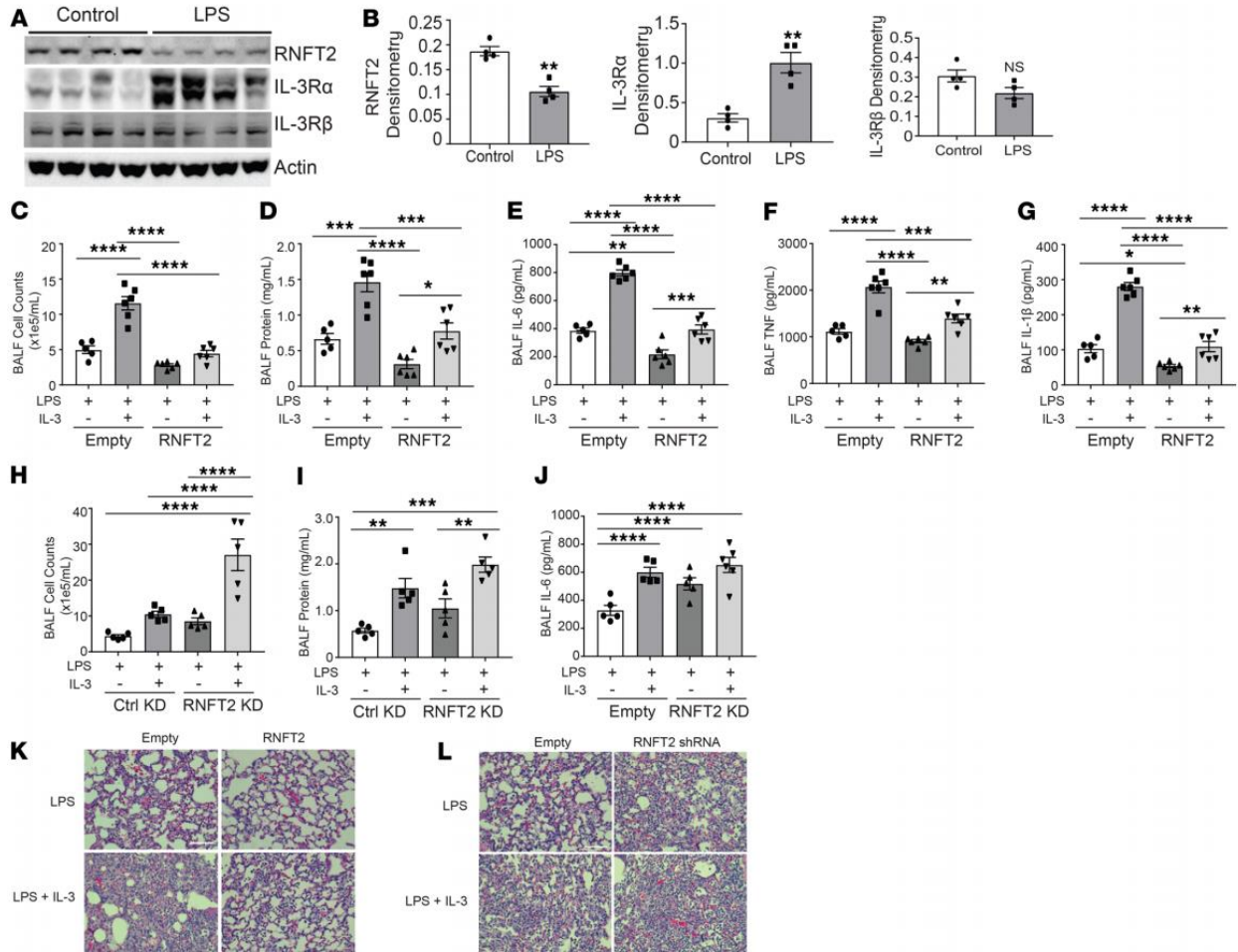
Figure 54 The RNFT2/IL3Rα axis regulates lung innate immunity and inflammation in vivo

(A) Immunoblot analysis of RNFT2, IL3Rα, and IL3Rβ from mice intratracheally treated with control or LPS, as indicated. Data and means ± SEM of 4 mice per group. (C) Cell concentration, (D) total protein analysis, (E-G) ELISA analysis of (E) IL-6 (F), TNF, (G) IL-1β from BAL fluid of mice intratracheally treated with Lenti-Empty or Lenti-RNFT2 and then treated with LPS and PBS or recombinant IL3, as indicated. Data and means ± SEM pooled of 3 mice per group are from 2 independent experiments. (H) Cell concentration, (I) total protein analysis, (J) ELISA analysis of IL-6 from BAL fluid of mice intratracheally treated with Lenti-control shRNA or Lenti-RNFT2 shRNA and then treated with LPS and PBS or recombinant IL3, as indicated. Data and means ± SEM pooled of 3 mice per group are from 2 independent experiments. (K-L) Histological analysis of lung samples from mice treated as indicated. Images are representative of all independent experiments. Scale bar, 100 μm. *P ＜0.05, **P ＜0.01, ***P ＜0.001, ****P ＜0.0001, by Student's t-test (B) or by one-way ANOVA with Tukey's post hoc test (C-J).

169
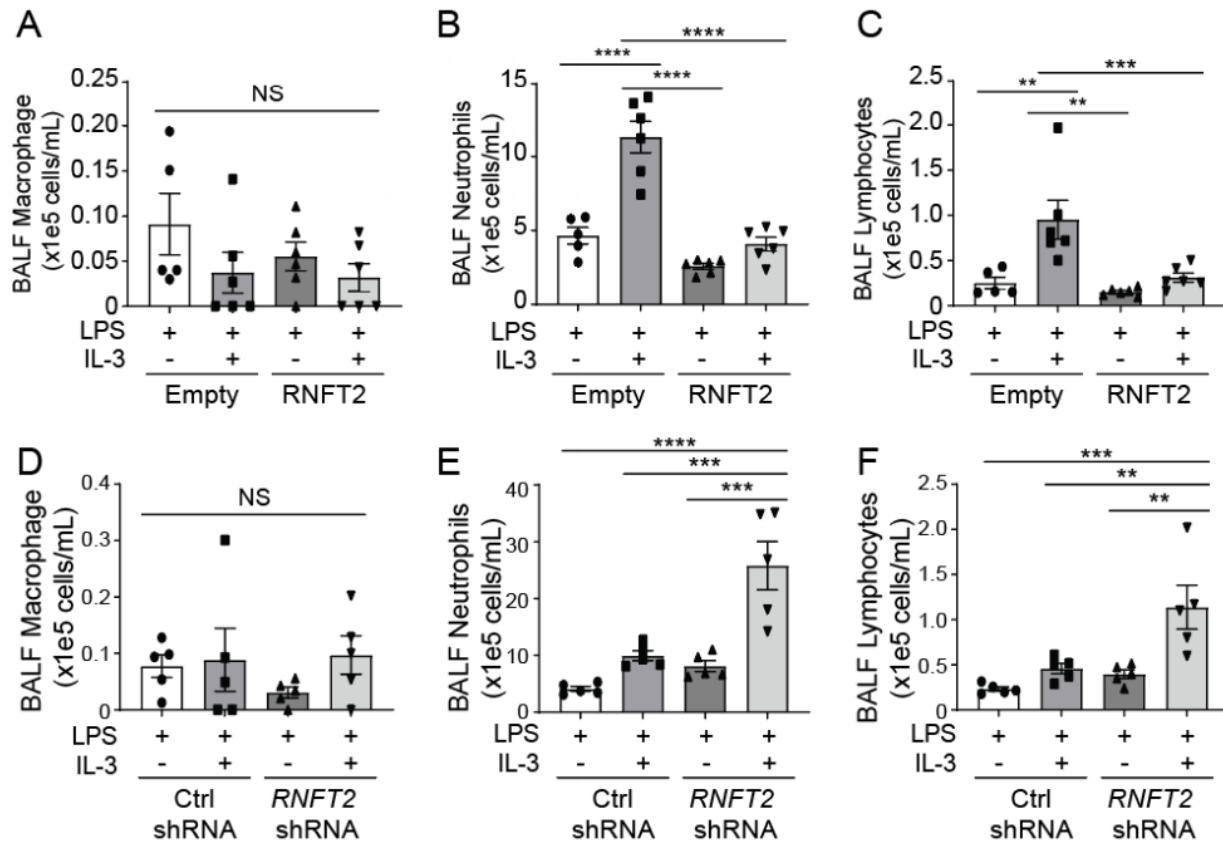
Figure 55 RNFT2 regulates neutrophils counts in lung inflammation and injury

(A to C) Total number of cells (A), neutrophils (B), and lymphocytes (C) in BAL fluid from mice that received LentiEmpty or Lenti-RNFT2 intratracheally before treatment with LPS with rIL-3, as indicated. Mice were euthanized after 18h, and lungs were lavaged with saline, and lavage cells were then processed for WrightGiemsa stain; lavage macrophages, neutrophils, and lymphocytes were counted and graphed (A-C). (D to F) Total number of macrophages (D), neutrophils (B), and lymphocytes (C) in BAL fluid from mice that received Lenti-control shRNA or Lenti-RNFT2 shRNA intratracheally before treatment with LPS and rIL3, as indicated. All data and means ± SEM of 2-3 mice per group are from 2 independent experiments. *P ＜0.05, **P ＜0.01, and ***P ＜0.001 by one-way ANOVA with Tukey's post hoc test (A-F).

170

3.3.9 The IL3/IL3Rα/RNFT2 axis is relevant in human inflammatory lung disease

To determine protein expression patterns of IL3Rα and RNFT2 in clinically relevant human disease, we assayed parenchymal explant lung samples from human cystic-fibrosis patients colonized with PA by immunoblot for RNFT2 and IL3Rα protein amounts, and we quantified their relative expression normalized to Tubulin. We observed a significant negative correlation between RNFT2 and IL3Rα protein signal (Figure 56A) (Pearson r^2=0.278). These studies suggest that the RNFT2/IL3Rα pathway may be relevant in response to *PA* infection in patients, where decreased amounts of RNFT2 result in reciprocally increased IL3Rα abundance.

Circulating IL3 may be a potentiator of cytokine storm, and in a cohort of 60 patients with septic shock, high IL3 (>89.4 pg/mL) amount were associated with mortality. In this cohort, there was no significant difference in circulating IL3 protein abundance at Day 0 vs. Day 1 or Day 2 of following sepsis diagnosis (326). However, in a separate cohort, IL3 was significantly elevated in septic patients relative to healthy controls (342). We sought out to determine if circulating IL3 differed in a more homogenous population at risk for ARDS (acute respiratory distress syndrome), as a subset of patients at risk or with ARDS have excessive inflammation and cytokine storm in the lung (343, 344). We assayed IL3 in plasma from mechanically-ventilated subjects at risk for ARDS vs. mechanically-ventilated subjects without lung injury (Table 3). Subjects at-risk for ARDS had increased plasma IL3 compared to subjects without lung injury (Figure 56B). Further, IL3 levels were associated with other plasma pro-inflammatory cytokines in this cohort, including TNFα and IL1β (Figure 56C-D). We also measured RNFT2 gene expression through RT-qPCR from white blood cell pellets from the same subjects, but found no significant correlations to the same pro-inflammatory cytokines (Figure 56E-F). Thus, high circulating IL3 may be an additional biomarker to identify subjects at risk for ARDS with excessive lung inflammation. Further studies

with increased power are warranted to determine if IL3 could be a new biomarker in patients with or at risk for ARDS.

In summary, our studies demonstrate IL3Rα stability is regulated through the ubiquitin-proteasome system, dependent on the previously uncharacterized E3 ligase RNFT2. These findings may have implications for pulmonary inflammatory disorders including acute lung injury. We characterize RNFT2 as an authentic E3 ligase that directs IL3Rα ubiquitination and degradation and identify Lysine 357 on IL3Rα as a critical residue regulating its stability, as K357R IL3Rα mutants are resistant to RNFT2-directed degradation. In vivo, we show 1.) IL3 exacerbates LPS-induced lung injury, 2.) IL3 neutralization reduced inflammation in LPS-induced lung injury, 3.) RNFT2 over-expression is protective in LPS/IL3-induced lung injury and mitigates the effects of IL3, and 4.) *Rnft2* knock-down exacerbates LPS/IL3 induced lung injury, and exacerbates the effects of IL3.
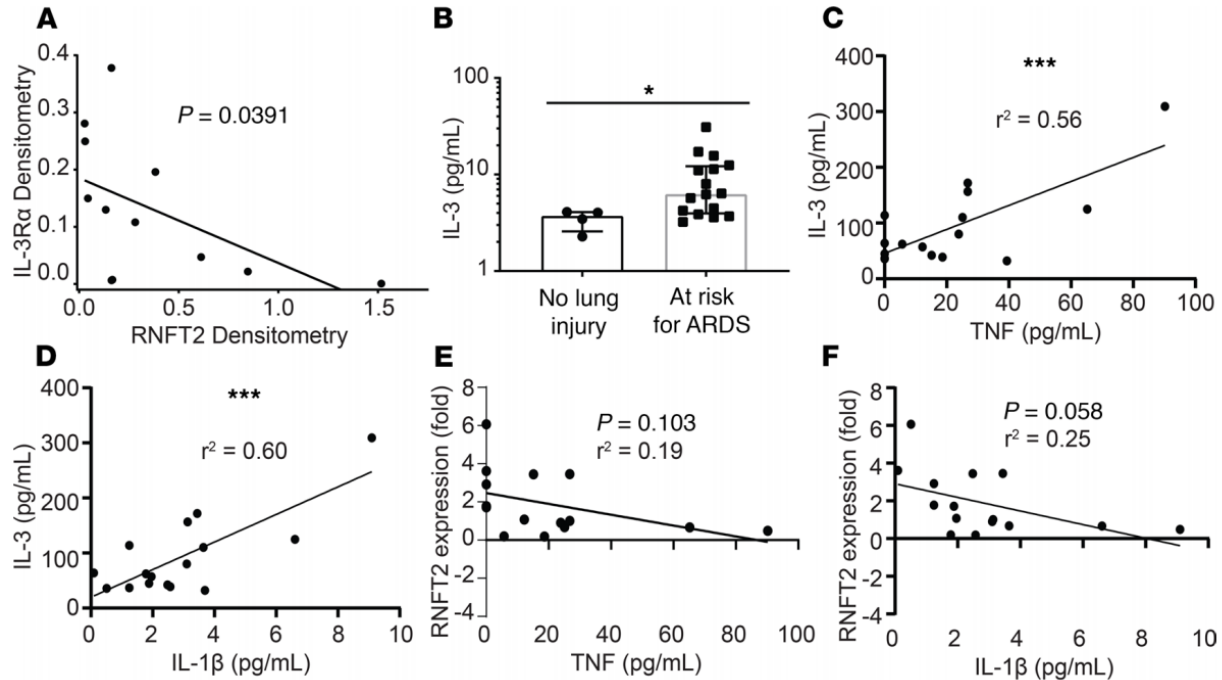
Figure 56 The IL3Rα/RNFT2 signaling axis is relevant in human lung disease

(A) Immunoblot analysis of RNFT2, IL3Rα and tubulin from Human CF subjects lung explants with Pseudomonas colonization. Data and means ± SEM (n=12). (B) ELISA analysis of plasma IL3 in mechanically ventilated patients without lung injury (n=4) or At Risk for ARDS (n=16). Subject classification was blinded to the operator. Bars and error bars represent median and IQR, respectively. Data were analyzed by Mann Whitney U test. *P<0.05 by Mann-Whitney U Test. (C-D) Linear regression of plasma IL3 vs. plasma TNF (C) and IL1β (D) in ARFA subjects (n=16); *<P<0.05, ***P<0.001. (E-F) Linear regression of RNFT2 gene expression normalized to control patient vs. plasma TNF (E) and IL1β (F) in ARFA subjects (n=15).

Table 3 Acute Lung Injury Biospecimen Repository baseline parameters analyzed for plasma IL3 Levels

Variable	No Lung Injury	At Risk for ARDS (ARFA)
N	4	16
Age, mean (SD), yrs	64.9 (12.8)	51.8 (14.8)
Males, N (%)	4 (100)	10 (62.5)
SOFA score, median (IQR)*	5.0 (4.5-5.5)	7.0 (5.75-9.25)
PaO2:FIO2 ratio, mean (SD), mmHg	281.5 (187.7)	217.1 (101.5)
WBC, mean (SD), x 10⁻⁹ per liter	14.5 (10.8)	13.6 (8.7)
ICU LOS, median (IQR), days	4.5 (3.75-7.25)	6.5 (4.75-9.75)
30 Day mortality, N (%)	1 (25)	2 (12)

Data are presented as mean (standard deviation) for normally distributed continuous variables or median (interquartile range) for not normally distributed continuous variables, and N (%) for categorical variables.

3.3.10 Discussion

IL3 has recently been implicated in the pathogenesis of several inflammatory disorders, including collagen-induced arthritis (345), autoimmune encephalitis (346), and lupus nephritis (347). In some of these models, IL3 blockade reduced disease severity scores and was associated with decreased systemic inflammatory markers, whereas administration of IL3 exacerbated these effects (346, 347). Our findings are in line with these studies, as we show that IL3 blockade reduces lung injury and inflammatory markers in a murine model of severe lung injury, and that addition of IL3 exacerbates organ damage. Our results are also consistent with those of Weber, et al, who demonstrated that IL3 alone is not sufficient to induce a systemic inflammatory response, but rather serves to "amplify" signaling initiated by an initial insult (CLP, or intra-tracheal LPS) (326). Here we extensively studied the role of the IL3/IL3Rα axis in lung innate immunity and inflammation. We found IL3 amounts were increased in BALF of mice subjected to LPS or *Pseudomonas* (PA) treatment, and rIL3 co-treatment with LPS drastically enhanced pro-inflammatory cytokine release and immune cell activation in murine lungs. We observed IL3 treatment synergizes with bacterial PAMP-exposure to strongly activate downstream signaling through NF-κB activation, leading to pro-inflammatory cytokine release. Our model is consistent with the 'second-hit' theory or multi-causal effect mentioned in previous studies (348, 349).

IL3 classically signals through the JAK/STAT pathway (333) , but has also been linked to NF-κB through tumor necrosis factor receptor (TNFR)-associated factor 6 (TRAF6) (332). TRAF6 is one of the six well-characterized TRAF proteins, which are critical contributors to inflammatory, innate, and adaptive immune responses(342, 350, 351). Specifically, TRAF6 is a key mediator of TLR signaling and downstream NF-κB signaling(352-354). We found TRAF6 increased in MLE cells treated with rIL3, suggesting TRAF6 is a candidate contributor to the synergy of IL3 and NF-

κB activation. We also observed that ectopic expression of the IL3 receptor (IL3Rα) significantly increased TRAF6 amount and enhanced cytokine release upon IL3/LPS co-treatment. These studies suggest that IL3 along with its receptor IL3Rα synergize with bacterial PAMP exposure through downstream NF-κB signaling.

In this study, we found that IL3Rα protein abundance is regulated post-translationally through ubiquitination. Protein ubiquitination is a universal cellular mechanism controlling protein amount and innate immunity (336, 355-358). Recently, we have shown that several E3 ligases regulate substrate ubiquitination in pulmonary inflammatory conditions(141, 232, 283). During systemic insults induced by infection, alterations of E3 ligase activity or targeting can affect substrate protein abundance and their downstream effector functions. We showed that intratracheal treatment of LPS or PA in vivo increases substrate IL3Rα protein amount, and that LPS treatment of MLE cells increases IL3Rα. Lung tissue from PA-treated mice showed decreased abundance of the putative E3 ligase RNFT2, with a correlative increase in IL3Rα protein, suggesting the exogenous insult manipulated RNFT2 protein amount, and thus the protein stability of its substrate IL3Rα. We characterized RNFT2 as an authentic E3 ligase by showing its interaction with the E2 enzyme UBE2D in vitro. We further found that RNFT2 regulated the rIL3-induced increase in TRAF6 protein and affected CXCL-1 secretion in MLE cells. Specifically, ectopic expression of RNFT2 in MLE cells significantly suppressed co-treatment (LPS with rIL3) induced cytokine release, whereas *Rnft2* knockdown enhanced CXCL-1 secretion. RNFT2 gene transfer and knockdown in vivo also has similar phenotype in cytokine release and immune cell activation such as neutrophils in lung. Our data imply that RNFT2 functions as an inflammatory suppressor protein that controls IL3 signaling in innate immunity, and the RNFT2/IL3Rα axis may be important in the lung innate immune response chain.

175

This study also provided two additional human translational links that suggest the IL3/IL3Rα signaling axis may play a role in human inflammatory lung diseases. We show that plasma IL3 protein amounts are increased in humans at risk for ARDS compared to mechanically ventilated subjects without lung injury. These findings warrant examination in larger lung injury cohorts and suggest that IL3 may be a previously unrecognized cytokine associated with excessive inflammation. We also examined protein abundance of RNFT2 and IL3Rα in explanted lung tissue from patients with chronic pseudomonas infection. We discovered there was an inverse correlation between RNFT2 and IL3Rα protein amount, suggesting that our newly described mechanism of RNFT2-dependent IL3Rα degradation may be operant in humans with chronic infection. Further studies are warranted to delineate the role of RNFT2 in these inflammatory disorders.

There are limitations to these studies. While our in vivo work clearly identifies a role for IL3 in LPS and PA murine acute lung injury, we do not identify the cell type responsible for IL3 secretion. In murine sepsis models, IRA-B cells are thought to be responsible for IL3 secretion (326, 359). Further, T cells and B cells are classically regarded as the main IL3 producers in other models of disease(331, 333, 345, 346). Whether IRA-B cells are also responsible for IL3 secretion in acute lung injury models is an active area of investigation. Further, whether these cells express RNFT2 is also unknown. Recent single cell RNA sequencing studies on murine airway cells showed no detection or extremely low levels of Il3 gene expression, which was not significantly altered among different airway cell types(360-362), suggesting that lung cells are not a primary producer of IL3. Additionally, while we show in vitro that IL3Rα abundance increases and RNFT2 abundance decreases in LPS-stimulated MLE12 cells, the changes in RNFT2 and IL3Rα abundance in lung homogenates after in vivo during lung injury could also be explained by differences in infiltrating immune cells between control and LPS/PA-treated mice. Thus, while

our in vitro work provides mechanistic insight into RNFT2/IL3Rα, additional work remains to further characterize this pathway in vivo.

We use the MLE12 cell line to characterize IL3Rα stability and test the role of RNFT2 in modulating IL3Rα-dependent downstream effects. MLE12 cells are an immortalized cell line that closely resembles, but does not fully mirror, Type II alveolar epithelial cells. We have identified several E3 ligase/substrate interactions relevant in pulmonary inflammatory conditions using the MLE-12 cells(59, 60, 363, 364). Future studies will focus on examining the RNFT2/IL3Rα expression in other pulmonary cell types, including primary human cells. We chose to examine NF-κB signaling (TRAF6 abundance, IL-6 secretion, CXLC-1 secretion) because our laboratory has previously shown role for TRAFs in experimental lung injury(60), and IL3 signaling has been linked to TRAF6 recruitment (332). However, whether RNFT2 also has similar effects on IL3Rα-dependent signaling in immune cells is unknown.

Lastly, our in vitro findings provide a framework to interrogate the role of RNFT2 in vivo in pathological disease states where IL3 is implicated. Related to our studies, it will be critical to determine which cell types are responsible for mediating the effects we observed after intratracheal lentiviral RNFT2 over-expression or knockdown. More broadly, these findings could have implications in other disease states where IL3Rα expression is altered. For example, IL3Rα is over-expressed in several hematologic malignancies and is the basis for novel therapies including chimeric antigen receptor (CAR) T cell therapies (365, 366). The role of RNFT2 in these conditions is unknown, and one could postulate that reduced RNFT2 expression or function could be partially responsible for aberrant IL3Rα expression. Further, pharmacological targeting of RNFT2 with a small molecule inhibitor could potentially enhance IL3Rα expression.

In conclusion, we showed that IL3 synergizes with LPS to exacerbate lung inflammatory injury, resulting in increased NF-κB activation and lung injury. This synergy proceeds through the IL3Rα subunit, whose protein stability is weakened by IL3 treatment but preserved by LPS exposure. IL3Rα protein is processed by the ubiquitin proteasome system, and the previously uncharacterized RING E3 Ligase, RNFT2, targets IL3Rα for proteasomal degradation by ubiquitinating it at lysine 357. The RNFT2/IL3Rα axis controls pro-inflammatory cytokine and immune cell release in murine lung inflammation models. Taken together, this study characterized a regulatory mechanism involving RNFT2-targeted degradation of the IL3 cytokine receptor IL3α.

3.3.11 Methods

3.3.11.1 Reagents

Anti-IL3Rα antibodies (MBS2542745; sc-74522) were obtained from MYBioSource and Santa Cruz Biotechnology. Anti-IL3Rβ (MBS2534790) antibody was from MYBioSource. Monoclonal anti-HA-Tag (clone 6E2) (Cat# 2367S RRID:AB_10691311), Anti-TRAF6 (Cat# 8028, RRID:AB_10858223), Anti-RelB (Cat# 10544, RRID:AB_2797727), and Anti-Phos-P100 (Cat# 4810, RRID:AB_659925) were from Cell Signaling Technology. Anti-V5 antibody (R960, RRID: AB_159298) was from Invitrogen. Anti-Actin antibody (A5441, RRID: AB_476744) and leupeptin (L2884) were from Sigma Aldrich. Goat anti-Rabbit IgG-HRP (Cat# 170-6515 RRID:AB_11125142), Goat anti-Mouse IgG-HRP (Cat# 170-6516 RRID:AB_11125547), and CFX96 Touch Real-Time qPCR (1855196) were from BioRad. MG-132 (F1100) was from UBPBio. Recombinant Murine IL3 was from PeproTech. Murine CXCL1 (DY453) and Murine TNF-a (DY410) ELISA kits were from R&D Systems. Murine IL-1β (88–7261) and murine IL-6 (88–7064, RRID: AB_2574986) ELISA kits were from eBioscience. SYBR Select Master Mix

(4472918) was from Life Technologies. QuikChange II XL Site-Directed Mutagenesis Kit (200522) was from Aglient Technologies. High capacity RNA-to-cDNA kits (4387406) were from Applied Biosystems.

3.3.11.2 Cell Culture

Murine Lung Epithelial 12 cells (MLE) (CRL-2110) were obtained from ATCC and cultured in Dulbecco's Modified Eagle Medium-F12 (Gibco) with 10% fetal bovine serum (DMEM-F12-10). For RNFT2 overexpression in MLE cells, electroporation was used, and 24 or 48hr later, cells were treated with stimulators. For RNFT2 knockdown, scramble siRNA and RNFT2 siRNA were used to transfect MLE cells for 48hr by electroporation. Cell lysates were collected in Lysis Buffer (150 mM NaCl, 50 mM Tris, 1.0 mM EDTA, 2 mM dithiothreitol, 0.025% sodium azide, and 1 mM phenylmethylsulfonyl fluoride), and prepared by brief sonication at 4˚C. Additionally, MLE cells were treated with cycloheximide (100μg/ml) for half-life studies. RAW264.7 cells were from ATCC (TIB-71) and cultured in DMEM with 10% fetal bovine serum. THP-1 cells were from ATCC (TIB-202) PBMCs and THP-1 cells were cultured in RPMI Medium 1640 (Gibco) with 10% fetal bovine serum. Pseudomonas aeruginosa (PA103) was from ATCC (29260).

3.3.11.3 RT–qPCR, cloning, and mutagenesis

Total RNA was isolated and reverse transcription was performed followed by real-time quantitative PCR with SYBR Green qPCR mixture as described (141).

3.3.11.4 In vitro ubiquitin conjugation assays

The assay was performed in a volume of 20μl containing 50 mM Tris, pH 7.6, 5mM MgCl2, 0.6mM DTT, 2mM adenosine triphosphate (ATP), 10μM MG132, 100nM Ubiquitin activating enzyme, 0.5 μM UBE2D, 2μM ubiquitin, and 1μM ubiquitin aldehyde. TnT-coupled reticulocyte in vitro–synthesized proteins (tagless-RNFT2 and HIS-purified IL3Rα-V5) and reaction products were processed for V5 immunoblotting.

3.3.11.5 Plasmid Transfection

For protein overexpression in MLE-12 cells, cells were nucleofected using Nucleofector 2B (Amaxa), program T-13. For protein overexpression in HEK293T cells, XtremeGENE transfection reagents were used following the manufacturer's protocol. Expression was confirmed by western blotting.

3.3.11.6 Recombinant DNA Constructs

Total RNA was isolated from untreated human PBMCs using RNeasy Mini Kit, and reverse transcribed to cDNA using High-Capacity RNA to cDNA kits. RNFT2 cDNA were PCR amplified, isolated, and sequence confirmed prior to PCR-cloning into pcDNA3.1D-V5-HIS vector. Deletion mutants were generated by PCR-cloning. Point mutants of RNFT2 and IL3Rα were generated using the QuikChange II XL kit, per the manufacturer's protocol. pRK5-HA-Ubiquitin-WT was a gift from Ted Dawson (Addgene plasmid # 17608, (322)) (Johns Hopkins University School of Medicine, Baltimore, MD)

3.3.11.7 In vitro protein binding assays

RNFT2 protein was immunoprecipitated from 1 mg MLE cell lysate using 1:100 dilution of RNFT antibody (rabbit) for four hours at 25°C in IP buffer (50 mM Tris HCl pH 7.6, 150 mM NaCl, 0.25 % v/v Triton-X-100) and coupled to protein A/G agarose resin for an additional hour. V5-Ubiquitin E2 enzymes (20 µl) were in vitro synthesized using TnT translation kits for 90 minutes at 30°C. RNFT2-bound resin was then incubated with the in vitro synthesized proteins for 18 hours at 4°C. Following binding, resin was washed with IP buffer, and eluted by dilution in denaturing loading buffer, with a final 1X formulation of: 50 mM Tris HCl pH 6.8, 2% SDS, 10% Glycerol and 100 mM DTT and incubation at 88°C for five minutes prior to immunoblotting analysis.

3.3.11.8 Immunoprecipitation Assays

MLE cells were cultured and treated as indicated prior to collection. Cell pellets were lysed with IP buffer (0.25% Triton-X-100 in 1x PBS, pH 7.6, 0.025% sodium azide, and 1 mM phenylmethylsulfonyl fluoride) on ice. Lysates were prepared by brief sonication at 4°C. Insoluble cellular debris was precipitated through centrifugation at 15,000x rcf for 10 min at 4°C. Lysate supernatant was normalized for protein concentration. Supernatants were exposed to a 1:50 dilution of the indicated antibody for three hours at 25°C. Immunoprecipitated protein was captured with 10µL magnetic protein A/G resin for 1 hour prior to two rounds of washing with IP buffer (1 mL). Protein was eluted by dilution in denaturing loading buffer, with a final 1X formulation of: 50 mM Tris HCl pH 6.8, 2% SDS, 10% Glycerol and 100 mM DTT and incubation at 88°C for five minutes. Eluted samples were resolved by SDS-PAGE and subjected to immunoblotting.

3.3.11.9 HIS-Pulldowns Assays

MLE cells were cultured and treated as indicated prior to collection. Lysate was recovered in PD buffer (0.25% Triton-X-100 in 1x PBS pH 8.0, 30mM imidazole, and 1 mM phenylmethylsulfonyl fluoride) on ice, before brief sonication and sedimentation by centrifugation (15,000x rcf, 10min, 4°C). Lysate supernatants were subjected to HIS-pulldown by 10µL magnetic HisPur resin for 1 hour prior to two rounds of washing with PD buffer (1mL). Protein was eluted by dilution in denaturing loading buffer, with a final 1X formulation of: 50mM Tris HCl pH 6.8, 2% SDS, 10% Glycerol and 100mM DTT and boiling for 5 minutes. Eluted samples were resolved by SDS-PAGE and subjected to Immunoblotting.

3.3.11.10 Animal studies

C57BL/6J mice were purchased from the Jackson Laboratory. Animals were between 7-9 weeks of age and around 25g weight at time of experiment. All procedures were approved by the University of Pittsburgh Institutional Animal Care and Use Committee. Models of endotoxin-induced lung injury (IT LPS) or Lung Injury by Live Bacteria (IT *Pseudomonas)* were employed in accordance with ATS guidelines on animal models of experimental lung injury (367). The principal objective in these models is the physiological assessment of lung injury, and studies were powered to detect a two-fold difference BAL protein amount, which is a well-established primary end point for animal models of ALI, and based on our prior published results using these models of lung injury(59, 60, 141, 232, 283, 341, 368). For intratracheal injection studies, C57BL/6J mice were anesthetized using a ketamine/xylazine mixture, and the larynx was well visualized under a fiber optic light source before endotracheal intubation with a 3/400 24-gauge plastic catheter. LPS with or without IL3 (rIL3) (LPS: 1.5mg/kg; rIL3: 6µg) were administered i.t. for 18h, after which animals were euthanized and assayed for BAL protein amounts by Lowry assay and

immunoblotting, cell count by TC20 automated cell counter, cytokine abundance by ELISA, and lung tissue H&E staining. In another study, LPS with or without IL3 neutralization antibody (Cell Signaling, Cat#D6C1) (LPS: 1.5mg/kg; α-IL3: 5µg) were administered i.t. for 18h, after which animals were euthanized and assayed for BAL protein amounts by immunoblotting, cell count, cytokine abundance by ELISA, and lung tissue H&E staining. For lentiviral study, $1x10^7$ PFU of lentivirus encoding genes for RNFT2 or *Rnft2* shRNA was treated i.t. for 144 hr before the administration of LPS with or without rIL3 (LPS: 1.5mg/kg; rIL3: 6µg in RNFT2 overexpression mice, 3µg in RNFT2 shRNA mice) for 18 hr, after which animals were euthanized and assayed for BAL protein amounts by immunoblotting, cell count, cytokine abundance by ELISA, and lung tissue H&E staining.

3.3.11.11 Human Studies (Acute Respiratory Distress Syndrome (ARDS))

De-identified human plasma samples were obtained from the University of Pittsburgh Acute Lung Injury Biospecimen Repository (IRB number #PRO10110387). Informed consent was provided by all participants or their surrogates in accordance with the Declaration of Helsinki. Adults aged 18-90 admitted to the Medical ICU in the UPMC Presbyterian Hospital with acute respiratory failure requiring mechanical ventilation by endotracheal tube were enrolled as patients if the onset of acute respiratory failure was associated with established risk factors for developing acute lung injury (sepsis, pneumonia, aspiration, blood transfusion, pancreatitis, or trauma) or if intubation was performed for airway protection in the setting of non-pulmonary critical illness. Enrollment took place within 48 h of the initiation of mechanical ventilation. After enrollment, patients were retrospectively sub-classified by an expert clinical panel into categories: 1) 'ARDS', as defined by Berlin criteria and agreed upon by a minimum of three members of an expert clinical panel, 2) 'at risk,' as defined as Lung Injury Prediction Score (LIPS) score >4 and the presence of

a clinically identifiable risk factor for ARDS, and 3) 'ventilated control,' as defined by intubation and mechanical ventilation for non-pulmonary critical illness without risk factor for ARDS. We performed a preliminary sample size calculation to detect a three-fold difference in two means (30 pg/mL vs. 90 pg/mL) between ventilated control and lung injured-patients with a power of 0.8, α of 0.05, an estimated standard deviation of 35, and a sampling ratio of 0.25 ventilated control/lung-injured patients (given there are fewer control patients enrolled in our study). We chose values of 30 and 90 pg/mL based on published literature showing an IL3 of >89.4 pg/mL is associated with poor outcomes in sepsis(326), and estimated baseline amounts from manufacturer data and published literature. The predicted samples size was 4 "control" patients and 14 "lung-injured" patients. With this, $n=4$ 'ventilated control,' $n=16$ 'at risk for ARDS,' were randomly selected from the cohort for analysis.

3.3.11.12 Human Studies (Cystic Fibrosis, CF)

Following attainment of informed consent, CF lung tissue was obtained from excess pathological tissue following lung transplantation in accordance with a protocol approved by the University of Pittsburgh Investigational Review Board. 1cm^2 sections of lung parenchyma were frozen and stored at -80 until use. ~100mg of lung tissue were homogenized in RIPA buffer followed by protein immunoblotting.

3.3.11.13 Statistics

Protein Signal densitometry was quantified by ImageJ. Comparisons of two groups were carried out with unpaired, two-tailed Student's T-test. Comparisons of more than two groups were tested with One-ANOVA with Tukey or Dunnett's post-hoc test for multiple comparisons as noted. Non-linear regression plots were tested with F-Test. All tests used $p < 0.05$ as indicative of

statistical significance. All statistical analyses were carried out using the Graph Pad Prism 8.0 program.

3.3.11.14 Study Approval

C57BL/6J mice were purchased from the Jackson Laboratory. All procedures were approved by the University of Pittsburgh Institutional Animal Care and Use Committee. For ARDS human studies, de-identified human plasma samples were obtained from the University of Pittsburgh Acute Lung Injury Biospecimen Repository (IRB number #PRO10110387). Informed consent was provided by all participants or their surrogates in accordance with the Declaration of Helsinki. Following attainment of informed consent, CF lung tissue was obtained from excess pathological tissue following lung transplantation in accordance with a protocol approved by the University of Pittsburgh Investigational Review Board.

3.3.11.15 Author contributions

B.B.C., Y.L., and M.J.J designed the study, analyzed the data; Y.T., T.L., J.E. and B.B.C. wrote the manuscript; Y.T., T.L., J.E., K.C.L, Y.C., and J.D.L. performed all in vitro experiments and animal experiments; J.E., M.M.M, Y.Z., I.D.P., J.F.M, and B.J.M. designed and executed the human studies. B.B.C. directed the study

3.4 RNF113A Regulates CXCR4 stability and signaling

As an inflammatory response in the lung progresses, immune cells for the vasculature extravasate the pulmonary endothelia barrier. The influx of these cells is reliant on specific molecular signals known as chemokines. The chemokine CXCL-12 is an important signal for cellular motility and is recognized by the chemokine receptor CXCR4. In addition to cell migratory ability, CXCR4 is a receptor important for HIV cellular invasion (370). In this short study we investigated CXCR4 protein stability, and its regulation by the E3 ligase RNF113A.

3.4.1 Overview

As an α-chemokine receptor specific for stromal-derived-factor-1 (SDF-1, also called CXCL12), C-X-C chemokine receptor type 4 (CXCR4) plays a vital role in chemotactically attracting lymphocytes during inflammation. CXCR4 also regulates HIV infection due to its role as one of the chemokine coreceptors for HIV entry into CD4+ T cells. Chemokine receptors and their signaling pathways have been shown to be regulated by the process of ubiquitination, a posttranslational modification, guided by ubiquitin E3 ligases, which covalently links ubiquitin chains to lysine residues within target substrates. Here we describe a novel mechanism regulating CXCR4 protein levels and subsequent CXCR4/CXCL12 signaling pathway through the

186

ubiquitination and degradation of the receptor in response to ligand stimulation. We identify that an uncharacterized really interesting new gene (RING) finger ubiquitin E3 ligase, RING finger protein 113A (RNF113A), directly ubiquitinates CXCR4 in cells, leading to CXCR4 degradation, and therefore disrupts the signaling cascade. We determined that the K331 residue within CXCR4 is essential for RNF113A-mediated ubiquitin conjugation. Overexpression of RNF113A significantly reduces CXCL12-induced kinase activation in HeLa cells, whereas RNF113A knockdown enhances CXCL12-induced downstream signaling. Further, RNF113A expression and silencing directly affect cell motility in a wound healing assay. These results suggest that RNF113A plays an important role in CXCR4 signaling through the ubiquitination and degradation of CXCR4. This mechanistic study might provide new understanding of HIV immunity and neutrophil activation and motility regulated by CXCR4.

3.4.1.1 Chemokine Receptor Type 4 Signaling in Inflammation

C-X-C Chemokine Receptor Type 4 (CXCR4) is a G-protein coupled receptor on the cellular membrane, and is expressed across many tissue types. It serves as the main receptor for the chemokine stromal cell-derived factor 1 (CXCL12). The binding of CXCL12 leads to signaling through several G-Protein dependent pathways (371). Specifically, this activates G-protein subunits and phosphorylates SRK kinases, leading to signaling through the ERK pathway (372). This signaling pathway is critical for cellular processes such as chemotaxis and proliferation. Concurrently, CXCR4 signaling activates phosphatidylinositide 3-kinases (PI3Ks), initiating a signaling cascade of second messengers resulting in downstream activation of RAC-alpha serine/threonine-protein kinase (Akt) and mitogen associated protein kinase (MAPK) (373, 374). As with ERK, these kinases are important regulators of cell adhesion, migration, and survival. Following ligand binding, CXCR4 is extensively phosphorylated by G protein-coupled receptor

kinases, causing desensitization, and leading to its internalization (375, 376). Following internalization, CXCR4 can be recycled back to the membrane for additional signaling, or sorted to endosomes for eventual degradation.

3.4.1.2 Dysregulation of CXCR4 Activity in Disease

Dysregulated CXCR4 activity exists in human pathologies. CXCR4 was initially characterized as one of two co-receptors aiding HIV-1 viral entry into cells (370). Classically, HIV-1 uses the CD4-lymphocyte receptor as the main coordinating anchor, with CCR5 or CXCR4 receptors as a secondary receptor. Use of CXCR4 as a co-receptor is primarily associated with the later stages of infection, for reasons that remain unclear (377). CCR5 has been the focus of several receptor antagonist therapeutics currently approved or in clinical trials (378). However, efforts to inhibit CXCR4 have not proven clinically meaningful, despite its importance as a co-receptor. CXCR4 plays a role in patients with co-morbidities as well. Macrophages from patients with TB show higher pulmonary expression of CXCR4, which leads to an acceleration of HIV infection (379). While CXCR4 functions as a co-receptor most notably for T-cell invasion, pulmonary epithelia are susceptible to CXCR4-mediated HIV infection (380). Due to the chemotactic consequences of its signaling, CXCR4 is implicated in cancer progression (381). Li *et al.* have demonstrated CXCR4 is linked to HER2-mediated breast cancer metastasis (382). Specifically, they observed that HER2 prevents ligand-induced CXCR4 degradation and increases the protein expression of CXCR4, thus facilitating cell migration. Moreover, depletion of CXCR4 through siRNA can block the ability of breast and liver cancer cells to migrate *in vitro* (383, 384). Overall, CXCR4 protein level is known to be elevated in cancerous tissue, and to be associated with worsened patient outcomes (385). Thus, CXCR4 protein expression, regulation, and stability are directly tied to disease progression.

3.4.1.3 Molecular Mechanisms of CXCR4 Regulation

There are multiple mechanisms regulating the expression and stability of CXCR4 (371). CXCR4 is regulated as the transcriptional level by transcription factors such as Nuclear Respiratory Factor-1 (NRF-1), SP-1, and negatively regulated by YY1 (386). This has disease implications, as infections such as HIV hijack NRF-1 to increase CXCR4 expression, and increase the infectivity of cells. Post-translational modifications also regulate the stability of CXCR4. The extensive phosphorylation that occurs following ligand binding not only regulates receptor activity, but serves as a scaffold for protein binding. These binding sites have been recognized as phospho-degrons for subsequent ubiquitination and degradation (375). In fact, ligand binding actually promotes ubiquitination leading to internalization and sorting prior to recycling (387). It has been reported that a HECT-domain Ubiquitin E3 ligase ITCH (E3 ubiquitin-protein ligase Itchy homolog) mediates ubiquitination of CXCR4 (301). ITCH specifically interacts with Arrestins on the ESCRT machinery leading to CXCR4 ubiquitination and endosomal transport to the lysosome (388). However, researchers have also observed other E3 ligases to manipulate CXCR4, specifically DTX3L, which antagonizes ITCH activity, maintaining CXCR4 stability (389). Regulation of CXCR4 degradation is a highly regulated and complex process (390). These recent discoveries suggest multiple proteins and multiple ubiquitin E3 ligases work to regulate CXCR4 stability.

3.4.1.4 The search for new regulators of CXCR4

We screened a library of RING E3 ligases to assay their activity on CXCR4 stability and observed a previously uncharacterized E3 ligase, RING finger protein 113A (RNF113A), mediates CXCR4 degradation. Here we report RNF113A is a bona-fide RING E3 ligase that directly binds

CXCR4, shortens CXCR4 protein half-life, downregulates CXCR4 signaling, and impairs cellular motility. This study represents a new means in regulating CXCR4 stability.

3.4.2 RNF113A is an ubiquitin E3 ligase regulating CXCR4

We prepared a library of over 200 E3 ligases and expressed them in HeLa cells to assess their effect on the protein abundance of CXCR4 (141, 283). A representative panel of E3 ligase overexpression was shown in Figure 57A. We observed RNF113A expression decreases protein abundance of CXCR4 (Figure 57A). Ligand binding is known to stimulate CXCR4 ubiquitination and degradation (387). To examine the role of RNF113A and CXCL12 on CXCR4 ubiquitination, we co-expressed HIS-tagged CXCR4 with RNF113A prior to treatment with CXCL12 (6 nM) for 1 hour. Lysates were subjected to HIS pull-down, washed, and the eluate was processed for Ubiquitin immunoblotting (Figure 57B). We recapitulated that CXCR4 protein is degraded upon CXCL12 exposure, as well as increased ubiquitin signal with pulled-down CXCR4 following CXCL12 treatment. Furthermore, we observed an even greater degradation and greater ubiquitin signal upon co-expression of RNF113A, suggesting RNF113A aids in CXCR4 ubiquitination and degradation in response to CXCL12 stimulant (Figure 57B). Next, we observed that the overexpression of RNF113A resulted in the decrease in CXCR4 protein level in a dose-dependent manner, but not of its paralogue RNF113B (Figure 57C). RING E3 ligases have a canonical RING domain containing critical Cys and His residues for zinc coordination (391). To validate the activity of RNF113A, we mutated two critical residues within the RING domain of RNF113A: C262 and C277. We observed that C262A and C277A mutants were unable to reduce CXCR4 protein levels as compared to wild-type RNF113A (Figure 57D). Upon the blockage of protein synthesis by exposure to cycloheximide (CHX), the overexpression of RNF113A led to an

accelerated degradation of CXCR4, compared to the empty vector control group (Figure 58A). Silencing of RNF113A via several different shRNA all led to the increased CXCR4 protein abundance (Figure 58B). Combination of shRNA silencing of RNF113A and CHX treatment significantly slowed down CXCR4 protein turnover (Figure 58C).
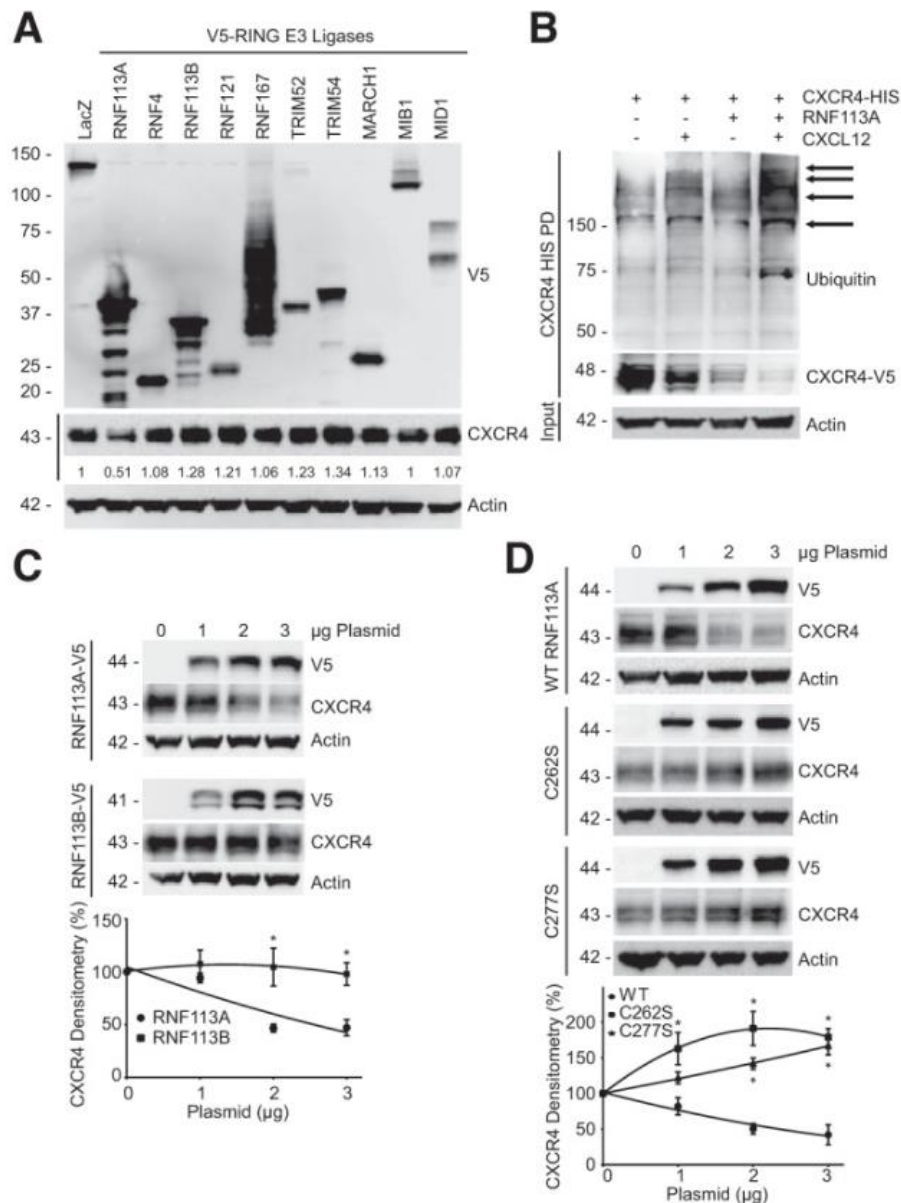
Figure 57 RNF113A facilitates C-X-C chemokine receptor type 4 (CXCR4) degradation

A: RING E3 ligase screening. A library of RING E3 ligases were transfected in HeLa cells before CXCR4 immunoblotting. CXCR4 densitometry relative to LacZ is shown beneath immunoblot. B: HeLa cells were cotransfected with CXCR4-HIS and RNF113A before CXCL12 treatment (6 nM, 1 h.), HIS pull-down, and immunoblotting. C, top: V5-tagged RNF113A and its paralogue RNF113B were expressed in HeLa cells in a dose course before CXCR4 immunoblotting. Bottom: densitometry on CXCR4 protein signal normalized to 0 µg for each treatment. Data represent mean values ± SE (n = 4, *P < 0.05, significant compared with RNF113A, two-way ANOVA, Bonferroni multiple comparisons). D, top: point mutants of RNF113A RING domain (V5-tagged) were expressed in HeLa cells before CXCR4 immunoblotting. Bottom: densitometry on CXCR4 protein signal normalized to 0 µg for each treatment. Data represent mean values ± SE (n = 4, *P < 0.05, significant compared with RNF113A WT signal at indicated dose, two-way ANOVA, Bonferroni multiple comparisons).
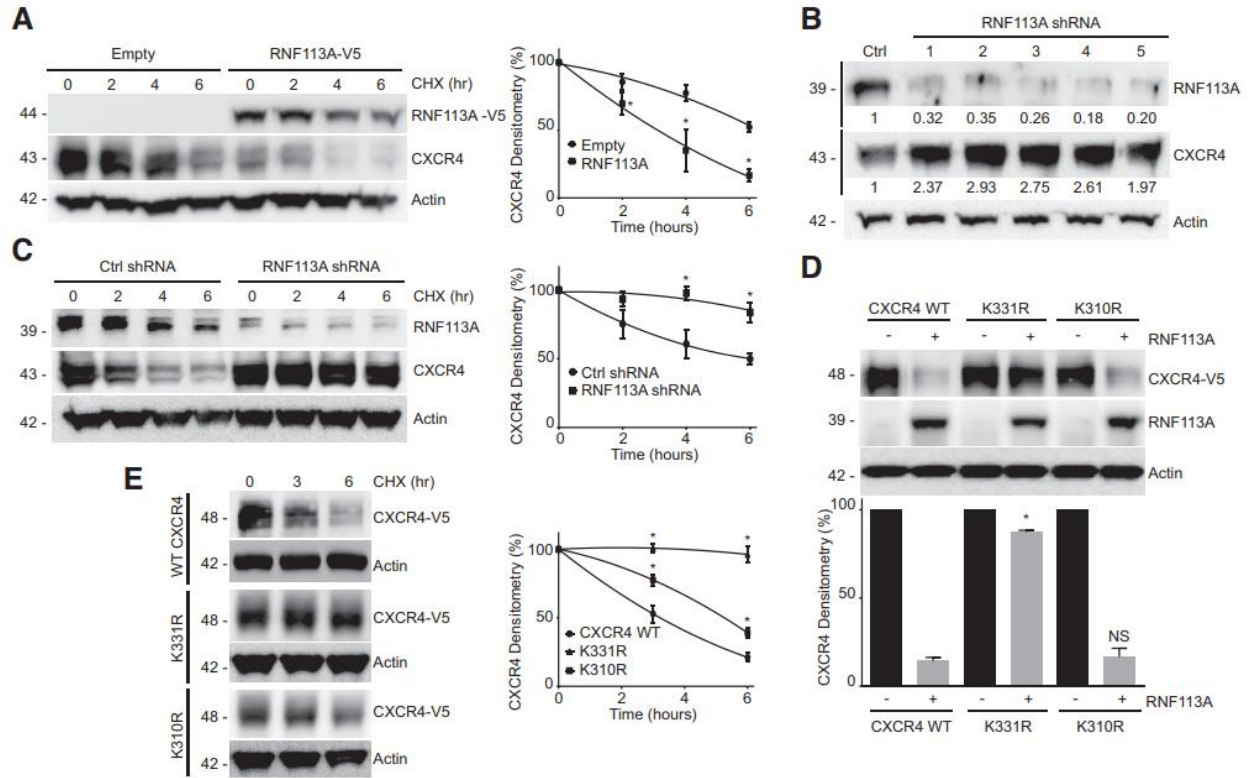
Figure 58 RNF113A decreases CXCR4 stability and half-life

A, left: HeLa cells were transfected with RN113A-V5 plasmid before cycloheximide (CHX) chase (50 μg/ml), and CXCR4 immunoblotting. Right: densitometry on CXCR4 protein signal normalized to time 0 for each treatment. Data represent mean values ± SE (n = 4, *P < 0.05, significant compared with Empty at indicated time, two-way ANOVA, Bonferroni multiple comparisons). B: screening of shRNA against RNF113A. HeLa cells were transfected with shRNA plasmids targeted against RNF113A before CXCR4 immunoblotting. Densitometry of RNF113A and CXCR4 signal relative to control (Ctrl) shRNA is shown beneath immunoblots. C, left: HeLa cells were transfected with shRNA scramble or shRNA plasmids targeted against RNF113A before CHX chase (50 μg/ml). Cells were then subjected to immunoblotting. Right: densitometry on CXCR4 protein signal normalized to time 0 for each treatment. Data represent mean values ± SE (n = 4, *P < 0.05, significant compared with Ctrl at indicated time, two-way ANOVA, Bonferroni multiple comparisons). D, top: HeLa cells were cotransfected with RNF113A and CXCR4 K-R lysine mutants before immunoblotting. Bottom: densitometry on CXCR4-V5 protein signal normalized to (−) RNF113A for each treatment. Data represent mean values ± SE (n = 3, NS, P > 0.05, not significant, *P < 0.05, significant compared with CXCR4 WT + RNF113A, one-way ANOVA, Bonferroni multiple comparisons). E, left: candidate lysine point mutants were transfected into HeLa cells before CHX chase (50 μg/ml). Right: densitometry on CXCR4-V5 protein signal normalized to time 0 for each treatment. Data represent mean values ± SE (n = 3, *P < 0.05, significant compared with WT at indicated time, two-way ANOVA, Bonferroni multiple comparisons).

3.4.3 CXCR4 K331 is critical for RNF113A-mediated degradation

We next sought to identify a potential ubiquitin lysine site within CXCR4. The intracellular C-terminal tail of CXCR4 contains several lysines. Previous reports have shown that the CXCR4 triple mutant of lysine to arginine (lysines 327, 331, and 333) is resistant to ubiquitin mediated degradation (387, 392). We further constructed single CXCR4 K-R point mutants, and observed K331R to be resistant to RNF113A-mediated degradation (Figure 58D). As a negative control, K310R remained susceptible to RNF113A-dependent degradation. Further, K331R CXCR4 exhibited a prolonged half-life during CHX chase, compared to CXCR4 wild-type (WT) and K310R mutant (Figure 58E)

3.4.4 RNF113A binds CXCR4 through a positively charged region

E3 ligases are known to target substrates through specific motifs on the E3 ligase and the target substrate (261, 393). ITCH uses a specific targeting sequencing, called a WW domain containing conserved tryptophan residues, to target CXCR4 for binding and ubiquitination (394). To further characterize the interaction of RNF113A and CXCR4, we employed a reductionist mapping approach to elucidate the putative binding regions within RNF113A and CXCR4. A series of N-terminal and C-terminal truncation mutants of RNF113A were prepared, *in vitro* expressed and subjected to CXCR4 binding (Figure 59A). We observed a loss of association between CXCR4 immunoprecipitate and RNF113A when the 15-residue region between 50 and 65 was deleted (Figure 59B). Finer mapping experiments narrowed this region down to ten residues (Figure 59C). The RNF113A construct with an internal deletion of these 10 residues largely decreased the interaction between RNF113A and CXCR4 (Figure 59D), and its

overexpression in HeLa cells failed to induce CXCR4 degradation (Figure 59E). This led to the conclusion that this ten-residue region is the putative binding site. Conversely, we designed C-terminal truncation mutants of CXCR4 and conducted binding assays with immunoprecipitated RNF113A (Figure 59F). We observed that a loss of association between RNF113A immunoprecipiate and CXCR4 when the region between residues 322-333 was deleted (Figure 59G). As serine 324 and 325 within this region have been described to be phosphorylated (375), we hypothesized they are critical for RNF113A association. Mutation of these serines to alanine prevented the binding of CXCR4 to RNF113A (Figure 59H). These residues have also been implicated as critical facilitators for ITCH-mediated ubiquitination of CXCR4 (394). However, as a positive control, deletion of the final 19 residues of CXCR4 preserved its binding affinity to RNF113A (Figure 59H).
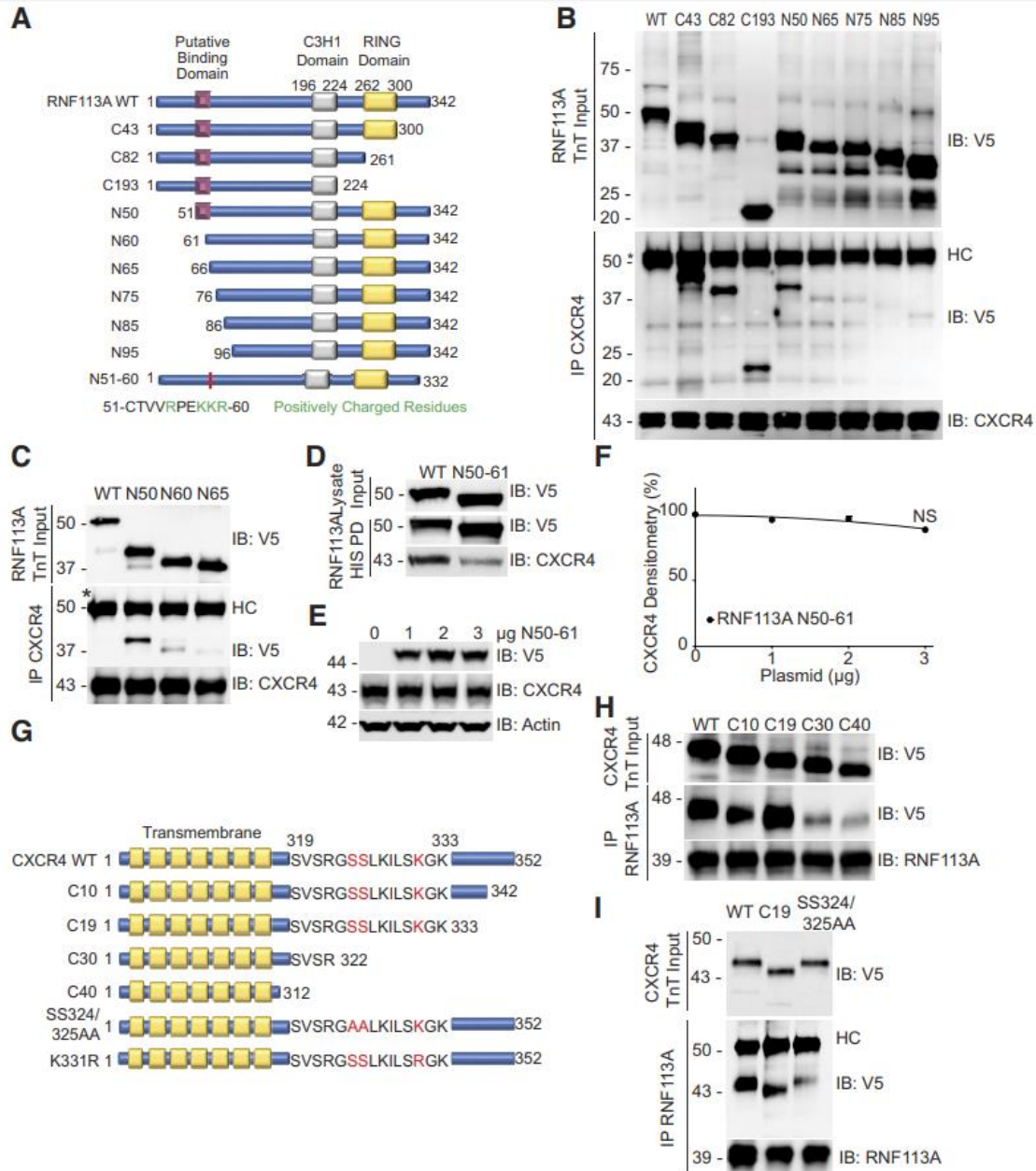
Figure 59 RNF113A binds CXCR4 in a positively charged region

A: schematic of RNF113A deletion mutants constructed for the binding studies. B and C: binding assays between RNF113A and CXCR4. HeLa cell lysate (100 μg protein) was subjected to CXCR4 immunoprecipitation (IP). RNF113A mutants were synthesized via in vitro transcription and translation (TnT), and allowed to bind to overnight with immunoprecipitated resin. Eluates were subjected to immunoblotting (IB). Asterisk (*) indicates full-length RNF113A, which runs at the same size as IgG heavy chain (HC). D: V5-tagged RNF113A internal deletion mutant was expressed in HeLa cells before HIS pull-down (PD) and CXCR4 immunoblotting. E: V5-tagged RNF113A internal deletion mutant was expressed in HeLa cells in a dose course before CXCR4 immunoblotting. F: densitometry of E. Data represent mean values ± SE (n = 3, NS, P > 0.05, slope not significantly different from 0, F-test). G: schematic of CXCR4 deletion mutants constructed for the binding studies. H and I: binding assays between RNF113A and CXCR4. HeLa cell lysate (100 μg protein) was subjected to RNF113A immunoprecipitation. CXCR4 mutants were synthesized via in vitro transcription and translation (TnT) and allowed to bind to overnight with immunoprecipitated resin. Eluates were subjected to immunoblotting.

3.4.5 RNF113A regulates CXCR4 signaling

Next, we investigated the effect of RNF113A on the CXCR4 signaling pathway. HeLa cells were transfected with RNF113A and treated with 6 nM CXCL12 in a time course before immunoblotting. RNF113A expression accelerates CXCL12-mediated degradation of CXCR4 (Figure 60A). Further, RNF113A expression decreased the activation of downstream kinases in CXCR4 signaling, specifically the phosphorylation of Akt1 and ERK1/2, without affecting total kinase levels (Figure 60A). Next, we silenced RNF113A in HeLa cells before CXCL12 treatment. We observed RNF113A depletion led to increased CXCR4 protein signal. Further, RNF113A depletion increases the activation of downstream kinases in CXCR4 signaling, specifically the phosphorylation of Akt1 and ERK1/2 (Figure 60B).
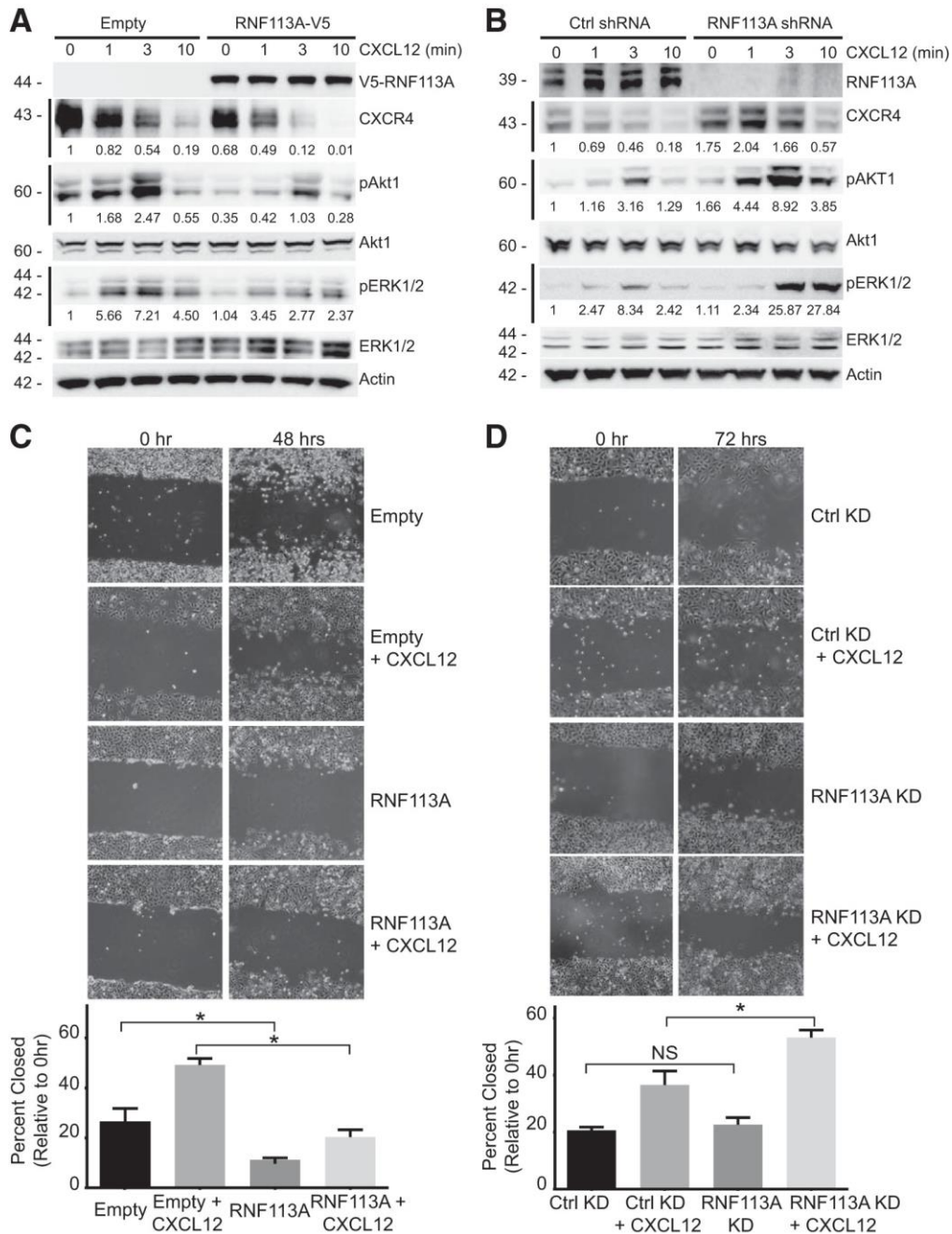
Figure 60 RNF113A regulates CXCR4 signaling and cellular motility

A: HeLa cells were transfected with RNF113A-V5 before CXCL12 treatment and immunoblotting for phosphorylated kinases. Densitometry relative to Empty at time 0 is shown beneath immunoblots. B: HeLa cells were transfected with plasmid encoding shRNA targeting RNF113A before treatment with CXCL12 (6 nM) for the indicated times. Cells were collected and immunoblotted for activation of downstream CXCR4 signalers. Densitometry relative to Ctrl shRNA at time 0 is shown beneath immunoblots. C and D: wound healing assay. HeLa cells were transfected with empty or RNF113A-encoded plasmids, or with plasmids encoding shRNA against scramble or RNF113A and allowed to grow to 80–90% confluency before starvation and wounding with pipette tip. Extent of gap closure was measured at 48 or 72 h and in the absence or presence of CXCL12. Gap closure is quantified below. Data represent mean values ± SE (n = 3–4 per group; *P < 0.05, significant between indicated groups, NS, P > 0.05, not significant between indicated groups, two-sided t-test). "KD" refers to shRNA.

3.4.6 RNF113A affects cell motility

Finally, we investigated the functional role of RNF113A on cellular motility through its regulation of CXCR4. The CXCR4 signaling cascade mediates cellular motility, especially in the presence of CXCL12. Manipulation of CXCR4 signaling through antagonist inhibition or siRNA silencing has been shown to affect cellular motility in a wound healing assay (384, 395). Further, CXCL12 treatment can accelerate wound healing (395). HeLa cells were transfected with RNF113A-V5 plasmid or *shRNA* against RNF113A, and seeded to a density of 80-90%. Confluent cells were starved and wounded using 200 µL pipette tip to create a 400 µm gap in the monolayer. Additionally, cells were exposed to CXCL12 (12 nM) during course of healing. The monolayer was imaged and gap closure was quantified (n=3-4). RNF113A overexpression significantly precluded gap closure, compared to empty plasmid (Figure 60C). Moreover, treatment with CXCL12 resulted in a significantly increased gap closure with empty plasmid cells. However, compared to CXCL12 treatment, additional overexpression of RNF113A only slightly increased gap closure, and only closely within significance (p = 0.0458). From these observations, we conclude RNF113A expression affects cell motility through regulating CXCR4. As a complementary assay, we used *shRNA* to silence RNF113A prior to wound healing assay (Figure 60D). We further confirmed that CXCL12 enhanced gap closure among the control *shRNA* plasmid group. Furthermore, additional depletion of RNF113A significantly increased gap closure, compared to CXCL12 treatment alone.

These data demonstrate that RNF113A is a negative regulator of CXCR4 protein stability, signaling, and CXCR4-mediated cellular motility.

3.4.7 Discussion

Here we report a new mechanism in the regulation of CXCR4 protein stability. We observed RING ubiquitin E3 ligase RNF113A promotes CXCR4 degradation, impairs downstream signaling, and affects cell motility. Depletion of RNF113A through *shRNA* preserves CXCR4 protein level, extends CXCR4 protein half-life and enhances CXCR4 signaling. CXCR4 has been shown to be mono-ubiquitinated, specifically by ubiquitin E3 ligase ITCH, leading to its endosomal sorting and degradation (301, 371). However, poly-ubiquitination of CXCR4 has also been observed, and is suggested to play a role in immune cell aging (396, 397). We demonstrated RNF113A expression and CXCL12 treatment can increase high molecular weight ubiquitin signal of CXCR4 compared to control (Figure 57B). This suggests RNF113A facilitates the poly-ubiquitination of CXCR4.

The ubiquitin system is a critical mediator of the dynamics of cellular motility and migration (398). Specifically, RING E3 ligases, such as inhibitors of apoptosis (IAP), can both positively or negatively regulate cell migration through the ubiquitination of substrates including plasma membrane surface proteins or members of the signaling cascade (399). We observed that RNF113A overexpression attenuates CXCL12-CXCR4-dependent activation of Akt and ERK, kinases classically associated with cellular movement (Figure 60A). Conversely, silencing of RNF113A enhanced Akt and ERK activation (Figure 60B). RNF113A mediation of CXCR4 degradation also has functional consequences. Cells with overexpressed RNF113A were less able to close the gap in a wound healing assay relative to empty vector plasmid (Figure 60C). However, among cells with RNF113A over-expression, the difference in gap closure between untreated and CXCL12-treatment trends toward insignificance (p = 0.0458). This suggests that RNF113A-expressing cells are less sensitive to CXCL12-stimulated motility, possibly due to RNF113A-

mediated degradation of the primary CXCL12 receptor, CXCR4. When RNF113A is silenced, which leads to the increased CXCR4 stability and abundance, cells exhibit a stronger response to CXCL12, with enhanced gap closure relative to control shRNA treatment (Figure 60D).

GPCR and chemokine receptor signaling are heavily regulated by the stability of the receptor, specifically through post-translational modification. Phosphorylation by G-protein specific kinases has been known to be a main regulator through desensitization. However, ubiquitination is increasingly understood to be a potent regulator of stability and downstream function (400). Indeed, several ubiquitin E3 ligases are known to regulate the function and signaling of CXCR4.

Substrates fated for ubiquitination are often characterized by specific targeting sequences that aid ubiquitin E3 ligases in identification and association. Specifically, protein binding motifs involving phosphorylation have proven critical for E3-substrate interaction (261, 393). Protein binding motifs have been shown to be critical in engaging CXCR4. Previous research has shown that ITCH binds CXCR4 with WW-motifs, which are binding regions with proline-rich affinity (394). We observed RNF113A to have a positively charged 10-residue region necessary for binding to CXCR4 (Figure 59A). Further, mutation of critical serine residues of CXCR4, known to be phosphorylated and thus negatively charged, led to decreased association with RNF113A (Figure 59H). These mechanistic studies suggest a complementary charge-dependent interaction facilitating the association between E3 ligase and substrate. Understanding of the mechanistic underpinnings of association will serve as the basis for future structure-based small molecule drug development. As a co-receptor for HIV-1, depletion of CXCR4 protein would be beneficial to prevent viral entry, similar to drug development efforts in antagonizing CCR5 (378). Enhancing

RNF113A-CXCR4 interaction or prolonging RNF113A half-life would function to decrease available co-receptor for viral entry, and potentially have therapeutic benefits for patients.

RNF113A may be working in concert with other proteins or E3 ligases. Arrestin-2 has been shown to cooperate with ITCH in promoting ubiquitination of CXCR4, leading to its degradation (388, 401). Conversely, Holleman and Marchese described antagonism between the RING E3 ligase Deltex-3L (DTX3L) and ITCH, as DTX3L inhibits ITCH ubiquitin ligase activity toward CXCR4 (389). Similarly, the downstream kinase CISK has been shown to inhibit ITCH activity in degrading CXCR4 (402). Interestingly, we observe that RNF113A protein signal also decays during cycloheximide chase (Figure 58A), suggesting RNF113A protein stability is subject to regulation. We have observed a similar multiple E3 ligase relationship in F-box only protein 3 (FBXO3) regulating F-box/LRR-repeat protein 2 (FBXL2) leading to pleiotropic cellular and pathological consequences (403). Substrates have been shown to be regulated by a variety of ubiquitin E3 ligases depending on the specific spatiotemporal environment, and in response to discrete stimuli; a classic example being the ubiquitin-mediated regulation of p53 (404). It is possible that the regulation of CXCR4 by RNF113A works within a comparable regulatory framework.

Aside from this study, the function of RNF113A remains unclear. Bioinformatics studies predict a RING domain in RNF113A (405). We observed that mutation of critical RING residues rescues substrate CXCR4 from degradation (Figure 57D). Genomic studies have shown that nonsense mutations within the catalytic RING domain of RNF113A occur in patients with the autosomal recessive disease Trichothiodystrophy (406). While trichothiodystrophy is a pathologically heterogenous disease, malfunction of DNA-repair mechanisms has been associated with patients (407). It could be that RNF113A is involved in regulation of these potentially disease-

causing repair mechanisms. Further investigation is needed for determining the regulation of RNF113A on biologic processes.

We believe this study is a stepping stone for further investigations into a novel regulator of CXCR4 stability and signaling.

3.4.8 Materials and Methods

3.4.8.1 Materials

Anti-CXCR4 antibody (UMB2) (ab124824) was from Abcam. Horseradish peroxidase-conjugated secondary antibodies (170-515/6) were from Bio-Rad. Antibodies against ERK1/2 (137F5; 4695), pERK1/2 (Thr202/Tyr204) (20G11; 4376), pAkt (Ser473) (D9E; 4060), and Akt (40D4; 2920) were from Cell Signaling Technologies. Anti-ubiquitin antibody (VU101) was from Life Sensors. Antibodies against RNF113A (V-25, sc-133965) were from Santa Cruz Biotechnology. Anti-actin antibody (A5441) was from Sigma Aldrich. Anti-V5 Tag (R960-25) was from Thermo Fisher Scientific. QuikChange II XL Site-Directed Mutagenesis Kit (200522) was from Aglient Technologies. Eagle's minimum essential medium (EMEM) (30-2003) and HeLa cells (CCL-2) were from ATCC. Thermal Cycler Life ECO (BYQ6078) was from BIOER Technology. Cytation5 Imager was from BioTek. Cycloheximide (BML-GR310) was from Enzo. Plasmids (pLKO.1) encoding shRNA against RNF113A were from GE Dharmacon. FBS (100-106) was from Gemini. DNA sequencing was performed at Genewiz. Phusion High-Fidelity DNA Polymerase (M0530) was from NEB. TnT T7 Quick Coupled Transcription/Translation System (L1170) was from Promega. Recombinant hCXCL12 (350-NS-010) was from R&D Systems. Agar (A5306) and XtremeGene HP (XTGHP-RO ROCHE) were from Sigma Aldrich. HisPur Ni-NTA Magnetic Beads (88831), PureLink Quick Plasmid Miniprep Kit (K210010), Pierce Protein

A/G Magnetic Beads (88802), and pcDNA3.1D V5/HIS/TOPO kit (K490040) were from Thermo Fisher Scientific.

3.4.8.2 Cell culture

HeLa cells were cultured in Eagle's minimum essential medium (ATCC) supplemented with 10% fetal bovine serum (EMEM-10). Cell line morphology was monitored via microscopy and immunoblotted for multiple markers. Mycoplasma contamination was checked using the MycoAlert Mycoplasma Detection Kit (Lonza, Switzerland). For plasmid overexpression in HeLa cells, plasmids were combined with XtremeGene HP kit following manufacturer's protocol. After 24 h, cells were treated with CXCL12 (6 nM) or cycloheximide (CHX; 50 µg/ml) for the indicated times. For RNF113A silencing studies in HeLa cells, scrambled shRNA control and RNF113A shRNA were transfected into cells for 48 h using XtremeGene HP kit following the manufacturer's protocol. Exposed cells were collected and processed for immunoblotting.

3.4.8.3 Cloning and mutagenesis

All wild-type (WT) and mutant CXCR4, RNF113A, and RING E3 ligase plasmid constructs were generated using PCR-based approaches using appropriate primers and were then subcloned into a pcDNA3.1D/V5-His vector (9, 34). Point mutants were generated using the QuikChange II XL kit (Aglient). All plasmid constructs were sequence-confirmed against NCBI reference sequences before experimentation, (e.g., NM_001008540 for CXCR4, NM_006978 for RNF113A).

3.4.8.4 Western blotting

Cell sample lysates were collected and digested in buffer A (150 mM NaCl, 50 mM Tris, 1.0 mM EDTA, 2 mM dithiothreitol, 0.025% sodium azide, and 1 mM phenylmethylsulfonyl fluoride) on ice. Lysates were prepared by brief sonication at 4°C. Insoluble cellular debris was precipitated through centrifugation at 15,000 g for 10 min at 4°C. Lysate supernatant was normalized for protein concentration and diluted in denaturing loading buffer, with a final 1× formulation of: 50 mM Tris·HCl (pH 6.8), 2% SDS, 10% glycerol, and 100 mM DTT. Samples were resolved via SDS-PAGE prior to immunoblotting. Signal was detected via chemiluminescence on a Kodak Imaging Station. Densitometry was calculated via ImageJ (National Institutes of Health, Bethesda, MD).

3.4.8.5 HIS-pull down

Full-length CXCR4-HIS-V5 plasmid was overexpressed in HeLa cells without and with coexpression of tagless RNF113A using the above protocol. Following 18 h of expression, cells were exposed to vehicle or CXCL12 (6 nM) for 1 h, before collection and lysis of cells. Clarified cell lysate was incubated with HisPur Ni-NTA agarose resin for 1 h at 25°C. Resin pull-downs were washed before elution at 70°C in 1× denaturing loading buffer and subsequent immunoblot analysis.

3.4.8.6 In vitro protein-binding assays

CXCR4 protein was immunoprecipitated from 1 mg HeLa cell lysate using CXCR4 antibody (rabbit) and coupled to protein A/G agarose resin. CXCR4 beads were then incubated with in vitro synthesized products (50 μl) expressing RNF113A-V5 deletion mutants. After washing, the proteins were eluted and processed for V5 immunoblotting. Similarly, RNF113A

protein was immunoprecipitated from HeLa cell lysate using RNF113A antibody (rabbit), and subjected to binding against V5-tagged CXCR4 mutants.

3.4.8.7 RNF113A shRNA knockdown

pLKO.1 plasmids encoding nontargeting control (RHS6848) and shRNA against RNF113A were derived from the RNAi Consortium (TRC-Hs1.0, human) and purchased from GE Dharmacon. Mature antisense sequences are as follows: shRNA no. 1 (TRCN0000033729): TTTCCGGTCGAACCACAGTGC; shRNA no. 2 (TRCN0000033730): TAGCAATCAATTCTTTCGCTG; shRNA no. 3 (TRCN0000033731): TATCATTGGATTGTGGGTCAC; shRNA no. 4 (TRCN0000033732): AAAGATGGCTTGTGCATCGCG; and shRNA no. 5 (TRCN0000033733): ATTGAAGACGCCATTGGTCTG. Plasmids encoding shRNA were delivered to cells using transfection protocols described above.

3.4.8.8 Cellular migration assay

HeLa cells were transfected with empty plasmid, RNF113A-V5, control shRNA, or shRNA against RNF113A as described above. Transfected cells were seeded in six-well plates to 80–90% of confluence and starved for 24 h before scratching the monolayer with a pipette tip. CXCL12 (12 nM) was added to wounded monolayer immediately following injury and replaced every 24 h. Images were collected at 48 and 72 h post scratch. Images were collected with ×4 objective using BioTek Cytation5 Imager.

3.4.8.9 Statistical analysis

Statistical comparisons were performed with means ± SE for continuous variables. All data were statistically analyzed by the indicated statistical tests with $P < 0.05$ indicative of statistical significance. All analyses were performed using GraphPad Prism 6.

4.0 Ubiquitination in Nutrient Sensing

In the final aim of this dissertation, we conducted pilot studies into the role of ubiquitin E3 ligase control of nutrient sensing mechanisms. Many of the previously described lung diseases disproportionately afflict the elderly. ARDS incidence and mortality is highest in the elderly (268). Likewise, individuals over 60 are the highest proportion of patients presenting with idiopathic pulmonary fibrosis (408, 409). As humanity enters an age where elders assume a hitherto unseen proportion of total persons, diseases such as ARDS, fibrosis, and other age-related co-morbidities will increase in prevalence (410). One route to intervene against these age-associated diseases is to investigate the mechanisms of aging itself; among these, nutrient sensing, and its dysfunction, has been implicated in longevity and health span. Understanding of the mechanisms controlling nutrient sensing may yield new protein relationships associated with health and disease, and present new targets for therapeutic intervention. In this pilot study, we investigated the E3 ligase RNF186 and its control of Sestrin-2, a protein that senses the amino acid leucine to regulate metabolic signaling through mTORC1.

4.1 The RING-type E3 ligase RNF186 ubiquitinates Sestrin-2 and thereby controls nutrient sensing

Adapted from: Lear et al., The RING-type E3 ligase RNF186 ubiquitinates Sestrin-2 and thereby controls nutrient sensing J. Biol. Chem. 2019 294: 16527-. doi:10.1074/jbc.AC119.010671, (411)

4.1.1 Introduction

Nutrient sensing is a critical process controlling metabolism and growth function for cells and tissues (412). The primary signaling pathway controlling nutrient sensing is the mechanistic target of rapamycin complex 1 (mTORC1) pathway (413). During nutrient availability, mTORC1 phosphorylates several key signaling proteins such as P70S6K, 4E-BP1, and ULK1, working to activate anabolic processes and inhibit processes such as autophagy (70). Specific amino acid sensors such as Sestrin-2 sense intracellular nutrient levels, and integrate this signal to the mTORC1 complex (414).

4.1.1.1 The nutrient sensing role of Sestrin-2

Sestrin-2 (also known as Hi95) exerts inhibitory control over mTORC1 by associating with an mTORC1 activating protein complex called GATOR2 (415). This function is in a leucine-dependent manner, such that when leucine is abundant, the Sestrin-2-GATOR2 interaction is impeded, allowing activation and anabolic mTORC1 activity (415, 416). Sestrin-2 loss-of-function and mutational studies demonstrate the sensor's criticality for mTORC1 activity, as Sestrin-2 depleted cells result in constitutively active mTORC1, even in the absence of nutrients such as leucine (415). Further Sestrin-2 has been shown to regulate autophagic flux in numerous cell types (417-419). Transcriptional control of Sestrin-2 has been well-characterized (420-422), however, the post-translational mechanisms of Sestrin-2 regulation remain unclear. Our group and others have noted distinct mechanisms of E3 ligase control of disease, such as lung innate immunity, fibrosis, and of mTORC1 activity (176, 261, 423). E3 ligases are also a growing field for therapeutic targeting and inhibition (424). We sought to determine if Sestrin-2 was subject to ubiquitin E3-ligase mediated degradation, and the effect of this control on mTORC1 activity.

4.1.1.2 RNF186 as a new regulator of Sestrin-2 stability and activity

Here we report the mechanistic study of Sestrin-2 ubiquitination and degradation by the RING E3 ligase RNF186. We observed Sestrin-2 has a short half-life in Beas-2b cells that is prolonged by inhibiting the proteasome or the ubiquitination cascade. We used unbiased high throughput screening of Sestrin-2-GFP expressing cells with a library of siRNA targeting ubiquitin proteins and E3 ligases to uncover the E3 ligase RNF186 as a regulator of Sestrin-2 stability. RNF186 silencing prolongs Sestrin-2 stability while RNF186 expression accelerated Sestrin-2 degradation. RNF186 ubiquitinates and binds Sestrin-2 through specific domains. Silencing of RNF186 leads to decreased mTORC1 activity, potentially through increased Sestrin-2 protein abundance. This study adds a new mechanism for control of nutrient sensing through protein ubiquitination and suggests RNF186 may be potential target for inhibition to increase the level of the mTORC1 inhibitor Sestrin-2.

4.1.2 The ubiquitin-proteasome system potently controls Sestrin-2 stability in airway cells

We first investigated the stability of Sestrin-2 in human primary airway epithelial Beas-2B cells. Cycloheximide (CHX) time course revealed endogenous Sestrin-2 has a half-life around 4 hours, which is prolonged with proteasomal inhibition by MG132 (Figure 61A). Treatment with the lysosomal inhibitor leupeptin did not increase Sestrin-2 protein stability. MG132 treatment also resulted in a time dependent increase in endogenous Sestrin-2 level (Figure 61B). While the proteasome is the endpoint for most protein degradation, the ubiquitination pathway is a major upstream mechanism controlling proteins fated for proteasomal degradation. Co-treatment of Beas-2B cells with CHX and the ubiquitin E1 inhibitor MLN7243 resulted in enhanced Sestrin-2 stability, suggesting a role for ubiquitin-control of Sestrin-2 stability (Figure 61C) (425).

Expression of HA-tagged ubiquitin with CHX treatment led to Sestrin-2 degradation, which was also prevented with proteasomal inhibition (Figure 61D). Ubiquitin is often assembled in polymeric chains upon proteins to be degraded; this poly-ubiquitination is a canonical signal for degradation (94). Sestrin-2 pull-down in the presence of MG132 displayed extensive high molecular weight ubiquitin signal, characteristic of poly-ubiquitination (Figure 61E). These poly-ubiquitin chains have the capacity to assemble different linkage types, forming a cellular code (426). We used the UbiCREST assay to unravel the specific poly-ubiquitin chain type assembled on Sestrin-2. UbiCREST utilizes the differential reactivity of de-ubiquitinase enzymes for specific poly-ubiquitin-linkage types (427). We observed Sestrin-2 assembles predominately -K48 and -K63 poly-ubiquitin chains as evidenced by the degradation of Sestrin-2 poly-ubiquitin signal upon treatment with deubiquitinases specific for these linkage-types (Figure 61F).

Figure 61 Sestrin-2 is ubiquitinated and degraded in the proteasome

(A) Immunoblot analysis of Sestrin-2 protein from Beas-2b cells following CHX time course with MG132 or leupeptin co-treatment. Data and means ± SD of 3 independent experiments. (B) Sestrin-2 blotting from Beas-2b cells treated with vehicle, MG132, or leupeptin for indicated times. Data and means ± SD of 3 independent experiments. (C) Immunoblot analysis of Sestrin-2 protein from Beas-2b cells following CHX time course with the Ubiquitin E1 inhibitor MLN7243 or leupeptin co-treatment. Data and means ± SD of 3 independent experiments. (D) HA-tagged ubiquitin was expressed prior to CHX time course with MG132 co-treatment and Sestrin-2 immunoblotting. Data and means ± SD of 3 independent experiments. (E) Sestrin-2-V5-HIS was expressed in Beas-2b cells prior to MG132 treatment, HIS pulldown, and ubiquitin immunoblotting. (F) UbiCREST analysis of Sestrin-2 poly-ubiquitination pattern. Sestrin-2-V5-HIS was expressed in Beas-2b cells, treated with MG132, and pulled-down prior to digestion with different deubiquitinases and immunoblot analysis. *P < 0.05, by F-test comparisons of nonlinear regression relative to controls (A-D).

212

4.1.3 The Ubiquitin E3 ligase RNF186 ubiquitinates and degrades Sestrin-2

Ubiquitin E3 ligases are the critical substrate-recognition mechanism of the ubiquitination pathway. To understand the mechanism of Sestrin-2 degradation, we prepared a stable Sestrin-2-GFP expressing cell line and utilized an RNAi library targeting proteins involved in ubiquitination (E1, E2, E3, etc) to screen for Sestrin-2 regulators. Sestrin-2-GFP cells were transfected with the siRNA library, and GFP fluorescence was measured after 72 hours and ranked by median absolute deviation Z-score. We observed several key regulators of Sestrin-2 stability (Figure 62A). Specifically, the ubiquitin E3 ligases RNF186 and PRFP19 resulted in potent Sestrin-2-GFP signal relative to ctrl siRNA (Figure 62B). Top hits from the screen were evaluated by immunoblotting, and RNF186 knockdown resulted in increased SESN2 protein signal (Figure 62C). Further, RNF186 expression resulted in dose dependent decrease in Sestrin-2 protein (Figure 62D). In contrast, mutation of a key residue within the RNF186 active site, His-60 to Trp (428), led to inability to decrease Sestrin-2 protein (Figure 62E). Beas-2B cells were treated with siRNA against RNF186 prior to CHX chase, and we observed that RNF186 knockdown resulted in prolonged Sestrin-2 stability relative to control siRNA (Figure 62F). Conversely, RNF186 overexpression led to accelerated Sestrin-2 degradation in CHX chase (Figure 62G). Finally, co-expression of RNF186 with ubiquitin and Sestrin-2 in an *in vivo* ubiquitination assay resulted in increased poly-ubiquitination signal detected from Sestrin-2 pull-down, suggesting RNF186 facilitates the ubiquitination of Sestrin-2 (Figure 62H).
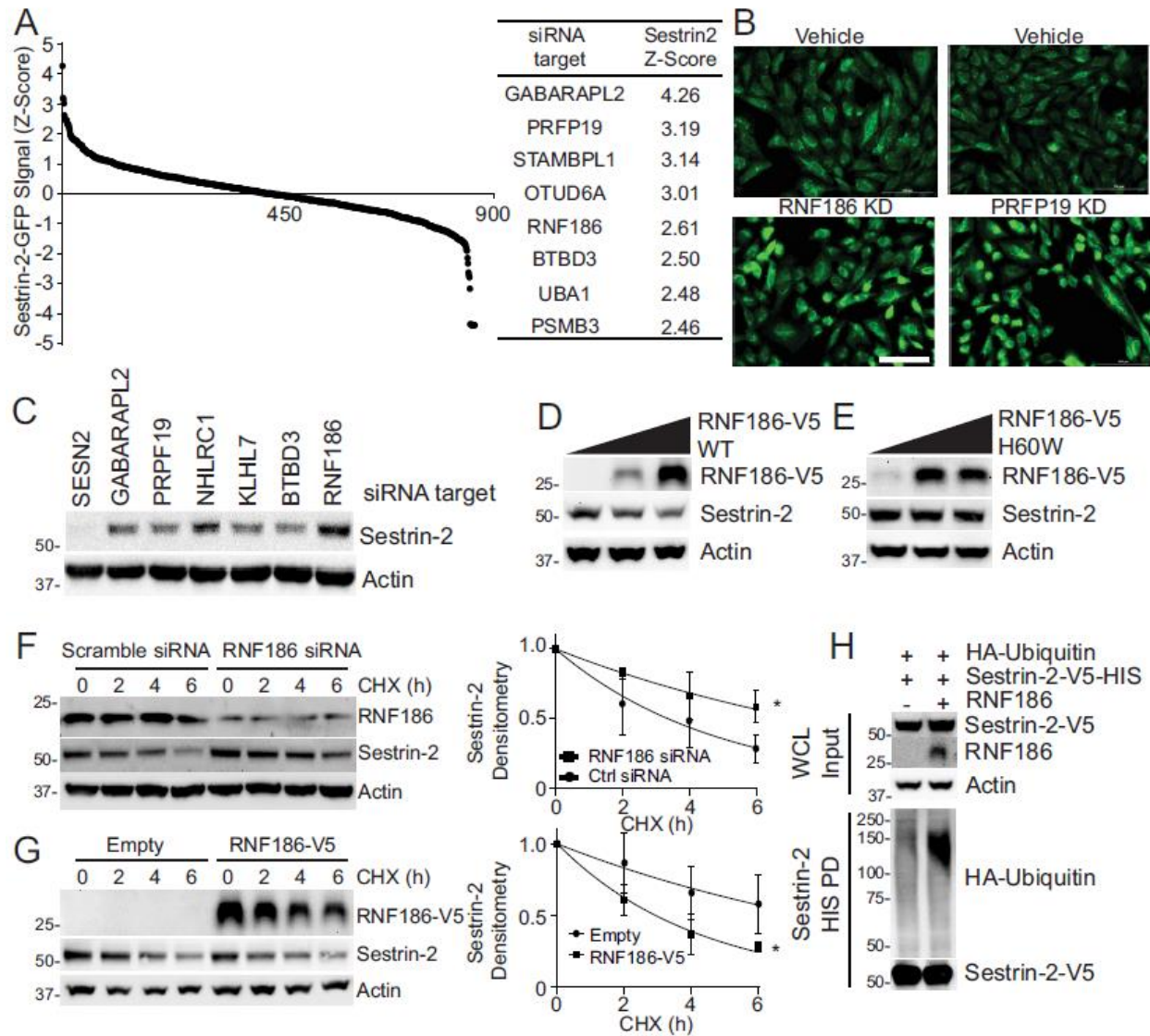
Figure 62 Ubiquitin RING E3 ligase RNF186 controls Sestrin-2 ubiquitination and degradation

(A) Screening of an siRNA library targeting ubiquitin E3 ligases for effect on Sestrin-2-GFP signal. Fluorescence was measured by Cytation 5 automated microcopy. Sestrin-2-GFP signal was reported as median absolute deviation Z-score. Top hits are ranked and displayed. (B) Representative Sestrin-2-GFP images from scramble siRNA and candidate E3 ligase siRNA from screen in (A). Scale bar indicates 100μm. (C) Immunoblot analysis of candidate E3 ligases identified from screen in (A). (D) RNF186 was expressed dose-wise in Beas-2b prior to Sestrin-2 immunoblotting. (E) Immunoblot analysis of Sestrin-2 following expression of RNF186 H60W mutant. (F) CHX chase of Sestrin-2 protein following siRNA knockdown of *RNF186* in Beas-2b cells. Data and means ± SD of 3 independent experiments. (G) CHX chase of Sestrin-2 protein following expression of RNF186 in Beas-2b cells. Data and means ± SD of 3 independent experiments. (H) Immunoblot analysis of Sestrin-2 ubiquitination following *in vivo* ubiquitination assay and pull-down of Sestrin-2 protein. *P $<$0.05, by F-test comparisons of nonlinear regression compared to controls (F, G).

214

4.1.4 RNF186 and Sestrin-2 bind each other through C-terminal motifs

To further examine the mechanism of the RNF186/Sestrin-2 interaction, we conducted reductionist mapping experiments to find the critical protein motif for binding. We prepared RNF186 deletion mutants (Figure 63A), synthesized the protein fragments in vitro, and exposed them to immunoprecipitated Sestrin-2 in binding assays. We observed that the RNF186 ΔC27 mutant lost binding with Sestrin-2, and upon further deletion mapping, we observe the C10-20 region of RNF186 is critical for Sestrin-2 binding (Figure 63B-C). We also prepare deletion mutants of Sestrin-2 encompassing critical protein domains (Figure 63D). Sestrin-2 mutants lost binding with RNF186 with the ΔC173 mutant (Figure 63E). Further mapping studies show the key region for RNF186-engagement to exist between residue 308 and 380 of Sestrin-2 (Figure 63F).

4.1.5 Lysine 13 is a critical ubiquitin-acceptor site for Sestrin-2

Substrates are ubiquitinated through covalent isopeptide bond between ubiquitin's C-terminus and an acceptor amino acid on the substrate. The key substrate amino acid is often lysine (429). We sought to identify the critical ubiquitin-acceptor lysine site within Sestrin-2. Previous ubiquitin proteomics studies detected a ubiquitinated peptide corresponding to Sestrin-2 Lys13 (430). To confirm this, we prepared Sestrin-2 point mutants, and co-expressed with RNF186 in Beas-2B cells. Sestrin-2 K13R mutant demonstrated resistance to RNF186 expression relative to wild-type (Figure 63G). Further, Sestrin-2 K13R mutant displayed a prolonged half-life in CHX time course (Figure 63H). As a negative control, mutation of non-ubiquitin-associated Sestrin-2 lysine (K452R) did not confer protection from degradation (Figure 63I).
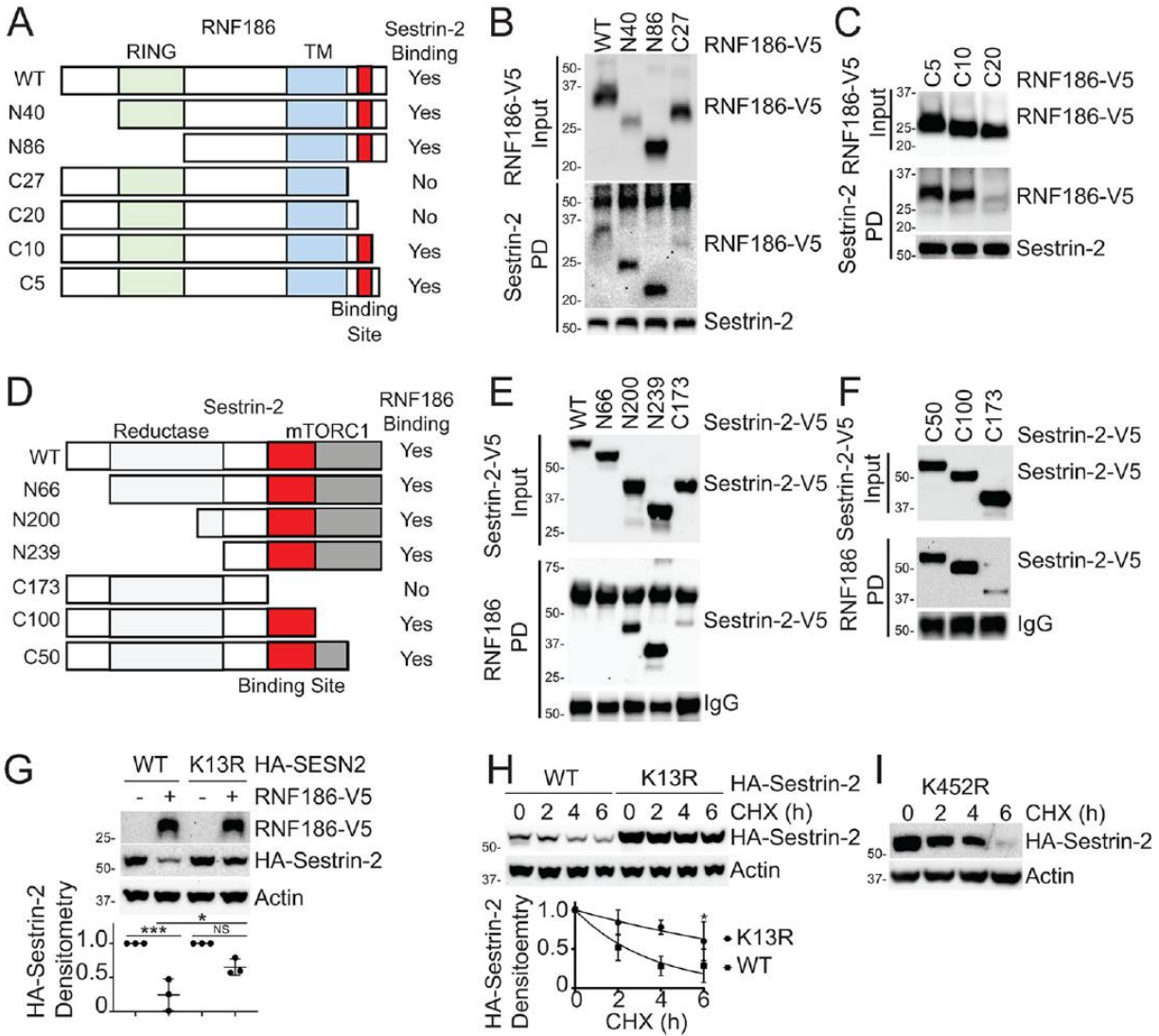
Figure 63 RNF186 and Sestrin-2 bind through discrete C-terminal Motifs

(A) Schematic of RNF186 deletion mutant strategy and individual binding status with Sestrin-2. (B-C) Binding assay of in vitro synthesized RNF186 deletion mutants and Sestrin-2. (D) Sestrin-2 deletion mutant strategy and binding status with RNF186. (E-F) Immunoblot analysis of Sestrin-2 mutant binding with RNF186 protein. (G) Wild-type or K13R mutant Sestrin-2 was expressed in Beas-2b cells without or with expression of RNF186 prior to blotting. Data and means ± SD of 3 independent experiments. (H) Immunoblot analysis of Sestrin-2 wild-type or K13R expression prior to CHX time course. Data and means ± SD of 3 independent experiments. (I) Immunoblot analysis of Sestrin-2 K452R mutant in CHX assay. NS, P > 0.05; *P ＜0.05; ***P < 0.001 by ANOVA, with Tukey's test for multiple comparisons (G) or by F-test comparisons of nonlinear regression relative to control (H).

4.1.6 RNF186 affects Sestrin-2 regulation of mTORC1

We next sought to explore the effect of the RNF186-Sestrin-2 axis on downstream mTORC1 signaling. As a leucine sensor, Sestrin-2 acts to inhibit mTORC1 activity by interacting with GATOR2, and preventing its downstream regulation of the Rag GTPases (415). The inhibitory effect of Sestrin-2 is most potent during leucine starvation. *SESN2* silencing in Beas-2B cells led to increased mTORC1 activity as measured by phosphorylation of P70S6K (Thr389) Figure 64A-C). This effect persists even during cellular leucine starvation. Silencing of *RNF186* led to increased SESN2 protein relative to control (Figure 64D, E). Of note, *RNF186* knockdown led to decreased mTORC1 activity relative to control (Figure 64).
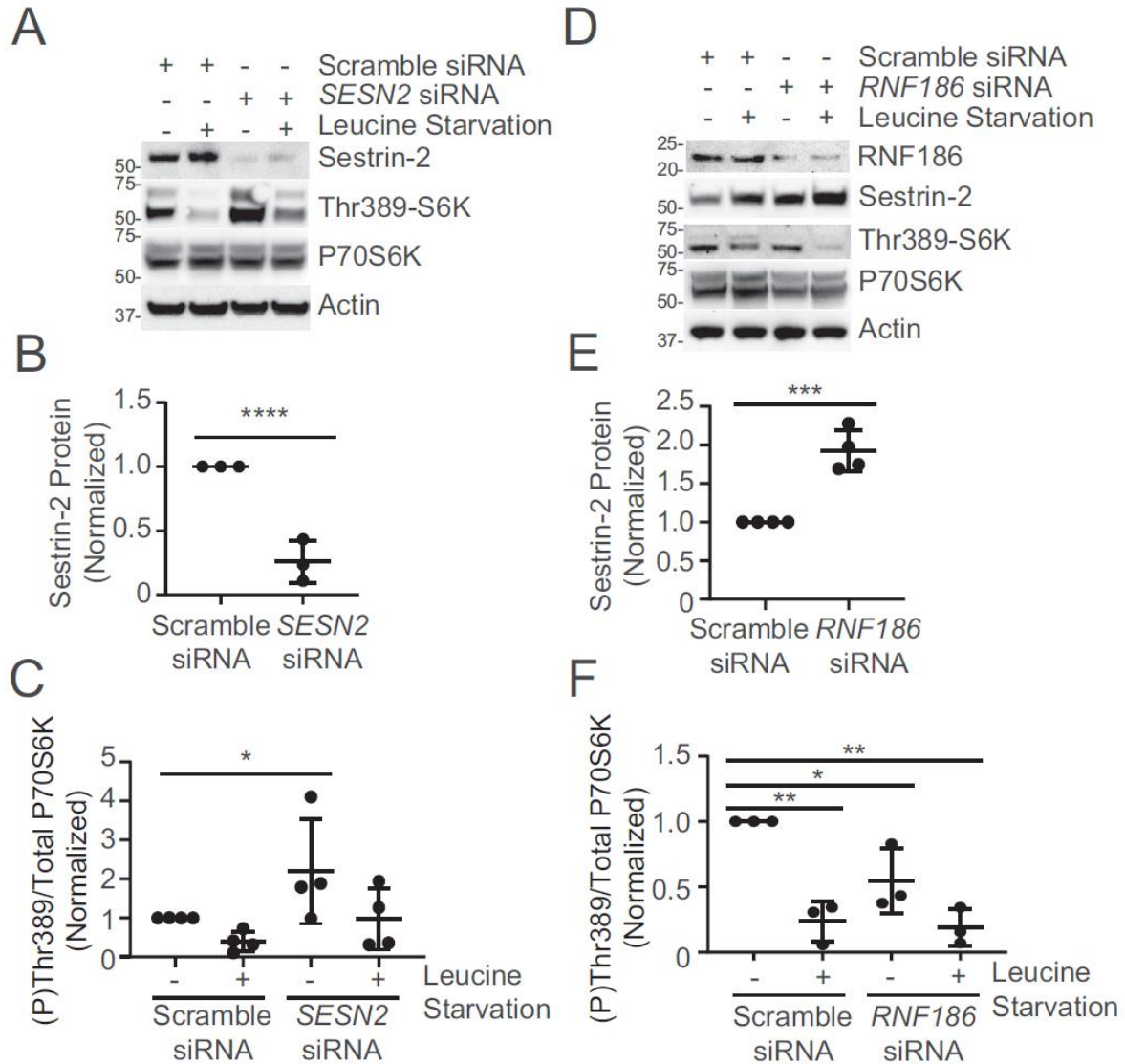
Figure 64 RNF186 knockdown impairs leucine-dependent nutrient sensing

(A) Immunoblot analysis of mTORC1 activity and autophagic flux from Beas-2b cells treated with control or SESN2 siRNA prior to leucine starvation. Protein densitometry of (B) Sestrin-2 and (C) ratio of phosphorylated (Thr389) to total P70S6K was quantified. Data and means ± SD of 3-4 independent experiments. (D) Immunoblot analysis of mTORC1 activity and autophagic flux from Beas-2b cells treated with control or RNF186 siRNA prior to leucine starvation. Protein densitometry of (E) Sestrin-2 and (F) ratio of phosphorylated (Thr389) to total P70S6K was quantified. Data and means ± SD of 3-4 independent experiments. *P<0.05, **P < 0.01, ****P < 0.0001 by two-sided unpaired t-test (B, E) or by one-way ANOVA, with Tukey's test for multiple comparisons (C, F).

As a complementary assay, we utilized LC3-GFP-RFP reporter cells to measure the effect

of RNF186 and SESN2 interaction. This autophagic tool exploited the instability of GFP at low

pH to create a reporter sensitive to lysosomal maturation. The LC3 construct also has constitutively

cleaved RFP fusion protein is expressed in cells, serving as a loading control. The ratio of GFP/RFP is a surrogate for autophagic flux in a cell (431). As autophagy is an endpoint of mTORC1 regulation, we utilized this tool as a readout for mTORC1 activity. We knocked down *SESN2* and *RNF186* in Beas-2B cells that stability expresses LC3-GFP-RFP reporter prior to leucine starvation, fixation and automated microscopy. We observed control siRNA during leucine starvation resulted in 70% decrease in GFP/RFP ratio relative to baseline, consistent with previous studies into the effect of amino acid starvation on autophagic flux (Figure 65A, B) (431). *SESN2* knockdown resulted in a significantly higher GFP/RFP ratio, suggesting less autophagic flux (Figure 65A, C). Interestingly, *RNF186* silencing decreased the GFP/RFP further, suggestive of increased autophagic flux (Figure 65A, D). These assays suggest the RNF186/Sestrin-2 axis plays a role in regulating cellular nutrient sensing and metabolic flux.
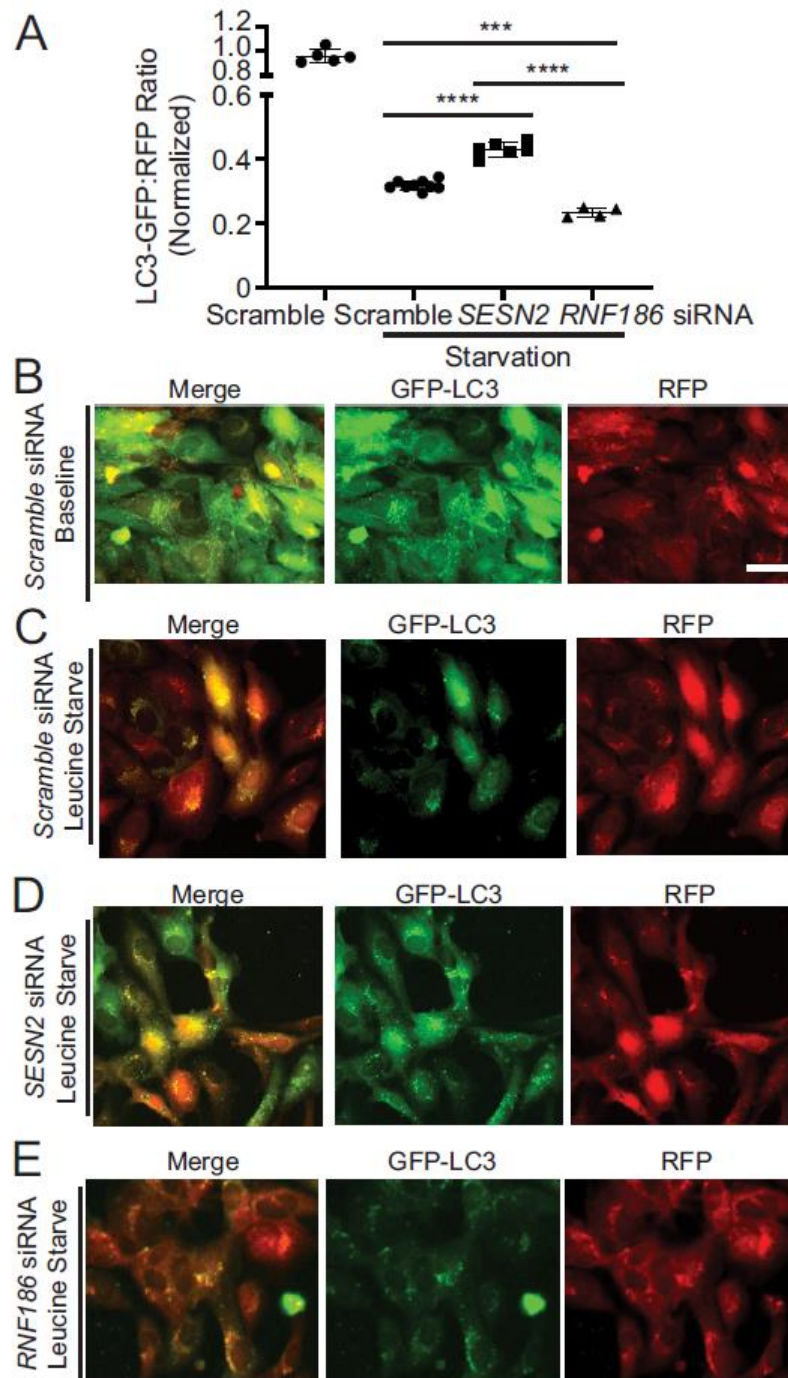
Figure 65 Sestrin-2 and RNF186 depletion affect starvation-mediated autophagic flux

(A) Quantification of LC3B GFP to RFP ratio in cells starved of leucine. Data are normalized to Control siRNA baseline ratio. Data and means ± SD (n = 4-8). (B) Representative image of LC3B-GFP-RFP reporter cells transfected with scramble siRNA at baseline conditions. (C-E) Representative images of LC3B-GFP-RFP reporter cells starved of leucine and transfected with siRNA targeting (C) scramble, (D) SESN2, or (E) RNF186. ***$P < 0.001$; ****$P < 0.0001$ by ANOVA, with Tukey's test for multiple comparisons (A). Scale bar indicates 50μm.

4.1.7 Discussion

E3 ligases are increasingly appreciated regulators of nutrient sensing and mTORC1 activity (423). A recent study has shown the GATOR1 subunit DEPDC5 to be potently regulated by the Cullin-3 substrate-receptor KLHL22 (81). Our data show that RNF186 plays a similar role in targeting Sestrin-2 for ubiquitination and degradation, which in turn affects mTORC1 activity and downstream autophagic flux. Dysfunction of nutrient sensing is recognized as a hallmark of aging; better understanding of the regulation of nutrient sensing will afford new potential targets for inhibition and intervention (68).

RNF186 has been characterized as RING (Really new interesting gene)-type ubiquitin E3 ligase (432). RING E3 ligases function through Zinc-finger domains that are critical for engaging the E2 ubiquitin conjugating enzyme (254). We observed that mutation of a critical residue within the RING-domain impaired RNF186 ability to degrade Sestrin-2 (Figure 62E), suggesting that the ubiquitin E3 ligase activity of RNF186 drives its effect on Sestrin-2 (428). We observed that RNF186 and Sestrin-2 binding was lost upon the deletion of a 72-residue region between amino acid 308 and 380 of the Sestrin-2 C-terminus (Figure 63F). Interestingly, this same region has been described as key for regulating mTORC1 activity, and for binding leucine (residues 374-377) (416, 433). Future studies are needed to investigate the distinct mechanism of RNF186/Sestrin-2 interaction, and if leucine plays a role.

K48 poly-ubiquitination is the canonical signal for proteasomal degradation, and has been reported as a predominant linkage type among cellular poly-ubiquitin chains (434). Through UbiCREST assay, we observed Sestrin-2 poly-ubiquitination with K48-linkages, consistent with previous studies in neuronal cells (435). We also observed that Sestrin-2 contains poly-ubiquitin chains with K63 linkages. This linkage type has been implicated in several processes, notably

cellular trafficking (436). It remains unclear if Sestrin-2 ubiquitination plays a non-degradation role in its cellular localization.

mTORC1 plays an important role in the lung epithelia and disease. Research has suggested mTORC1 activity plays a pathogenic role in epithelia during acute lung injury (437). Similarly, mTOR-driven signaling affects the pathophysiology of pulmonary fibrosis in fibroblasts (438). One study suggested Sestrin-2 inhibition to be protective in a mouse model of COPD (439). More research is needed to see if RNF186 and Sestrin-2 play a role in these lung diseases.

In conclusion, we describe a new mechanism of ubiquitin E3-ligase mediated control of nutrient sensing through the interaction of RNF186 with Sestrin-2.

4.1.8 Materials and Methods

4.1.8.1 Materials

BEAS2-B (Cat# CRL-9609, RRID:CVCL_0168) were from ATCC. BioRad (Cat# 170-6515 RRID:AB_11125142), Goat anti-Mouse HRP (Cat# 170-6516 RRID:AB_11125547), Rabbit anti-Goat HRP (Cat# 172-1034 RRID:AB_11125144 were from BioRad. UbiCREST assay kit was from BostonBiochem. Mouse Monoclonal anti-HA-Tag (clone 6E2) (Cat# 2367S RRID:AB_10691311), Rabbit anti-Phospho-p70 S6 Kinase (Thr389) (108D2) (Cat# 9234, RRID:AB_2269803), Rabbit anti-p70 S6 Kinase (49D7) (Cat# 2708, RRID:AB_390722), Rabbit anti-Sestrin-2 (D1B6) (Cat# 8487, RRID:AB_11178663), Mouse anti-Ubiquitin (P4D1) (Cat# 3936, RRID:AB_331292), and Rabbit anti-LC3B (D11) XP (Cat# 3868, RRID:AB_2137707) were from Cell Signaling Technology. Cycloheximide (Cat# BML- GR310) was from Ubiquitinylation kit (Cat# BML-UW9920-0001) were from Enzo. Sequencing was conducted at Genewiz. DNA primers and dsiRNA were from IDT. pcDNA3.1D-V5-HIS-TOPO (Cat#

K490001), was from Invitrogen. TnT T7 Quick Coupled Transcription/Translation (Cat# L1170) was from Promega. Leupeptin (Cat# L2884) and Mouse Monoclonal anti-beta-Actin (clone AC-15) (Cat# A5441 RRID:AB_476744) were from Sigma-Aldrich. Mouse Monoclonal anti-V5 Tag (Cat# R960-25 RRID:AB_2556564), Protein A/G Magnetic Beads (Cat# 88802), pcDNA3.1 Directional TOPO Expression Kit (Cat# K490001), were from Thermo Fisher Scientific. pRK5-HA-Ubiquitin-WT (Cat#17608, RRID:Addgene17608) Was a gift from Ted Dawson (440). Anti-RNF186 antibody (Cat# ab86547, RRID:AB_2180433) was from Abcam. WesternBright Sirius HRP substrate (Cat# K-12043) was from Advansta. QuikChange II XL Site-Directed Mutagenesis Kit (Cat# 200521) was from Agilent Technologies. pLenti CMV GFP Puro (658-5) was a gift from Eric Campeau & Paul Kaufman (Addgene plasmid # 17448 ; http://n2t.net/addgene:17448; RRID:Addgene_17448). pMRX-IP-GFP-LC3-RFP was a gift from Noboru Mizushima (Addgene plasmid # 84573; http://n2t.net/addgene:84573; RRID:Addgene_84573)(431). pRK5-HA-Sestrin2 was a gift from David Sabatini (Addgene plasmid # 72593 ; http://n2t.net/addgene:72593 ; RRID:Addgene_72593)(441).

4.1.8.2 Cell Culture

Beas-2b cells were from ATCC and cultured in HITES media supplemented with 10% FBS. Cells were treated with cycloheximide (100μg/mL), MG132 (20μM), leupeptin (20μM), and MLN7243 (10μM) for indicated times. Cells were transfected with Nucleofector 2b (Amaxa) or XtremeGene siRNA reagent (Roche). Cells were starved by two washes, then incubation with EBSS supplemented with amino acids minus leucine (Gibco).

4.1.8.3 UbiCREST Assay

Ubiquitination Linkage-type analysis was measured by UbiCREST assay(427) (BostonBiochem). Briefly, Sestrin-2 was expressed in Beas-2b, treated with MG132 (20μM, 4 hours), and lysed prior to HIS-pull down with HisPur Resin (ThermoFisher). Following UbiCREST digestion, resin eluate was assayed by immunoblotting.

4.1.8.4 Ubiquitination siRNA Screen

Stably expressing Beas-2b Sestrin-2-GFP cells in 384-well glass-bottom plates were transfected with MISSION esiRNA targeting ubiquitination proteins (E1, E2, E3 ligases etc) (Sigma-Aldrich) using XtremeGene siRNA transfection reagent (Roche). Knockdown proceeded for 72 hours prior to washing, fixation, and fluorescent imaging using BioTek Cytation5.

4.1.8.5 LC3 Fluorescent Reporter Assay

LC3 reporter cells were transfected with dsiRNA against scramble, *SESN2*, or *RNF186* and seeded to 96-well glass-bottle plates for 60 hours before starvation in EBSS + amino acids minus leucine for 18 hours. Cells were fixed in 4% paraformaldehyde and imaged using ImageXpress Micro XLS. Fluorescence was quantified and GFP:RFP ratio was calculated with CellProfiler (231).

4.1.8.6 In vitro protein binding assays

Protein binding assays were conducted as previously described (261). Briefly, Sestrin-2 or RNF186 protein was immunoprecipitated from 1mg of Beas-2b cell lysate using 1:100 antibody dilution. Protein was precipitated in IP buffer (50 mM Tris HCl pH 7.6, 150 mM NaCl, 0.25 % v/v Triton-X-100) for four hours at +4C, then coupled to protein A/G agarose resin for an additional

two hours. Binding mutants were in vitro synthesized using TnT expression kits and allowed to bind overnight. Resin was washed and protein was eluted in 1x Laemmli buffer at 88°C for five minutes prior to immunoblotting analysis.

4.1.8.7 Statistics

All statistical tests were calculating using Graphpad Prism 8. $P < 0.05$ was used to indicate significance. Densitometry was calculated using ImageJ (NIH).

4.1.9 Acknowledgements

4.1.10 Conflict of interest

The authors acknowledge no conflicts of interest with the contents of this article

5.0 Concluding Remarks

5.1 Ubiquitin E3 Ligase Mediated Lung Disease and Public Health in an Aging World

These data show that Ubiquitin E3 ligases play intricate and important roles in lung disease and progression, including fibrosis, inflammation, and nutrient sensing disorder. These new mechanistic understandings are needed more than ever as humanity enters a more aged world. Public health initiatives, medical advances, and numerous other factors have led to the phenomena of an increasingly aged human population. This is pointedly shown in that the proportion of humans over 65 now outnumbers those under 5; it is estimated this inflection point is occurring in this decade (442). The public health consequences of an aging population are numerous, but lung diseases are a key effect. Several lung diseases are disproportionately represented among the elderly. Inflammatory lung diseases show sharp increases in incidence among older patients; Acute Lung Injury incidence peaks among those aged 75-84 (268). Further, fibrotic lung disease afflict the elderly; patients aged 60 to 70 make up the largest percentage of those presenting with Idiopathic pulmonary fibrosis (409, 443). As a key hallmark of aging, nutrient sensing dysregulation will continue to be an underlying biological mechanism for aging-related diseases (68). Studies into the ubiquitin-proteasome based control of key regulator proteins in lung disease, including the research in this thesis, not only expand understanding of the networks of ubiquitin-based control, but provide new targets for future therapeutic development. These studies show that targeting Ubiquitin E3 ligases has experimental efficacy, which may translate to therapeutic efficacy in future studies.

5.2 Future Directions for E3 ligase-based intervention

As ubiquitin E3 ligases are increasingly recognized as avenues for therapeutic intervention, new technologies are under development to target their activity. Researchers have utilized established E3 ligase-binding chemicals to pharmacologically develop *proteolysis targeting chimeras* or PROTAC chemicals (444, 445). These small molecules are comprised of an E3 ligase ligand connected to a substrate-specific ligand by a linker region in the attempt to bring E3 ligases near substrates to facilitate substrate degradation (446). PROTAC utilizes a number of E3 ligases for targeted degradation; the two primary E3 ligases are the VHL E3 ligase, and the CRL4 subunit Cereblon which binds to thalidomide-based chemicals (447, 448). These E3 ligase chemicals form the basis of a combinatorial chemical which can be exchanged for whatever ligand binds the desired substrate. Research has shown PROTAC is extremely potent in targeted degradation of substrate proteins such as STAT3 and Bromodomains, which potential application to inflammation, cancer and other diseases (449-451). Further, recent research has shown efficacy in animal models, which will further aid in the evaluation of PROTAC as a potential therapeutic strategy (452). Currently, clinical studies are underway to determine the efficacy of PROTAC for use in human patients with cancer (NCT03888612).

5.3 Conclusion

These studies demonstrate that Ubiquitin E3 ligases are biologically relevant in lung diseases through their targeted ligase activity against critical cell signaling substrates, leading to substrate degradation. We explored E3 ligase-mediated control of fibrotic signaling in interstitial

lung disease, including idiopathic pulmonary fibrosis and systemic sclerosis (Aim 1). We documented the biologic effect of E3 ligases in various stages and aspects of lung inflammation through epithelial cell recognition of pathogen signals, transduction of inflammatory signaling, modulation of signaling by exogenous host cytokines, and the regulation of motility signaling (Aim 2). Finally, we explored mechanisms related to aging itself through nutrient sensing in lung epithelial cells and mechanisms of control by E3 ligases (Aim 3). Collectively these studies support a model in which ubiquitin E3 ligases are central to the pathogenesis and perpetuation of disease in the lung (Figure 66).
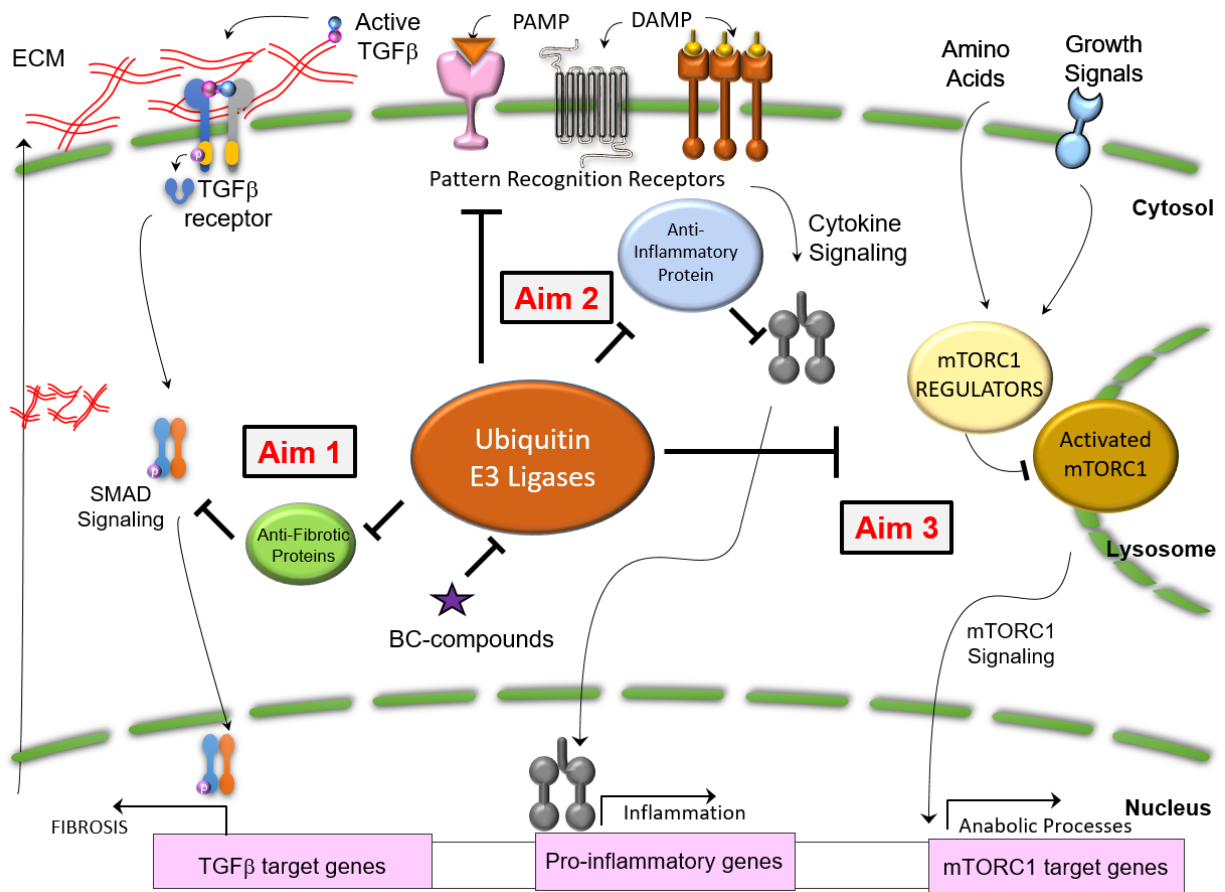
Figure 66 Ubiquitin E3 ligases at the center of lung disease signaling

Schematic model of dissertation studies. Ubiquitin E3 ligases play a central role in regulation of numerous pathologic signaling mechanisms in the lung, including fibrotic signaling in TGF-β-driven interstitial lung disease (Aim 1), inflammatory signaling related to bacterial infection and lung injury (Aim 2), and in controlling nutrient

sensing apparatus for metabolic control (Aim 3). Ubiquitin E3 ligases also present an opportunity for therapuetic internvetion through small molecule targeting to inhibit E3 ligases.

Bibliography

1. Coles E, and Mensah GA. The Burden of Heart, Lung, and Blood Diseases in the United States, 1990 to 2016: Perspectives from the National Heart, Lung, and Blood Institute. *Glob Heart.* 2017;12(4):349-58.
2. Societies FoIR. The Global Impact of Respiratory Disease – Second Edition. *Sheffield, European Respiratory Society, 2017.* 2017.
3. Mizgerd JP. Acute lower respiratory tract infection. *N Engl J Med.* 2008;358(7):716-27.
4. Carroll KC, and Adams LL. Lower Respiratory Tract Infections. *Microbiol Spectr.* 2016;4(4).
5. Matthay MA, Zemans RL, Zimmerman GA, Arabi YM, Beitler JR, Mercat A, et al. Acute respiratory distress syndrome. *Nat Rev Dis Primers.* 2019;5(1):18.
6. Antoniou KM, Margaritopoulos GA, Tomassetti S, Bonella F, Costabel U, and Poletti V. Interstitial lung disease. *Eur Respir Rev.* 2014;23(131):40-54.
7. Weiskirchen R, Weiskirchen S, and Tacke F. Organ and tissue fibrosis: Molecular signals, cellular mechanisms and translational implications. *Mol Aspects Med.* 2019;65:2-15.
8. Belloli EA, Martinez FJ, and Flaherty KR. Update in Interstitial Lung Disease 2014. *Am J Respir Crit Care Med.* 2015;192(5):538-43.
9. Wells AU, and Denton CP. Interstitial lung disease in connective tissue disease--mechanisms and management. *Nat Rev Rheumatol.* 2014;10(12):728-39.
10. Richeldi L, Collard HR, and Jones MG. Idiopathic pulmonary fibrosis. *Lancet.* 2017;389(10082):1941-52.
11. Lear T, and Chen BB. Therapeutic targets in fibrotic pathways. *Cytokine.* 2016;88:193-5.
12. Wolters PJ, Collard HR, and Jones KD. Pathogenesis of idiopathic pulmonary fibrosis. *Annual review of pathology.* 2014;9:157-79.
13. Armanios M. Telomerase and idiopathic pulmonary fibrosis. *Mutation research.* 2012;730(1-2):52-8.
14. Peljto AL, Zhang Y, Fingerlin TE, Ma SF, Garcia JG, Richards TJ, et al. Association between the MUC5B promoter polymorphism and survival in patients with idiopathic pulmonary fibrosis. *Jama.* 2013;309(21):2232-9.
15. Kurundkar AR, Kurundkar D, Rangarajan S, Locy ML, Zhou Y, Liu RM, et al. The matricellular protein CCN1 enhances TGF-beta1/SMAD3-dependent profibrotic signaling in fibroblasts and contributes to fibrogenic responses to lung injury. *FASEB journal : official publication of the Federation of American Societies for Experimental Biology.* 2016.
16. Sheppard D. Epithelial-mesenchymal interactions in fibrosis and repair. Transforming growth factor-beta activation by epithelial cells and fibroblasts. *Annals of the American Thoracic Society.* 2015;12 Suppl 1:S21-3.
17. Luzina IG, Todd NW, Sundararajan S, and Atamas SP. The cytokines of pulmonary fibrosis: Much learned, much more to learn. *Cytokine.* 2015;74(1):88-100.
18. Reed NI, Jo H, Chen C, Tsujino K, Arnold TD, DeGrado WF, et al. The alphavbeta1 integrin plays a critical in vivo role in tissue fibrosis. *Science translational medicine.* 2015;7(288):288ra79.

19. Shi Y, and Massague J. Mechanisms of TGF-beta signaling from cell membrane to the nucleus. *Cell.* 2003;113(6):685-700.

20. Macias MJ, Martin-Malpartida P, and Massague J. Structural determinants of Smad function in TGF-beta signaling. *Trends in biochemical sciences.* 2015;40(6):296-308.

21. Gao S, Alarcon C, Sapkota G, Rahman S, Chen PY, Goerner N, et al. Ubiquitin ligase Nedd4L targets activated Smad2/3 to limit TGF-beta signaling. *Molecular cell.* 2009;36(3):457-68.

22. Imoto S, Ohbayashi N, Ikeda O, Kamitani S, Muromoto R, Sekine Y, et al. Sumoylation of Smad3 stimulates its nuclear export during PIASy-mediated suppression of TGF-beta signaling. *Biochemical and biophysical research communications.* 2008;370(2):359-65.

23. Imoto S, Sugiyama K, Muromoto R, Sato N, Yamamoto T, and Matsuda T. Regulation of transforming growth factor-beta signaling by protein inhibitor of activated STAT, PIASy through Smad3. *The Journal of biological chemistry.* 2003;278(36):34253-8.

24. Network TIPFCR. Prednisone, Azathioprine, and N-Acetylcysteine for Pulmonary Fibrosis. *New England Journal of Medicine.* 2012;366(21):1968-77.

25. Richeldi L, du Bois RM, Raghu G, Azuma A, Brown KK, Costabel U, et al. Efficacy and Safety of Nintedanib in Idiopathic Pulmonary Fibrosis. *New England Journal of Medicine.* 2014;370(22):2071-82.

26. King TE, Bradford WZ, Castro-Bernardini S, Fagan EA, Glaspole I, Glassberg MK, et al. A Phase 3 Trial of Pirfenidone in Patients with Idiopathic Pulmonary Fibrosis. *New England Journal of Medicine.* 2014;370(22):2083-92.

27. Selvaggio AS, and Noble PW. Pirfenidone Initiates a New Era in the Treatment of Idiopathic Pulmonary Fibrosis. *Annual review of medicine.* 2016;67:487-95.

28. Rangarajan S, Locy ML, Luckhardt TR, and Thannickal VJ. Targeted Therapy for Idiopathic Pulmonary Fibrosis: Where To Now? *Drugs.* 2016;76(3):291-300.

29. Weitnauer M, Mijosek V, and Dalpke AH. Control of local immunity by airway epithelial cells. *Mucosal Immunol.* 2016;9(2):287-98.

30. Park BS, and Lee JO. Recognition of lipopolysaccharide pattern by TLR4 complexes. *Exp Mol Med.* 2013;45:e66.

31. Amarante-Mendes GP, Adjemian S, Branco LM, Zanetti LC, Weinlich R, and Bortoluci KR. Pattern Recognition Receptors and the Host Cell Death Molecular Machinery. *Front Immunol.* 2018;9:2379.

32. Kang R, Chen R, Zhang Q, Hou W, Wu S, Cao L, et al. HMGB1 in health and disease. *Mol Aspects Med.* 2014;40:1-116.

33. Leiva-Juarez MM, Kolls JK, and Evans SE. Lung epithelial cells: therapeutically inducible effectors of antimicrobial defense. *Mucosal Immunol.* 2018;11(1):21-34.

34. Manicone AM. Role of the pulmonary epithelium and inflammatory signals in acute lung injury. *Expert Rev Clin Immunol.* 2009;5(1):63-75.

35. Pouwels SD, Hesse L, Faiz A, Lubbers J, Bodha PK, Ten Hacken NH, et al. Susceptibility for cigarette smoke-induced DAMP release and DAMP-induced inflammation in COPD. *Am J Physiol Lung Cell Mol Physiol.* 2016;311(5):L881-l92.

36. Pan C, Wang J, Liu W, Liu L, Jing L, Yang Y, et al. Low tidal volume protects pulmonary vasomotor function from "second-hit" injury in acute lung injury rats. *Respir Res.* 2012;13:77.

37. Aoshiba K, Tsuji T, Yamaguchi K, Itoh M, and Nakamura H. The danger signal plus DNA damage two-hit hypothesis for chronic inflammation in COPD. *European Respiratory Journal.* 2013;42(6):1689-95.

38. Davies LC, Jenkins SJ, Allen JE, and Taylor PR. Tissue-resident macrophages. *Nat Immunol.* 2013;14(10):986-95.

39. Levy BD, and Serhan CN. Resolution of Acute Inflammation in the Lung. *Annu Rev Physiol.* 2014;76(1):467-92.

40. Ware LB, and Matthay MA. The Acute Respiratory Distress Syndrome. *New England Journal of Medicine.* 2000;342(18):1334-49.

41. Zemans RL, Colgan SP, and Downey GP. Transepithelial migration of neutrophils: mechanisms and implications for acute lung injury. *Am J Respir Cell Mol Biol.* 2009;40(5):519-35.

42. Cardinal-Fernandez P, Lorente JA, Ballen-Barragan A, and Matute-Bello G. Acute Respiratory Distress Syndrome and Diffuse Alveolar Damage. New Insights on a Complex Relationship. *Annals of the American Thoracic Society.* 2017;14(6):844-50.

43. Matthay MA, Ware LB, and Zimmerman GA. The acute respiratory distress syndrome. *J Clin Invest.* 2012;122(8):2731-40.

44. Moldoveanu B, Otmishi P, Jani P, Walker J, Sarmiento X, Guardiola J, et al. Inflammatory mechanisms in the lung. *J Inflamm Res.* 2009;2:1-11.

45. Rubenfeld GD, Caldwell E, Peabody E, Weaver J, Martin DP, Neff M, et al. Incidence and outcomes of acute lung injury. *The New England journal of medicine.* 2005;353(16):1685-93.

46. Ware LB, and Matthay MA. The acute respiratory distress syndrome. *The New England journal of medicine.* 2000;342(18):1334-49.

47. Rahman A, and Fazal F. Blocking NF-kappaB: an inflammatory issue. *Proc Am Thorac Soc.* 2011;8(6):497-503.

48. Zimmerman GA, Albertine KH, Carveth HJ, Gill EA, Grissom CK, Hoidal JR, et al. Endothelial activation in ARDS. *Chest.* 1999;116(1 Suppl):18S-24S.

49. Schwartz MD, Moore EE, Moore FA, Shenkar R, Moine P, Haenel JB, et al. Nuclear factor-kappa B is activated in alveolar macrophages from patients with acute respiratory distress syndrome. *Critical Care Medicine.* 1996;24(8):1285-92.

50. Blackwell TS, and Christman JW. The Role of Nuclear Factor- κ B in Cytokine Gene Regulation. *Am J Respir Cell Mol Biol.* 1997;17(1):3-9.

51. Lawrence T. The Nuclear Factor NF-κB Pathway in Inflammation. *Cold Spring Harb Perspect Biol.* 2009;1(6):a001651.

52. Orfanos SE, Mavrommati I, Korovesi I, and Roussos C. In: Hedenstierna G, Mancebo J, Brochard L, and Pinsky MR eds. *Applied physiology in intensive care medicine.* Berlin, Heidelberg: Springer Berlin Heidelberg; 2009:215-27.

53. Schuliga M. NF-kappaB Signaling in Chronic Inflammatory Airway Disease. *Biomolecules.* 2015;5(3):1266-83.

54. Hosokawa S, Haraguchi G, Sasaki A, Arai H, Muto S, Itai A, et al. Pathophysiological roles of nuclear factor kappaB (NF-kB) in pulmonary arterial hypertension: effects of synthetic selective NF-kB inhibitor IMD-0354. *Cardiovascular research.* 2013;99(1):35-43.

55. Yoshimura A, Ito M, Chikuma S, Akanuma T, and Nakatsukasa H. Negative Regulation of Cytokine Signaling in Immunity. *Cold Spring Harb Perspect Biol.* 2018;10(7).

56. Liongue C, Sertori R, and Ward AC. Evolution of Cytokine Receptor Signaling. *J Immunol.* 2016;197(1):11-8.

57. Krebs DL, and Hilton DJ. SOCS proteins: negative regulators of cytokine signaling. *Stem Cells.* 2001;19(5):378-87.

58. Chen BB, Coon TA, Glasser JR, and Mallampalli RK. Calmodulin antagonizes a calcium-activated SCF ubiquitin E3 ligase subunit, FBXL2, to regulate surfactant homeostasis. *Mol Cell Biol.* 2011;31(9):1905-20.

59. Zhao J, Wei J, Mialki RK, Mallampalli DF, Chen BB, Coon T, et al. F-box protein FBXL19-mediated ubiquitination and degradation of the receptor for IL-33 limits pulmonary inflammation. *Nat Immunol.* 2012;13(7):651-8.

60. Chen BB, Coon TA, Glasser JR, McVerry BJ, Zhao J, Zhao Y, et al. A combinatorial F box protein directed pathway controls TRAF adaptor stability to regulate inflammation. *Nat Immunol.* 2013;14(5):470-9.

61. Chen BB, Glasser JR, Coon TA, and Mallampalli RK. Skp-cullin-F box E3 ligase component FBXL2 ubiquitinates Aurora B to inhibit tumorigenesis. *Cell Death Dis.* 2013;4:e759.

62. Mallampalli RK, Coon TA, Glasser JR, Wang C, Dunn SR, Weathington NM, et al. Targeting F box protein Fbxo3 to control cytokine-driven inflammation. *J Immunol.* 2013;191(10):5247-55.

63. Ben-Sahra I, and Manning BD. mTORC1 signaling and the metabolic control of cell growth. *Curr Opin Cell Biol.* 2017;45:72-82.

64. Lee G, Zheng Y, Cho S, Jang C, England C, Dempsey JM, et al. Post-transcriptional Regulation of De Novo Lipogenesis by mTORC1-S6K1-SRPK2 Signaling. *Cell.* 2017;171(7):1545-58.e18.

65. Zhang Y, Nicholatos J, Dreier JR, Ricoult SJH, Widenmaier SB, Hotamisligil GS, et al. Coordinated regulation of protein synthesis and degradation by mTORC1. *Nature.* 2014;513(7518):440-3.

66. Blenis J. TOR, the gateway to cellular metabolism, cell growth, and disease. *Cell.* 2017;171(1):10-3.

67. Sabatini DM. Twenty-five years of mTOR: Uncovering the link from nutrients to growth. *Proc Natl Acad Sci USA.* 2017;114(45):11818-25.

68. López-Otín C, Blasco MA, Partridge L, Serrano M, and Kroemer G. The hallmarks of aging. *Cell.* 2013;153(6):1194-217.

69. Rabanal-Ruiz Y, Otten EG, and Korolchuk VI. mTORC1 as the main gateway to autophagy. *Essays Biochem.* 2017;61(6):565-84.

70. Saxton RA, and Sabatini DM. mTOR Signaling in Growth, Metabolism, and Disease. *Cell.* 2017;168(6):960-76.

71. Johnson SC, Rabinovitch PS, and Kaeberlein M. mTOR is a key modulator of ageing and age-related disease. *Nature.* 2013;493(7432):338-45.

72. Lamming DW. Inhibition of the Mechanistic Target of Rapamycin (mTOR)-Rapamycin and Beyond. *Cold Spring Harb Perspect Med.* 2016;6(5).

73. Li J, Kim SG, and Blenis J. Rapamycin: one drug, many effects. *Cell Metab.* 2014;19(3):373-9.

74. Stoica L, Zhu PJ, Huang W, Zhou H, Kozma SC, and Costa-Mattioli M. Selective pharmacogenetic inhibition of mammalian target of Rapamycin complex I (mTORC1)

blocks long-term synaptic plasticity and memory storage. *Proc Natl Acad Sci USA*. 2011;108(9):3791-6.

75. Benjamin D, Colombi M, Moroni C, and Hall MN. Rapamycin passes the torch: a new generation of mTOR inhibitors. *Nat Rev Drug Discov.* 2011;10(11):868-80.

76. Finkel T. The metabolic regulation of aging. *Nat Med.* 2015;21(12):1416-23.

77. Wolfson RL, Chantranupong L, Saxton RA, Shen K, Scaria SM, Cantor JR, et al. Sestrin2 is a leucine sensor for the mTORC1 pathway. *Science.* 2016;351(6268):43-8.

78. Shimobayashi M, and Hall MN. Multiple amino acid sensing inputs to mTORC1. *Cell Res.* 2016;26(1):7-20.

79. Wolfson RL, and Sabatini DM. The Dawn of the Age of Amino Acid Sensors for the mTORC1 Pathway. *Cell Metab.* 2017;26(2):301-9.

80. Ishida S, Picard F, Rudolf G, No├─ E, Achaz G, Thomas P, et al. Mutations of DEPDC5 cause autosomal dominant focal epilepsies. *Nat Genet.* 2013;45(5):552-5.

81. Chen J, Ou Y, Yang Y, Li W, Xu Y, Xie Y, et al. KLHL22 activates amino-acid-dependent mTORC1 signalling to promote tumorigenesis and ageing. *Nature.* 2018;557(7706):585-9.

82. Pajusalu S, Reimand T, and ├òunap K. Novel homozygous mutation in KPTN gene causing a familial intellectual disability-macrocephaly syndrome. *Am J Med Genet A.* 2015;167A(8):1913-5.

83. Baple EL, Maroofian R, Chioza BA, Izadi M, Cross HE, Al-Turki S, et al. Mutations in KPTN cause macrocephaly, neurodevelopmental delay, and seizures. *Am J Hum Genet.* 2014;94(1):87-94.

84. Bar-Peled L, Chantranupong L, Cherniack AD, Chen WW, Ottina KA, Grabiner BC, et al. A Tumor suppressor complex with GAP activity for the Rag GTPases that signal amino acid sufficiency to mTORC1. *Science.* 2013;340(6136):1100-6.

85. Eden E, Geva-Zatorsky N, Issaeva I, Cohen A, Dekel E, Danon T, et al. Proteome half-life dynamics in living human cells. *Science.* 2011;331(6018):764-8.

86. Toyama BH, and Hetzer MW. Protein homeostasis: live long, won't prosper. *Nat Rev Mol Cell Biol.* 2013;14(1):55-61.

87. Zhou P. In: Dickson RC, and Mendenhall MD eds. *Signal Transduction Protocols*. Totowa, NJ: Humana Press; 2004:67-77.

88. Martin-Perez M, and Villen J. Determinants and Regulation of Protein Turnover in Yeast. *Cell Syst.* 2017;5(3):283-94.e5.

89. Alber AB, Paquet ER, Biserni M, Naef F, and Suter DM. Single Live Cell Monitoring of Protein Turnover Reveals Intercellular Variability and Cell-Cycle Dependence of Degradation Rates. *Molecular cell.* 2018;71(6):1079-91.e9.

90. Jager S, Kim DY, Hultquist JF, Shindo K, LaRue RS, Kwon E, et al. Vif hijacks CBF-beta to degrade APOBEC3G and promote HIV-1 infection. *Nature.* 2011;481(7381):371-5.

91. Mahon C, Krogan NJ, Craik CS, and Pick E. Cullin E3 ligases and their rewiring by viral factors. *Biomolecules.* 2014;4(4):897-930.

92. Chen M, and Gerlier D. Viral hijacking of cellular ubiquitination pathways as an anti-innate immunity strategy. *Viral Immunol.* 2006;19(3):349-62.

93. Gandolfi S, Laubach JP, Hideshima T, Chauhan D, Anderson KC, and Richardson PG. The proteasome and proteasome inhibitors in multiple myeloma. *Cancer Metastasis Rev.* 2017;36(4):561-84.

94.   Hershko A, and Ciechanover A. The ubiquitin system. *Annu Rev Biochem.* 1998;67:425-79.

95.   Swatek KN, and Komander D. Ubiquitin modifications. *Cell Res.* 2016;26(4):399-422.

96.   Spit M, Rieser E, and Walczak H. Linear ubiquitination at a glance. *J Cell Sci.* 2019;132(2):jcs208512.

97.   Komander D, and Rape M. The ubiquitin code. *Annu Rev Biochem.* 2012;81:203-29.

98.   Yau R, and Rape M. The increasing complexity of the ubiquitin code. *Nat Cell Biol.* 2016;18(6):579-86.

99.   Duncan LM, Piper S, Dodd RB, Saville MK, Sanderson CM, Luzio JP, et al. Lysine-63-linked ubiquitination is required for endolysosomal degradation of class I molecules. *EMBO J.* 2006;25(8):1635-45.

100.   Iwai K, and Tokunaga F. Linear polyubiquitination: a new regulator of NF-kappaB activation. *EMBO Rep.* 2009;10(7):706-13.

101.   Grice GL, and Nathan JA. The recognition of ubiquitinated proteins by the proteasome. *Cell Mol Life Sci.* 2016;73(18):3497-506.

102.   Sun H, Mali SM, Singh SK, Meledin R, Brik A, Kwon YT, et al. Diverse fate of ubiquitin chain moieties: The proximal is degraded with the target, and the distal protects the proximal from removal and recycles. *Proceedings of the National Academy of Sciences.* 2019;116(16):7805-12.

103.   Jin J, Li X, Gygi SP, and Harper JW. Dual E1 activation systems for ubiquitin differentially regulate E2 enzyme charging. *Nature.* 2007;447(7148):1135-8.

104.   Hatakeyama S, Yada M, Matsumoto M, Ishida N, and Nakayama KI. U box proteins as a new family of ubiquitin-protein ligases. *J Biol Chem.* 2001;276(35):33111-20.

105.   Skaar JR, Pagan JK, and Pagano M. Mechanisms and function of substrate recruitment by F-box proteins. *Nature reviews Molecular cell biology.* 2013;14(6):369-81.

106.   Dikic I, and Robertson M. Ubiquitin ligases and beyond. *BMC Biology.* 2012;10(1):1-3.

107.   Huibregtse JM, Scheffner M, Beaudenon S, and Howley PM. A family of proteins structurally and functionally related to the E6-AP ubiquitin-protein ligase. *Proceedings of the National Academy of Sciences of the United States of America.* 1995;92(7):2563-7.

108.   Petroski MD, and Deshaies RJ. Function and regulation of cullin–RING ubiquitin ligases. *Nature Reviews Molecular Cell Biology.* 2005;6(1):9-20.

109.   Cheng J, Guo J, Wang Z, North BJ, Tao K, Dai X, et al. Functional analysis of Cullin 3 E3 ligases in tumorigenesis. *Biochim Biophys Acta Rev Cancer.* 2018;1869(1):11-28.

110.   Deshaies RJ, Emberley ED, and Saha A. Control of cullin-ring ubiquitin ligase activity by nedd8. *Subcell Biochem.* 2010;54:41-56.

111.   Duda DM, Borg LA, Scott DC, Hunt HW, Hammel M, and Schulman BA. Structural insights into NEDD8 activation of cullin-RING ligases: conformational control of conjugation. *Cell.* 2008;134(6):995-1006.

112.   Lydeard JR, Schulman BA, and Harper JW. Building and remodelling Cullin-RING E3 ubiquitin ligases. *EMBO Rep.* 2013;14(12):1050-61.

113.   Borden KL, and Freemont PS. The RING finger domain: a recent example of a sequence-structure family. *Current opinion in structural biology.* 1996;6(3):395-401.

114.   Freemont PS, Hanson IM, and Trowsdale J. A novel cysteine-rich sequence motif. *Cell.* 1991;64(3):483-4.

115. Lovering R, Hanson IM, Borden KL, Martin S, O'Reilly NJ, Evan GI, et al. Identification and preliminary characterization of a protein motif related to the zinc finger. *Proceedings of the National Academy of Sciences of the United States of America.* 1993;90(6):2112-6.

116. Deshaies RJ, and Joazeiro CAP. RING domain E3 ubiquitin ligases. *Annu Rev Biochem.* 2009;78:399-434.

117. Joazeiro CA, and Weissman AM. RING finger proteins: mediators of ubiquitin ligase activity. *Cell.* 2000;102(5):549-52.

118. Rotin D, and Kumar S. Physiological functions of the HECT family of ubiquitin ligases. *Nature reviews Molecular cell biology.* 2009;10(6):398-409.

119. Coon TA, McKelvey AC, Lear T, Rajbhandari S, Dunn SR, Connelly W, et al. The proinflammatory role of HECTD2 in innate immunity and experimental lung injury. *Science Translational Medicine.* 2015;7(295):295ra109-295ra109.

120. Fang S, Jensen JP, Ludwig RL, Vousden KH, and Weissman AM. Mdm2 is a RING finger-dependent ubiquitin protein ligase for itself and p53. *J Biol Chem.* 2000;275(12):8945-51.

121. Joazeiro CA, and Weissman AM. RING finger proteins: mediators of ubiquitin ligase activity. *Cell.* 2000;102(5):549-52.

122. Lorick KL, Jensen JP, Fang S, Ong AM, Hatakeyama S, and Weissman AM. RING fingers mediate ubiquitin-conjugating enzyme (E2)-dependent ubiquitination. *Proceedings of the National Academy of Sciences of the United States of America.* 1999;96(20):11364-9.

123. Metzger MB, Hristova VA, and Weissman AM. HECT and RING finger families of E3 ubiquitin ligases at a glance. *Journal of cell science.* 2012;125(Pt 3):531-7.

124. Karni-Schmidt O, Lokshin M, and Prives C. The Roles of MDM2 and MDMX in Cancer. *Annual Review of Pathology: Mechanisms of Disease.* 2016;11(1):617-44.

125. Oliner JD, Saiki AY, and Caenepeel S. The Role of MDM2 Amplification and Overexpression in Tumorigenesis. *Cold Spring Harb Perspect Med.* 2016;6(6).

126. Wade M, Li YC, and Wahl GM. MDM2, MDMX and p53 in oncogenesis and cancer therapy. *Nat Rev Cancer.* 2013;13(2):83-96.

127. Burgess A, Chia KM, Haupt S, Thomas D, Haupt Y, and Lim E. Clinical Overview of MDM2/X-Targeted Therapies. *Front Oncol.* 2016;6:7.

128. Yee-Lin V, Pooi-Fong W, and Soo-Beng AK. Nutlin-3, A p53-Mdm2 Antagonist for Nasopharyngeal Carcinoma Treatment. *Mini Rev Med Chem.* 2018;18(2):173-83.

129. Starita LM, and Parvin JD. Substrates of the BRCA1-dependent ubiquitin ligase. *Cancer Biol Ther.* 2006;5(2):137-41.

130. Yoshida K, and Miki Y. Role of BRCA1 and BRCA2 as regulators of DNA repair, transcription, and cell cycle in response to DNA damage. *Cancer Sci.* 2004;95(11):866-71.

131. Kuchenbaecker KB, Hopper JL, Barnes DR, Phillips K-A, Mooij TM, Roos-Blom M-J, et al. Risks of breast, ovarian, and contralateral breast cancer for BRCA1 and BRCA2 mutation carriers. *The Journal of the American Medical Association.* 2017;317(23):2402-16.

132. Carbine NE, Lostumbo L, Wallace J, and Ko H. Risk-reducing mastectomy for the prevention of primary breast cancer. *Cochrane Database Syst Rev.* 2018;4:Cd002748.

133. Arkinson C, and Walden H. Parkin function in Parkinson's disease. *Science.* 2018;360(6386):267-8.

134. Pickrell AM, and Youle RJ. The roles of PINK1, parkin, and mitochondrial fidelity in Parkinson's disease. *Neuron.* 2015;85(2):257-73.

135. Seirafi M, Kozlov G, and Gehring K. Parkin structure and function. *FEBS J.* 2015;282(11):2076-88.
136. Lisztwan J, Imbert G, Wirbelauer C, Gstaiger M, and Krek W. The von Hippel–Lindau tumor suppressor protein is a component of an E3 ubiquitin–protein ligase activity. *Genes & Development.* 1999;13(14):1822-33.
137. Blagosklonny MV. Do VHL and HIF-1 mirror p53 and Mdm-2? Degradation-transactivation loops of oncoproteins and tumor suppressors. *Oncogene.* 2001;20(3):395-8.
138. Walmsley SR, McGovern NN, Whyte MK, and Chilvers ER. The HIF/VHL pathway: from oxygen sensing to innate immunity. *Am J Respir Cell Mol Biol.* 2008;38(3):251-5.
139. Kapitsinou PP, and Haase VH. The VHL tumor suppressor and HIF: insights from genetic studies in mice. *Cell Death Differ.* 2008;15(4):650-9.
140. Gossage L, Eisen T, and Maher ER. VHL, the story of a tumour suppressor gene. *Nat Rev Cancer.* 2015;15(1):55-64.
141. Lear T, McKelvey AC, Rajbhandari S, Dunn SR, Coon TA, Connelly W, et al. Ubiquitin E3 ligase FIEL1 regulates fibrotic lung injury through SUMO-E3 ligase PIAS4. *The Journal of Experimental Medicine.* 2016;213(6):1029-46.
142. Gross TJ, and Hunninghake GW. Idiopathic pulmonary fibrosis. *The New England journal of medicine.* 2001;345(7):517-25.
143. Noble PW, Barkauskas CE, and Jiang D. Pulmonary fibrosis: patterns and perpetrators. *The Journal of clinical investigation.* 2012;122(8):2756-62.
144. King TE, Jr., Pardo A, and Selman M. Idiopathic pulmonary fibrosis. *Lancet.* 2011;378(9807):1949-61.
145. Sheppard D. ROCKing pulmonary fibrosis. *The Journal of clinical investigation.* 2013;123(3):1005-6.
146. Raghu G, Collard HR, Egan JJ, Martinez FJ, Behr J, Brown KK, et al. An official ATS/ERS/JRS/ALAT statement: idiopathic pulmonary fibrosis: evidence-based guidelines for diagnosis and management. *Am J Respir Crit Care Med.* 2011;183(6):788-824.
147. Annes JP, Munger JS, and Rifkin DB. Making sense of latent TGFbeta activation. *Journal of cell science.* 2003;116(Pt 2):217-24.
148. Kage H, and Borok Z. EMT and interstitial lung disease: a mysterious relationship. *Current opinion in pulmonary medicine.* 2012;18(5):517-23.
149. Chapman HA. Epithelial-Mesenchymal Interactions in Pulmonary Fibrosis. *Annual Review of Physiology.* 2011;73(1):413-35.
150. Massague J. TGF[beta] signalling in context. *Nat Rev Mol Cell Biol.* 2012;13(10):616-30.
151. Wick G, Grundtman C, Mayerl C, Wimpissinger T-F, Feichtinger J, Zelger B, et al. The Immunology of Fibrosis. *Annual Review of Immunology.* 2013;31(1):107-35.
152. Attisano L, and Wrana JL. Smads as transcriptional co-modulators. *Curr Opin Cell Biol.* 2000;12(2):235-43.
153. Bonniaud P, Margetts PJ, Ask K, Flanders K, Gauldie J, and Kolb M. TGF-beta and Smad3 signaling link inflammation to chronic fibrogenesis. *J Immunol.* 2005;175(8):5390-5.
154. Yingling JM, Blanchard KL, and Sawyer JS. Development of TGF-beta signalling inhibitors for cancer therapy. *Nat Rev Drug Discov.* 2004;3(12):1011-22.
155. Derynck R, and Zhang YE. Smad-dependent and Smad-independent pathways in TGF-beta family signalling. *Nature.* 2003;425(6958):577-84.

156.   Jonk LJ, Itoh S, Heldin CH, ten Dijke P, and Kruijer W. Identification and functional characterization of a Smad binding element (SBE) in the JunB promoter that acts as a transforming growth factor-beta, activin, and bone morphogenetic protein-inducible enhancer. *The Journal of biological chemistry.* 1998;273(33):21145-52.

157.   Wang XM, Zhang Y, Kim HP, Zhou Z, Feghali-Bostwick CA, Liu F, et al. Caveolin-1: a critical regulator of lung fibrosis in idiopathic pulmonary fibrosis. *J Exp Med.* 2006;203(13):2895-906.

158.   Hecker L, Vittal R, Jones T, Jagirdar R, Luckhardt TR, Horowitz JC, et al. NADPH oxidase-4 mediates myofibroblast activation and fibrogenic responses to lung injury. *Nature medicine.* 2009;15(9):1077-81.

159.   Rytinki MM, Kaikkonen S, Pehkonen P, Jaaskelainen T, and Palvimo JJ. PIAS proteins: pleiotropic interactors associated with SUMO. *Cell Mol Life Sci.* 2009;66(18):3029-41.

160.   Gross M, Liu B, Tan J, French FS, Carey M, and Shuai K. Distinct effects of PIAS proteins on androgen-mediated gene activation in prostate cancer cells. *Oncogene.* 2001;20(29):3880-7.

161.   Long J, Matsuura I, He D, Wang G, Shuai K, and Liu F. Repression of Smad transcriptional activity by PIASy, an inhibitor of activated STAT. *Proceedings of the National Academy of Sciences of the United States of America.* 2003;100(17):9791-6.

162.   Imoto S, Sugiyama K, Yamamoto T, and Matsuda T. The RING domain of PIASy is involved in the suppression of bone morphogenetic protein-signaling pathway. *Biochemical and biophysical research communications.* 2004;319(1):275-82.

163.   Lee PS, Chang C, Liu D, and Derynck R. Sumoylation of Smad4, the common Smad mediator of transforming growth factor-beta family signaling. *The Journal of biological chemistry.* 2003;278(30):27853-63.

164.   Kim J-B, Kim SY, Kim BM, Lee H, Kim I, Yun J, et al. Identification of a novel anti-apoptotic E3 ubiquitin ligase that ubiquitinates antagonists of inhibitor of apoptosis proteins SMAC, HtrA2, and ARTS. *The Journal of biological chemistry.* 2013;288(17):12014-21.

165.   Tager AM, LaCamera P, Shea BS, Campanella GS, Selman M, Zhao Z, et al. The lysophosphatidic acid receptor LPA1 links pulmonary fibrosis to lung injury by mediating fibroblast recruitment and vascular leak. *Nature medicine.* 2008;14(1):45-54.

166.   Jiang D, Liang J, Campanella GS, Guo R, Yu S, Xie T, et al. Inhibition of pulmonary fibrosis in mice by CXCL10 requires glycosaminoglycan binding and syndecan-4. *The Journal of clinical investigation.* 2010;120(6):2049-57.

167.   Umadevi N, Kumar S, and Narayana N. Crystallization and preliminary X-ray diffraction studies of the WW4 domain of the Nedd4-2 ubiquitin-protein ligase. *Acta crystallographica Section F, Structural biology and crystallization communications.* 2005;61(Pt 12):1084-6.

168.   Kamadurai HB, Souphron J, Scott DC, Duda DM, Miller DJ, Stringer D, et al. Insights into ubiquitin transfer cascades from a structure of a UbcH5B approximately ubiquitin-HECT(NEDD4L) complex. *Molecular cell.* 2009;36(6):1095-102.

169.   Wilson MS, and Wynn TA. Pulmonary fibrosis: pathogenesis, etiology and regulation. *Mucosal Immunol.* 2009;2(2):103-21.

170.   Li M, Krishnaveni MS, Li C, Zhou B, Xing Y, Banfalvi A, et al. Epithelium-specific deletion of TGF-beta receptor type II protects mice from bleomycin-induced pulmonary fibrosis. *J Clin Invest.* 2011;121(1):277-87.

171.   Jiang D, Liang J, Fan J, Yu S, Chen S, Luo Y, et al. Regulation of lung injury and repair by Toll-like receptors and hyaluronan. *Nature medicine.* 2005;11(11):1173-9.

172.   Baarsma HA, Engelbertink LH, van Hees LJ, Menzen MH, Meurs H, Timens W, et al. Glycogen synthase kinase-3 (GSK-3) regulates TGF-beta(1)-induced differentiation of pulmonary fibroblasts. *Br J Pharmacol.* 2013;169(3):590-603.

173.   Takeda M, Babazono T, Nitta K, and Iwamoto Y. High glucose stimulates hyaluronan production by renal interstitial fibroblasts through the protein kinase C and transforming growth factor-beta cascade. *Metabolism.* 2001;50(7):789-94.

174.   Mulsow JJ, Watson RW, Fitzpatrick JM, and O'Connell PR. Transforming growth factor-beta promotes pro-fibrotic behavior by serosal fibroblasts via PKC and ERK1/2 mitogen activated protein kinase cell signaling. *Ann Surg.* 2005;242(6):880-7, discussion 7-9.

175.   Mallampalli RK, Coon TA, Glasser JR, Wang C, Dunn SR, Weathington NM, et al. Targeting F box protein Fbxo3 to control cytokine-driven inflammation. *Journal of immunology.* 2013;191(10):5247-55.

176.   Chen BB, Coon TA, Glasser JR, McVerry BJ, Zhao J, Zhao Y, et al. A combinatorial F box protein directed pathway controls TRAF adaptor stability to regulate inflammation. *Nat Immunol.* 2013;14(5):470-9.

177.   Akhmetshina A, Venalis P, Dees C, Busch N, Zwerina J, Schett G, et al. Treatment with imatinib prevents fibrosis in different preclinical models of systemic sclerosis and induces regression of established fibrosis. *Arthritis Rheum.* 2009;60(1):219-24.

178.   Daniels CE, Lasky JA, Limper AH, Mieras K, Gabor E, and Schroeder DR. Imatinib treatment for idiopathic pulmonary fibrosis: Randomized placebo-controlled trial results. *Am J Respir Crit Care Med.* 2010;181(6):604-10.

179.   Denton CP, Merkel PA, Furst DE, Khanna D, Emery P, Hsu VM, et al. Recombinant human anti-transforming growth factor beta1 antibody therapy in systemic sclerosis: a multicenter, randomized, placebo-controlled phase I/II trial of CAT-192. *Arthritis Rheum.* 2007;56(1):323-33.

180.   Pope J, McBain D, Petrlich L, Watson S, Vanderhoek L, de Leon F, et al. Imatinib in active diffuse cutaneous systemic sclerosis: Results of a six-month, randomized, double-blind, placebo-controlled, proof-of-concept pilot study at a single center. *Arthritis and rheumatism.* 2011;63(11):3547-51.

181.   Ray NB, Durairaj L, Chen BB, McVerry BJ, Ryan AJ, Donahoe M, et al. Dynamic regulation of cardiolipin by the lipid pump Atp8b1 determines the severity of lung injury in experimental pneumonia. *Nat Med.* 2010;16(10):1120-7.

182.   Chen BB, and Mallampalli RK. Calmodulin binds and stabilizes the regulatory enzyme, CTP: phosphocholine cytidylyltransferase. *The Journal of biological chemistry.* 2007;282(46):33494-506.

183.   Kesava Reddy G, and Enwemeka CS. A simplified method for the analysis of hydroxyproline in biological tissues. *Clin Biochem.* 1996;29(3):225-9.

184.   Neuman RE, and Logan MA. THE DETERMINATION OF HYDROXYPROLINE. *Journal of Biological Chemistry.* 1950;184(1):299-306.

185.   Butler PL, and Mallampalli RK. Cross-talk between remodeling and de novo pathways maintains phospholipid balance through ubiquitination. *J Biol Chem.* 2010;285(9):6246-58.

186. Lear TB, Lockwood KC, Larsen M, Tuncer F, Kennerdell JR, Morse C, et al. Kelch-like protein 42 is a profibrotic ubiquitin E3 ligase involved in systemic sclerosis. *Journal of Biological Chemistry.* 2020;295(13):4171-80.

187. Gao T, Liu Z, Wang Y, Cheng H, Yang Q, Guo A, et al. UUCD: a family-based database of ubiquitin and ubiquitin-like conjugation. *Nucleic Acids Res.* 2013;41(Database issue):D445-D51.

188. Denton CP, and Khanna D. Systemic sclerosis. *Lancet.* 2017;390(10103):1685-99.

189. Poudel DR, Jayakumar D, Danve A, Sehra ST, and Derk CT. Determinants of mortality in systemic sclerosis: a focused review. *Rheumatol Int.* 2018;38(10):1847-58.

190. Barnes J, and Mayes MD. Epidemiology of systemic sclerosis: incidence, prevalence, survival, risk factors, malignancy, and environmental triggers. *Curr Opin Rheumatol.* 2012;24(2):165-70.

191. Denton CP, Wells AU, and Coghlan JG. Major lung complications of systemic sclerosis. *Nat Rev Rheumatol.* 2018;14(9):511-27.

192. Korman B. Evolving insights into the cellular and molecular pathogenesis of fibrosis in systemic sclerosis. *Transl Res.* 2019;209:77-89.

193. Giacomelli R, Liakouli V, Berardicurti O, Ruscitti P, Di Benedetto P, Carubbi F, et al. Interstitial lung disease in systemic sclerosis: current and future treatment. *Rheumatol Int.* 2017;37(6):853-63.

194. Lafyatis R. Transforming growth factorβ--at the centre of systemic sclerosis. *Nat Rev Rheumatol.* 2014;10(12):706-19.

195. Imoto S, Sugiyama K, Muromoto R, Sato N, Yamamoto T, and Matsuda T. Regulation of transforming growth factor-beta signaling by protein inhibitor of activated STAT, PIASy through Smad3. *The Journal of biological chemistry.* 2003;278(36):34253-8.

196. Lee PSW, Chang C, Liu D, and Derynck R. Sumoylation of Smad4, the common Smad mediator of transforming growth factor-beta family signaling. *The Journal of biological chemistry.* 2003;278(30):27853-63.

197. Abdollah S, Macías-Silva M, Tsukazaki T, Hayashi H, Attisano L, and Wrana JL. TbetaRI phosphorylation of Smad2 on Ser465 and Ser467 is required for Smad2-Smad4 complex formation and signaling. *The Journal of biological chemistry.* 1997;272(44):27678-85.

198. Macías-Silva M, Abdollah S, Hoodless PA, Pirone R, Attisano L, and Wrana JL. MADR2 is a substrate of the TGFbeta receptor and its phosphorylation is required for nuclear accumulation and signaling. *Cell.* 1996;87(7):1215-24.

199. Derynck R, and Zhang YE. Smad-dependent and Smad-independent pathways in TGF-beta family signalling. *Nature.* 2003;425(6958):577-84.

200. Inoue Y, and Imamura T. Regulation of TGF-beta family signaling by E3 ubiquitin ligases. *Cancer Sci.* 2008;99(11):2107-12.

201. Izzi L, and Attisano L. Regulation of the TGFbeta signalling pathway by ubiquitin-mediated degradation. *Oncogene.* 2004;23(11):2071-8.

202. Gao S, Alarcón C, Sapkota G, Rahman S, Chen P-Y, Goerner N, et al. Ubiquitin ligase Nedd4L targets activated Smad2/3 to limit TGF-beta signaling. *Molecular cell.* 2009;36(3):457-68.

203. Kavsak P, Rasmussen RK, Causing CG, Bonni S, Zhu H, Thomsen GH, et al. Smad7 binds to Smurf2 to form an E3 ubiquitin ligase that targets the TGF beta receptor for degradation. *Molecular cell.* 2000;6(6):1365-75.

204. Li S, Zhao J, Shang D, Kass DJ, and Zhao Y. Ubiquitination and deubiquitination emerge as players in idiopathic pulmonary fibrosis pathogenesis and treatment. *JCI Insight.* 2018;3(10).

205. Collison AM, Li J, de Siqueira AP, Lv X, Toop HD, Morris JC, et al. TRAIL signals through the ubiquitin ligase MID1 to promote pulmonary fibrosis. *BMC Pulm Med.* 2019;19(1):31.

206. Zuscik MJ, Rosier RN, and Schwarz EM. Altered negative regulation of transforming growth factor beta signaling in scleroderma: potential involvement of SMURF2 in disease. *Arthritis Rheum.* 2003;48(7):1779-80.

207. Deng Q, Zhang J, Gao Y, She X, Wang Y, Wang Y, et al. MLN4924 protects against bleomycin-induced pulmonary fibrosis by inhibiting the early inflammatory process. *Am J Transl Res.* 2017;9(4):1810-21.

208. Liu S-S, Lv X-X, Liu C, Qi J, Li Y-X, Wei X-P, et al. Targeting Degradation of the Transcription Factor C/EBPβ Reduces Lung Fibrosis by Restoring Activity of the Ubiquitin-Editing Enzyme A20 in Macrophages. *Immunity.* 2019;51(3):522-34.e7.

209. Valenzi E, Bulik M, Tabib T, Morse C, Sembrat J, Trejo Bittar H, et al. Single-cell analysis reveals fibroblast heterogeneity and myofibroblasts in systemic sclerosis-associated interstitial lung disease. *Ann Rheum Dis.* 2019;78(10):1379-87.

210. Mori Y, Chen S-J, and Varga J. Expression and regulation of intracellular SMAD signaling in scleroderma skin fibroblasts. *Arthritis Rheum.* 2003;48(7):1964-78.

211. Zhang JH, Chung TD, and Oldenburg KR. A Simple Statistical Parameter for Use in Evaluation and Validation of High Throughput Screening Assays. *J Biomol Screen.* 1999;4(2):67-73.

212. Petroski MD, and Deshaies RJ. Function and regulation of cullin-RING ubiquitin ligases. *Nat Rev Mol Cell Biol.* 2005;6(1):9-20.

213. Cummings CM, Bentley CA, Perdue SA, Baas PW, and Singer JD. The Cul3/Klhdc5 E3 ligase regulates p60/katanin and is required for normal mitosis in mammalian cells. *The Journal of biological chemistry.* 2009;284(17):11663-75.

214. Hjerpe R, Aillet F, Lopitz-Otsoa F, Lang V, England P, and Rodriguez MS. Efficient protection and isolation of ubiquitylated proteins using tandem ubiquitin-binding entities. *EMBO Rep.* 2009;10(11):1250-8.

215. Azkargorta M, Escobes I, Elortza F, Matthiesen R, and Rodríguez MS. TUBEs-Mass Spectrometry for Identification and Analysis of the Ubiquitin-Proteome. *Methods Mol Biol.* 2016;1449:177-92.

216. Eden E, Navon R, Steinfeld I, Lipson D, and Yakhini Z. GOrilla: a tool for discovery and visualization of enriched GO terms in ranked gene lists. *BMC Bioinformatics.* 2009;10:48.

217. McCright B, and Virshup DM. Identification of a new family of protein phosphatase 2A regulatory subunits. *The Journal of biological chemistry.* 1995;270(44):26123-8.

218. Cristóbal I, Cirauqui C, Castello-Cros R, Garcia-Orti L, Calasanz MJ, and Odero MD. Downregulation of PPP2R5E is a common event in acute myeloid leukemia that affects the oncogenic potential of leukemic cells. *Haematologica.* 2013;98(9):e103-4.

219. Xia H, Seeman J, Hong J, Hergert P, Bodem V, Jessurun J, et al. Low α(2)β(1) integrin function enhances the proliferation of fibroblasts from patients with idiopathic pulmonary fibrosis by activation of the β-catenin pathway. *Am J Pathol.* 2012;181(1):222-33.

220. Samuel GH, Bujor AM, Nakerakanti SS, Hant FN, and Trojanowska M. Autocrine transforming growth factor β signaling regulates extracellular signal-regulated kinase 1/2

241

phosphorylation via modulation of protein phosphatase 2A expression in scleroderma fibroblasts. *Fibrogenesis Tissue Repair.* 2010;3:25.

221. Rizvi F, Siddiqui R, DeFranco A, Homar P, Emelyanova L, Holmuhamedov E, et al. Simvastatin reduces TGF-β1-induced SMAD2/3-dependent human ventricular fibroblasts differentiation: Role of protein phosphatase activation. *Int J Cardiol.* 2018;270:228-36.

222. Hornbeck PV, Zhang B, Murray B, Kornhauser JM, Latham V, and Skrzypek E. PhosphoSitePlus, 2014: mutations, PTMs and recalibrations. *Nucleic Acids Res.* 2015;43(Database issue):D512-20.

223. Asano Y, Ihn H, Yamane K, Jinnin M, Mimura Y, and Tamaki K. Increased expression of integrin alpha(v)beta3 contributes to the establishment of autocrine TGF-beta signaling in scleroderma fibroblasts. *J Immunol.* 2005;175(11):7708-18.

224. Bhattacharyya S, Chen S-J, Wu M, Warner-Blankenship M, Ning H, Lakos G, et al. Smad-independent transforming growth factor-beta regulation of early growth response-1 and sustained expression in fibrosis: implications for scleroderma. *Am J Pathol.* 2008;173(4):1085-99.

225. Chen Y, Leask A, Abraham DJ, Pala D, Shiwen X, Khan K, et al. Heparan sulfate-dependent ERK activation contributes to the overexpression of fibrotic proteins and enhanced contraction by scleroderma fibroblasts. *Arthritis Rheum.* 2008;58(2):577-85.

226. Meiners S, Evankovich J, and Mallampalli RK. The ubiquitin proteasome system as a potential therapeutic target for systemic sclerosis. *Transl Res.* 2018;198:17-28.

227. Long Y, Chen W, Du Q, Zuo X, and Zhu H. Ubiquitination in scleroderma fibrosis and its treatment. *Front Immunol.* 2018;9:2383.

228. Mikamo M, Kitagawa K, Sakai S, Uchida C, Ohhata T, Nishimoto K, et al. Inhibiting Skp2 E3 Ligase Suppresses Bleomycin-Induced Pulmonary Fibrosis. *Int J Mol Sci.* 2018;19(2).

229. Seiler CY, Park JG, Sharma A, Hunter P, Surapaneni P, Sedillo C, et al. DNASU plasmid and PSI:Biology-Materials repositories: resources to accelerate biological research. *Nucleic Acids Res.* 2014;42(Database issue):D1253-60.

230. Morse C, Tabib T, Sembrat J, Buschur KL, Bittar HT, Valenzi E, et al. Proliferating SPP1/MERTK-expressing macrophages in idiopathic pulmonary fibrosis. *Eur Respir J.* 2019;54(2).

231. Carpenter AE, Jones TR, Lamprecht MR, Clarke C, Kang IH, Friman O, et al. CellProfiler: image analysis software for identifying and quantifying cell phenotypes. *Genome Biol.* 2006;7(10):R100.

232. McKelvey AC, Lear TB, Dunn SR, Evankovich J, Londino JD, Bednash JS, et al. RING finger E3 ligase PPP1R11 regulates TLR2 signaling and innate immunity. *elife.* 2016;5.

233. Chuang TH, and Ulevitch RJ. Triad3A, an E3 ubiquitin-protein ligase regulating Toll-like receptors. *Nat Immunol.* 2004;5(5):495-502.

234. Crespo-Lessmann A, Juarez-Rubio C, and Plaza-Moral V. [Role of toll-like receptors in respiratory diseases]. *Arch Bronconeumol.* 2010;46(3):135-42.

235. Delgado MA, Elmaoued RA, Davis AS, Kyei G, and Deretic V. Toll-like receptors control autophagy. *The EMBO journal.* 2008;27(7):1110-21.

236. Esen N, and Kielian T. Central role for MyD88 in the responses of microglia to pathogen-associated molecular patterns. *Journal of immunology.* 2006;176(11):6802-11.

237. Chalifour A, Jeannin P, Gauchat JF, Blaecke A, Malissard M, N'Guyen T, et al. Direct bacterial protein PAMP recognition by human NK cells involves TLRs and triggers alpha-defensin production. *Blood.* 2004;104(6):1778-83.

238. Tobian AA, Potter NS, Ramachandra L, Pai RK, Convery M, Boom WH, et al. Alternate class I MHC antigen processing is inhibited by Toll-like receptor signaling pathogen-associated molecular patterns: Mycobacterium tuberculosis 19-kDa lipoprotein, CpG DNA, and lipopolysaccharide. *J Immunol.* 2003;171(3):1413-22.

239. O'Neill LA. The interleukin-1 receptor/Toll-like receptor superfamily: signal transduction during inflammation and host defense. *Science's STKE : signal transduction knowledge environment.* 2000;2000(44):re1.

240. Fitzgerald KA, Palsson-McDermott EM, Bowie AG, Jefferies CA, Mansell AS, Brady G, et al. Mal (MyD88-adapter-like) is required for Toll-like receptor-4 signal transduction. *Nature.* 2001;413(6851):78-83.

241. Xu Y, Tao X, Shen B, Horng T, Medzhitov R, Manley JL, et al. Structural basis for signal transduction by the Toll/interleukin-1 receptor domains. *Nature.* 2000;408(6808):111-5.

242. Raby AC, Holst B, Le Bouder E, Diaz C, Ferran E, Conraux L, et al. Targeting the TLR co-receptor CD14 with TLR2-derived peptides modulates immune responses to pathogens. *Science translational medicine.* 2013;5(185):185ra64.

243. Charles PE, Tissieres P, Barbar SD, Croisier D, Dufour J, Dunn-Siegrist I, et al. Mild-stretch mechanical ventilation upregulates toll-like receptor 2 and sensitizes the lung to bacterial lipopeptide. *Crit Care.* 2011;15(4):R181.

244. Hertz CJ, Wu Q, Porter EM, Zhang YJ, Weismuller KH, Godowski PJ, et al. Activation of Toll-like receptor 2 on human tracheobronchial epithelial cells induces the antimicrobial peptide human beta defensin-2. *J Immunol.* 2003;171(12):6820-6.

245. Hoth JJ, Wells JD, Yoza BK, and McCall CE. Innate immune response to pulmonary contusion: identification of cell type-specific inflammatory responses. *Shock.* 2012;37(4):385-91.

246. Takeuchi O, Hoshino K, and Akira S. Cutting edge: TLR2-deficient and MyD88-deficient mice are highly susceptible to Staphylococcus aureus infection. *Journal of immunology.* 2000;165(10):5392-6.

247. Bronkhorst MW, Boye ND, Lomax MA, Vossen RH, Bakker J, Patka P, et al. Single-nucleotide polymorphisms in the Toll-like receptor pathway increase susceptibility to infections in severely injured trauma patients. *J Trauma Acute Care Surg.* 2013;74(3):862-70.

248. Janardhanan J, Joseph Martin S, Astrup E, Veeramanikandan R, Aukrust P, Abraham OC, et al. Single-nucleotide polymorphisms in Toll-like receptor (TLR)-2, TLR4 and heat shock protein 70 genes and susceptibility to scrub typhus. *Journal of human genetics.* 2013;58(11):707-10.

249. Nachtigall I, Tamarkin A, Tafelski S, Weimann A, Rothbart A, Heim S, et al. Polymorphisms of the toll-like receptor 2 and 4 genes are associated with faster progression and a more severe course of sepsis in critically ill patients. *The Journal of international medical research.* 2014;42(1):93-110.

250. Stappers MH, Thys Y, Oosting M, Plantinga TS, Ioana M, Reimnitz P, et al. TLR1, TLR2, and TLR6 gene polymorphisms are associated with increased susceptibility to complicated skin and skin structure infections. *J Infect Dis.* 2014;210(2):311-8.

251. Coon TA, McKelvey AC, Lear T, Rajbhandari S, Dunn SR, Connelly W, et al. The proinflammatory role of HECTD2 in innate immunity and experimental lung injury. *Science translational medicine.* 2015;7(295):295ra109.

252. Borden KL. RING fingers and B-boxes: zinc-binding protein-protein interaction domains. *Biochemistry and cell biology = Biochimie et biologie cellulaire.* 1998;76(2-3):351-8.

253. Amemiya Y, Azmi P, and Seth A. Autoubiquitination of BCA2 RING E3 ligase regulates its own stability and affects cell migration. *Molecular cancer research : MCR.* 2008;6(9):1385-96.

254. Deshaies RJ, and Joazeiro CA. RING domain E3 ubiquitin ligases. *Annu Rev Biochem.* 2009;78:399-434.

255. Hudson LD, Milberg JA, Anardi D, and Maunder RJ. Clinical risks for development of the acute respiratory distress syndrome. *American journal of respiratory and critical care medicine.* 1995;151(2 Pt 1):293-301.

256. Zhang J, Zhang L, Zhao S, and Lee EY. Identification and characterization of the human HCG V gene product as a novel inhibitor of protein phosphatase-1. *Biochemistry.* 1998;37(47):16728-34.

257. Han Y, Song XX, Feng HL, Cheung CK, Lam PM, Wang CC, et al. Mutations of t-complex testis expressed gene 5 transcripts in the testis of sterile t-haplotype mutant mouse. *Asian journal of andrology.* 2008;10(2):219-26.

258. Pilder SH, Lu J, Han Y, Hui L, Samant SA, Olugbemiga OO, et al. The molecular basis of "curlicue": a sperm motility abnormality linked to the sterility of t haplotype homozygous male mice. *Society of Reproduction and Fertility supplement.* 2007;63:123-33.

259. Skaar JR, D'Angiolella V, Pagan JK, and Pagano M. SnapShot: F Box Proteins II. *Cell.* 2009;137(7):1358, e1.

260. Zhao J, Wei J, Mialki RK, Mallampalli DF, Chen BB, Coon T, et al. F-box protein FBXL19-mediated ubiquitination and degradation of the receptor for IL-33 limits pulmonary inflammation. *Nature immunology.* 2012;13(7):651-8.

261. Lear T, McKelvey AC, Rajbhandari S, Dunn SR, Coon TA, Connelly W, et al. Ubiquitin E3 ligase FIEL1 regulates fibrotic lung injury through SUMO-E3 ligase PIAS4. *The Journal of experimental medicine.* 2016;213(6):1029-46.

262. Hospenthal MK, Mevissen TE, and Komander D. Deubiquitinase-based analysis of ubiquitin chain architecture using Ubiquitin Chain Restriction (UbiCRest). *Nat Protoc.* 2015;10(2):349-61.

263. Lear TB, McKelvey AC, Evankovich JW, Rajbhandari S, Coon TA, Dunn SR, et al. KIAA0317 regulates pulmonary inflammation through SOCS2 degradation. *JCI Insight.* 2019;4(19).

264. Pham T, and Rubenfeld GD. Fifty years of research in ARDS. the epidemiology of acute respiratory distress syndrome. A 50th birthday review. *Am J Respir Crit Care Med.* 2017;195(7):860-70.

265. Hiemstra PS, McCray PB, and Bals R. The innate immune function of airway epithelial cells in inflammatory lung disease. *European Respiratory Journal.* 2015;45(4):1150-62.

266. Weitnauer M, Mijošek V, and Dalpke AH. Control of local immunity by airway epithelial cells. *Mucosal Immunol.* 2016;9(2):287-98.

267. Ware LB, and Matthay MA. The acute respiratory distress syndrome. *N Engl J Med.* 2000;342(18):1334-49.

268. Rubenfeld GD, Caldwell E, Peabody E, Weaver J, Martin DP, Neff M, et al. Incidence and outcomes of acute lung injury. *N Engl J Med.* 2005;353(16):1685-93.

269. Rahman A, and Fazal F. Blocking NF-κB: an inflammatory issue. *Proc Am Thorac Soc.* 2011;8(6):497-503.

270. Blackwell TS, and Christman JW. The role of nuclear factor-kappa B in cytokine gene regulation. *Am J Respir Cell Mol Biol.* 1997;17(1):3-9.
271. Lawrence T. The nuclear factor NF-kappaB pathway in inflammation. *Cold Spring Harb Perspect Biol.* 2009;1(6):a001651.
272. Yoshimura A, Naka T, and Kubo M. SOCS proteins, cytokine signalling and immune regulation. *Nat Rev Immunol.* 2007;7(6):454-65.
273. Trengove MC, and Ward AC. SOCS proteins in development and disease. *American journal of clinical and experimental immunology.* 2013;2(1):1-29.
274. Kazi JU, and Rönnstrand L. Suppressor of cytokine signaling 2 (SOCS2) associates with FLT3 and negatively regulates downstream signaling. *Mol Oncol.* 2013;7(3):693-703.
275. Gan L, Liu Z, Zhang Z, Yang X, Liu J, and Sun C. SOCS2 inhibited mitochondria biogenesis via inhibiting p38 MAPK/ATF2 pathway in C2C12 cells. *Mol Biol Rep.* 2014;41(2):627-37.
276. Tannahill GM, Elliott J, Barry AC, Hibbert L, Cacalano NA, and Johnston JA. SOCS2 can enhance interleukin-2 (IL-2) and IL-3 signaling by accelerating SOCS3 degradation. *Mol Cell Biol.* 2005;25(20):9115-26.
277. Vesterlund M, Zadjali F, Persson T, Nielsen ML, Kessler BM, Norstedt G, et al. The SOCS2 ubiquitin ligase complex regulates growth hormone receptor levels. *PLoS ONE.* 2011;6(9):e25358.
278. Park S-H, Kim K-E, Hwang H-Y, and Kim TY. Regulatory effect of SOCS on NF-kappaB activity in murine monocytes/macrophages. *DNA Cell Biol.* 2003;22(2):131-9.
279. Shi D-D, Shi H, Lu D, Li R, Zhang Y, and Zhang J. NDR1/STK38 potentiates NF-κB activation by its kinase activity. *Cell Biochem Funct.* 2012;30(8):664-70.
280. Paul I, Batth TS, Iglesias-Gato D, Al-Araimi A, Al-Haddabi I, Alkharusi A, et al. The ubiquitin ligase Cullin5SOCS2 regulates NDR1/STK38 stability and NF-κB transactivation. *Sci Rep.* 2017;7:42800.
281. McBerry C, Gonzalez RMS, Shryock N, Dias A, and Aliberti J. SOCS2-induced proteasome-dependent TRAF6 degradation: a common anti-inflammatory pathway for control of innate immune responses. *PLoS ONE.* 2012;7(6):e38384.
282. Machado FS, Johndrow JE, Esper L, Dias A, Bafica A, Serhan CN, et al. Anti-inflammatory actions of lipoxin A4 and aspirin-triggered lipoxin are SOCS-2 dependent. *Nat Med.* 2006;12(3):330-4.
283. Coon TA, McKelvey AC, Lear T, Rajbhandari S, Dunn SR, Connelly W, et al. The proinflammatory role of HECTD2 in innate immunity and experimental lung injury. *Science translational medicine.* 2015;7(295):295ra109.
284. Hippenstiel S, Opitz B, Schmeck B, and Suttorp N. Lung epithelium as a sentinel and effector system in pneumonia--molecular mechanisms of pathogen recognition and signal transduction. *Respir Res.* 2006;7:97.
285. Kristariyanto YA, Choi S-Y, Rehman SAA, Ritorto MS, Campbell DG, Morrice NA, et al. Assembly and structure of Lys33-linked polyubiquitin reveals distinct conformations. *Biochem J.* 2015;467(2):345-52.
286. Michel MA, Elliott PR, Swatek KN, Simicek M, Pruneda JN, Wagstaff JL, et al. Assembly and specific recognition of k29- and k33-linked polyubiquitin. *Molecular cell.* 2015;58(1):95-109.
287. Skaar JR, Pagan JK, and Pagano M. Mechanisms and function of substrate recruitment by F-box proteins. *Nat Rev Mol Cell Biol.* 2013;14(6):369-81.

288. Blom N, Gammeltoft S, and Brunak S. Sequence and structure-based prediction of eukaryotic protein phosphorylation sites. *J Mol Biol.* 1999;294(5):1351-62.

289. Blom N, Gammeltoft S, and Brunak S. Sequence and structure-based prediction of eukaryotic protein phosphorylation sites. *Journal of molecular biology.* 1999;294(5):1351-62.

290. Kim H, Zamel R, Bai X-H, and Liu M. PKC activation induces inflammatory response and cell death in human bronchial epithelial cells. *PLoS ONE.* 2013;8(5):e64182.

291. Kontny E, Ziółkowska M, Ryzewska A, and Maśliński W. Protein kinase c-dependent pathway is critical for the production of pro-inflammatory cytokines (TNF-alpha, IL-1beta, IL-6). *Cytokine.* 1999;11(11):839-48.

292. Loegering DJ, and Lennartz MR. Protein kinase C and toll-like receptor signaling. *Enzyme Res.* 2011;2011:537821.

293. Pelletier S, Gingras S, and Green DR. Mouse genome engineering via CRISPR-Cas9 for study of immune function. *Immunity.* 2015;42(1):18-27.

294. Rotin D, and Kumar S. Physiological functions of the HECT family of ubiquitin ligases. *Nat Rev Mol Cell Biol.* 2009;10(6):398-409.

295. Huang L, Kinnucan E, Wang G, Beaudenon S, Howley PM, Huibregtse JM, et al. Structure of an E6AP-UbcH7 complex: insights into ubiquitination by the E2-E3 enzyme cascade. *Science.* 1999;286(5443):1321-6.

296. Umadevi N, Kumar S, and Narayana N. Crystallization and preliminary X-ray diffraction studies of the WW4 domain of the Nedd4-2 ubiquitin-protein ligase. *Acta Crystallogr Sect F Struct Biol Cryst Commun.* 2005;61(Pt 12):1084-6.

297. Kamadurai HB, Souphron J, Scott DC, Duda DM, Miller DJ, Stringer D, et al. Insights into ubiquitin transfer cascades from a structure of a UbcH5B approximately ubiquitin-HECT(NEDD4L) complex. *Molecular cell.* 2009;36(6):1095-102.

298. Kuratomi G, Komuro A, Goto K, Shinozaki M, Miyazawa K, Miyazono K, et al. NEDD4-2 (neural precursor cell expressed, developmentally down-regulated 4-2) negatively regulates TGF-beta (transforming growth factor-beta) signalling by inducing ubiquitin-mediated degradation of Smad2 and TGF-beta type I receptor. *Biochem J.* 2005;386(Pt 3):461-70.

299. Cao XR, Lill NL, Boase N, Shi PP, Croucher DR, Shan H, et al. Nedd4 Controls Animal Growth by Regulating IGF-1 Signaling. 2008;1(38):ra5-ra.

300. Torrino S, Visvikis O, Doye A, Boyer L, Stefani C, Munro P, et al. The E3 ubiquitin-ligase HACE1 catalyzes the ubiquitylation of active Rac1. *Dev Cell.* 2011;21(5):959-65.

301. Marchese A, Raiborg C, Santini F, Keen JH, Stenmark H, and Benovic JL. The E3 ubiquitin ligase AIP4 mediates ubiquitination and sorting of the G protein-coupled receptor CXCR4. *Dev Cell.* 2003;5(5):709-22.

302. Xu H, Wang W, Li C, Yu H, Yang A, Wang B, et al. WWP2 promotes degradation of transcription factor OCT4 in human embryonic stem cells. *Cell Res.* 2009;19(5):561-73.

303. Zhong Q, Gao W, Du F, and Wang X. Mule/ARF-BP1, a BH3-Only E3 Ubiquitin Ligase, Catalyzes the Polyubiquitination of Mcl-1 and Regulates Apoptosis. *Cell.* 2005;121(7):1085-95.

304. Miyazaki K, Fujita T, Ozaki T, Kato C, Kurose Y, Sakamoto M, et al. NEDL1, a novel ubiquitin-protein isopeptide ligase for dishevelled-1, targets mutant superoxide dismutase-1. *The Journal of biological chemistry.* 2004;279(12):11327-35.

305. Zhu H, Kavsak P, Abdollah S, Wrana JL, and Thomsen GH. A SMAD ubiquitin ligase targets the BMP pathway and affects embryonic pattern formation. *Nature.* 1999;400(6745):687-93.

306. Krishnamoorthy V, Khanna R, and Parnaik VK. E3 ubiquitin ligase HECW2 mediates the proteasomal degradation of HP1 isoforms. *Biochemical and biophysical research communications.* 2018;503(4):2478-84.

307. Lin X, Liang M, and Feng XH. Smurf2 is a ubiquitin E3 ligase mediating proteasome-dependent degradation of Smad2 in transforming growth factor-beta signaling. *The Journal of biological chemistry.* 2000;275(47):36818-22.

308. Seo SR, Lallemand F, Ferrand N, Pessah M, L'Hoste S, Camonis J, et al. The novel E3 ubiquitin ligase Tiul1 associates with TGIF to target Smad2 for degradation. *EMBO J.* 2004;23(19):3780-92.

309. Yu Y, and Hayward GS. The ubiquitin E3 ligase RAUL negatively regulates type i interferon through ubiquitination of the transcription factors IRF7 and IRF3. *Immunity.* 2010;33(6):863-77.

310. Cheon S, Kaur K, Nijem N, Tuncay IO, Kumar P, Dean M, et al. The ubiquitin ligase UBE3B, disrupted in intellectual disability and absent speech, regulates metabolic pathways by targeting BCKDK. *Proc Natl Acad Sci U S A.* 2019;116(9):3662-7.

311. Mishra A, Godavarthi SK, and Jana NR. UBE3A/E6-AP regulates cell proliferation by promoting proteasomal degradation of p27. *Neurobiology of disease.* 2009;36(1):26-34.

312. Hochrainer K, Pejanovic N, Olaseun VA, Zhang S, Iadecola C, and Anrather J. The ubiquitin ligase HERC3 attenuates NF-kappaB-dependent transcription independently of its enzymatic activity by delivering the RelA subunit for degradation. *Nucleic Acids Res.* 2015;43(20):9889-904.

313. Letellier E, and Haan S. SOCS2: physiological and pathological functions. *Front Biosci (Elite Ed).* 2016;8:189-204.

314. Qureshi N, Morrison DC, and Reis J. Proteasome protease mediated regulation of cytokine induction and inflammation. *Biochim Biophys Acta.* 2012;1823(11):2087-93.

315. Hu M-M, Xie X-Q, Yang Q, Liao C-Y, Ye W, Lin H, et al. TRIM38 Negatively Regulates TLR3/4-Mediated Innate Immune and Inflammatory Responses by Two Sequential and Distinct Mechanisms. *J Immunol.* 2015;195(9):4415-25.

316. Zhen-jin Z, Peng L, Fa-yu L, Liyan S, and Chang-fu S. PKCα take part in CCR7/NF-κB autocrine signaling loop in CCR7-positive squamous cell carcinoma of head and neck. *Mol Cell Biochem.* 2011;357(1-2):181-7.

317. Melino G, Gallagher E, Aqeilan RI, Knight R, Peschiaroli A, Rossi M, et al. Itch: a HECT-type E3 ligase regulating immunity, skin and cancer. *Cell Death Differ.* 2008;15(7):1103-12.

318. Humphreys IR, Walzl G, Edwards L, Rae A, Hill S, and Hussell T. A critical role for OX40 in T cell-mediated immunopathology during lung viral infection. *The Journal of Experimental Medicine.* 2003;198(8):1237-42.

319. Marshall RP, Gohlke P, Chambers RC, Howell DC, Bottoms SE, Unger T, et al. Angiotensin II and the fibroproliferative response to acute lung injury. *Am J Physiol Lung Cell Mol Physiol.* 2004;286(1):L156-64.

320. Gelinck LBS, van der Bijl AE, Beyer WEP, Visser LG, Huizinga TWJ, van Hogezand RA, et al. The effect of anti-tumour necrosis factor alpha treatment on the antibody response to influenza vaccination. *Ann Rheum Dis.* 2008;67(5):713-6.

321. Sweeney DA, Danner RL, Eichacker PQ, and Natanson C. Once is not enough: clinical trials in sepsis. *Intensive Care Med.* 2008;34(11):1955-60.

322. Lim KL, Chew KCM, Tan JMM, Wang C, Chung KKK, Zhang Y, et al. Parkin mediates nonclassical, proteasomal-independent ubiquitination of synphilin-1: implications for Lewy body formation. *J Neurosci.* 2005;25(8):2002-9.

323. Datta A, Datta A, Kamthan A, and Kamthan M. A simple protocol to detect interacting proteins by GST pull down assay coupled with MALDI or LC-MS/MS analysis. *Protoc exch.* 2015.

324. Tong Y, Lear TB, Evankovich J, Chen Y, Londino JD, Myerburg MM, et al. The RNFT2/IL-3Rα axis regulates IL-3 signaling and innate immunity. *JCI Insight.* 2020;5(3).

325. Broughton SE, Dhagat U, Hercus TR, Nero TL, Grimbaldeston MA, Bonder CS, et al. The GM-CSF/IL-3/IL-5 cytokine receptor family: from ligand recognition to initiation of signaling. *Immunol Rev.* 2012;250(1):277-302.

326. Weber GF, Chousterman BG, He S, Fenn AM, Nairz M, Anzai A, et al. Interleukin-3 amplifies acute inflammation and is a potential therapeutic target in sepsis. *Science.* 2015;347(6227):1260-5.

327. Takai S, Yamada K, Hirayama N, Miyajima A, and Taniyama T. Mapping of the human gene encoding the mutual signal-transducing subunit (beta-chain) of granulocyte-macrophage colony-stimulating factor (GM-CSF), interleukin-3 (IL-3), and interleukin-5 (IL-5) receptor complexes to chromosome 22q13.1. *Hum Genet.* 1994;93(2):198-200.

328. Hu J, Tang Z, Xu J, Ge W, Hu Q, He F, et al. The inhibitor of interleukin-3 receptor protects against sepsis in a rat model of cecal ligation and puncture. *Mol Immunol.* 2019;109:71-80.

329. Bentzer P, Fjell C, Walley KR, Boyd J, and Russell JA. Plasma cytokine levels predict response to corticosteroids in septic shock. *Intensive Care Med.* 2016;42(12):1970-9.

330. Broughton SE, Nero TL, Dhagat U, Kan WL, Hercus TR, Tvorogov D, et al. The βc receptor family - Structural insights and their functional implications. *Cytokine.* 2015;74(2):247-58.

331. Hercus TR, Kan WLT, Broughton SE, Tvorogov D, Ramshaw HS, Sandow JJ, et al. Role of the β common (βc) family of cytokines in health and disease. *Cold Spring Harb Perspect Biol.* 2018;10(6).

332. Meads MB, Li Z-W, and Dalton WS. A novel TNF receptor-associated factor 6 binding domain mediates NF-kappa B signaling by the common cytokine receptor beta subunit. *J Immunol.* 2010;185(3):1606-15.

333. Borriello F, Galdiero MR, Varricchi G, Loffredo S, Spadaro G, and Marone G. Innate Immune Modulation by GM-CSF and IL-3 in Health and Disease. *Int J Mol Sci.* 2019;20(4).

334. Jin J, Xiao Y, Hu H, Zou Q, Li Y, Gao Y, et al. Proinflammatory TLR signalling is regulated by a TRAF2-dependent proteolysis mechanism in macrophages. *Nat Commun.* 2015;6:5930.

335. Hu H, Wang H, Xiao Y, Jin J, Chang J-H, Zou Q, et al. Otud7b facilitates T cell activation and inflammatory responses by regulating Zap70 ubiquitination. *The Journal of Experimental Medicine.* 2016;213(3):399-414.

336. Chang M, Jin W, and Sun S-C. Peli1 facilitates TRIF-dependent Toll-like receptor signaling and proinflammatory cytokine production. *Nat Immunol.* 2009;10(10):1089-95.

337. Jia Y, Vong JS-L, Asafova A, Garvalov BK, Caputo L, Cordero J, et al. Lamin B1 loss promotes lung cancer development and metastasis by epigenetic derepression of RET. *The Journal of Experimental Medicine.* 2019;216(6):1377-95.

338. Hospenthal MK, Mevissen TET, and Komander D. Deubiquitinase-based analysis of ubiquitin chain architecture using Ubiquitin Chain Restriction (UbiCRest). *Nat Protoc.* 2015;10(2):349-61.

339. Ravid T, and Hochstrasser M. Diversity of degradation signals in the ubiquitin-proteasome system. *Nat Rev Mol Cell Biol.* 2008;9(9):679-90.

340. Evankovich J, Lear T, McKelvey A, Dunn S, Londino J, Liu Y, et al. Receptor for advanced glycation end products is targeted by FBXO10 for ubiquitination and degradation. *The FASEB Journal.* 2017;31(9):3894-903.

341. Chen BB, Coon TA, Glasser JR, Zou C, Ellis B, Das T, et al. E3 ligase subunit Fbxo15 and PINK1 kinase regulate cardiolipin synthase 1 stability and mitochondrial function in pneumonia. *Cell Rep.* 2014;7(2):476-87.

342. Min J, Nothing M, Coble B, Zheng H, Park J, Im H, et al. Integrated Biosensor for Rapid and Point-of-Care Sepsis Diagnosis. *ACS Nano.* 2018;12(4):3378-84.

343. Calfee CS, Delucchi K, Parsons PE, Thompson BT, Ware LB, Matthay MA, et al. Subphenotypes in acute respiratory distress syndrome: latent class analysis of data from two randomised controlled trials. *Lancet Respir Med.* 2014;2(8):611-20.

344. Delucchi K, Famous KR, Ware LB, Parsons PE, Thompson BT, Calfee CS, et al. Stability of ARDS subphenotypes over time in two randomised controlled trials. *Thorax.* 2018;73(5):439-45.

345. Srivastava RK, Tomar GB, Barhanpurkar AP, Gupta N, Pote ST, Mishra GC, et al. IL-3 attenuates collagen-induced arthritis by modulating the development of Foxp3+ regulatory T cells. *J Immunol.* 2011;186(4):2262-72.

346. Renner K, Hellerbrand S, Hermann F, Riedhammer C, Talke Y, Schiechl G, et al. IL-3 promotes the development of experimental autoimmune encephalitis. *JCI Insight.* 2016;1(16):e87157.

347. Renner K, Hermann FJ, Schmidbauer K, Talke Y, Rodriguez Gomez M, Schiechl G, et al. IL-3 contributes to development of lupus nephritis in MRL/lpr mice. *Kidney Int.* 2015;88(5):1088-98.

348. Middelburg RA, and van der Bom JG. Transfusion-related acute lung injury not a two-hit, but a multicausal model. *Transfusion.* 2015;55(5):953-60.

349. Birukova AA, Tian Y, Meliton A, Leff A, Wu T, and Birukov KG. Stimulation of Rho signaling by pathologic mechanical stretch is a "second hit" to Rho-independent lung injury induced by IL-6. *Am J Physiol Lung Cell Mol Physiol.* 2012;302(9):L965-75.

350. Walsh MC, Lee J, and Choi Y. Tumor necrosis factor receptor- associated factor 6 (TRAF6) regulation of development, function, and homeostasis of the immune system. *Immunol Rev.* 2015;266(1):72-92.

351. Inoue Ji, Ishida T, Tsukamoto N, Kobayashi N, Naito A, Azuma S, et al. Tumor necrosis factor receptor-associated factor (TRAF) family: adapter proteins that mediate cytokine signaling. *Exp Cell Res.* 2000;254(1):14-24.

352. Häcker H, Redecke V, Blagoev B, Kratchmarova I, Hsu L-C, Wang GG, et al. Specificity in Toll-like receptor signalling through distinct effector functions of TRAF3 and TRAF6. *Nature.* 2006;439(7073):204-7.

353. Cohen P. The TLR and IL-1 signalling network at a glance. *J Cell Sci.* 2014;127(Pt 11):2383-90.
354. Kawasaki T, and Kawai T. Toll-like receptor signaling pathways. *Front Immunol.* 2014;5:461.
355. Hu H, and Sun S-C. Ubiquitin signaling in immune responses. *Cell Res.* 2016;26(4):457-83.
356. Yang X-D, and Sun S-C. Targeting signaling factors for degradation, an emerging mechanism for TRAF functions. *Immunol Rev.* 2015;266(1):56-71.
357. Fang R, Jiang Q, Zhou X, Wang C, Guan Y, Tao J, et al. MAVS activates TBK1 and IKKε through TRAFs in NEMO dependent and independent manner. *PLoS Pathog.* 2017;13(11):e1006720.
358. Shi M, Deng W, Bi E, Mao K, Ji Y, Lin G, et al. TRIM30 alpha negatively regulates TLR-mediated NF-kappa B activation by targeting TAB2 and TAB3 for degradation. *Nat Immunol.* 2008;9(4):369-77.
359. Chousterman BG, and Swirski FK. Innate response activator B cells: origins and functions. *Int Immunol.* 2015;27(10):537-41.
360. Du Y, Kitzmiller JA, Sridharan A, Perl AK, Bridges JP, Misra RS, et al. Lung Gene Expression Analysis (LGEA): an integrative web portal for comprehensive gene expression data analysis in lung development. *Thorax.* 2017;72(5):481-4.
361. Du Y, Guo M, Whitsett JA, and Xu Y. 'LungGENS': a web-based tool for mapping single-cell gene expression in the developing lung. *Thorax.* 2015;70(11):1092-4.
362. Montoro DT, Haber AL, Biton M, Vinarsky V, Lin B, Birket SE, et al. A revised airway epithelial hierarchy includes CFTR-expressing ionocytes. *Nature.* 2018;560(7718):319-24.
363. Liu Y, Lear T, Iannone O, Shiva S, Corey C, Rajbhandari S, et al. The Proapoptotic F-box Protein Fbxl7 Regulates Mitochondrial Function by Mediating the Ubiquitylation and Proteasomal Degradation of Survivin. *The Journal of biological chemistry.* 2015;290(19):11843-52.
364. Han S, Lear TB, Jerome JA, Rajbhandari S, Snavely CA, Gulick DL, et al. Lipopolysaccharide primes the NALP3 inflammasome by inhibiting its ubiquitination and degradation mediated by the SCFFBXL2 E3 ligase. *The Journal of biological chemistry.* 2015;290(29):18124-33.
365. Townsend MH, Shrestha G, Robison RA, and O'Neill KL. The expansion of targetable biomarkers for CAR T cell therapy. *J Exp Clin Cancer Res.* 2018;37(1):163.
366. Testa U, Pelosi E, and Frankel A. CD 123 is a membrane biomarker and a therapeutic target in hematologic malignancies. *Biomark Res.* 2014;2(1):4.
367. Matute-Bello G, Downey G, Moore BB, Groshong SD, Matthay MA, Slutsky AS, et al. An official American Thoracic Society workshop report: features and measurements of experimental acute lung injury in animals. *Am J Respir Cell Mol Biol.* 2011;44(5):725-38.
368. Zou C, Li J, Xiong S, Chen Y, Wu Q, Li X, et al. Mortality factor 4 like 1 protein mediates epithelial cell death in a mouse model of pneumonia. *Science translational medicine.* 2015;7(311):311ra171.
369. Lear T, Dunn SR, McKelvey AC, Mir A, Evankovich J, Chen BB, et al. RING finger protein 113A regulates C-X-C chemokine receptor type 4 stability and signaling. *Am J Physiol, Cell Physiol.* 2017;313(5):C584-C92.
370. Klasse PJ. The molecular basis of HIV entry. *Cellular microbiology.* 2012;14(8):1183-92.

371. Busillo JM, and Benovic JL. Regulation of CXCR4 Signaling. *Biochim Biophys Acta.* 2007;1768(4):952-63.

372. Pozzobon T, Goldoni G, Viola A, and Molon B. CXCR4 signaling in health and disease. *Immunology Letters.* 2016;177:6-15.

373. Sun Y, Cheng Z, Ma L, and Pei G. Beta-arrestin2 is critically involved in CXCR4-mediated chemotaxis, and this is mediated by its enhancement of p38 MAPK activation. *The Journal of biological chemistry.* 2002;277(51):49212-9.

374. Mellado M, Rodriguez-Frade JM, Vila-Coro AJ, Fernandez S, Martin de Ana A, Jones DR, et al. Chemokine receptor homo- or heterodimerization activates distinct signaling pathways. *EMBO J.* 2001;20(10):2497-507.

375. Busillo JM, Armando S, Sengupta R, Meucci O, Bouvier M, and Benovic JL. Site-specific phosphorylation of CXCR4 is dynamically regulated by multiple kinases and results in differential modulation of CXCR4 signaling. *The Journal of biological chemistry.* 2010;285(10):7805-17.

376. Orsini MJ, Parent JL, Mundell SJ, Marchese A, and Benovic JL. Trafficking of the HIV coreceptor CXCR4. Role of arrestins and identification of residues in the c-terminal tail that mediate receptor internalization. *The Journal of biological chemistry.* 1999;274(43):31076-86.

377. Feng Y, Broder CC, Kennedy PE, and Berger EA. HIV-1 Entry Cofactor: Functional cDNA Cloning of a Seven-Transmembrane, G Protein-Coupled Receptor. *Science.* 1996;272(5263):872.

378. Henrich TJ, and Kuritzkes DR. HIV-1 Entry Inhibitors: Recent Development and Clinical Use. *Current opinion in virology.* 2013;3(1):51-7.

379. Hoshino Y, Tse DB, Rochford G, Prabhakar S, Hoshino S, Chitkara N, et al. *Mycobacterium tuberculosis*-Induced CXCR4 and Chemokine Expression Leads to Preferential X4 HIV-1 Replication in Human Macrophages. *The Journal of Immunology.* 2004;172(10):6251-8.

380. Chinnapaiyan S, Parira T, Dutta R, Agudelo M, Morris A, Nair M, et al. HIV Infects Bronchial Epithelium and Suppresses Components of the Mucociliary Clearance Apparatus. *PLoS ONE.* 2017;12(1):e0169161.

381. Chatterjee S, Behnam Azad B, and Nimmagadda S. The intricate role of CXCR4 in cancer. *Advances in cancer research.* 2014;124:31-82.

382. Li YM, Pan Y, Wei Y, Cheng X, Zhou BP, Tan M, et al. Upregulation of CXCR4 is essential for HER2-mediated tumor metastasis. *Cancer Cell.* 2004;6(5):459-69.

383. Liang Z, Yoon Y, Votaw J, Goodman MM, Williams L, and Shim H. Silencing of CXCR4 blocks breast cancer metastasis. *Cancer Res.* 2005;65(3):967-71.

384. Niu J, Huang Y, and Zhang L. CXCR4 silencing inhibits invasion and migration of human laryngeal cancer Hep-2 cells. *Int J Clin Exp Pathol.* 2015;8(6):6255-61.

385. Zhao H, Guo L, Zhao H, Zhao J, Weng H, and Zhao B. CXCR4 over-expression and survival in cancer: a system review and meta-analysis. *Oncotarget.* 2015;6(7):5022-40.

386. Moriuchi M, Moriuchi H, Margolis DM, and Fauci AS. USF/c-Myc enhances, while Yin-Yang 1 suppresses, the promoter activity of CXCR4, a coreceptor for HIV-1 entry. *J Immunol.* 1999;162(10):5986-92.

387. Marchese A, and Benovic JL. Agonist-promoted ubiquitination of the G protein-coupled receptor CXCR4 mediates lysosomal sorting. *The Journal of biological chemistry.* 2001;276(49):45509-12.

388. Bhandari D, Trejo J, Benovic JL, and Marchese A. Arrestin-2 interacts with the ubiquitin-protein isopeptide ligase atrophin-interacting protein 4 and mediates endosomal sorting of the chemokine receptor CXCR4. *The Journal of biological chemistry.* 2007;282(51):36971-9.

389. Holleman J, and Marchese A. The ubiquitin ligase deltex-3l regulates endosomal sorting of the G protein-coupled receptor CXCR4. *Molecular biology of the cell.* 2014;25(12):1892-904.

390. Kennedy JE, and Marchese A. Regulation of GPCR Trafficking by Ubiquitin. *Progress in molecular biology and translational science.* 2015;132:15-38.

391. Metzger MB, Pruneda JN, Klevit RE, and Weissman AM. RING-type E3 ligases: Master manipulators of E2 ubiquitin-conjugating enzymes and ubiquitination. *Biochimica et Biophysica Acta (BBA) - Molecular Cell Research.* 2014;1843(1):47-60.

392. Mines MA, Goodwin JS, Limbird LE, Cui F-F, and Fan G-H. Deubiquitination of CXCR4 by USP14 Is Critical for Both CXCL12-induced CXCR4 Degradation and Chemotaxis but Not ERK Activation. *Journal of Biological Chemistry.* 2009;284(9):5742-52.

393. Skaar JR, Pagan JK, and Pagano M. Mechanisms and function of substrate recruitment by F-box proteins. *Nat Rev Mol Cell Biol.* 2013;14(6):369-81.

394. Bhandari D, Robia SL, and Marchese A. The E3 ubiquitin ligase atrophin interacting protein 4 binds directly to the chemokine receptor CXCR4 via a novel WW domain-mediated interaction. *Molecular biology of the cell.* 2009;20(5):1324-39.

395. Ghosh MC, Makena PS, Gorantla V, Sinclair SE, and Waters CM. CXCR4 regulates migration of lung alveolar epithelial cells through activation of Rac1 and matrix metalloproteinase-2. *Am J Physiol Lung Cell Mol Physiol.* 2012;302(9):L846-56.

396. Cane S, Ponnappan S, and Ponnappan U. Altered regulation of CXCR4 expression during aging contributes to increased CXCL12-dependent chemotactic migration of CD4(+) T cells. *Aging Cell.* 2012;11(4):651-8.

397. Lapham CK, Romantseva T, Petricoin E, King LR, Manischewitz J, Zaitseva MB, et al. CXCR4 heterogeneity in primary cells: possible role of ubiquitination. *Journal of leukocyte biology.* 2002;72(6):1206-14.

398. Schaefer A, Nethe M, and Hordijk Peter L. Ubiquitin links to cytoskeletal dynamics, cell adhesion and migration. *Biochemical Journal.* 2012;442(1):13-25.

399. Dubrez L, and Rajalingam K. IAPs and cell migration. *Seminars in Cell & Developmental Biology.* 2015;39:124-31.

400. Marchese A, and Trejo J. Ubiquitin-dependent regulation of G protein-coupled receptor trafficking and signaling. *Cell Signal.* 2013;25(3):707-16.

401. Malik R, and Marchese A. Arrestin-2 interacts with the endosomal sorting complex required for transport machinery to modulate endosomal sorting of CXCR4. *Molecular biology of the cell.* 2010;21(14):2529-41.

402. Slagsvold T, Marchese A, Brech A, and Stenmark H. CISK attenuates degradation of the chemokine receptor CXCR4 via the ubiquitin ligase AIP4. *EMBO J.* 2006;25(16):3738-49.

403. Chen BB, Coon TA, Glasser JR, McVerry BJ, Zhao J, Zhao Y, et al. A combinatorial F box protein directed pathway controls TRAF adaptor stability to regulate inflammation. *Nat Immunol.* 2013;14(5):470-9.

404. Jain AK, and Barton MC. Regulation of p53: TRIM24 enters the RING. *Cell Cycle.* 2009;8(22):3668-74.

405. Frattini A, Faranda S, Bagnasco L, Patrosso C, Nulli P, Zucchi I, et al. Identification of a new member (ZNF183) of the Ring finger gene family in Xq24-25. *Gene.* 1997;192(2):291-8.

406. Corbett MA, Dudding-Byth T, Crock PA, Botta E, Christie LM, Nardo T, et al. A novel X-linked trichothiodystrophy associated with a nonsense mutation in RNF113A. *Journal of medical genetics.* 2015;52(4):269-74.

407. Czugala M, Karolak JA, Nowak DM, Polakowski P, Pitarque J, Molinari A, et al. Novel mutation and three other sequence variants segregating with phenotype at keratoconus 13q32 susceptibility locus. *European journal of human genetics : EJHG.* 2012;20(4):389-97.

408. King TE, Pardo A, and Selman M. Idiopathic pulmonary fibrosis. *Lancet.* 2011;378(9807):1949-61.

409. King TE, Tooze JA, Schwarz MI, Brown KR, and Cherniack RM. Predicting survival in idiopathic pulmonary fibrosis: scoring system and survival model. *Am J Respir Crit Care Med.* 2001;164(7):1171-81.

410. Partridge L, Deelen J, and Slagboom PE. Facing up to the global challenges of ageing. *Nature.* 2018;561(7721):45-56.

411. Lear TB, Lockwood KC, Ouyang Y, Evankovich JW, Larsen MB, Lin B, et al. The RING-type E3 ligase RNF186 ubiquitinates Sestrin-2 and thereby controls nutrient sensing. *Journal of Biological Chemistry.* 2019;294(45):16527-34.

412. Yuan H-X, Xiong Y, and Guan K-L. Nutrient sensing, metabolism, and cell growth control. *Molecular cell.* 2013;49(3):379-87.

413. Sabatini DM. Twenty-five years of mTOR: Uncovering the link from nutrients to growth. *Proceedings of the National Academy of Sciences.* 2017;114(45):11818-25.

414. Wolfson RL, and Sabatini DM. The Dawn of the Age of Amino Acid Sensors for the mTORC1 Pathway. *Cell Metab.* 2017;26(2):301-9.

415. Wolfson RL, Chantranupong L, Saxton RA, Shen K, Scaria SM, Cantor JR, et al. Sestrin2 is a leucine sensor for the mTORC1 pathway. *Science.* 2016;351(6268):43-8.

416. Saxton RA, Knockenhauer KE, Wolfson RL, Chantranupong L, Pacold ME, Wang T, et al. Structural basis for leucine sensing by the Sestrin2-mTORC1 pathway. *Science.* 2016;351(6268):53-8.

417. Liang Y, Zhu J, Huang H, Xiang D, Li Y, Zhang D, et al. SESN2/sestrin 2 induction-mediated autophagy and inhibitory effect of isorhapontigenin (ISO) on human bladder cancers. *Autophagy.* 2016;12(8):1229-39.

418. Kumar A, and Shaha C. SESN2 facilitates mitophagy by helping Parkin translocation through ULK1 mediated Beclin1 phosphorylation. *Sci Rep.* 2018;8(1):615.

419. Kim MJ, Bae SH, Ryu JC, Kwon Y, Oh JH, Kwon J, et al. SESN2/sestrin2 suppresses sepsis by inducing mitophagy and inhibiting NLRP3 activation in macrophages. *Autophagy.* 2016;12(8):1272-91.

420. Byun J-K, Choi Y-K, Kim J-H, Jeong JY, Jeon H-J, Kim M-K, et al. A Positive Feedback Loop between Sestrin2 and mTORC2 Is Required for the Survival of Glutamine-Depleted Lung Cancer Cells. *Cell Rep.* 2017;20(3):586-99.

421. Ding B, Parmigiani A, Divakaruni AS, Archer K, Murphy AN, and Budanov AV. Sestrin2 is induced by glucose starvation via the unfolded protein response and protects cells from non-canonical necroptotic cell death. *Sci Rep.* 2016;6:22538.

422. Lee JH, Budanov AV, Park EJ, Birse R, Kim TE, Perkins GA, et al. Sestrin as a feedback inhibitor of TOR that prevents age-related pathologies. *Science.* 2010;327(5970):1223-8.

423. Jiang Y, Su S, Zhang Y, Qian J, and Liu P. Control of mTOR signaling by ubiquitin. *Oncogene.* 2019;38(21):3989-4001.

424. Zheng N, and Shabek N. Ubiquitin Ligases: Structure, Function, and Regulation. *Annu Rev Biochem.* 2017;86:129-57.

425. Hyer ML, Milhollen MA, Ciavarri J, Fleming P, Traore T, Sappal D, et al. A small-molecule inhibitor of the ubiquitin activating enzyme for cancer treatment. *Nat Med.* 2018;24(2):186-93.

426. Komander D, and Rape M. The Ubiquitin Code. *Annual Review of Biochemistry.* 2012;81(1):203-29.

427. Hospenthal MK, Mevissen TET, and Komander D. Deubiquitinase-based analysis of ubiquitin chain architecture using Ubiquitin Chain Restriction (UbiCRest). *Nature Protocols.* 2015;10:349.

428. Fujimoto K, Kinoshita M, Tanaka H, Okuzaki D, Shimada Y, Kayama H, et al. Regulation of intestinal homeostasis by the ulcerative colitis-associated gene RNF186. *Mucosal immunology.* 2017;10(2):446-59.

429. Akutsu M, Dikic I, and Bremm A. Ubiquitin chain diversity at a glance. *J Cell Sci.* 2016;129(5):875-80.

430. Udeshi ND, Svinkina T, Mertins P, Kuhn E, Mani DR, Qiao JW, et al. Refined preparation and use of anti-diglycine remnant (K-ε-GG) antibody enables routine quantification of 10,000s of ubiquitination sites in single proteomics experiments. *Mol Cell Proteomics.* 2013;12(3):825-31.

431. Kaizuka T, Morishita H, Hama Y, Tsukamoto S, Matsui T, Toyota Y, et al. An Autophagic Flux Probe that Releases an Internal Control. *Mol Cell.* 2016;64(4):835-49.

432. Wang P, Wu Y, Li Y, Zheng J, and Tang J. A novel RING finger E3 ligase RNF186 regulate ER stress-mediated apoptosis through interaction with BNip1. *Cellular signalling.* 2013;25(11):2320-33.

433. Kim H, An S, Ro SH, Teixeira F, Park GJ, Kim C, et al. Janus-faced Sestrin2 controls ROS and mTOR signalling through two separate functional domains. *Nat Commun.* 2015;6:10025.

434. Kim W, Bennett Eric J, Huttlin Edward L, Guo A, Li J, Possemato A, et al. Systematic and Quantitative Assessment of the Ubiquitin-Modified Proteome. *Molecular Cell.* 2011;44(2):325-40.

435. Kumar A, and Shaha C. RBX1-mediated ubiquitination of SESN2 promotes cell death upon prolonged mitochondrial damage in SH-SY5Y neuroblastoma cells. *Mol Cell Biochem.* 2018;446(1-2):1-9.

436. Swatek KN, and Komander D. Ubiquitin modifications. *Cell Research.* 2016;26:399.

437. Hu Y, Lou J, Mao YY, Lai TW, Liu LY, Zhu C, et al. Activation of MTOR in pulmonary epithelium promotes LPS-induced acute lung injury. *Autophagy.* 2016;12(12):2286-99.

438. Romero Y, Bueno M, Ramirez R, Álvarez D, Sembrat JC, Goncharova EA, et al. mTORC1 activation decreases autophagy in aging and idiopathic pulmonary fibrosis and contributes to apoptosis resistance in IPF fibroblasts. *Aging Cell.* 2016;15(6):1103-12.

439. Wempe F, De-Zolt S, Koli K, Bangsow T, Parajuli N, Dumitrascu R, et al. Inactivation of sestrin 2 induces TGF-β signaling and partially rescues pulmonary emphysema in a mouse model of COPD. *Disease Models & Mechanisms.* 2010;3(3-4):246-53.

440. Lim KL, Chew KC, Tan JM, Wang C, Chung KK, Zhang Y, et al. Parkin mediates nonclassical, proteasomal-independent ubiquitination of synphilin-1: implications for Lewy body formation. *J Neurosci.* 2005;25(8):2002-9.

441. Chantranupong L, Wolfson RL, Orozco JM, Saxton RA, Scaria SM, Bar-Peled L, et al. The Sestrins interact with GATOR2 to negatively regulate the amino-acid-sensing pathway upstream of mTORC1. *Cell reports.* 2014;9(1):1-8.

442. Nations U. World Population Prospects: the 2010 Revision. *http://esaunorg/unpd/wpp/.* 2010.

443. Castriotta RJ, Eldadah BA, Foster WM, Halter JB, Hazzard WR, Kiley JP, et al. Workshop on idiopathic pulmonary fibrosis in older adults. *Chest.* 2010;138(3):693-703.

444. Burslem GM, and Crews CM. Proteolysis-Targeting Chimeras as Therapeutics and Tools for Biological Discovery. *Cell.* 2020.

445. Sakamoto KM, Kim KB, Kumagai A, Mercurio F, Crews CM, and Deshaies RJ. Protacs: chimeric molecules that target proteins to the Skp1-Cullin-F box complex for ubiquitination and degradation. *Proc Natl Acad Sci USA.* 2001;98(15):8554-9.

446. Paiva SL, and Crews CM. Targeted protein degradation: elements of PROTAC design. *Curr Opin Chem Biol.* 2019;50:111-9.

447. Zengerle M, Chan K-H, and Ciulli A. Selective Small Molecule Induced Degradation of the BET Bromodomain Protein BRD4. *ACS Chem Biol.* 2015;10(8):1770-7.

448. Winter GE, Buckley DL, Paulk J, Roberts JM, Souza A, Dhe-Paganon S, et al. DRUG DEVELOPMENT. Phthalimide conjugation as a strategy for in vivo target protein degradation. *Science (New York, NY).* 2015;348(6241):1376-81.

449. Raina K, Lu J, Qian Y, Altieri M, Gordon D, Rossi AM, et al. PROTAC-induced BET protein degradation as a therapy for castration-resistant prostate cancer. *Proc Natl Acad Sci U S A.* 2016;113(26):7124-9.

450. Bai L, Zhou H, Xu R, Zhao Y, Chinnaswamy K, McEachern D, et al. A Potent and Selective Small-Molecule Degrader of STAT3 Achieves Complete Tumor Regression In Vivo. *Cancer Cell.* 2019;36(5):498-511.e17.

451. Yang CY, Qin C, Bai L, and Wang S. Small-molecule PROTAC degraders of the Bromodomain and Extra Terminal (BET) proteins - A review. *Drug Discov Today Technol.* 2019;31:43-51.

452. Sun X, Wang J, Yao X, Zheng W, Mao Y, Lan T, et al. A chemical approach for global protein knockdown from mice to non-human primates. *Cell Discovery.* 2019;5(1):10.